Evolution of the Kamuikotan high-*P/T* metamorphic belt in central Hokkaido, Japan

- with special reference to the relation between white mica K-Ar ages and deformation

Tsutomu OTA

Course of Environmental Science
Graduate School of Science and Technology
Niigata University

Contents

Evolution of the Kamuikotan high-*P/T* metamorphic belt in central Hokkaido, Japan

- with special reference to the relation between white mica K-Ar ages and deformation

Tsutomu OTA

Abstract

The Kamuikotan metamorphic rocks in central Hokkaido, Japan, are typical example produced by subduction-related high pressure and low temperature (high-P/T) metamorphism in the world. They have preserved several lines of evidence showing that they had been formed in the subduction zone with a non-steady state thermal structure. Such evidence is based on investigations in the field, structural analyses, metamorphic petrology and radiometric dating of the Kamuikotan metamorphic rocks. They are summaried as follows.

The Kamuikotan metamorphic rocks in the Kamuikotan Gorge area, are divided into major two geologic sequences: melange with serpentinite matrix containing a large amount of metamorphic blocks (Tokiwayama melange unit) and coherent metamorphic sequence. The latter is subdivided into three units: Pankehoronai, Harushinai and Biei units, based on the geology, metamorphism and radiometric age. Major four stages of deformation, D1, D2, D3 and D4 stages, are discriminated based on available textural relation among meso- and microscopic deformation structures in the coherent metamorphic sequence. The D1 and D2 stages

correspond to subduction-related structures to produce melange complex at trench and underplating of the complex at deep level of subduction zone, respectively. The D3 stage is an exhumation process of the metamorphic complex accompanied with ductile deformation. Subsequently, the metamorphic complex has been gently bent in the D4 stage. Judging from the mineral parageneses in the basic rocks, the Tokiwayama melange, Biei and Harushinai units are metamorphosed at higher-P/T conditions with geothermal gradient less than 10 °C/km than the Pankehoronai unit (geothermal gradient; about 15 °C/km). However, remnants of minerals of the Pankehoronai unit, which were produced in the earlier stage of deformation (D2 stage), shows that the Pankehoronai unit had been metamorphosed at similar conditions to the Biei and Harushinai units. Radiometric ages of phengite dated by K-Ar method are considarably scattered and range from 133 Ma to 62 Ma. The ages of units with higher P/T conditions are older than those of units with lower P/T conditions. Detailed investigations of dated specimens in term of deformation and recrystallization degree indicate that each apparent age of specimen with complicated history never denotes a specific time, and that the intermediate ages within the above range are mixture ages of different events due to incomplete recrystallization during the later metamorphic event. The specimens showing older ages are nearly free from the later metamorphic event (lower P/T conditions). Thus, the Kamuikotan metamorphic rocks are clearly divided into two types, i.e., typical high-P/T metamorphic rocks formed in Early Cretaceous time and rocks belonging to high-P/T intermediate group metamorphosed in Early Eocene time. Such change of the Kamuikotan metamorphic P/T gradient is related that the ages and the relative motions of subducted oceanic plates had been changed in early Cretaceous to early Paleogene time.

1. Introduction

1-1. High-P/T metamorphic belt in the subduction zone

A broad spectrum of variably altered rocks with miscellaneous processing formations and origins are compressed and heated over a wide range of pressure and temperature conditions in subduction zones. Nevertheless the rocks undergone such changes of conditions in the subduction zones mostly have several lines of evidence that they have been produced under a unique geothermal gradient. The geothermal gradient is unusual and approximately a half of that in a common continental crust. Thus, the above-mentioned rocks have been called high-pressure and low-temperature (high-P/T) metamorphic rocks or simply high pressure metamorphic rocks, which one of their representatives are blueschist and eclogite (ultrahigh-pressure metamorphic rocks in several continental collision zones, as reviewed after Liou et al.(1994), have not been handled in this thesis). Although subduction zones have long been of interest because they are the builders of continents, collecting material from the ocean basins and constructing magmatic arcs, and the high-P/T metamorphic rocks are essentially connected to the subduction-related orogen.

Cordilleran-type orogenic belts (e.g., Dewey and Bird, 1970), which has developed at western continental margin of North America, Japanese Island on the East Asian continental margin and other circum-Pacific, are convergent-type orogens based on plate tectonics. After 1980 s, a concept of accretional complex has been established by advance of microfossil study, and the subduction-related process that forms subduction-accretion complexes in the Cordilleran-type orogenic belts is

under discussion. In recent years, the schematic diagrams showing subduction-accretion processes at trench and subduction-related high-P/T metamorphism at lower domains of the accreted complexes has been illustrated (Isozaki et al., 1990; Matsuda and Isozaki, 1991; Isozaki and Maruyama, 1991). The plate tectonics can explain the processing formation of high-P/T metamorphic rocks; cool lithosphere has subducted in deep level under continental or island arc crusts and has been metamorphosed at a typically lower geothermal gradient due to cooler itself subducted than the upper part. Some models for exhumation of the high-P/T metamorphic belts from the deep level to the earth surface have been proposed by many workers, however, the mechanism has been not fully clarified yet. Maruyama (1990) has presented an idealized mode of occurrence of high-P/T metamorphic belts based on compilations of the mode of occurrences, ages and petrological features for a huge amount of high-P/T metamorphic belts in the world. The idealized mode of occurrence is called the sandwich structure (Fig. 1-1), which the high-P/T metamorphic unit is intervened between two lower P/T metamorphic units by a pair of normal and reverse faults (Maruyama, 1990; Isozaki and Maruyama, 1991). Such a sandwich structure requires that a pair of fault bordering with the high-P/T metamorphic unit and the neighboring lower grade units is formed at the same time. Then, Maruyama (1990) and Maruyama et al. (1994) have proposed a model of wedge extrusion of high-P/T metamorphic belt. This wedge extrusion model is fundamentally based upon general features of the high-P/T metamorphic belts. But natures of individual high-P/T metamorphic belts are notably different from each other.

Ernst (1988) suggests that retrograde pressure-temperature (P-T) paths of high-P/T metamorphic rocks, expected to record changes of

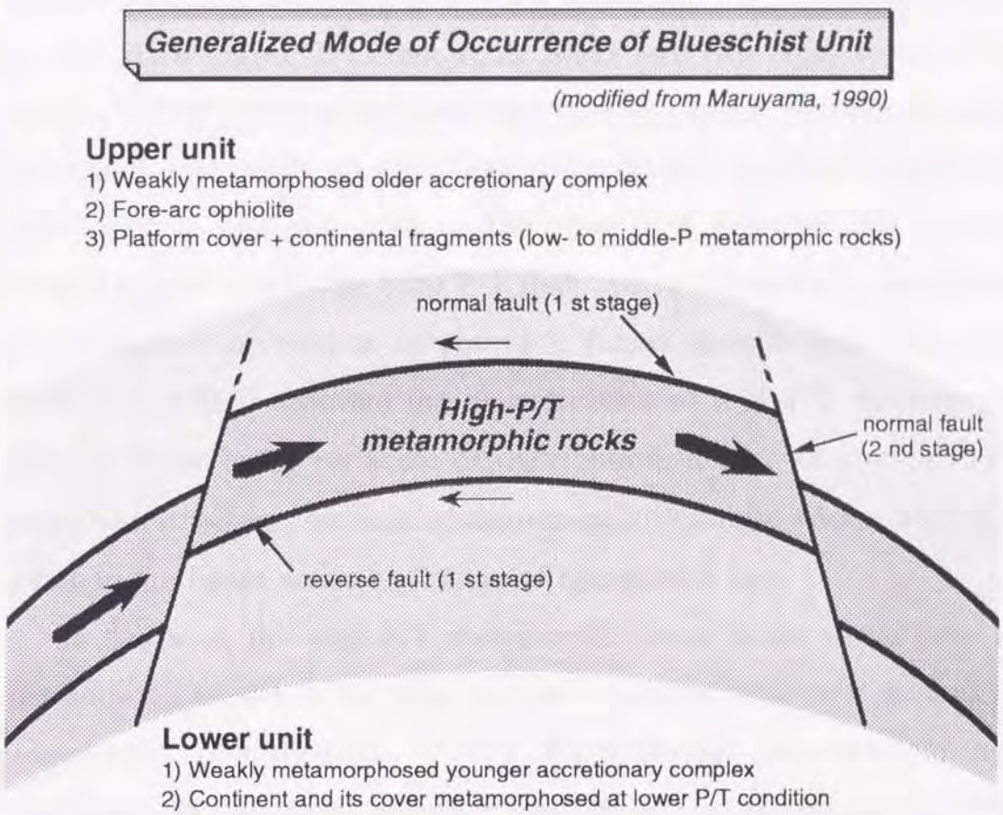

Upper unit Weakly metamorphosed older accretionary complex or Fore-arc ophiolite	normal fault	High-P/T metamorphic rocks	reverse fault	Lower unit Weakly metamorphosed younger accretionary complex
Sorachi ophiolite		Kamuikotan (Hokkaido)		Idon'nappu belt
Coast Range ophiolite		Franciscan (North California)		Coastal belt of Franciscan
Chichibu belt		Sanbagawa (Southwest Japan)		Shimanto belt

Fig. 1-1. Generalized mode of occurrence of blueschist unit modified from Maruyama (1990). Note the "sandwich" structure of high-pressure type unit intervened between two low-pressure type units by a pair of normal and reverse faults.

conditions in the exhumation process, provide important constrains on the tectonic evolution of convergent plate junctions, i.e., subduction zones, and classified high-P/T metamorphic rocks into two types based on the retrograde P-T paths as follows: one type has been metamorphosed at particularly low geothermal gradient and recorded a unique retrograde P-T path such as hair-pin curve. The other type, however, has evidence traced a typical clockwise loop P-T path and retrogressively overprinted by greenschist or epidote-amphibolite facies assemblages (Fig. 1-2). Hashimoto (1985) reported the classification of high-P/T metamorphic rocks in Japan based on scale of distribution, degree of complexity in geological structure, amount of associated ultramafic rocks, variety of metamorphic facies series and range of radiometric age.

In this way, the high-P/T metamorphic belts in the world have not only some generalities but also obvious varieties, and their natures are exceedingly complicated. The Kamuikotan metamorphic belt, investigated in this study, is one of the high-P/T metamorphic belts with such complexities.

The Kamuikotan metamorphic rocks in central Hokkaido, Japan, which have been subjected to subduction-related high-P/T metamorphism during early Cretaceous to early Eocene time. The metamorphic rocks have many lines of evidence of obviously wide range of variety for metamorphic P/T ratio and radiometric age (Fig. 1-3), and have a huge amount of serpentinite included exotic blocks with variable metamorphic grades (reviews in Ota et al., 1993; Iwasaki et al., 1994; Sakakibara and Ota, 1994). As mentioned in detail in the later chapters, the Kamuikotan metamorphic rocks are extraordinary high-P/T metamorphic rocks and have an intensely complicated nature, combined traits of some types which are classified by Ernst (1988), Hashimoto (1985) and so on.

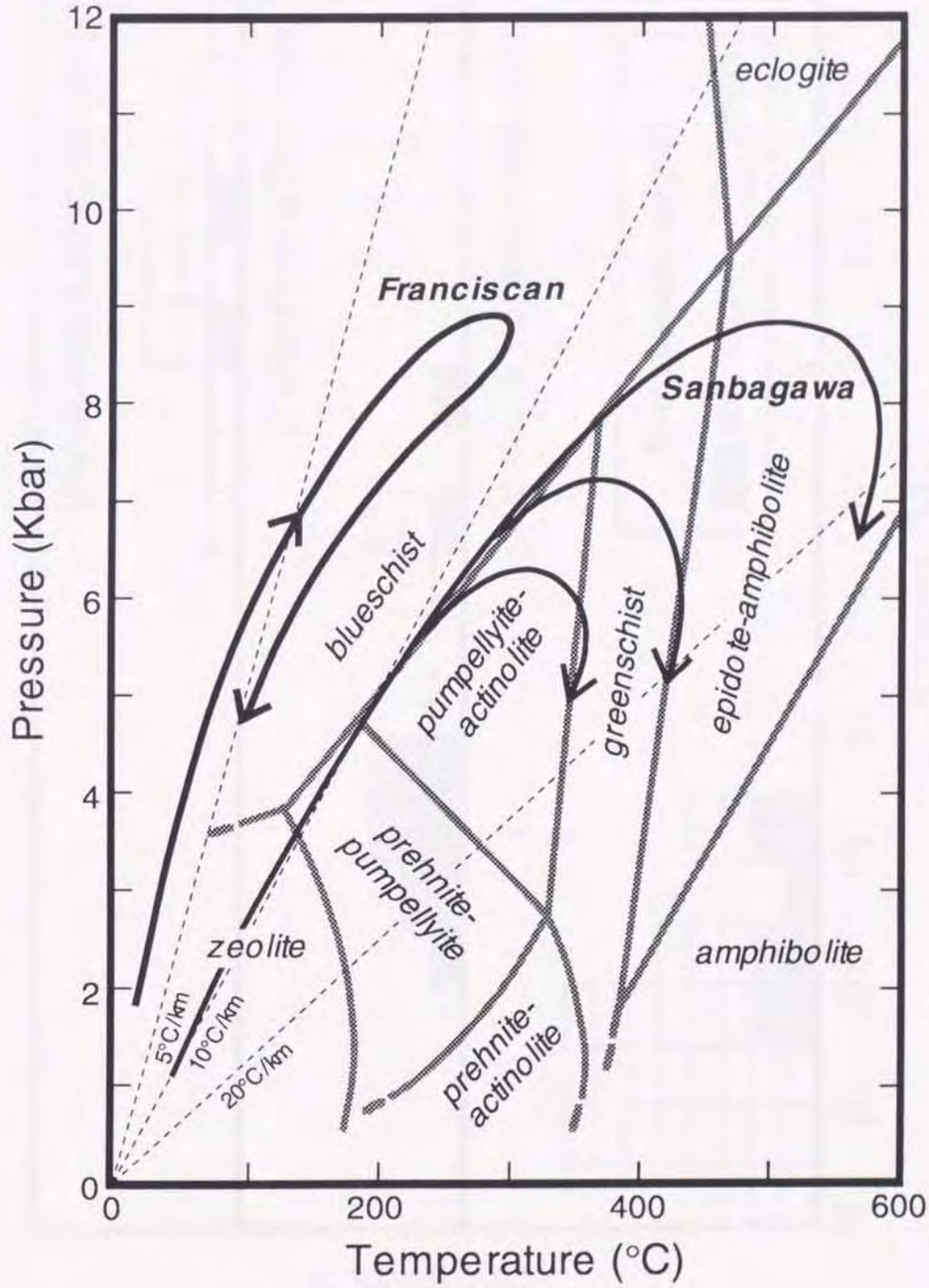

Fig. 1-2. A pressure-temperature diagram for low- and medium-grade metamorphic facies developed in rocks of roughly basaltic composition and generalized prograde and retrograde paths modified from Ernst (1988).

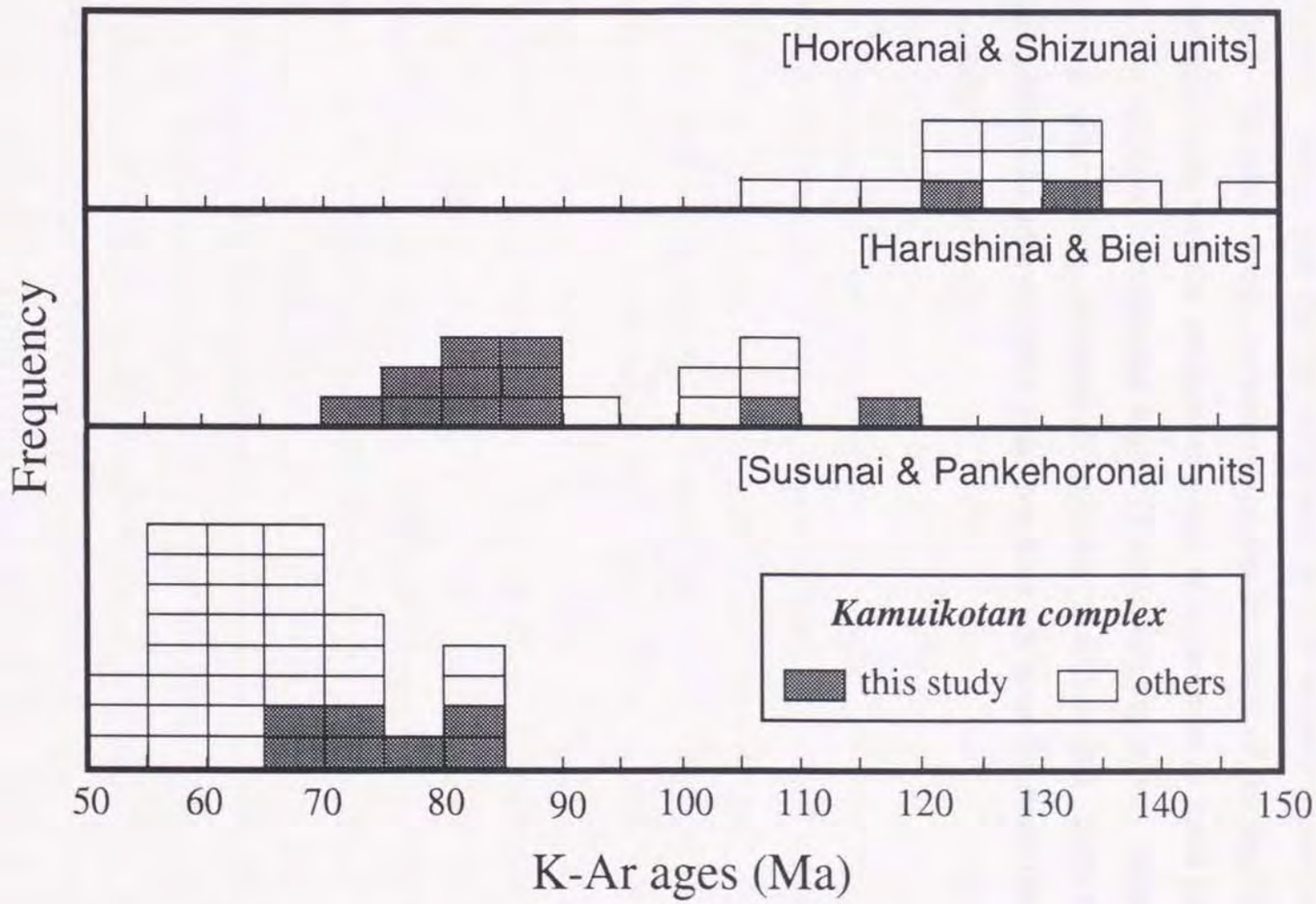

Fig. 1-3. Frequency distribution diagram of K-Ar ages of the Kamuikotan high-P/T metamorphic rocks. The sources of data are this study, Imaizumi and Ueda (1981), Iwasaki et al. (1991), Nakagawa and Nakano (1987), Shibakusa and Itaya (1992), Gouchi et al. (1992) and Ota et al. (1993).

The complexity of high-P/T metamorphic rocks is an evidence that various tectonics has affected the subduction zone formed the high-P/T metamorphic rocks, and that the influences of such tectonics have been recorded. In other words, to understand the tectonics of the high-P/T metamorphic belts and the subduction zones, it is essential to make clear the details of more complicated high-P/T metamorphic belts. Hence, clarifying processing formation of the Kamuikotan high-P/T metamorphic rocks with complex traits has been set up as the main theme in this study.

1-2. K-Ar ages of low-grade metamorphic rocks: recognition of mixture age

To reveal evolution of high-P/T metamorphic rocks, it is essential to clarify the metamorphic history, in particular, retrograde P-T paths recording changes of conditions in the exhumation process, the deformation history suggesting conversions of pictures of movements in the formation and exhumation process, and the accurate times when the high-P/T metamorphic rocks have formed. The most later is commonly examined by radiometric dating. The advance of radiometric dating by K-Ar method, together with microfossil study, gives important constraints to discussions of low-grade metamorphic rocks included high-P/T metamorphic rocks, resulting that geotectonic framework of Southwest Japan and new geotectonic subdivision of the Japanese Island are established (Isozaki and Itaya, 1990; 1991). In general, white micas in pelitic rocks are used to dating of low-grade metamorphic rocks. White mica K-Ar ages, however, are often discordant by differences of metamorphic grades and history, areas, and lithofacies of dating specimens (e.g., Itaya and Takasugi, 1988; Hirajima et al., 1992), and many investigaters have regarded that the significance of K-Ar ages of metamorphic rocks is uncertain.

Times inferred K-Ar ages of metamorphic rocks are defined by a concept of closure temperature (Fig. 1-4). Thus, the K-Ar ages of metamorphic rocks denote when the rocks have gotten cold less than closure temperature of dated minerals. In this case, the ages are called cooling ages and are regarded as a time during exhumation process of the rocks. On the other hand, in the case that the metamorphic peak temperature is lower than the closure temperature of dating minerals, K-

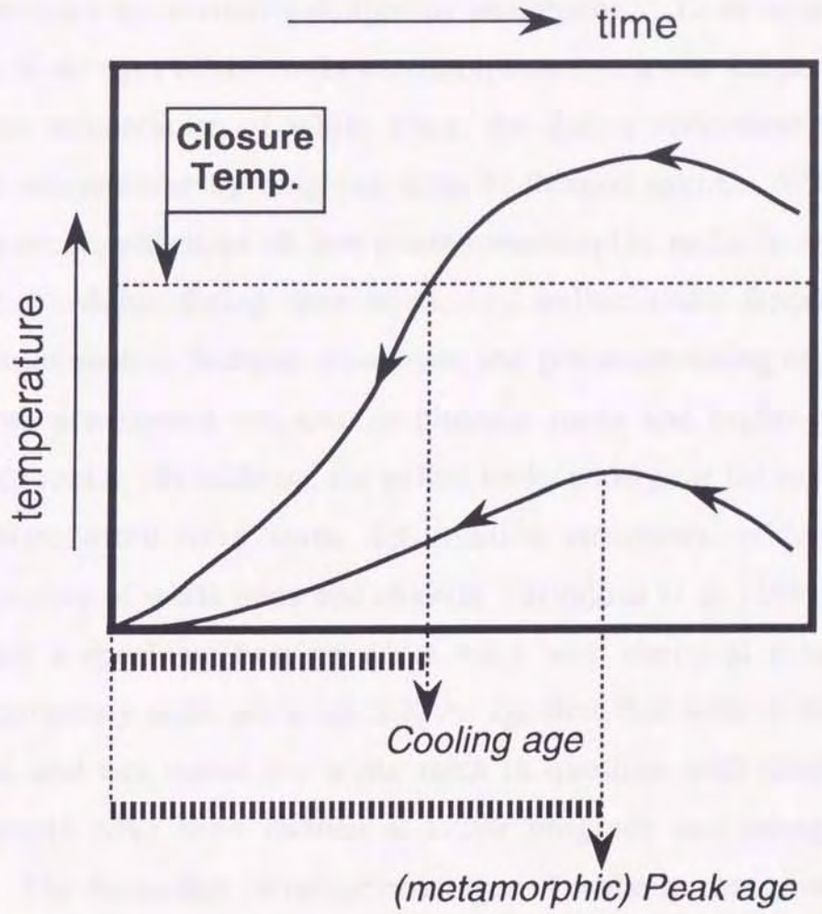

Fig. 1-4. Correlation of closure temperature, cooling age and metamorphic peak age for K-Ar age of metamorphic rocks.

Ar ages derived from such rocks are regarded as a time that temperature has begun to be lower than the peak temperature during the metamorphism, i.e., approximately metamorphic peak age. Definition of the latter includes an obviously dangerous assumption. To be available white mica K-Ar ages of the rocks metamorphosed at lower temperature than closure temperature of white mica, the dating specimens must completely recrystallize by only one time of thermal event. Without saying, the recrystallization of low-grade metamorphic rocks is mostly incomplete. Major dating specimens, i.e., pelitic rocks frequently include detritus such as feldspar, muscovite and grains consisting of them derived from pre-existed volcanic or plutonic rocks and higher-grade metamorphic rocks. In addition, the pelitic rocks undergone the regional metamorphism often have some deformation structures, which are composed mainly of white mica and chlorite. Hirajima et al. (1992) has reported that a specimen bearing white mica with chemical zonation shows an apparently older white mica K-Ar age than that without such a white mica, and has stated the white mica in question with chemical zonation would have been formed at either prograde and retrograde processes. The discordant in radiometric ages of white micas, grown in some stages of different conditions, has been documented by Scaillet et al.(1990, 1992) as well. Their spot-fusion and ^{40}Ar-^{39}Ar continuous laser-probe techniques on single grains reveal a significant zonation of radiometric ages, and they suggest that the white micas composing of earlier textures have preserved the ages when they have been formed until present, within a specific high-P/T metamorphic rocks.

In this study, taking the previous works mentioned above into consideration, it has been thoroughly investigated how are white micas in

fractions prepared for dating and what time shows white mica K-Ar ages derived from such fractions.

In this thesis, minute investigations in the field, structural analyses, metamorphic petrology and radiometric ages of the Kamuikotan high-P/T metamorphic rocks are described. These are integrated to clarify the nature of the Kamuikotan high-P/T metamorphism, the significance of the white mica K-Ar ages of low-grade metamorphic rocks, and the processing formation and exhuming mechanism of the Kamuikotan high-P/T metamorphic belt.

2. General geology of Hokkaido

2-1. Tectonic divisions of Hokkaido

Hokkaido island (Fig. 2-1) has been formed entirely by accretion since Jurassic time (Kiminami, 1986; Niida and Kito, 1986; Komatsu et al., 1992; Kimura et al., 1994). Five geologic provinces from west to east, Oshima, Sorachi-Yezo, Hidaka, Tokoro and Nemuro belts have been defined on the basis of facies, age, tectonic setting in the Mesozoic and historical tectonic divisions of Hokkaido by Kiminami et al.(1986). Kimura(1986) has separated the Hidaka belt after Kiminami et al.(1986) into the Idonnappu belt and the Hidaka belt. Subsequently, Komatsu et al.(1992) has modified the above division on the basis of recent available studied, and divided the basement of Hokkaido island into three major provinces, west, central and east Hokkaido. In this thesis, the tectonic division of Hokkaido follows fundamentally Komatsu et al.(1992).

West Hokkaido corresponds to the Oshima belt of Kiminami et al.(1986). The province has consisted of a Jurassic accretionary complex (Kawamura et al.,1986; Kawamura et al., 1994), where Early Cretaceous granitic rocks have intruded and calc-alkaline volcanic rocks covered. The volcanic rocks with a nature of island arc tholeiite are distributed along the eastern margin, which has defined as the Rebun-Kabato belt by Komatsu (1985). Central Hokkaido is composed of two belts of lower to upper Cretaceous subduction-accretion complexes from west to east, the Sorachi-Yezo and Hidaka belts. The Sorachi-Yezo belt principally consists of Early to Late Cretaceous accretionary complexes, two ophiolite complexes and fore arc sedimentary sequences overlying the

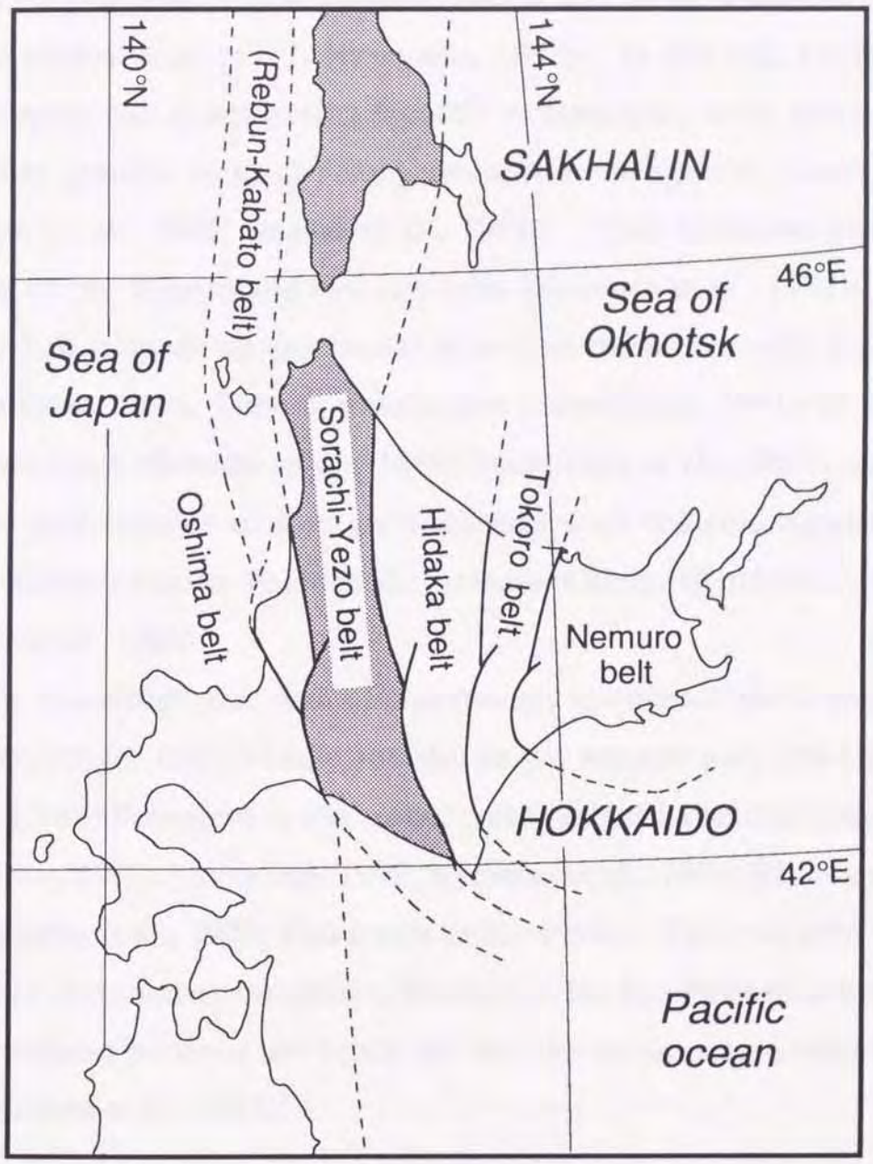

Fig. 2-1. Tectonic division map of Hokkaido and Sakhalin. Modified after Kiminami et al. (1986) and Komatsu et al. (1992).

accretionary complexes (Komatsu et al., 1992). Details of the belt are described in the following section. The Hidaka belt is composed mainly of Late Cretaceous to Early Paleogene trench-fill and accreted sedimentary complex, Nakanogawa Group and so on (Kontani et al., 1986; Komatsu et al., 1992; Nanayama, 1992). In this belt, the Hidaka metamorphic belt comprising a low P/T metamorphic rocks and a large amount of granitic rocks of Paleogene to Miocene age also occurs (e.g., Komatsu et al., 1986; Osanai et al., 1991). East Hokkaido province consists of the Tokoro and Nemuro belts (Komatsu et al., 1992). The Tokoro belt is made up subduction-accretion complexes with high-P/T metamorphic rocks, Tokoro metabasites (Sakakibara, 1991) of Upper Cretaceous age (Kontani et al., 1986; Sakakibara et al., 1986), and the Nemuro belt consists of fore arc sediments with volcanic materials of Upper Cretaceous to Paleogene, Nemuro Group (Kiminami, 1983; Kontani et al., 1986).

The biostratigraphic data of accretionary complexes show that they become younger from Middle Jurassic in the western part (the Oshima belt) to Lower Paleogene in the central part (the Hidaka belt) of Hokkaido (Kiyakawa, 1992; Nanayama, 1992; Komatsu et al., 1992; Kimura et al., 1994; Uyeda et al., 1993; Kawamura et al., 1994). This eastward zonal growth of accretionary complexes finished in the late Paleogene because of the collision between the Kurile arc and the Asian margin subduction zone (Kimura et al., 1983).

2-2. Sorachi-Yezo belt

The Sorachi-Yezo belt constitutes the central Hokkaido together with the Hidaka belt. The location of the boundary between the Sorachi-Yezo and Hidaka belts is still controversial, because the structure and age of the sedimentary rocks in both belts have not been fully clarified yet. In addition, the age of accretionary complexes consisting of each belt successively becomes younger from the western part of the Sorachi-Yezo belt to the eastern part of the Hidaka belt as mentioned above. The author has attached significance to the Hidaka Main Thrust (e.g., Miyashita and Maeda, 1978; Komatsu et al., 1979), which the Poroshiri ophiolite (an oceanic crust) borders on the Hidaka metamorphic belt (an island arc crust). These two geological sequences have entirely different natures, then Komatsu et al.(1992) has defined the Hidaka Main Thrust as the boundary between the Poroshiri ophiolite and the Hidaka metamorphic belt.

The Sorachi-Yezo belt is tectonostratigraphically divided into the Poroshiri ophiolite (Miyashita, 1981; 1983; Arai and Miyashita, 1994), the Early Cretaceous to Early Paleogene Idonnappu melange complex (Watanabe, 1981; Kiyokawa, 1992; Uyeda et al., 1994), the Early Cretaceous to Early Paleogene Kamuikotan complex consisting of high-P/T metamorphic rocks and serpentinite melange (e.g., Sakakibara and Ota, 1994), Sorachi ophiolite (Kito, 1987), and Yezo Supergroup of fore arc sediments (Okada, 1983), in ascending order. In the southern portion of the Sorachi-Yezo belt, its components thrust over the Tertiary sedimentary rocks or overturned (e.g., Niida and Kito, 1986), because the belt has been affected by a series of diastrophic disturbances which is

ascribed to the westward shift of the frontal Kurile Arc since the Tertiary (Kimura et al., 1983).

The structural, lithologic and biostratigraphic data (Kiyakawa, 1992; Nanayama, 1992; Komatsu et al., 1992; Uyeda et al., 1993; 1994) indicate that the Kamuikotan complex, Idonnappu complex, and the Hidaka belt were formed as a result of accretion during northward convergence of the Izanagi (or Kula) and Pacific plates (Sakakibara and Ota, 1994). Although the Early Cretaceous sequences are very thin and occur mostly as blocks in a melange shale matrix, the Late Cretaceous sequences are contrary composed of abundant terrigenous sediments with only a few relatively thin, shale-rich melange zones. The sedimentation pattern in the accretionary complex and the forearc basin sequence (Yezo Supergroup) have been changed during the Middle Cretaceous, i.e., Cenomanian to Turonian time (Kiyokawa, 1992).

2-3. Kamuikotan complex

The Kamuikotan complex, consisting of the Kamuikotan high-P/T metamorphic rocks and a large amount of serpentinite melange, lies within the Sorachi-Yezo belt, which extends about a distance of 300 km in Hokkaido and is traced to the north as far as Sakhalin, Russia Republic (Fig. 2-2). Since the complex is composed of not only so-called high-P/T metamorphic rocks but also serpentinite melange including abundant blocks of various metamorphic P/T types and grades such as jadeite-quartz rock, epidote amphibolite, amphibolitic rocks, crystalline schists, and so on (Ishibashi, 1939; Shido and Seki, 1959; Kato et al., 1979; Imaizumi and Kanehira, 1980; Ishizuka and Imaizumi, 1980; Maekawa, 1983; Imaizumi, 1984; Takayama, 1986; Nakagawa and Toda,1987), therefore it has been thought a chaotic terrain and also called the Kamuikotan tectonic belt or Kamuikotan zone, (e.g., Kato et al., 1979; Ishizuka et al., 1983a; Watanabe et al., 1986). As described below, however, the detailed geologic mapping in the Kamuikotan Gorge area by the author has revealed that both coherent natures of the Kamuikotan metamorphic rocks and domains or belts of serpentinite melange are actually present. The serpentinite melange is characteristic of only the insertion along the boundaries among each unit or shear zones within the units (Ota, 1993MS; Sakakibara and Ota, 1994).

The tectonic relation between the Sorachi ophiolite and Kamuikotan complex is observed in the Horokanai area. The Horokanai ophiolite, regarded as the lower sequence of the Sorachi ophiolite in the area, contains nearly all constituents of oceanic crusts (Asahina and Komatsu, 1979; Ishizuka, 1980). It has undergone a low P/T type metamorphism, which is broadly comparable to the ocean floor metamorphism, but the

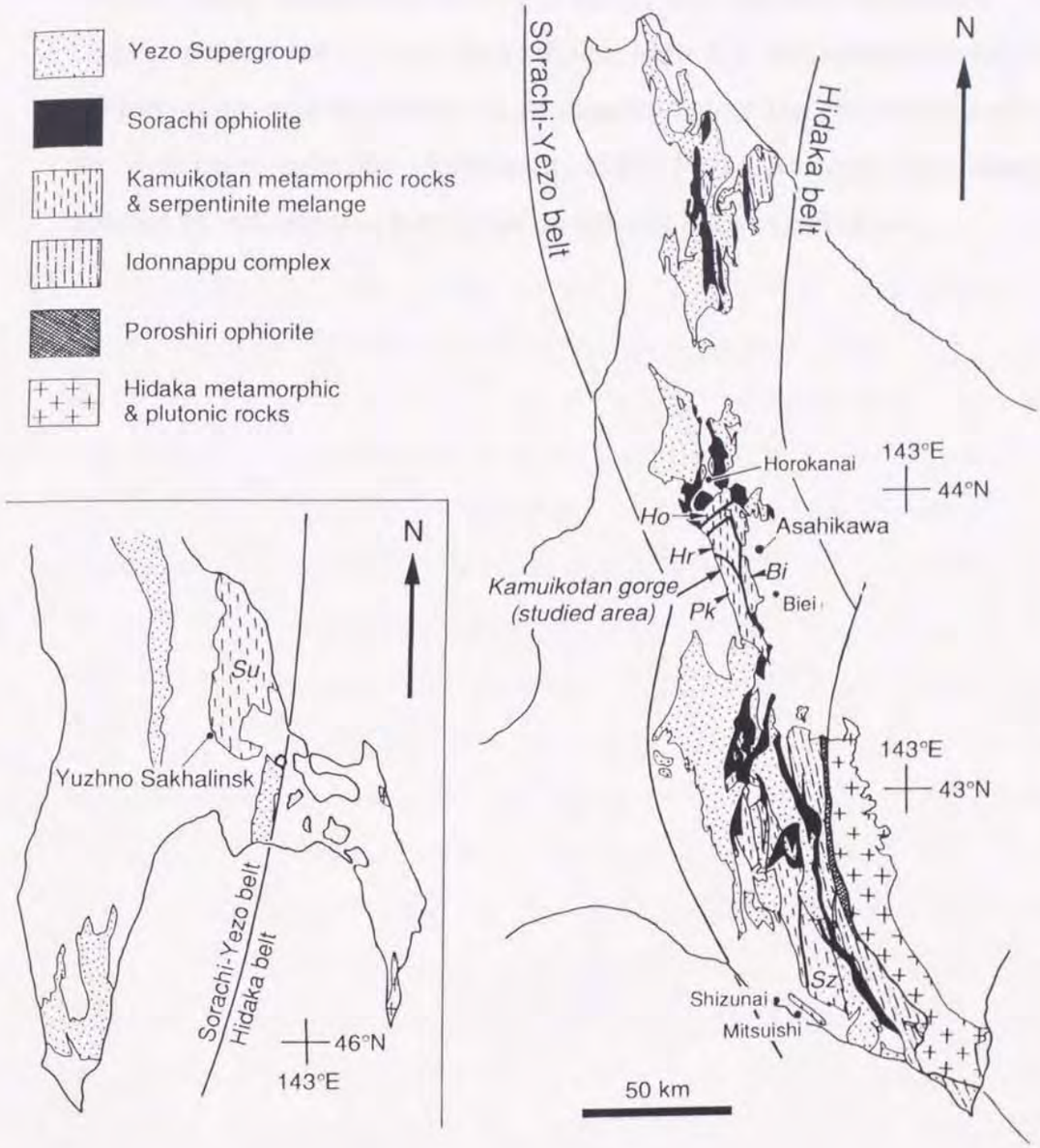

Fig. 2-2. Simplified geologic sketch map of central Hokkaido and Sakhalin showing the distribution of the Kamuikotan high-P/T metamorphic rocks, modified from Sakakibara and Ota (1994). Bi, Biei unit; Ho, Horokanai unit; Hr, Harushinai unit; Pk, Pankehoronai unit; Su, Susunai unit; Sz, Shizunai unit.

highest grade attains to the granulite facies (e.g., Ishizuka et al., 1985). The Horokanai ophiolite is overlain by Late Jurassic chert (Ishizuka et al., 1983b), Early Cretaceous siliceous shale, and volcanic sandstone. The highest grade rocks of the Kamuikotan high-P/T metamorphic complex, epidote-glaucophane schists, lie in directly below the ultramafic rocks of the Horokanai ophiolite (Shibakusa, 1989; 1991), however the formation process of this tectonic juxtaposition has not been clarified yet.

3. Geology of Kamuikotan complex

3-1. Outline of geology

The coherent Kamuikotan high-P/T metamorphic complex has been divided into two major units, unit I and unit II (Komatsu et al., 1992) or the upper unit and the lower unit (Ota et al., 1993), on the basis of lithology, metamorphic grade and radiometric age. Subsequently, the complex has been subdivided into the following six mappable units from north to south, on the basis of lithology, metamorphic grade and radiometric age: Susunai, Horokanai, Biei, Harushinai, Pankehoronai and Shizunai units (Fig. 2-2; Sakakibara and Ota, 1994). This thesis fundamentally follows the division of Sakakibara and Ota (1994). The six units occur originally as thrust sheets. The widespread serpentinite melange has assumed to predominate in the Kamuikotan metamorphic complex (e.g., Watanabe et al., 1986), but it is characteristic of only the insertion along the boundaries among each unit or the shear zone within the units. The outline of each unit is briefly described below.

The Susunai unit in the Sakhalin Island is situated between Cretaceous forearc sediments and the Cretaceous Aniva accretionary complex. This unit is composed of metabasites (derived from pillow lava, pillow breccia, hyaloclastite, reworked basaltic sedimentary rocks), chert, greywacke, and pelitic rocks (Kimura et al., 1992). The unit partly includes serpentinite melange on its northern and southern margins, and is rarely interbedded with high-grade amphibolitic rocks as small lenses, from meters to a few ten meters in thickness (Kimura et al., 1992; Sakakibara et al., 1992). In this unit, the deformation features in

outcrops were systematically analyzed and the successive history of deformation was established by Kimura et al.(1992).

The Horokanai unit crops out in a tectonic window of the Horokanai low-P/T metamorphosed ophiolite along the N-S axial part of an antiform plunging north in the Horokanai area (Shibakusa, 1974; Asahina and Komatsu, 1979). As mentioned above, the ophiolite directly overlies the Horokanai blueschist, but it has not suffered the Kamuikotan high-P/T metamorphism (Ishizuka, 1985). On the basis of geological, petrological and geochronological studies (Imaizumi, 1984; Ishizuka et al., 1983a; Shibakusa and Itaya, 1992; Ota et al., 1993), the Horokanai unit is inferred to tectonically overlie the Biei unit (Sakakibara and Ota, 1994). It seems that the boundary is identical with that between the zone I and the zone II by Ishizuka et al.(1983a) (Sakakibara and Ota, 1994). The Horokanai unit is composed mainly of basic schist (dolerite, pillow lava and hyaloclastite), pelitic schist, siliceous schist and calcareous schist (Shibakusa, 1974; 1991). The metamorphic grade within the unit successively increases upward (Shibakusa, 1989).

The Biei unit, and the Harushinai and Pankehoronai units described below are widespread in this study area around the Kamuikotan Gorge in the west of Asahikawa (Figs. 2-2 and 3-1). The relations among each unit are observed in the Kamuikotan Gorge area, so that the details will be described in the following section.

The Biei unit contains the Oichanunpe Formation by Maekawa (1986), and an eastern part of the Ino-gawa Greenstone Formation by Takayama (1988), which narrowly extends for approximately fifty kilometers with a north to south trend (Fig. 2-2). The unit consists mainly of basic rocks and small amounts of chert, limestone, and alternations of sandstone and mudstone (Maekawa, 1986; Kokubu et al.,

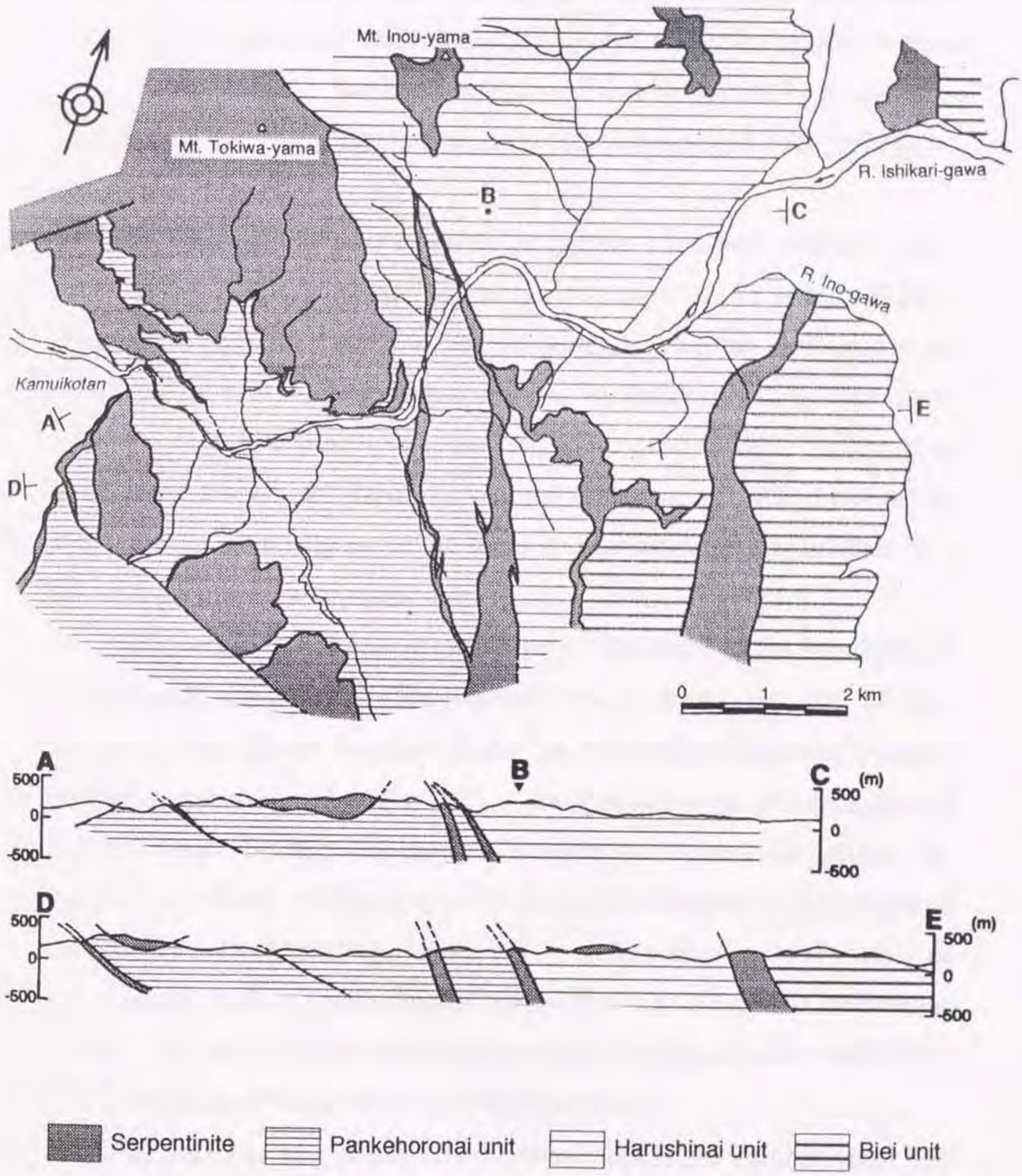

Fig. 3-1. Geologic sketch map showing the distribution of each unit and serpentinite melange in the Kamuikotan Gorge area.

1990). Along the eastern boundary of the unit, the Kamuikotan metamorphic rocks are unconformably overlain by the Pliocene welded tuff. The Biei unit has been interpreted as a fragment of a seamount province or oceanic plateau based on the petrological data (Maekawa, 1986).

The Harushinai unit consists of pelitic rock and contains some interbedded with psammitic, siliceous, and basic rocks (Ota, 1993MS; Sakakibara and Ota, 1994). This unit extends from the northeast of the Kamuikotan Gorge, Harushinai region, to the northward with about fifteen kilometers long and about ten kilometers wide. It has been termed the Harushinai Pelite Formation (Takayama, 1988), because the unit is occupied mostly by pelitic rocks and its constituent lithofacies does not vary so much as the other unit.

The Pankehoronai unit is extensively distributed in the southwest of the Kamuikotan Gorge. The western end is thrust over the Tertiary sediments and eastern boundary is cut by a northwest-southeast trending sheared serpentinite zone (Fig. 2-2). The Pankehoronai unit includes the western part of the Ino-gawa Greenstone Formation along the Kamuikotan Gorge by Takayama (1988) and the Pankehoronai Formation in the Biei area (Maekawa, 1986). The former is composed mainly of basic schist with a small amount of pelitic, siliceous, and calcareous schists. On the other hand, the latter consists largely of pelitic schist with a small amount of basic schist and siliceous schist.

The Shizunai unit is extensively distributed in the southernmost end of the Sorachi-Yezo belt (Fig. 2-2). It mainly consists of basic rocks with various lithofacies such as pillow lava, dolerite, hyaloclastite and volcanic sandstone, and varicolored shale. They are accompanied with minor chert, limestone, and alternations of sandstone and mudstone

(Nakano, 1981). The structures of original rocks are well preserved because of very weak deformation and recrystallization.

Various kinds of exotic high-grade metamorphic blocks appear in the serpentinite melange as follows; epidote amphibolites, garnet amphibolites, amphibolites, amphibolite schists, lawsonite-bearing blueschists, jadeite-quartz rocks, and high-P/T metamorphic rocks with various metamorphic grades (Ishibashi, 1939; Shido and Seki, 1959; Kato et al., 1979; Imaizumi and Kanehira, 1980; Ishizuka and Imaizumi, 1980; Maekawa, 1983; 1986; Imaizumi, 1984; Takayama, 1986; Nakagawa and Toda, 1987). These blocks commonly range from a half to fifty meters in diameter and are typically lenticular in form despite the difference in size. The blueschists locally occur as kilometer-order slabs in serpentinite melange. Although the direct contacts between the tectonic blocks and serpentinite matrix are rarely observed, some blocks have rinds of foliated serpentinite schist and actinolite nodules.

3-2. Geology around the Kamuikotan Gorge

Until recently, the geology around the Kamuikotan Gorge area has not been fully clarified. The abundant occurrence and irregular distribution of serpentinite in the area have also confused many workers. As a result, several different interpretations for the geology and metamorphism have been presented (e.g., Gouchi, 1983; Takayama, 1988). The author has investigated the area in detail with a main view of making clear the accurate distribution of serpentinite and the structural relation between serpentinite and coherent metamorphic sequence. Consequently, as shown in a geological map of Fig. 3-2, it became clear that some of serpentinite melange tectonically overlies the coherent sequences and the other serpentinites are the insertion along the boundaries among each unit or shear zones within the coherent units (Ota, 1993MS; Ota et al., 1993; Sakakibara and Ota, 1994). An example of the relation between the serpentinite melange and the coherent unit is presented in Fig. 3-3. As shown in the route map, the coherent sequence exposed in the geographically lower level, consisting of pelitic rocks and psammitic rocks, has NNW strike and steep or vertical dip, whereas serpentinite and associated basic rocks exposed in the geographically upper level overlie in the southern part of coherent sequence. Such a distribution of serpentinite indicates that the serpentinite melange tectonically overlies the coherent metamorphic sequence, bounded with a low-angle fault. In the investigated area, the similar structural relation is observed in some parts. The division of geological units in the Kamuikotan complex (e.g., Ota et al., 1993; Sakakibara and Ota, 1994) is fundamentally based on such many lines of geological evidence.

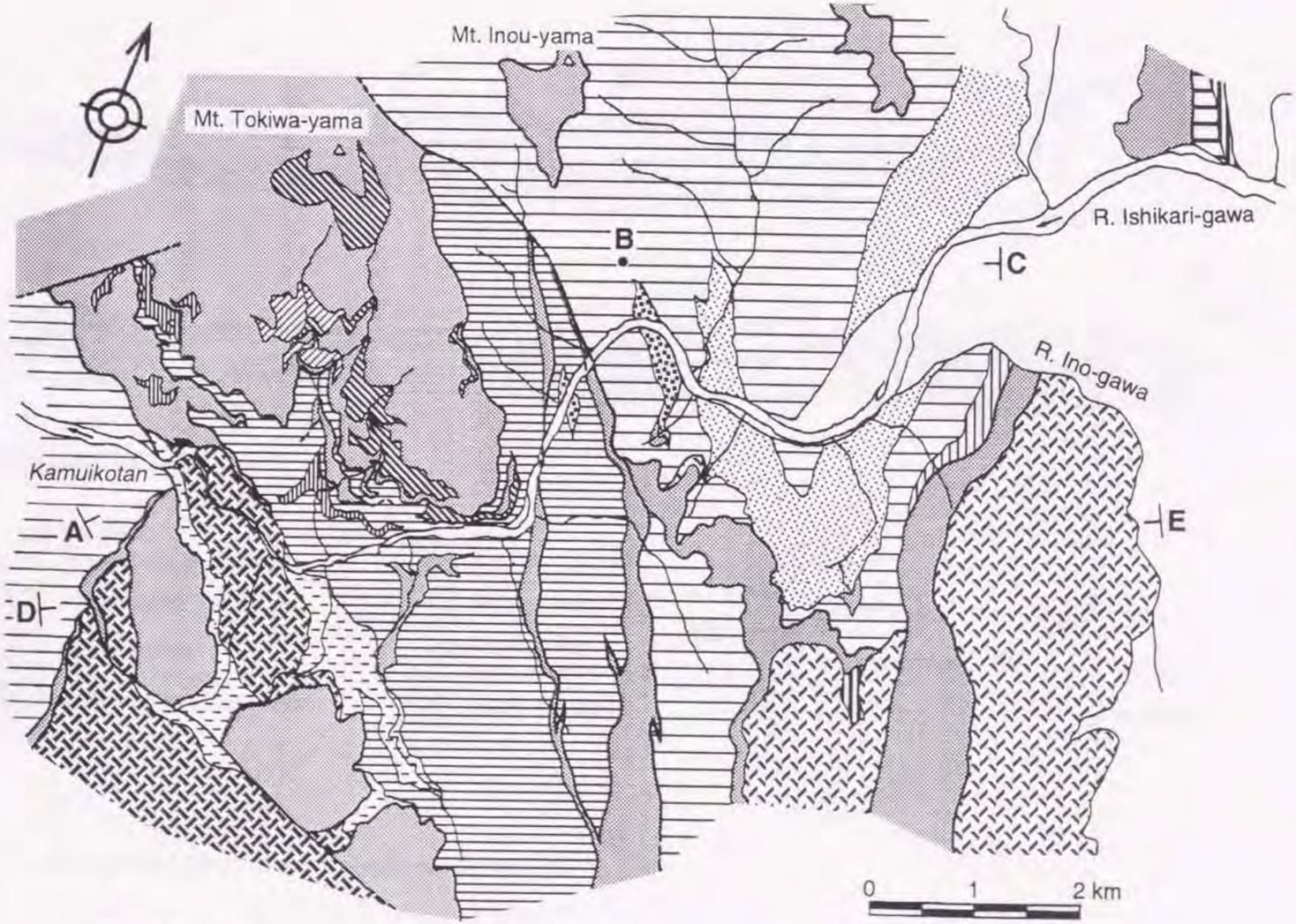

Fig. 3-2. a. Geologic map of the Biei, Harushinai and Pankehoronai units, and serpentinite melange in the Kamuikotan Gorge area.

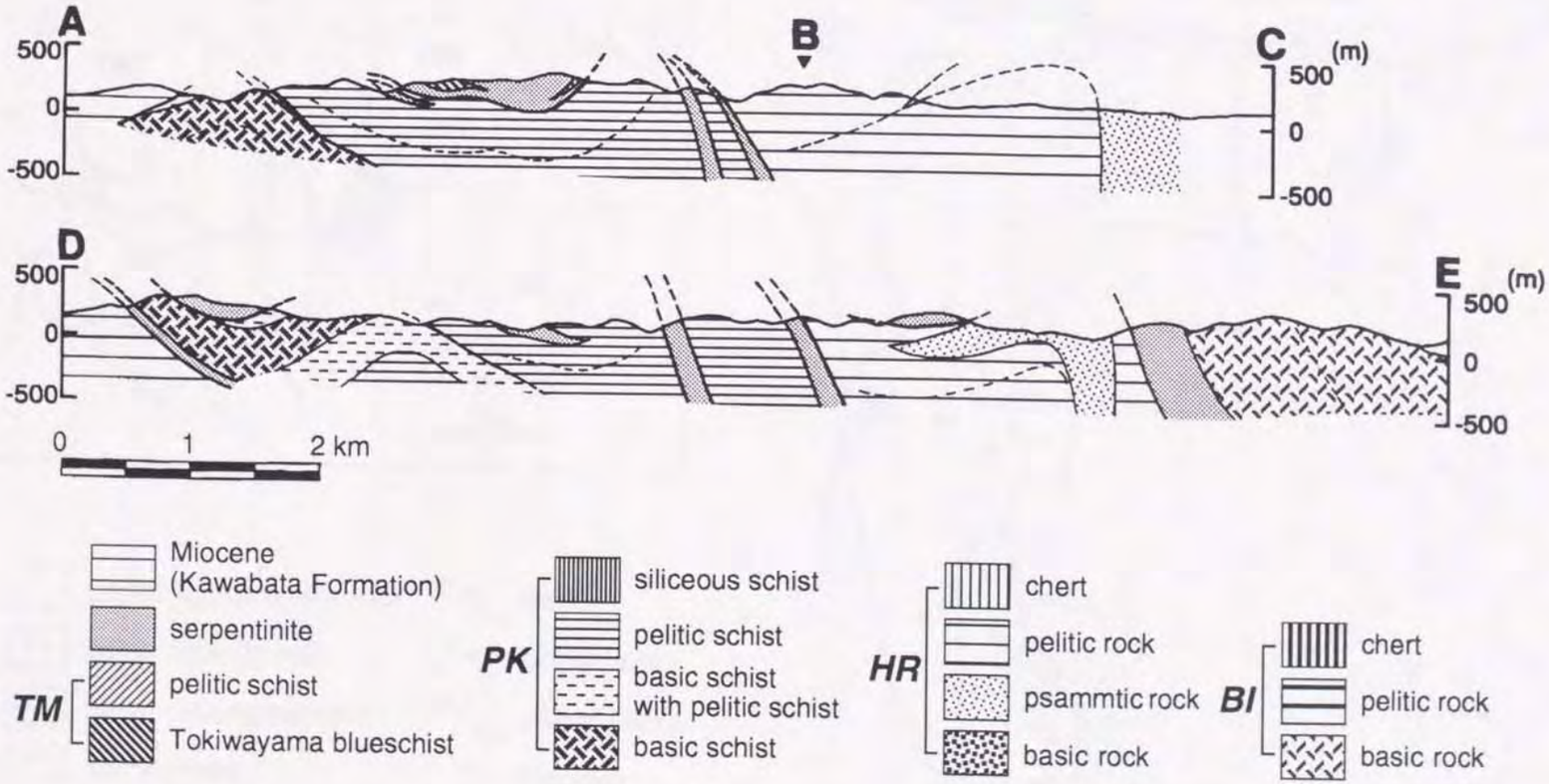

Fig. 3-2. b. Cross sections of the Kamuikotan Gorge area.

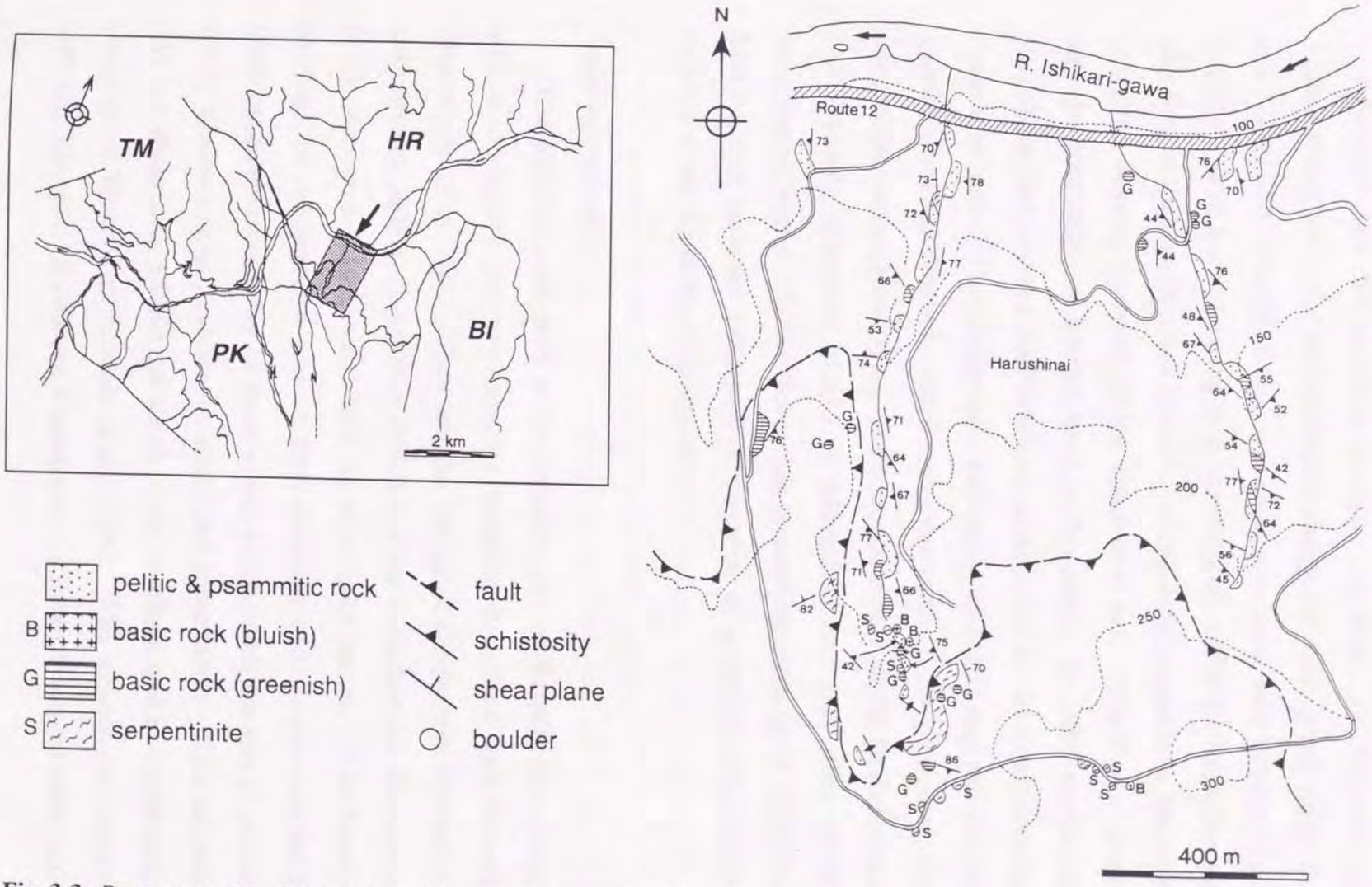

Fig. 3-3. Route map of the Harushinai unit showing an example of the relation between the serpentinite melange and the coherent unit.

Around the Kamuikotan Gorge, the Biei, Harushinai and Pankehoronai units, and serpentinite melange are widespread (Figs. 3-1 and 3-2). The Harushinai and Biei units are juxtaposed bounded by a low-angle fault accompanying with serpentinite, while the Pankehoronai unit lies in high-angle fault contact with sheared serpentinite insertion along the western boundary of the Harushinai unit. The Pankehoronai unit is structurally the lowest level in this area. In other words, the Harushinai unit overlies the Pankehoronai unit, and the Biei unit does the Harushinai unit. The serpentinite melanges regionally and tectonically overlie the Pankehoronai and Harushinai units. In particular, the serpentinite melange overlying on the northern part of the Pankehoronai unit includes abundant blocks of blueschist and the other exotic metamorphic rocks. In this thesis, this serpentinite melange is called the Tokiwayama melange unit, and is regarded as a typical serpentinite melange in the Kamuikotan Gorge area.

Pankehoronai unit

The Pankehoronai unit in the western part of Kamuikotan Gorge area is subdivided into two subunits, bounded by a fault with sheared serpentinite (Fig. 3-2). They are the Ino-gawa Greenstone Formation (the western part) by Takayama (1988) and the Pankehoronai Formation in the Biei area (Maekawa, 1986), as mentioned above. The former outcrops in the western part of Pankehoronai unit (lower structural level), and consists mostly of basic schist with a small amount of pelitic schist, siliceous schist, calcareous schist and serpentinite. This subunit dies out about four kilometers south of the southern end of study area, Oroen-gawa River (e.g., Iwasaki et al., 1994). The western end thrusts over the Miocene (Kawabata Formation). Sheared serpentinites and

serpentine schists, ranging in thickness from a few to about a hundred meters, are intercalated between the pelitic schist and the Miocene. The slickenside on the surface of serpentine schist, i.e., slickenside on the thrust plane, observed at the lower reaches of the Oroen-gawa River, strikes N30°E and dips 25°N (Ota, 1993MS). It indicates the direction of movemant that the Kamuikotan metamorphic rocks had thrust upon the Miocene. The metamorphic rocks are strongly recrystallized and have various deformation structures. The protoliths of basic schist are mainly hyaloclastite, basic tuff, hyaloclastic breccia, and minor massive basalt and pillow lava. The basic schist predominates in the upper structural level within this subunit, while a small amount of the other schists interbedded with finer-grained basic schist occurs in the lower level. The serpentinites overlie the part dominated by basic schist, and some of them are interbedded with the basic schist or pelitic schist as layers and lenses of a few meters in thickness. It has been deformed together with neighboring schists, resulting in sheared, foliated and folded.

The other subunit, which extends to the Pankehoronai Formation (Maekawa, 1986), is situated the eastern part (the upper structural level) of Pankehoronai unit. It is occupied by pelitic schist intercalated with siliceous schist, psammitic schist, basic schist and serpentinite as layers and lenses ranging in thickness from several to a few hundred meters. The siliceous schist is also included within serpentinite body between the two subunits of the Pankehoronai unit. An amount of psammitic domain intercalated with the pelitic schist tends to increase toward the northeast of this subunit, where psammitic layers of several centimeters in thickness and pelitic layers of about a centimeter are often interbedded. The basic schists are of hyaloclastite, basic tuff, massive basalt, and their reworked sediment origin. The schist commonly occurs as small lenticular

domains and scarcely continues as a bed in contrast with that of the above subunit. The serpentinite is widespread in the eastern part of the subunit. Insertions and lenticular domains of serpentinite, which trends northwest to southeast and steeply dips northeast, are often observed nearby the boundary between the Pankehoronai and Harushinai units. The Tokiwayama melange unit overlies in low-angle fault contact with this subunit in the northwestern part. Hereafter these two subunits are dealt with together, unless necessary to specify.

Harushinai unit

The unit is occupied mainly by pelitic rock and contains small amounts of psammitic rock, basic rock, chert, intermediate to acidic tuffs and serpentinite. Although variations of constituent lithofacies are minor as mentioned above, a minute geologic mapping in the Kamuikotan Gorge area indicates that beds and layers of the minor constitutions (e.g., psammitic rock, chert, tuff and serpentinite) are a notable key bed. In particular, the distribution of psammitic rock shows that the Harushinai unit forms a NNE-SSW trending asymmetric fold, slightly overturned eastward, while the east flank is cut by a north-south normal fault (Fig. 3-2). In the southern part of the study area, the Harushinai unit is completely covered by the Biei unit with sheared serpentinite, resulting in the disappearance on the map. The basic rock is intercalated by the pelitic rocks and usually appears as lenticular domains several meters wide. Rarely, it is accompanied with sheared serpentinite. The protoliths of basic rock are massive basalt, pillow breccia and hyaloclastite. The chert occurs as a lenticular domain in the eastern margin of the unit, and often as thin layers alternated with pelitic rocks. The intermediate to acidic tuffs are commonly interbedded with the

psammitic rocks and often form well successive layers. The serpentinite appears as layers or lenses intercalated with pelitic rocks and psammitic rocks. It sometimes overlies isolated on the geographically higher level, e.g., around the top of Inou-yama Mountain. This serpentinite body (melange) contains blocks of blueschist, pelitic schist and amphibolite as well as the Tokiwayama melange unit. Sheets of serpentinites, which load with basic rocks of the Biei unit, also bring boulders of minor blueschist to the Harushinai unit. Such blueschists and the other metamorphic rocks are similar to blocks of the Tokiwayama melange unit, but their amounts and sizes are less than those of the Tokiwayama melange unit. It is easy to distinguish the blueschist blocks from coherent basic rocks belonging to the Harushinai unit (or the Biei unit), because the blocks are exotic boulders and have a characteristic metamorphic mineral assemblage different from the that of coherent rocks, as described below.

Biei unit

The Biei unit is situated the most eastern part of Kamuikotan Gorge area (Fig. 3-2). Along the eastern boundary of this unit, the metamorphic rocks are unconformably overlain by the Pliocene welded tuff. The unit is in a high-angle fault with massive serpentinite body contact with the Harushinai unit, and overlies the Harushinai unit bordering by a low-angle fault with sheared serpentinite. The Biei unit is composed mostly of basic rocks, and minor amounts of chert and pelitic rock. The protoliths of basic rock are hyaloclastite, hyaloclastic breccia, massive basalt, pillow lava, dolerite, volcanic shale, and maybe their reworked sediments. The massive protoliths predominate in the northeastern part. The basic rocks in the southeastern part of the Biei

unit and those with serpentinite on the Harushinai unit are mainly of finer-grained origins, and relatively foliated. This unit is abundant in amounts of breccia and massive rock compared with the other unit. Most of basic rocks in the Biei unit, except ones of a finer-grained or reworked origin, do not show a visible schistosity. This is in part due to the trait of protolith, which influences the deformation and recrystallization, and in part due to the difference of metamorphic condition. The distribution of chert in mappable order is locally and the chert of lenticular domain usually underlies the basic rocks. In the northeastern part, pelitic rocks and volcanic shale occur together with a minor amount of chert. Serpentinites consisting of a trending north-south body between the Biei and Harushinai unit are mostly massive and often preserve original textures of peridotite, without ones along the boundaries among the two units and the internal shear zone of the body. In the study area, such serpentinite has found nowhere except for the above body. Sheets of serpentinites with basic rocks belonging to the Biei unit, which overlie the Harushinai unit, contain a small amount of blueschist and the other metamorphic rocks as mentioned above. The sheets are cut by high-angle faults with serpentinite bordering among the Biei, Harushinai and Pankehoronai units.

Tokiwayama melange unit

A typical serpentinite melange around the Kamuikotan Gorge, the Tokiwayama melange unit, overlies the eastern subunit of the Pankehoronai unit, and is in a low-angle fault contact with the subunit. The eastern end of the melange unit is cut by the fault with sheared serpentinite bordering the Pankehoronai and Harushinai units (Fig. 3-2). The melange unit includes large amounts of blueschist, pelitic schist,

siliceous schist and minor amphibolite, amphibole schist, calcareous schist, and green rocks. The slab of blueschist is exposed in a maximum area of about a half square kilometer, particularly called the Tokiwayama blueschist by Sakakibara and Ota (1994). The lenticular blocks of pelitic schist, siliceous schist and calcareous schist are also found, but their amounts and sizes are less than those of the blueschist. Amphibolite, amphibole schist and green rocks scatter as a small block in the melange unit. The blueschist is of massive basalt, hyaloclastite and basaltic tuff origin, while the protoliths of green stones are pillow lava, dolerite, gabbro, trachite and microdiorite. Serpentinites of melange matrix are sheared and form aggregate of flakes in various sizes. The contact relations between serpentinite matrix and the above blocks of metamorphic rocks are occasionally observed, e.g., around blueschist in the eastern margin of the Tokiwayama melange unit. In the boundary, serpentinites are considerably foliated to be serpentine schists of white or pale green in color, and some blocks have rinds of serpentine schists.

3-3. Deformation structure around the Kamuikotan Gorge

Major structure

The stereographic projections of structural elements from the Kamuikotan Gorge area are summarized in Figs. 3-4 and 3-5. Although the schistosity (S2- and S3-foliation described below) generally trends northwest-southeast and dips steeply northeast or southwest, it considerably changes due to some folds of mappable-order throughout the area. In this area, the schistosity is not always parallel to the lithologic boundary because the regional schistosity is mostly deformation structures such as shear planes and/or fold axial cleavages. Angles crossing each planer structure vary by differences of lithofacies and regions. The details are mentioned below.

Although the structure of the central part in the Pankehoronai unit (CPK) is particularly discordant, the change in the whole unit suggests the presence of a northwest-southeast trending fold (Fig. 3-5a). In the western margin (SWPK), a northwest-southeast trending and moderately to steeply eastward dipping schistosity predominates (Fig. 3-5a), the metamorphic rocks thrust over the Miocene system, bordering serpentinites as mentioned above. The foliation of metamorphic rocks in the eastern part of this unit (CSZ) trend northwest-southeast, and dip vertically and steeply westward or eastward. The boundary between the Pankehoronai and Harushinai units with sheared serpentinite zone is parallel to the regional foliation (Figs. 3-2 and 3-5a). The Harushinai unit forms a north-south trending asymmetric fold and the east flank is cut by a north-south normal fault (Fig. 3-2). The gradual change of predominating foliation, from a northwest-southeast trending and westward dipping in the northwestern part (NWHR) to a NNE-SSW

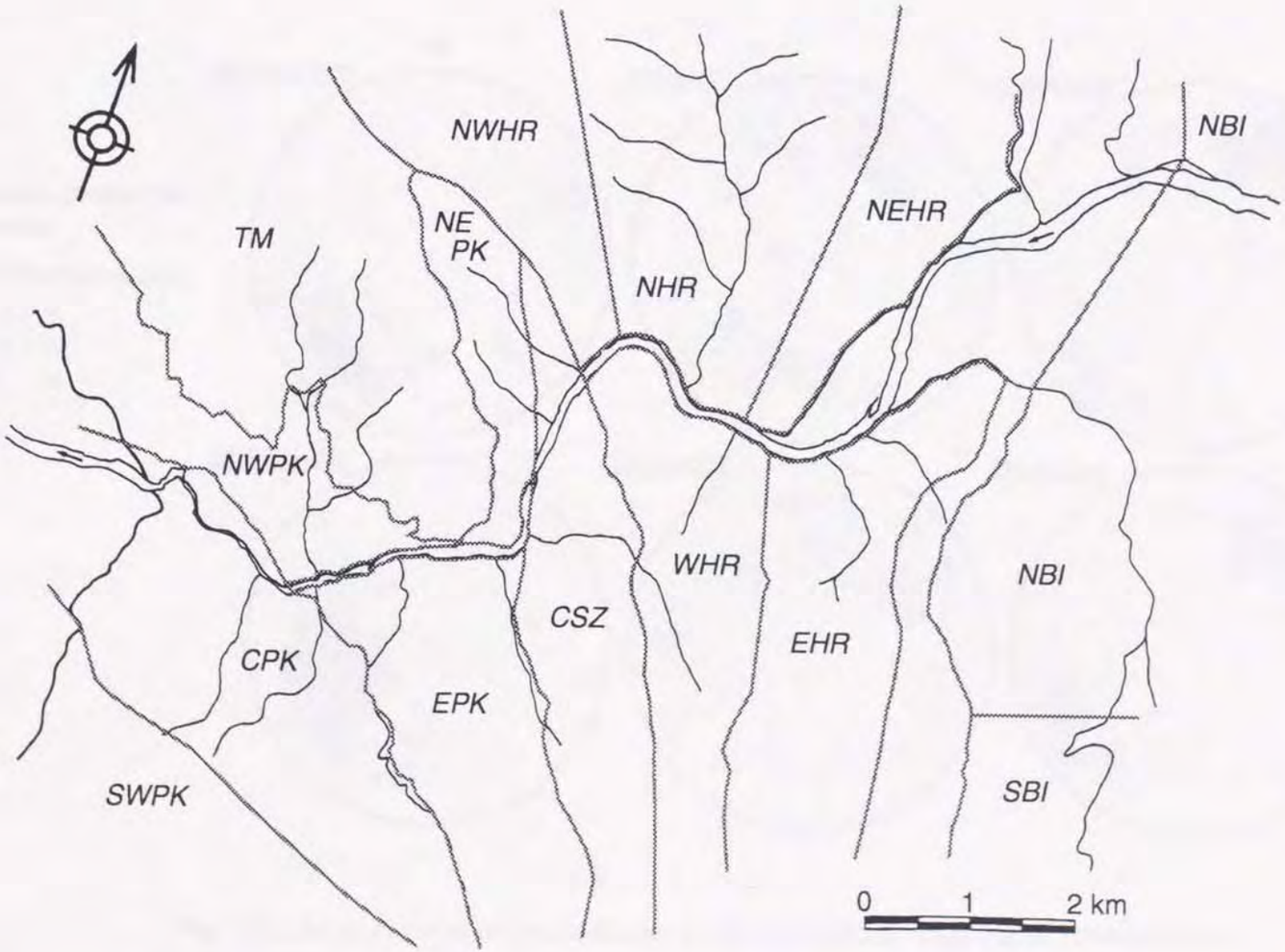

Fig. 3-4. Grid map of the Kamuikotan Gorge area divided by tectonic elements.

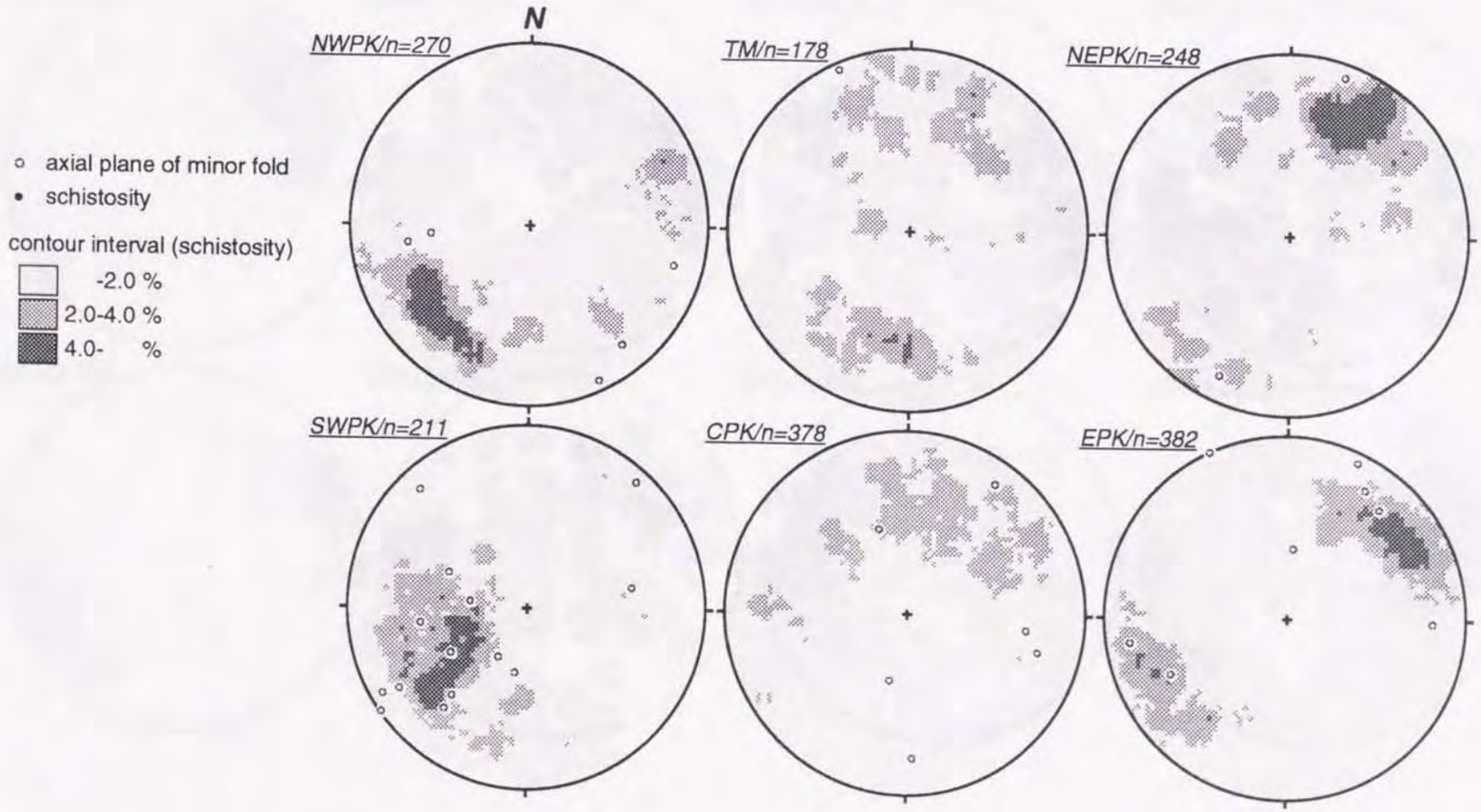

Fig. 3-5. Axial plane of minor fold(open circle) and contour diagrams of predominating foliation (S2- and S3-foliation) plotted on an equal area net (lower hemisphere). **a**. western part of the area (Pankehoronai and serpentinite melange units).

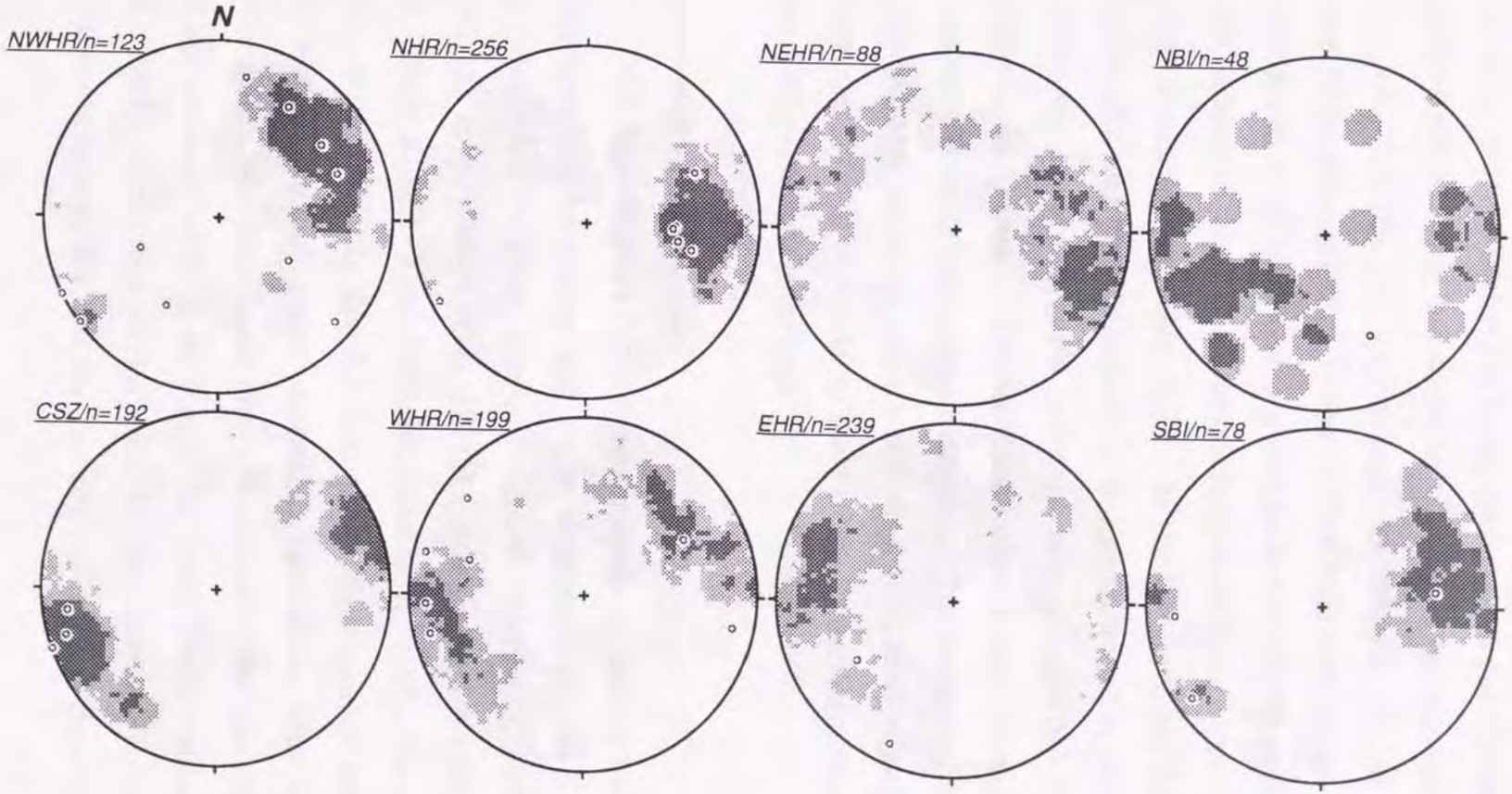

Fig. 3-5. b. eastern part of the area (Harushinai and Biei units).

trending and WNW dipping in the northeastern part (NEHR), through a north-south trending and westward dipping in the northern part (NHR), suggests that the fold axis plunges southward and the fold slightly overturns eastward (Fig. 3-5b). The foliations in the western part (WHR), trending northwest to southeast and steeply or vertically dipping, are parallel to those of the serpentinite zone between the Pankehoronai and Harushinai units (Fig. 3-5). In the Biei unit, the foliation trends NNW-SSE and dips moderately to steeply westward in the northern part (NBI) and steeply eastward in the southern part (SBI). Such a change suggests the presence of asymmetric fold with axial plane of northwest-southeast trending and eastward dipping. The metamorphic rocks in the Tokiwayama melange unit do not show a marked tendency but their foliations seem to be similar to those of the Pankehoronai unit overlain by the Tokiwayama melange unit.

Meso- and microstructure

The Kamuikotan coherent metamorphic rocks have been regionally undergone deformation and some deformation phases have been discriminated by many previous workers (Mizuochi, 1982; 1983MS; Ishizuka et al., 1989; Omata, 1991MS; Motoyama, 1991MS; Uemura, et al., 1991; Kimura et al., 1992; Komatsu et al., 1992; Ofuka, 1994MS). The deformation is divided into major four phases related to the following tectonic events: accretion, subduction with underplating, exhumation, and disturbance after exhumation. The last event, ascribed to the westward shift of the Kurile Arc since Tertiary time (Kimura et al., 1983), forms boundaries with sheared serpentinite between the metamorphic complex and the Tertiary system, and those among some

units within the metamorphic complex, e.g., the Pankehoronai, Harushinai and Biei units in the Kamuikotan Gorge area (Fig. 3-2).

The metamorphic rocks in the Kamuikotan Gorge area have suffered from ubiquitous ductile deformation except for the massive basic rocks of the Biei unit. The major four phases of deformation are discriminated in the field and under the microscope (Fig. 3-6). The characteristic deformation structures of each phase are schistosity (D1), shear plane (D2), axial cleavage (D3), open fold and shear zone (D4). Such a deformation history is the similar to that of Motoyama(1991MS) and Uemura et al.(1991). These phases are briefly described below. In the descriptions below, Asymmetric aspects of minor and micro structures are observed from a direction looking down a plane perpendicular to a foliation and a lineation formed during individual stages.

D1 stage is characterized by the formation of S1-foliation and F1-fold. The S1-foliation of originally sedimentary rocks is usually parallel to the bedding plane (S0-foliation). Although most of basaltic rocks do not show an apparent S1-foliation, an alignment and elongation of flatly deformed breccia define the foliation in some clastic rocks. Pinch and swell structures, and boudins are formed during the D1 stage (Fig. 3-7a). The F1 folds are intrafolial and ptygmatic folds, and their axial planes correspond to the S1-foliation (Fig. 3-7a). Under the microscope, detrital grains and carbonaceous materials lie on the S1-foliation of pelitic and psammitic rocks, and fractures perpendicular to the foliation and pull-apart structures parallel to the foliation of primary clinopyroxenes are often observed (Fig. 3-7b). The formation of such deformation structures suggests that the deformation feature of this stage seems to be a simple shortening.

Deformation	D0 (S0)	D1 (F1, S1)	D2 (F2, S2=Si, L2)	D3 (F3, S3=Sm, L3)	D4 (F4)
Deformation structure	bedding	schistosity intrafolial fold ptygmatic fold boudin fracture	asymmetric close fold crenulation fold kink fold S-C-C' structure	asymmetric close fold crenulation fold axial cleavage	upright open fold kink band minor fault
Type of strain	(?)		 (top to NE)	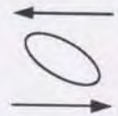 (top to SW)	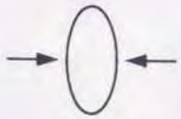
Metamorphic Facies		(Pmp-Act Facies)	**[initial stage]** Blueschist Facies *- max pressure -*	**[main stage]** Pmp-Act Facies *- max temperature -*	
Tectonics	subduction			exhumation	
	accretion (formation of melange)		underplating	formation of nappe	

Fig. 3-6. Summarized deformation structures and metamorphism related to the tectonic events of the Kamuikotan coherent metamorphic rocks.

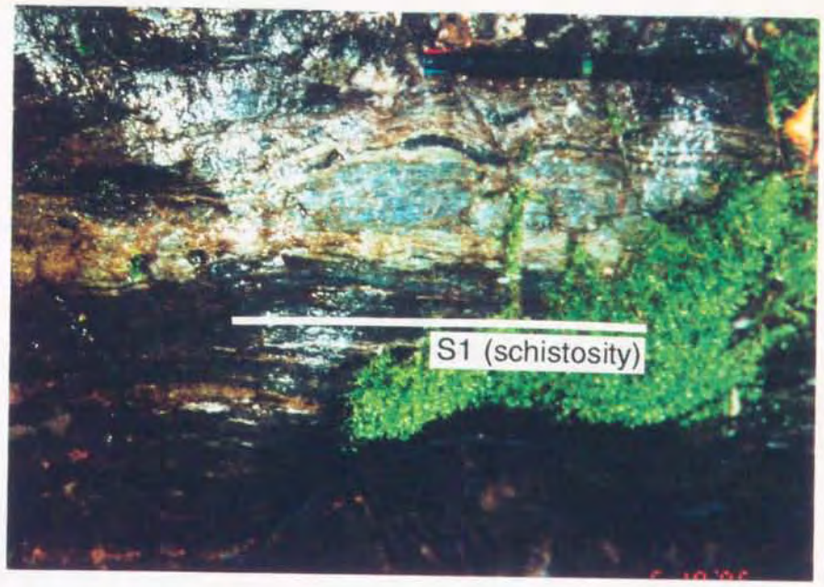

Fig. 3-7a. Representative deformation structures of the D1 stage. **above**: pinch and swell structure of tuff layer (pale blue and green in color) interbedded by pelitic schist of the Harushinai unit. **below**: ptygmatic fold of quartz-albite vein (white in color) in basic schist of the Pankehoronai unit.

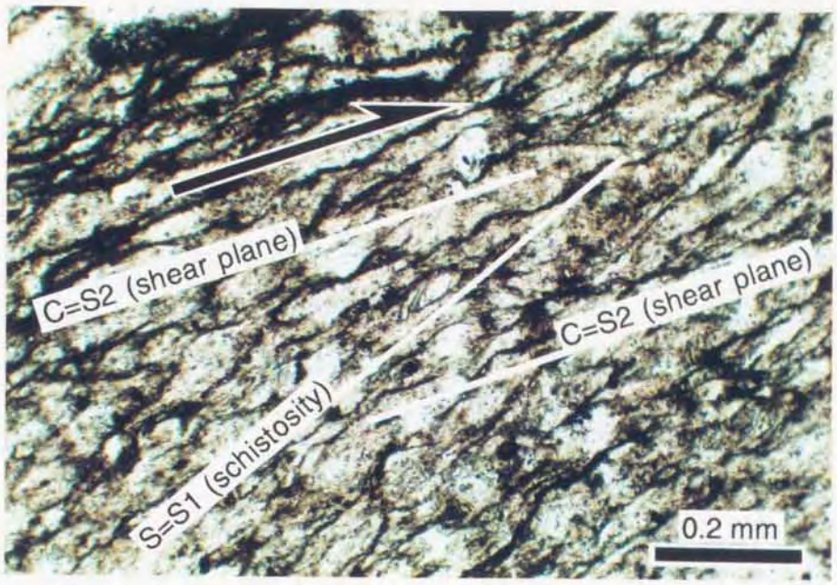

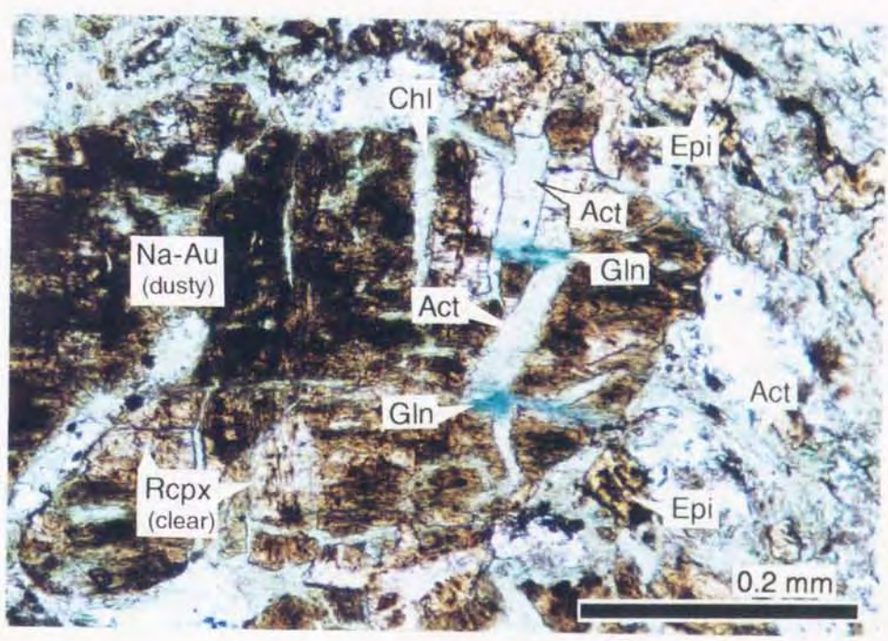

Fig. 3-7b. Relations between deformation structures of the D1 and D2 stages, and their constituent minerals (plane polarized light). **above**: D2 stage, S-C structure showing the dextral shear sense in pelitic rock of the Harushinai unit. The S1 and S2 foliations correspond to the S and C surfacies, respectively. The detrital grain remains on the S1 foliation. **below**: D1 stage, Fractures of the relic clinopyroxene in basic rock of the Pankehoronai unit. Fine-grained glaucophanes are elongating with perpendicular to the fractures.

D2 stage is characterized by the formation of S2-foliation, F2-fold and L2-lineation. The S2-foliations are shear planes and correspond to C-surface or C'-surface in mylonite of Lister and Snoke (1984) (Figs. 3-7b, 3-8a). The shear planes define a visible schistosity of massive basic rocks in the field and under the microscope. They obliquely cross the S1-foliation, corresponding to S-surface, with forty to sixty degrees. The detritus in the sedimentary rocks and the breccia in the basaltic clastics have deformed in this stage, resulting in asymmetric lenses with pressure shadows (Figs. 3-7b, 3-8a). The F2-folds are asymmetric close fold (Fig. 3-8b), kink fold (reverse, and angular or rounded type: Uemura and Long, 1987) and minor crenulation fold. Their fold axes and the intersection lines between the S1- and S2-foliations correspond to the L2-lineations. The asymmetric fold, the S-C-C' structure and accosiated structures (Figs. 3-7b, 3-8) commonly indicate dextral shear sense (top to NE), but the opposite sense is also found. Minor folds observed in the field are mostly the F2-folds. The S1- and S2-foliations of the sedimentary rocks, and S2-foliations of the massive basaltic rocks are a regional schistosity, but are commonly folded or cut by the deformation of next D3 stage (Figs. 3-9b, 3-9c), regarded as an initial schistosity (Si-schistosity). In addition, the D2 stage is called an initial stage from the view point of metamorphism, as mentioned the latter chapters.

D3 stage, the major deformation stage in the area, is characterized by the formation of S3-foliation, F3-fold and L3-lineation. The S3-foliations are axial cleavages, parallel to axial plane of the F3-fold such as asymmetric close to tight fold, associated with crenulation fold on the folded plane, and symmetric open to close fold (Fig. 3-9). The crenulation folds observed in the field are mainly formed during this

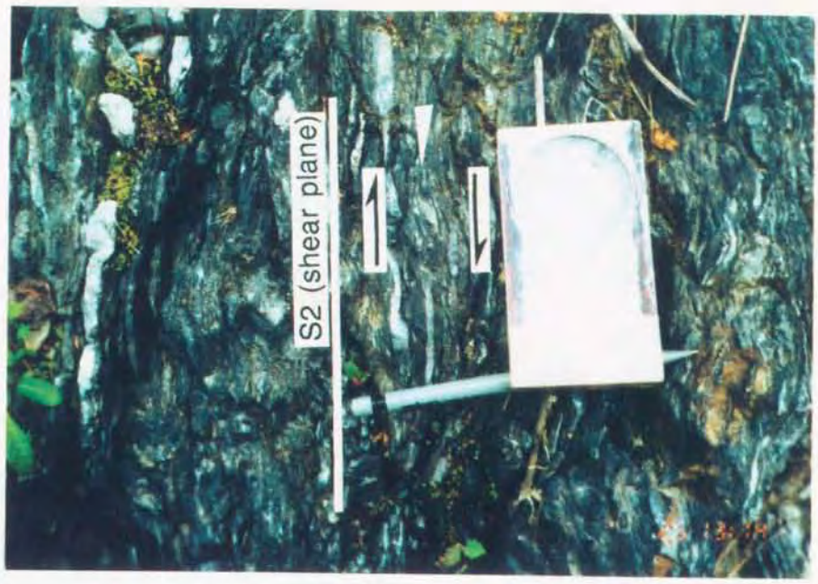

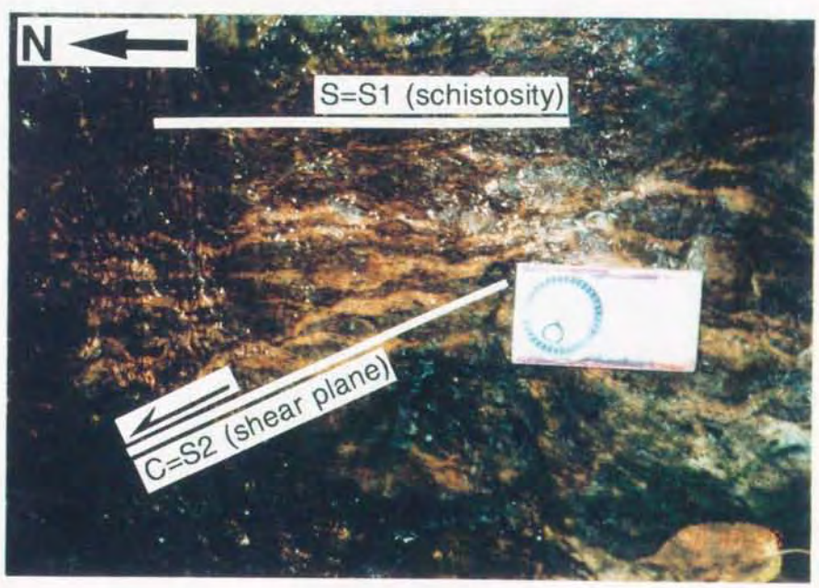

Fig. 3-8a. Representative deformation structures of the D2 stage. **above**: pebble of tuff asymmetrically deformed (white arrow) in pelitic schist of the Harushinai unit (dextral shear sense). **below**: S-C structure in basic schist of the Pankehoronai unit (top to the north).

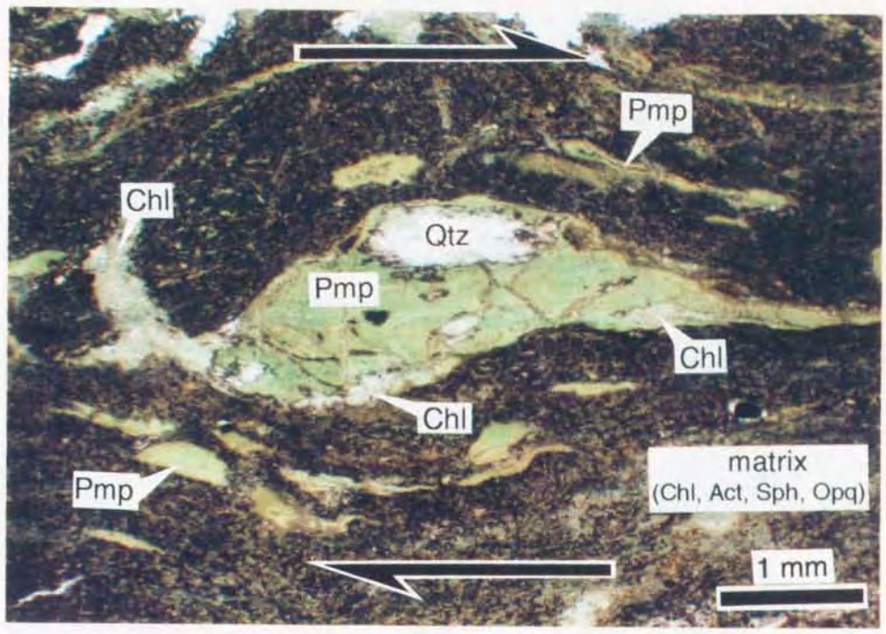

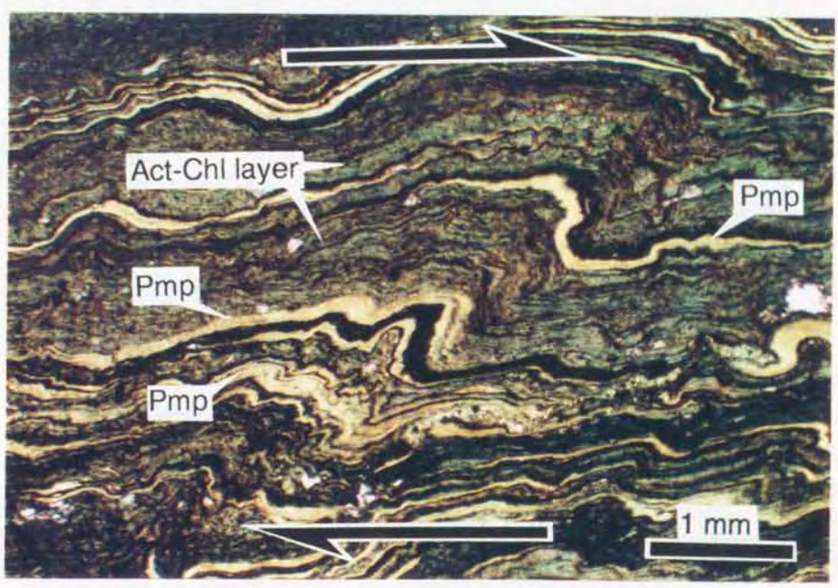

Fig. 3-8b. Relations between deformation structures of the D2 stage, and their constituent minerals (plane polarized light). **above**: Pumpellyite aggregates, which are asymmetrically deformed by the dextral shear, in basic rock of the Pankehoronai unit. **below**: Asymmetric micro fold formed by the dextral shear deformation in basic rock of the Pankehoronai unit. The S1 foliation, which is composed of pumpellyite, actinolite and chlorite, is folded.

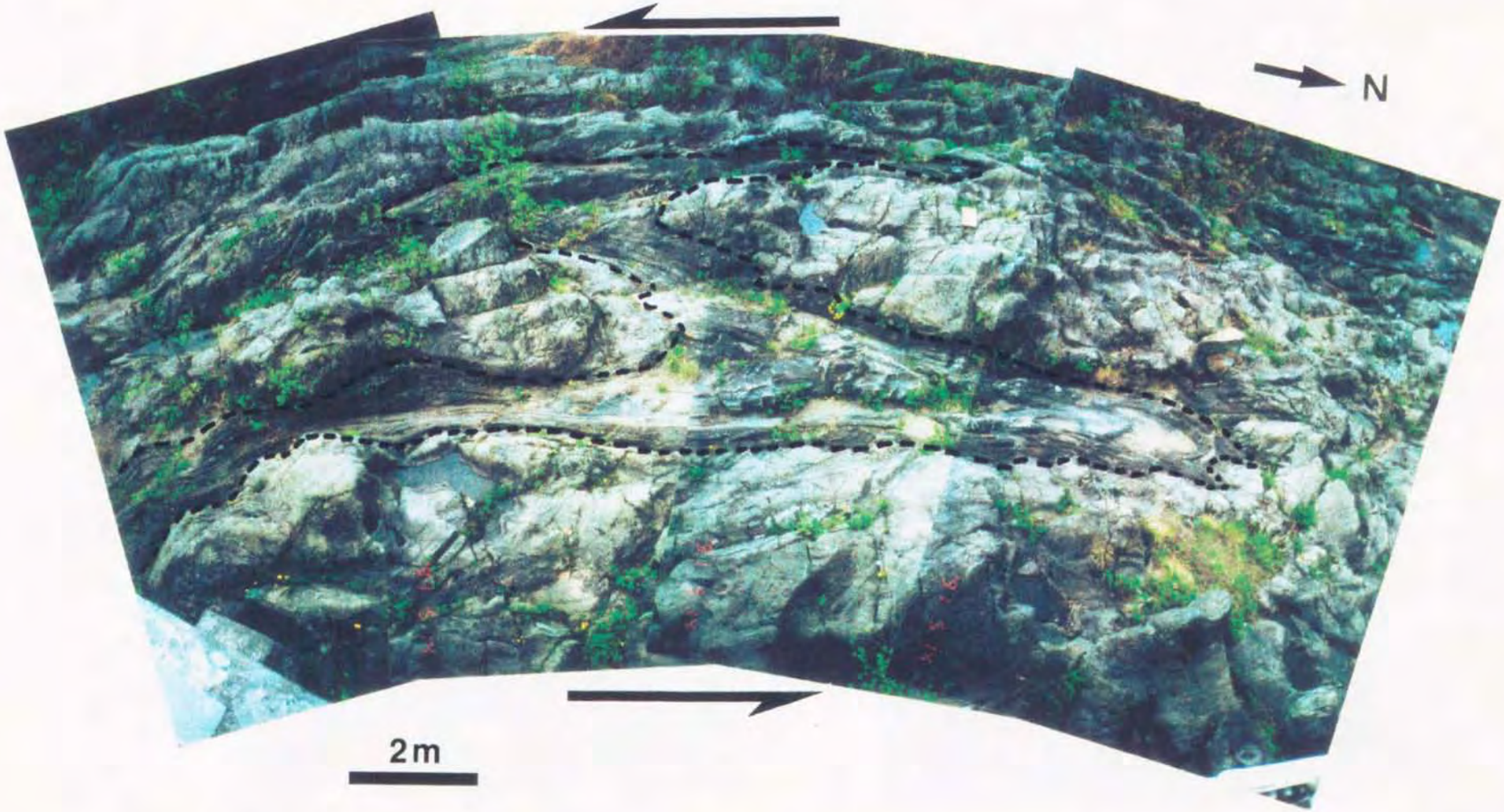

Fig. 3-9a. Asymmetric close fold (F3-fold) with sinistral shear sense of calcareous schist in the Pankehoronai unit (under the Kamuikotan suspension bridge). Dotted lines trace the folded calcareous schist.

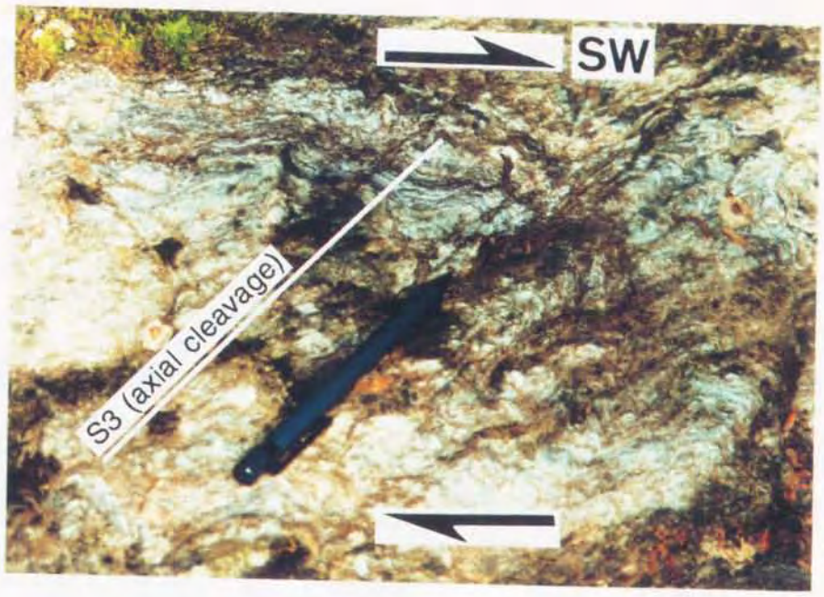

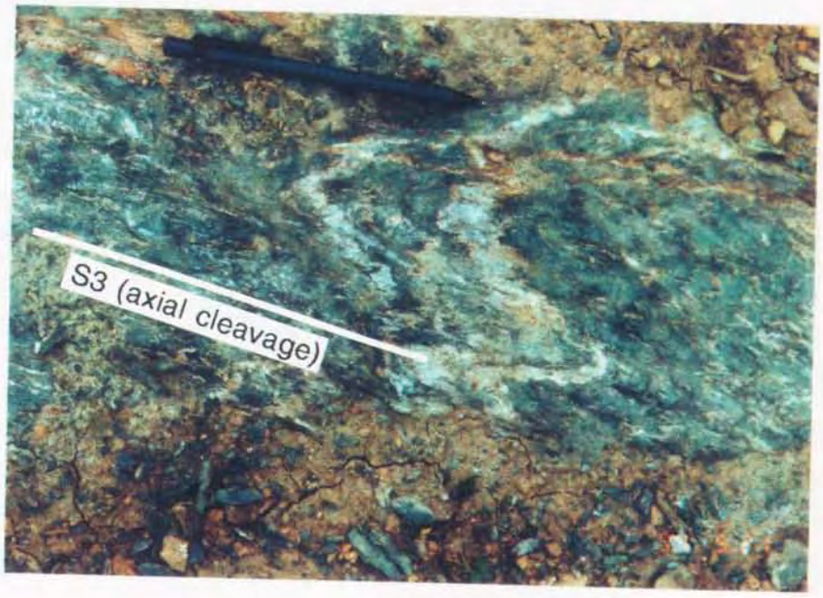

Fig. 3-9b. Representative deformation structures of the D3 stage. **above**: asymmetric fold with axial cleavage of pelitic schist in the Pankehoronai unit (top to the southwest). **below**: symmetric fold with axial cleavage of basic schist in the Pankehoronai unit.

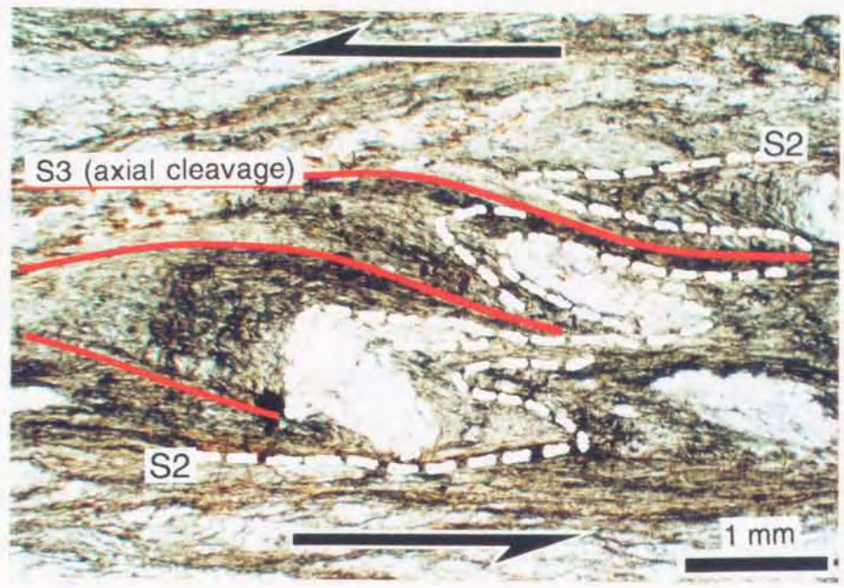

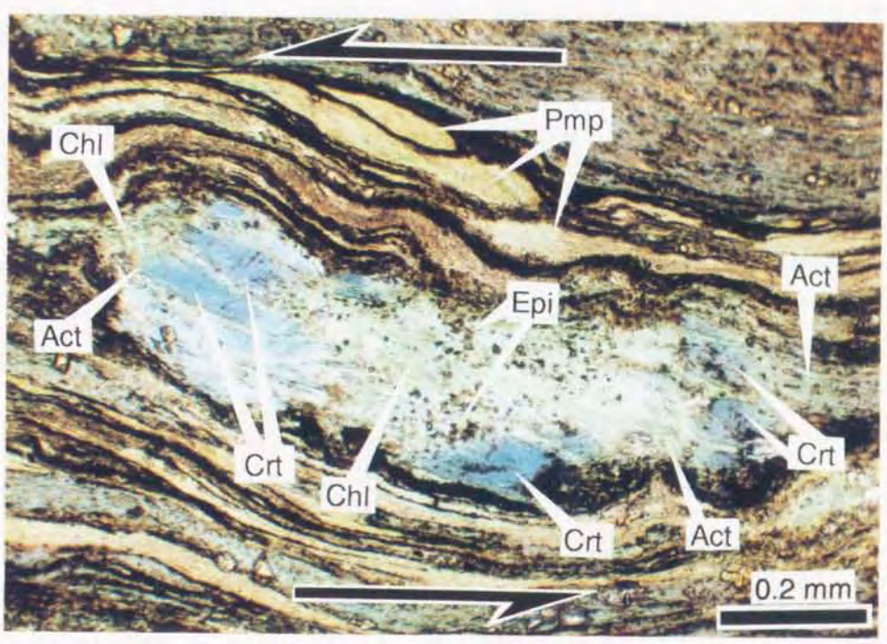

Fig. 3-9c. Relations between deformation structures of the D3 stage, and their constituent minerals (plane polarized light). **above**: Asymmetric micro fold with axial cleavage formed by the sinistral shear deformation in pelitic rock of the Pankehoronai unit. The S2 foliation folded is cut by the S3 foliation as axial cleavage. **below**: Porphyroblast of sodic amphibole (crossite), asymmetrically deformed by the sinistral shear, in basic rock of the Pankehoronai unit. Actinolites occur as surrounding sodic amphiboles and as the pressure shadow around the porphyroblast.

stage. The L3-lineations are defined by F3-fold axes and intersection lines between the S2-foliation and the F3-fold axial plane. Rarely, stretching lineations parallel to the L3-lineations, defining by elongations of pumpellyite aggregates in the finer-grained basaltic sediments, are observed in the field. The deformation structures during this stage are usually observed in the sedimentary rocks and finer-grained basaltic clastics, while shear planes and asymmetric pressure shadows are formed in the massive basaltic rocks as a whole area. As shown in Fig. 3-9, the asymmetric aspects of the F3-folds predominate the sinistral shear sense (top to S or SW). The F2-folds folded by the F3-fold are rarely observed, the L3-lineations intersect the L2-lineation with thirty to fifty degrees. The structure of the study area is mainly controlled by the deformation structures during this stage, and the S3-foliations are regarded as a main schistosity (Sm-schistosity). Then, the D3 stage is named a main stage from the view point of metamorphism, against the D2 stage as an initial stage. In the Pankehoronai unit, because the S3-foliations are subparallel to the S1- and S2-foliation folded by the close to tight F3-folds, it is difficult to discriminate the S3-foliations from the S1- and S2-foliations in many places. The F2-fold axial planes are also bent by the F3-folds to become subparallel to the S3-foliation. In the Harushinai unit, however, the development of the S3-foliation is less common than the Pankehoronai unit, and the close to tight F3-folds are also minor. Then, the S1- and S2-foliation refolded by the symmetric or asymmetric open to close F3-fold are easily discriminated from the S3-foliations as axial cleavages. The mappable ordered fold structures are formed during this stage, however, the trends of them are different from each unit as mentioned above. The change of S2-foliations and F2-fold axes in places with moderately dipping S2-foliations, and the trends of

F3-fold axes in places with steeply or vertically dipping S2-foliations imply that the trends of the major fold axes in the Pankehoronai, Harushinai and Biei units are northwest to southeast, north to south and north-northwest to south-southeast, respectively (Figs. 3-5 and 3-10).

D4 stage is characterized by the formation of F4-fold. It is gentle or open fold having upright axial plane and no visible axial cleavage. The fold axis trends mostly east-northeast to west-southwest and plunges gently westward. The deformation structures during D1, D2 and D3 stages are refolded by the F4-fold. In some places with a moderately dipping schistosity (e.g., CPK and NHR in Fig. 3-7), the effect is especially apparent. Kink bands (conjugate and angular type), tension gashes and minor faults are occasionally found, suggesting more brittle conditions during the D4 stage deformation than during the D2 and D3 stages.

After the D4 stage, the north-south to northwest-southeast trending and vertically or steeply eastward dipping faults with the insertion of serpentinite are formed, resulting that all deformation structures before the D4 stage are cut by the faults. They border each unit within the Kamuikotan complex, and the serpentinite melange overlying the coherent unit is also cut by the faults. In addition, they border the Kamuikotan complex and the Miocene system.

Summarized deformation structures and history from the D1 to D4 stage are presented in Figs. 3-6 and 3-11. The D1 deformation stage is related to the accretion of original materials and the formation of melange complex, and the D2 stage seems to be a deformation during subducting and underplating the complex. The change of shear sense from the D2 stage (top to NE) to the D3 stage (top to SW) infers that the deformation of the D3 stage corresponds to that during the exhumation of

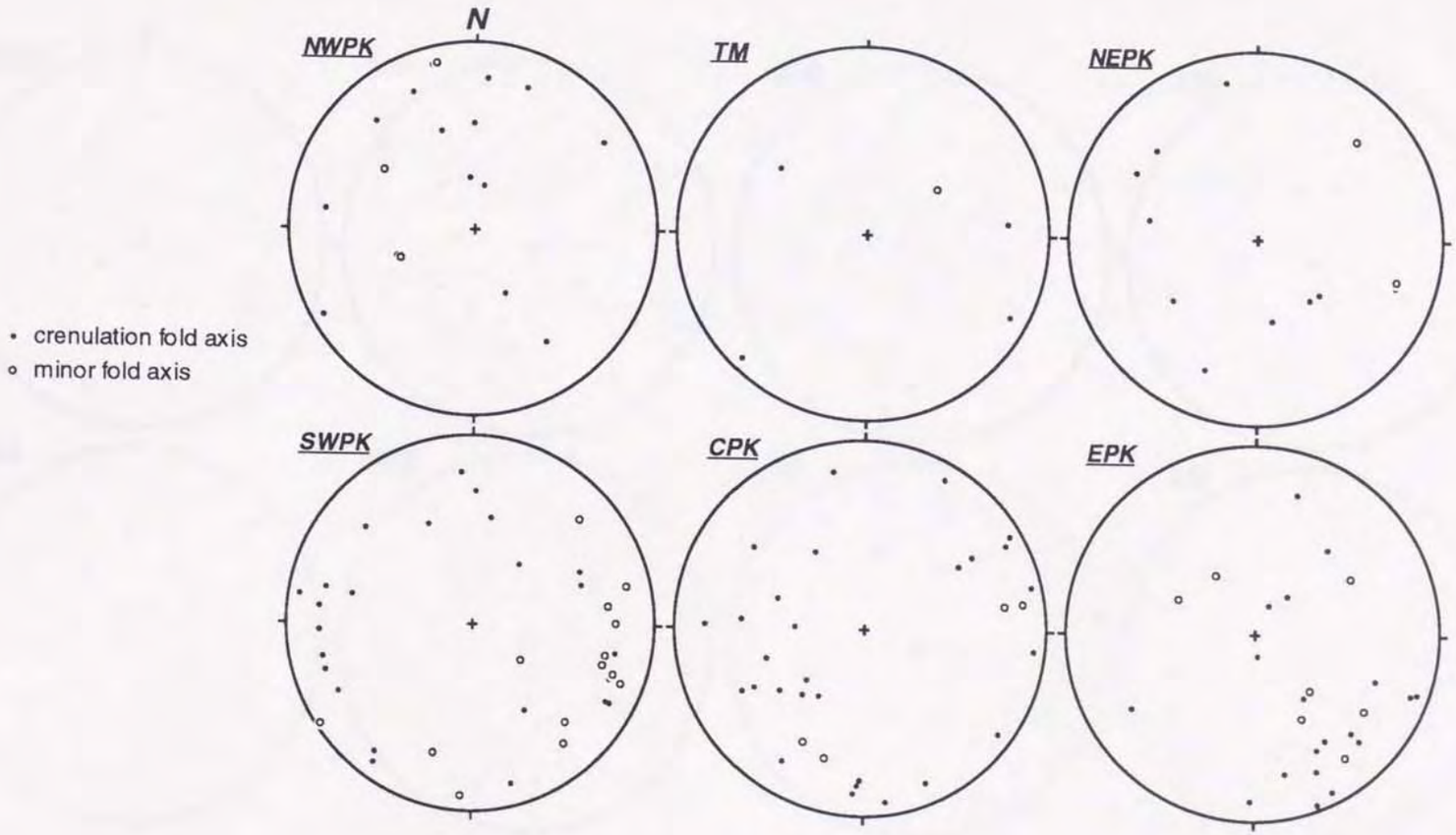

Fig. 3-10. Crenulation (solid circle) and minor fold axis (open circle) of the D2 and D3 stage plotted on an equal area net (lower hemisphere). **a**. western part of the area (Pankehoronai and serpentinite melange units).

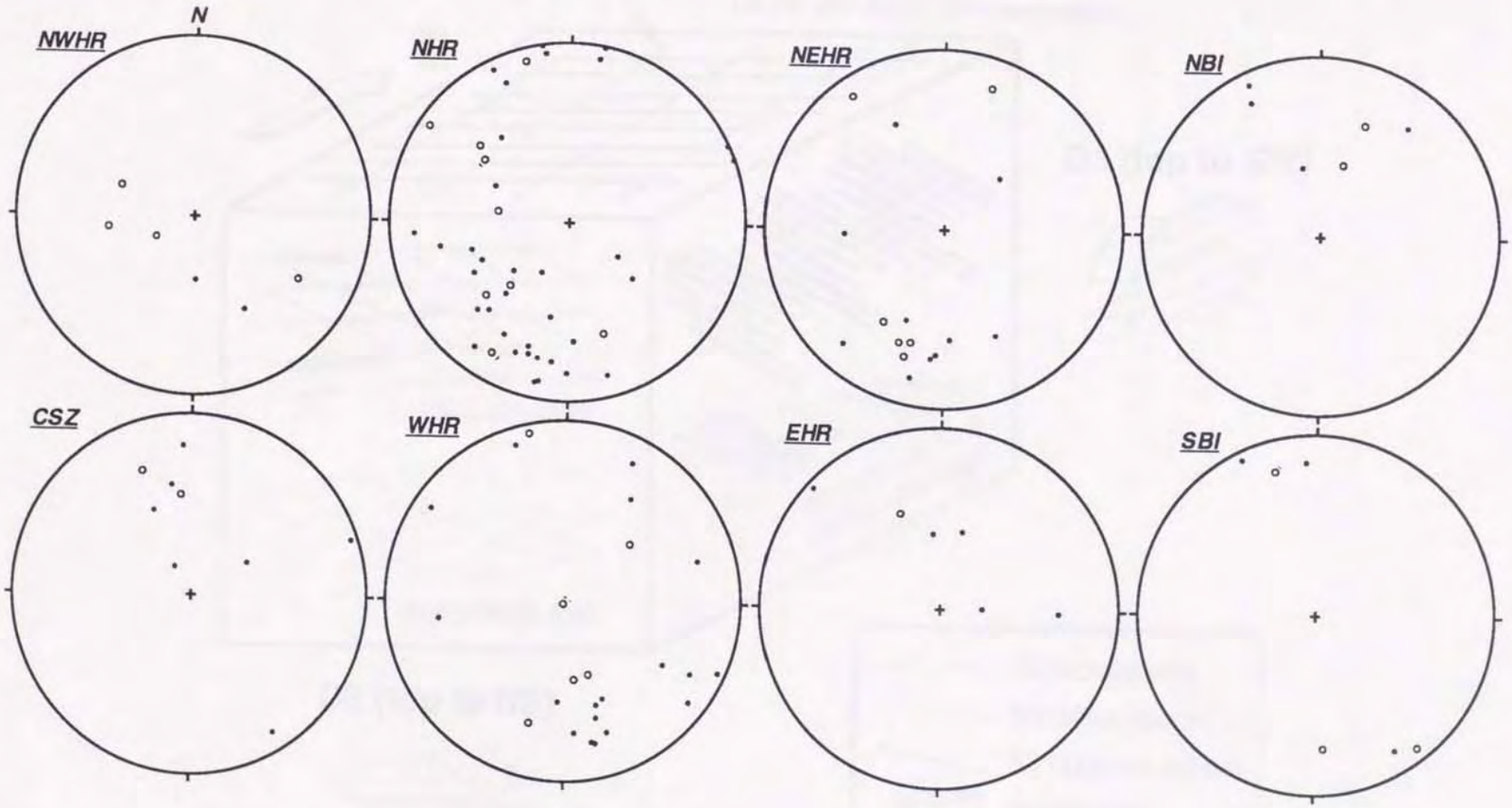

Fig. 3-10. b. eastern part of the area (Harushinai and Biei units).

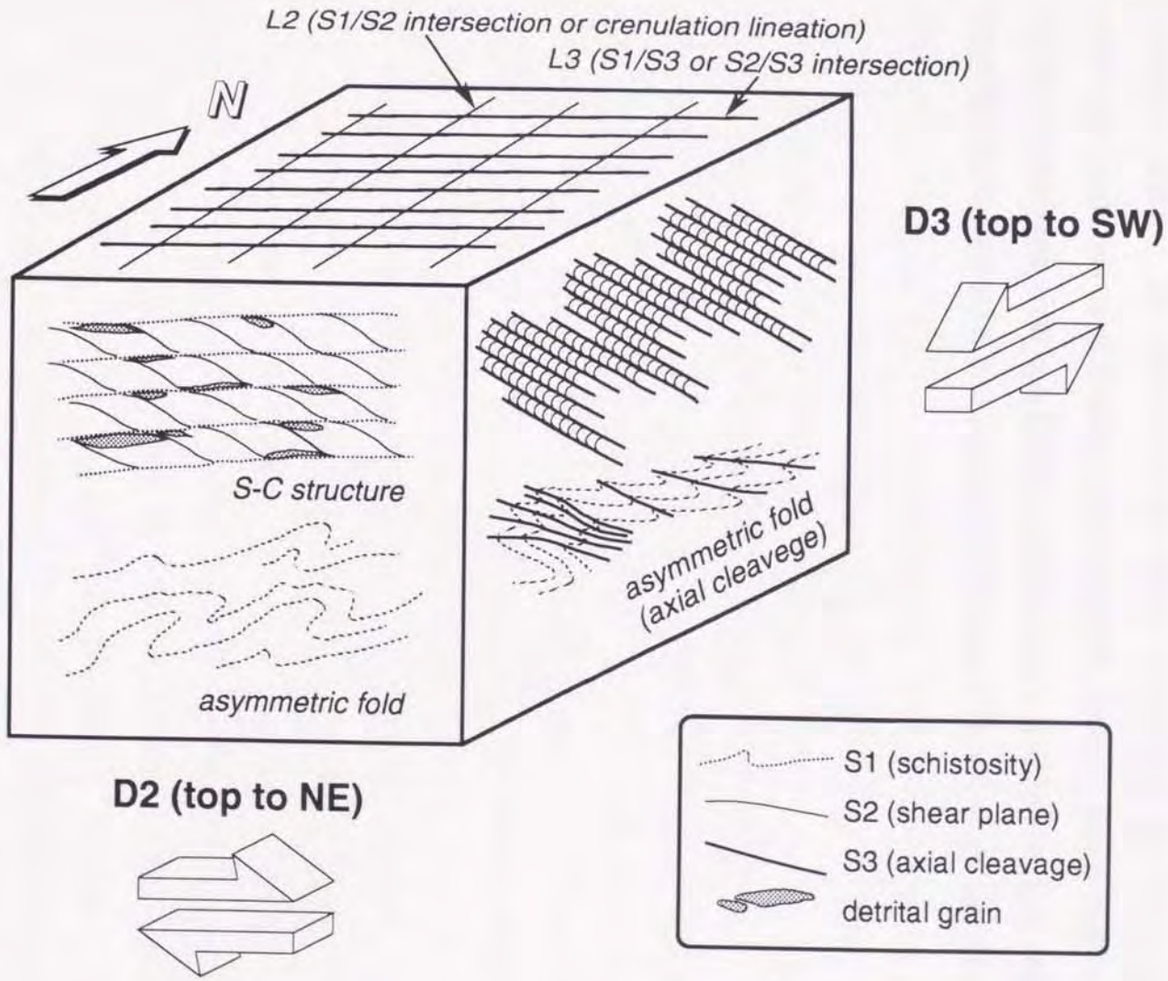

Fig. 3-11. Schematic block diagram shown correlation of the D2 and D3 stages and intersection of foliations and lineations in each stage. The three-dimensional arrows indicate the sense of shear.

the metamorphic complex. The major faults with the insertions of serpentinite border the Kamuikotan complex and the Miocene system. These suggest that the faults have acted after the exhumation of the Kamuikotan complex, and that the D4 stage is an event before the Miocene time. As mentioned the latter discussion, the Tokiwayama melange unit has a different metamorphic history from that of the Pankehoronai unit overlain by the melange unit, and so the fact suggests that the above two units had juxtaposed between the D3 stage and Miocene time.

4. Petrography

4-1. Basic rocks

Observations in the field

Basic rocks of the Kamuikotan Gorge area are divided into three types in the field, such as a) banded basic schist, b) basic schist and c) non-foliated basic rock. Basic schists of type a) are the typical in the Pankehoronai unit. Basic rocks of types b) and c) occur in all units but those in the Biei unit commonly belong to type c). Those of types a) and b) may be finer-grained basaltic pyroclastic rocks (e.g., hyaloclastic breccia, hyaloclastite and their reworked sediments), with some uncertainty due to their advance of recrystallization. Some mesoscopic deformation structures are observed in the basic schists of types a) and b), and schistosity, S-C structure, crenulation fold, ptygmatic fold, asymmetric and/or symmetric close folds and associated axial cleavages are often found in the schists of type b) (Figs. 3-7a, 3-8a and 3-9b). On the other hand, the protoliths of type c) are mainly massive basaltic rocks, such as pillow lava, massive basalt and dolerite. The basic rocks of type c) seldom show ductile deformation structures. Particularly in the Biei unit, they have rarely some undeformed vesicles derived from original structures of pillow lava, and are more weathered due to less recrystallization than those of the other types and units.

The type a) basic schists have quartz-albite layers of white color and epidote-chlorite layers of pale green, ranging in thickness from several millimeters to about a centimeter, in deep greenish matrix consisting of calcic amphibole and chlorite. Such banded basic schists are widespread in both sides of the Ishikari-gawa River nearby the Kamuikotan Gorge,

and have apparent schistosity (S1- and S2-foliations). In these schists, minor asymmetric close folds corresponding to F2-fold are also observed. The schistosity and minor folds are often cut by epidote-calcite-albite(-quartz) veins in irregular form.

The basic schists of type b) are common in the Pankehoronai. Harushinai and Tokiwayama melange units, and are minor in the Biei unit. The schists are pale green and green in color. They often alternate with pelitic schists in the Pankehoronai and Harushinai units. Some of them in the Tokiwayama melange and Biei units are composed of bluish layers dominated by sodic amphiboles, and greenish ones dominated by pumpellyites, chlorites and micas. These layers alternate with a few millimeters' orders. Bluish pebbles, which are lenticularly deformed and are ranging in diameter from a few millimeters to several centimeters, scatter in pale greenish matrix in the basic schists originated from pillow breccia or hyaloclastic breccia. Such a look results from occurrences of sodic amphiboles limited in the breccia being more mafic than matrix. In the Biei unit, the basic schists consisting of the above greenish layers and reddish ones comprised mainly of hematites are often found. The reddish laysers ma be varicolored shales. Sometimes, the basic schists in the Biei unit contain pale greenish pebbles less recrystallized than the matrix composed of chlorites, pumpellyites and hematites. In general, the basic schists are less advance of the deformation structures than the pelitic and psammitic rocks, but the type b) schists have schistosity corresponding to S1- and S2-foliations. The pebbles in the schist, derived from breccia, are flattened during the D1 stage and constitute the S1-foliations. Rarely, ptygmatic folds corresponding to the F1-folds are also observed in the type b) schists (Fig. 3-7a). The schists are also subjected to deformations of the D2 and

D3 stages, and the flattened pebbles show asymmetric lenticular shapes. Pressure solutions and shear planes (S2-foliation) develop around them. Although minor asymmetric close folds corresponding to F2- and F3-folds are also observed in the type b) schists, such fold structures are restricted in finer-grained and homogeneous parts. In some schists of type b) in the Pankehoronai unit, F3-fold axial cleavages as S3-foliations are found (Fig. 3-9b). This deformation feature in the D3 stage is different from that in the pelitic schist of the Pankehoronai unit, and the S3-foliations in the type b) basic schists are easily discriminated from the S1- and/or S2-folaitions in the field. In basic rocks of the other types and units, it is not so due to less advance of the S3-foliations.

The type c) basic rocks, in most case, do not have apparent deformation structures such as schistosity. The rocks derived from pillow lava are recrystallized along the margins of pillow and irregular quartz-albite veins, and the original structures are well preserved. In the Tokiwayama melange and Biei units, basic rocks of this type rarely show similar looks to the type b) basic schists of hyaloclastic breccia or pillow breccia origins, and have bluish rinds with the margins of pillow. The type c) basic rocks, which the protoliths are massive basalts, are also recrystallized along quartz-albite veins, and chlorites, epidotes and hematites occur along the veins. In the Tokiwayama melange and Pankehoronai units, basic rocks of this type often have schistosity (S2- or S3-foliation). Although the schistosity is an only deformation structure observed in the field, its development is partial. A sketch of basic rock with the schistosity, gotten from the Pankehoronai unit, is presented in Fig. 4-1. This basic rock, derived from massive basalt, are recrystallized along irregular quartz-albite veins in the massive part and finer veinlets consisting of epidote and chlorite extend from the veins to the matrix.

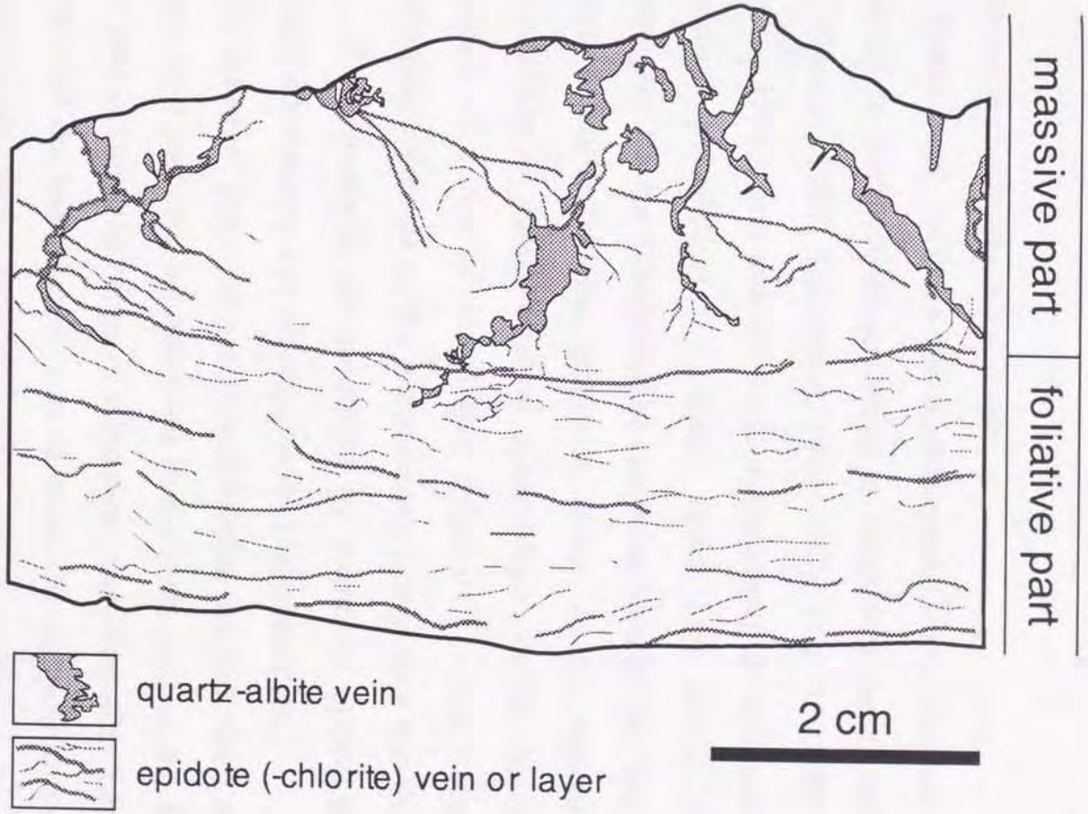

Fig. 4-1. A sketch of basic rock with the heterogeneous schistosity in the Pankehoronai unit (specimen K428).

On the other hand, the schistosity corresponding to S3-foliation is partly formed in the foliative part, and epidote and chlotite arrange along the foliation. As described below, the constitutions of the veins and schistosity are similar and correspond to index mineral assemblages of such basic rocks.

Observations under the microscope

These basic rocks in the Kamuikotan Gorge area are extensively subjected to pumpellyite-actinolite or blueschist facies metamorphism (e.g., Gouchi, 1983; Takayama, 1986; 1988; Ota, 1993MS; Sakakibara and Ota, 1994), and contain various metamorphic minerals as follow: lawsonite, pumpellyite, epidote, sodic and calcic amphiboles, metamorphic Ca-Na clinopyroxene (hereafter denoted as sodic pyroxene), chlorite, hematite, calcite, aragonite, albite, quartz, sphene, mica and stilpnomelane. Index mineral assemblages in the basic rocks are composed of some of the above minerals. The occurrences of metamorphic minerals in the Kamuikotan Gorge area are shown in Fig. 4-2. These minerals are identified by means of optical microscope, reflecting microscope and electron-probe microanalyser.

By the way, hereafter calcic amphiboles are described as actinolite because their chemical compositions in the basic rock of the Kamuikotan Gorge area occupy the range of actinolite, classified after Leake (1978), as mentioned the later chapter. In addition, the compositions of micas in the metamorphic rocks, especially pelitic and psammitic rocks, of the area have a wide range from muscovite to celadonite, but they are called metamorphic phengite or simply phengite, together.

The primary igneous textures (e.g., pebbles derived from pillow or hyaloclastic breccia) and phases (clinopyroxene and plagioclase) are

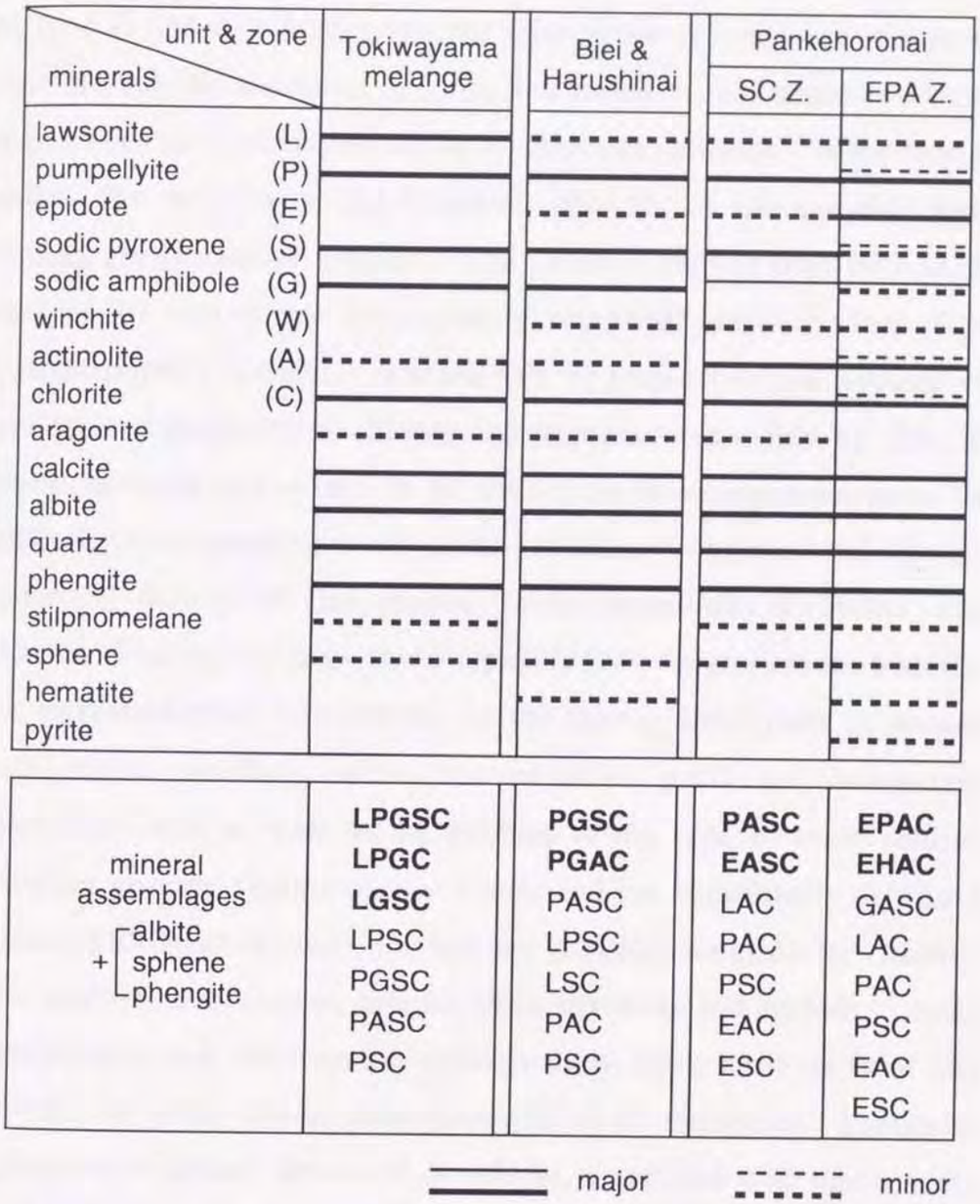

Fig. 4-2. Occurrence of metamorphic minerals (thick lines) and mineral assemblages for the basic rocks of Tokiwayama melange, Biei and Harushinai, and Pankehoronai units in the Kamuikotan Gorge area. Thin lines in the Pankehoronai unit show minerals in initial stage. Bold mineral assemblages show representative assemblages in each unit. See text for the details.

commonly preserved in the type b) and c) basic rocks. The schistosity in the type a) and b) schists under the microscope is composed mainly of sodic amphibole, actinolite, chlorite and phengite, and these two types basic schists show nematoblastic or lepidoblastic textures. In the type a) schists, the schistosity (S3-foliation) consists of idiomorphic platy chlorite, grown coarser-grained. The pebbles, derived from breccia, in the type b) schists are incompletely recrystallized and often show blastoporphyritic textures. Phenocrysts of plagioclase are replaced by finer-grained pumpellyite, chlorite and phengite, and matrix by chlorite, sphene, hematite and so on. In the finer-grained homogeneous parts, the schistosity corresponding to S2- or S3-foliations is observed and they are comprised mostly of fine-grained sodic amphibole, actinolite, and chlorite. The type c) basic rocks typically have heterogeneous textures. The recrystallization concentrates in the finer-grained parts or around quartz-albite veinlets, while the massive parts are commonly blastoporphyritic as well as the pebbles in the type b) basic schists. Abundant primary clinopyroxenes scatter and are occasionally deformed to show pull-apart textures. They are partially replaced by chlorite, sodic amphibole, actinolite, sphene, sodic pyroxene and epidote. In the Pankehoronai and Tokiwayama melange units, some basic rocks of this type have the schistosity as shear plane (S2- or S3-foliations). Lenticular aggregates of sphene, lawsonite or epidote, associated with minor sodic amphibole and actinolite are present on the schistosity. In the Pankehoronai unit, these minerals or mineral assemblages on the schistosity are similar to ones occurring around the quartz-albite veinlets which make active the recrystallizations in this type rock, nevertheless the schistosity rarely cut the quartz-albite veinlets and apparent textural relations are actually distinguished in such rocks of the Pankehoronai

unit. In this thesis, the mineral assemblages around the veinlets and on the schistosity are not classified because the assemblages in both occurrences can not be clearly discriminated and the textural relations between the veinlets and schistosity are uncertain in many cases.

Usually, it is regarded that the mineral parageneses in low-grade metabasites are sensitive to change of physical and chemical conditions during their growing processes, however, such metabasites are less recrystallized and often preserve their original textures and igneous minerals. Hence, they commonly included some local equilibrium domains, which are composed of metastable phases or have different effective bulk compositions, even if in the same thin section. In the previous works, Onuki and Takanashi (1986) concluded that the size of equilibrium domain is less than a half millimeter in diameter for the prehnite-pumpellyite facies' rocks. Although Nakajima (1982) and Maruyama and Liou (1985) regarded the size of one thin section as the equilibrium domain for the pumpellyite-actinolite facies' rocks, the basic rocks in the Kamuikotan Gorge area have some domains consisting of different mineral assemblages with a few millimeters' scale, e.g., layers showing different colors as described before, and the degree of recrystallization of the basic rocks is different by their protoliths and yielding units. In addition, some metastable phases which are not in equilibrium with neighboring ones are distinguished in many specimens. Consequently, the coexisting mineral assemblages in this thesis are fundamentally restricted to the clusters composed of homogeneous minerals in direct contact. For minerals with chemical zonations, it is decided that their rims in contact with neighboring minerals are in equilibrium with neighboring ones. In the case recognized apparent textural relations, coexisting mineral assemblages are selected for each

stage if possible, based on the above definitions for the equilibrium domains and deformation history. In fact, the index mineral assemblages in most basic rocks are constitutions on the S1- and S2-foliations. The assemblages on the these two foliations are not classified in Fig. 4-2. Because their assemblages are commonly similar, nevertheless apparent textural relations are often observed. In some basic rocks of the Pankehoronai unit, however, the minerals or the mineral assemblages resulting from different stages are discriminated. In such basic rocks, the assemblages on textures of later stage (the D3 stage) are regarded as the index assemblages of the rocks. Then, the later stage formed the index mineral assemblage is called the main stage, whereas the earlier stage formed the assemblages which had been pre-existed in the main stage is termed the initial stage. Although the initial stage corresponds to the D1 and/or D2 stages, it is decided that the initial stage contains both stages unless specified.

In Fig. 4-2, the mineral assemblages defined with taking the above into consideration are listed. Representative mineral parageneses in each unit are shown in Fig.4-3. The basic rocks in the Tokiwayama melange unit generally contain the index assemblage of lawsonite + sodic amphibole and the typical low-variance assemblages are lawsonite + pumpellyite + sodic amphibole + sodic pyroxene + chlorite, lawsonite + pumpellyite + sodic amphibole + chlorite, lawsonite + sodic amphibole + sodic pyroxene + chlorite (Figs. 4-2 and 4-3a). In the Harushinai and Biei units, the basic rocks have similar assemblages and the most common assemblages are pumpellyite + sodic pyroxene + chlorite. Representative assemblages are pumpellyite + sodic amphibole + sodic pyroxene + chlorite, lawsonite + pumpellyite + sodic pyroxene + chlorite and pumpellyite + actinolite + sodic pyroxene + chlorite (Figs. 4-2 and 4-3a).

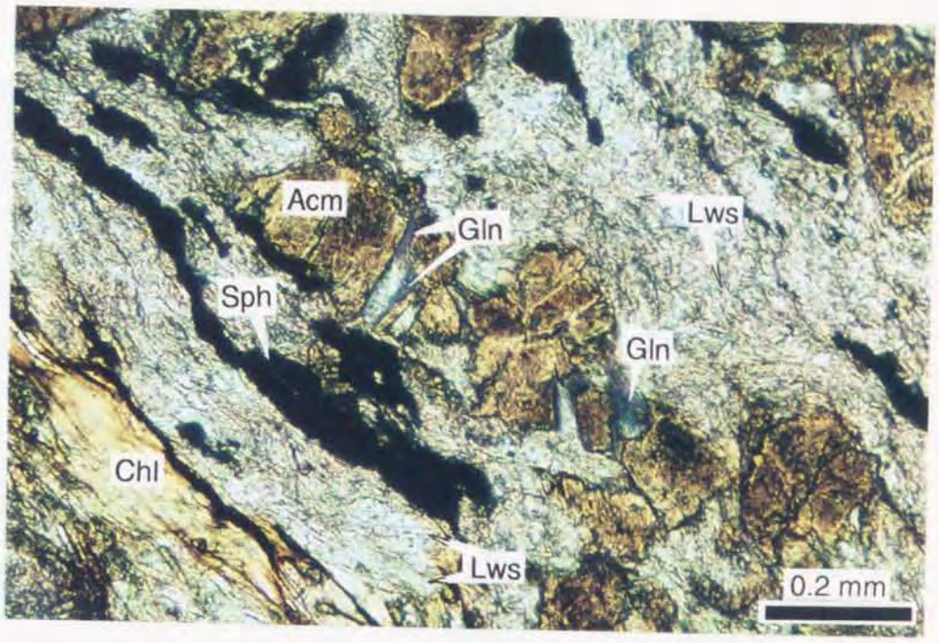

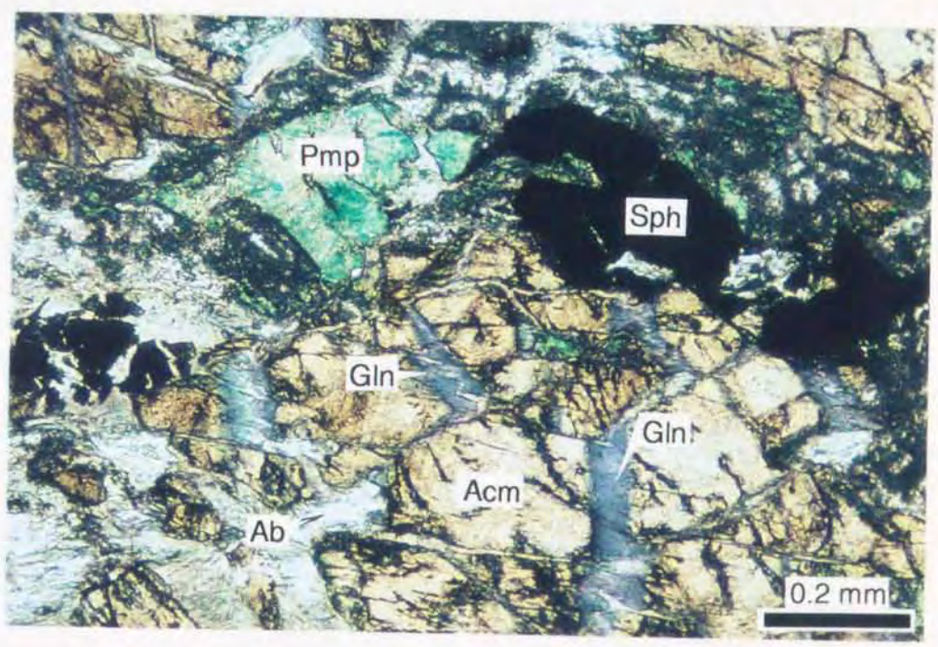

Fig. 4-3a. Representative mineral assembladges in the main stage in the basic rocks (plane polarized light). **above**: lawsonite + glaucophane + sodic pyroxene + chlorite in the Tokiwayama melange unit. **below**: pumpellyite + glaucophane + sodic pyroxene (aegirine) in the Biei unit.

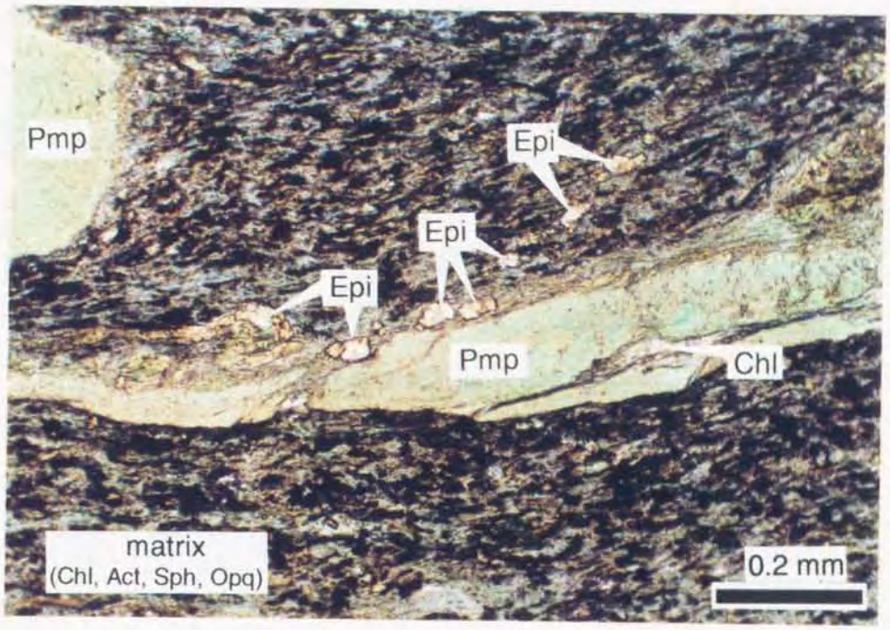

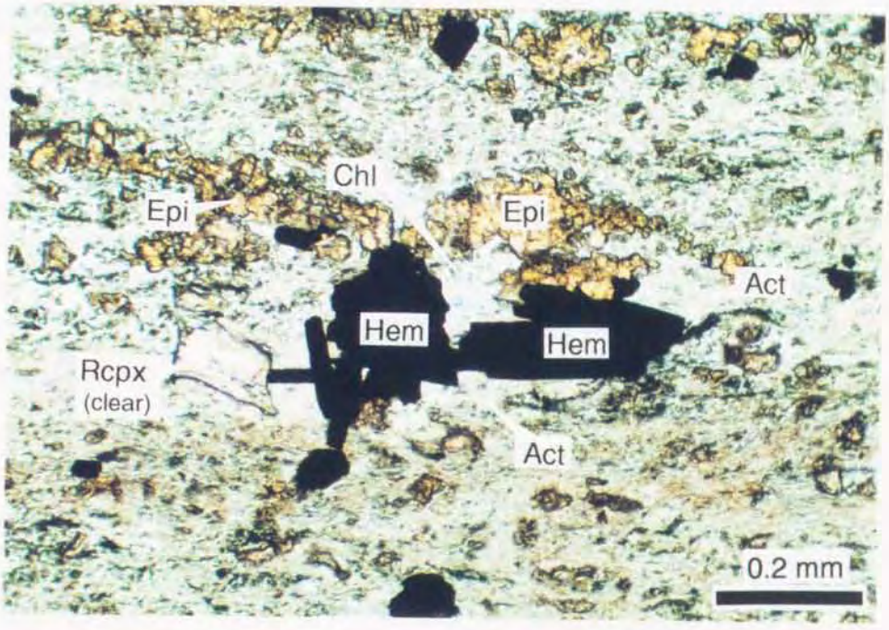

Fig. 4-3b. Representative mineral assembladges in the main stage in the basic rocks of the Pankehoronai unit (plane polarized light). **above**: epidote + pumpellyite + actinolite + chlorite. **below**: epidote + hematite + actinolite + chlorite.

Actinolite, lawsonite and hematite are common as additional phases, however, lawsonite never coexist with sodic amphibole. The basic rocks in these three units contain calcite and minor aragonite. Some metamorphic minerals in the above assemblages, in particular, sodic amphibole and sodic pyroxene occasionally show optical and chemical zonations, but the textures suggesting relation between such zonations and deformation structures has not been found. Of course, the assemblages described above are based on the definitions, mentioned before, and chemical compositions of the rims of minerals showing such zonations are used in the later discussions.

The basic rocks in the Pankehoronai unit are roughly divided into two metamorphic zones, from east to west within the Pankehoronai unit, sodic pyroxene-chlorite (SC) zone and epidote-pumpellyite-actinolite (EPA) zone (Fig. 4-2), based on the mineral assemblages in the main stage defined above. The SC zone is characterized by the association of sodic pyroxene + chlorite and representative assemblages are epidote + actinolite + sodic pyroxene + chlorite and pumpellyite + actinolite + sodic pyroxene + chlorite. Minor aragonite and no sodic amphibole occur in this zone. On the other hand, the EPA zone is defined by epidote + pumpellyite + actinolite + chlorite and epidote + hematite + actinolite + chlorite (Fig. 4-3b). In the basic rocks of this zone, no epidote is in direct contact with aragonite, and pumpellyite does coexist with neither sodic pyroxene nor calcite.

In the Pankehoronai unit, particularly, the EPA zone, the D1, D2 and D3 stages are discriminated based on the textural relations of some metamorphic minerals in the type b) and c) basic rocks. Some photomicrographs showing relations between deformation structures and their constituent minerals are presented in Figs. 3-7b, 3-8b and 3-9c.

The S1-foliations in the D1 stage are shown in flattened pumpellyites aggregates filling with amygdules (Fig. 3-8b). In the primary clinopyroxenes, showing pull-apart textures in many cases, fractures perpendicular to the foliations develop and sodic amphiboles elongated in parallel to the foliations is observed in the fractures (Fig. 3-7b). The flattened pumpellyite aggregates are subjected to deformation with dextral shear sense during the D2 stage, resulting in being lenticular shapes (Fig. 3-8b). The shear planes as S2-foliations are formed around them, and sodic amphiboles rarely appear along the fringes of the lenticular pumpellyites aggregates. Some pumpellyite aggregates constitute asymmetric close folds and crenulation folds (F2-folds) formed by the shear deformation in this stage (Fig. 3-8b), and the crenulation fold axes indicate L2-lineations. After that, i.e., in the D3 stage, asymmetric close folds (F3-folds) with axial cleavages (S3-foliations) are formed by shear deformation with sinistral sense. On the S3-foliations, fine-grained epidotes arrange. Intersections (L3-lineations) between folded S2-foliations and the S3-foliations apparently cut the L2-lineations. In the D3 stage, crenulation folds which have axes parallel to the L3-lineations are also formed and the folds slightly bend the L2-lineations. On the plane perpendicular to the S3-foliations and L3-lineations, asymmetrically deformed pumpellyites aggregates and porphyroblasts of sodic amphiboles are observed. Along the fringes of the former, finer-grained epidotes occur and the epidotes intergrow with fine-grained pumpellyites and fibrous chlorites and actinolites (Fig. 4-3b). Around these metamorphic minerals, although abundant sodic amphiboles appear, the amphiboles in direct contact with the epidotes are actinolites which are the rims of sodic amphiboles showing an optical zoning. The porphyroblasts of sodic amphiboles are asymmetrically deformed and elongated, and

their pressure shadows and boudin necks are composed of pale greenish actinolites with certainly different color from sodic amphiboles (Fig. 3-9c).

In the rocks observed such textural relations, sodic amphiboles, actinolite, pumpellyite, epidote, chlorite, phengite and sphene are observed in the matrix, however, the above textural relations suggest that the index mineral assemblage of main stage is epidote + pumpellyite + actinolite + chlorite, and sodic amphiboles and epidotes are not in equilibrium in the D3 stage (Fig. 4-2). Consequently, the sodic amphiboles in such rocks are regarded as relicts of the initial stage. On the basis of similar relations, the index mineral assemblages in main stage and the relic minerals derived from initial stage are discriminated in some other specimens of the Pankehoronai unit. As described the later chapter, the epidote which is the major phase in EPA zone often includes variable minerals such as sodic amphibole, actinolite, sodic pyroxene, pumpellyite and chlorite, and these inclusions are regarded as the relic minerals of initial stage (Figs. 4-2 and 4-4).

The occurrence, texture and chemical composition of each mineral phase are minutely described the next chapter.

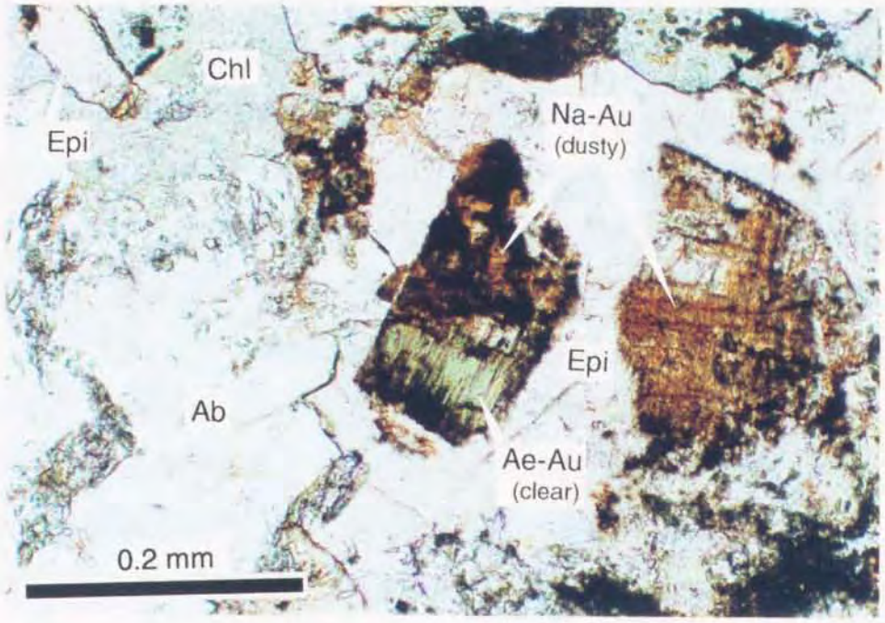

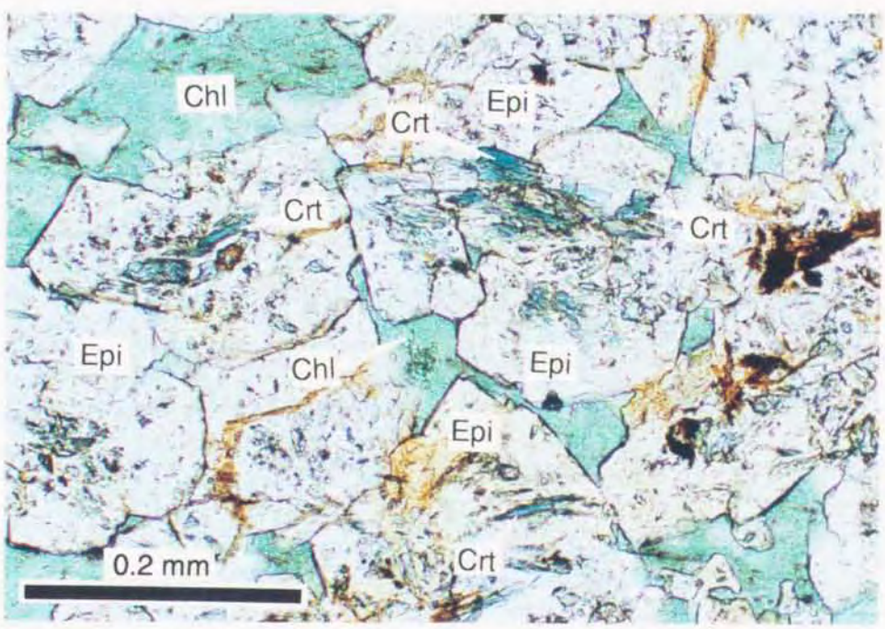

Fig. 4-4. Representative modes of occurrence of minerals in the initial stage in basic rocks of the Pankehoronai unit (plane polarized light). **above**: epidote porphyloblast around albite-chlorite vein, including sodic augite and aegirine-augite. **below**: epidote porphyloblast including abundant sodic amphiboles (crossite). Although pumpellyite and chlorite are also included, it is difficult to distinguish due to fine-grained under the microscope.

4-2. Pelitic and psammitic rocks

Observations in the field

Pelitic and psammitic rocks, widespreading in the eastern part of the Pankehoronai unit and whole of the Harushinai unit, tend to contain more psammitic domains toward the east, as described above. In particular, a large amount of psammitic rocks, with pelitic layers of a few millimeters thick, occur in the Harushinai unit. Commonly, the pelitic rocks are black or dark gray in color and show banded structure alternated with white quartz layers about a few millimeters thick. Some pelitic rocks consist only of pelitic portions. Sometimes, pelitic rocks containing pebbles of psammitic rock and intermediate to acidic tuff are found in the Harushinai unit. The tuff is often intercalated as layers of a few millimeters in thickness. The pebbles, less than several millimeters in diameter, are asymmerically or lenticularly deformed but are not very elongated (Fig. 3-8a). Pieces of sheared serpentinite and serpentine schist are also included within pelitic rocks around faults with the insertions of serpentinite. The pieces are highly deformed and elongated. The psammitic rocks show grayish color and occur as layers ranging in thickness from a few millimeters to ten centimeters, and as lenses of a centimeter in wide and several centimeters long in the pelitic rocks. In the Harushinai unit, those consisting mostly of psammitic portions are also found. They are not very foliated and the sizes of constituent grains are approximately a millimeter in diameter. Sometimes, the psammitic rocks are interbedded with pelitic and tuff layers of a few millimeters thick.

In the outcrops and under the microscope, the pelitic and psammitic rocks show various deformation structures, such as schistosity, boudin, pressure shadow, S-C-C' structure, kink band, symmetric and asymmetric

folds with various kinds of form and order, and associated linear and planer structures, e.g., shear plane, fold axis, axial plane, and axial cleavage (Figs. 3-7, 3-8 and 3-9). In the psammitic layer within pelitic rocks, tension gashes filled with quartz are often observed. The planer structures such as schistosity (S1-foliation), shear plane (S2-foliation) and axial cleavage (S3-foliation) are composed mainly of phengites, chlorites and carbonaceous materials (Figs. 3-7, 3-8 and 3-9). For the pelitic rocks in the Tokiwayama melange unit, stilpnomelane and actinolite are also the major constituent minerals of the S1- or S2-foliations. As mentioned the previous chapter, these structures have been mainly formed during the D1, D2 and D3 stages. Most of the planer structures are found in the pelitic and psammitic rocks, especially, in the pelitic rocks of the Pankehoronai and Harushinai units. Then, the relation between the planer structures observed under the microscope and their constitutions in pelitic rocks of the Pankehoronai and Harushinai units are described below.

Observations under the microscope

S1-foliations of the pelitic rocks, formed during the D1 stage, are subparallel to bedding planes (S0-foliation), and are composed of detritus, phengites, chlorites and carbonaceous materials (Fig. 3-7b). The detritus often appear in the pelitic rocks of the eastern part of the Pankehoronai unit and in those with psammitic parts of the Harushinai unit. They are deformed during the latter stages, resulting in a lenticular form with fifty micrometers in maximum thickness and two hundred micrometers in maximum length. The detritus is grains of quartz, feldspar, muscovite and fragments of rocks. The feldspar grains are partly and/or completely recrystallized to product tiny metamorphic phengites. The

detrital grains of muscovite and fragments of rocks are apparently recrystallized to become metamorphic phengites and chlorites, nevertheless the shapes have been preserved yet, under the microscope (Fig. 3-7b). The origins of fragments may be tuff but are uncertain. Such detritus typically occur in the pelitic rocks interbedded with psammitic rock and intermediate to acidic tuff of the Harushinai unit, but have not been found in the examined rocks of the Pankehoronai and the Tokiwayama melange units.

S2-foliations, shear planes formed during the D2 stage, consist of metamorphic phengites, chlorites and carbonaceous materials (Fig. 3-7b). The S2-foliations in the pelitic rocks are often subparallel to the S1-foliations, in particular, the pelitic rocks without the detritus. So, both foliations can not be distinguished in many pelitic rocks without observations under the microscope.

S3-foliations are the F3-fold axial cleavages in the pelitic rocks, formed during the D3 stage deformation, and cut the S1- and S2-foliations (Fig. 3-9c). The S3-foliations are composed of similar constitutions of the S2-foliations of the pelitic rocks and no detritus are on this foliations. In the pelitic rocks of the Pankehoronai unit, the S3-foliations as axial cleavages are partly subparallel to the S1- and S2-foliations bent by the F3-folds because the tightness of F3-folds produced the S3-foliations are close to tight (Fig. 3-9c). Then, the S3-foliations are regarded as the regional schistosity in many pelitic rocks of the Pankehoronai unit. On the contrary, the F3-folds observed in the Harushinai unit are commonly close or open folds. The S3-foliations in the pelitic rocks of the Harushinai unit, which are the F3-fold axial cleavages and minor crenulation cleavages oblique to the fold axial planes, are less advanced than those of the Pankehoronai unit. Hence, the

regional schistosity in the Harushinai unit is mostly the S1- and S2-foliations.

As mentioned the above chapter, the S2-foliations and S3-foliations correspond to the Si-schistosity (initial schistosity) and the Sm-schistosity (main schistosity), respectively. In other words, the regional schistosity of the Pankehoronai and Harushinai units is equal to the Sm-schistosity and the Si-schistosity, respectively.

4-3. Siliceous and calcareous rocks

Major distributions of chert are restricted in neighboring the north-south trending serpentinite body, bordering the Harushinai and Biei units. It is massive and pale red or red in color and commonly accompanies the basic rocks of the Biei unit. Sometimes, it contains layers of green and red shale, consisting of phengite and chlorite, and mostly hematite, respectively, but is usually not foliated. Minor siliceous schist, which is derived from layered cherts, occurs in the region dominated by pelitic and psammitic rocks of the Pankehoronai and Harushinai units, and as blocks in the Tokiwayama melange unit. Its discontinuous distribution is traced along the direction subparallel to the structure of neighboring pelitic and psammitic rocks. It appears as lenticularly elongated domains with changing the thickness and as layers ranging in thickness from a few millimeters to several centimeters. The siliceous schist, showing white or gray color, often alternates with pale greenish layers of about a millimeter in thickness, consisting mainly of phengite. In the Tokiwayama melange and Harushinai units, a few amounts of bluish and brownish siliceous schist, bearing sodic amphibole and stilpnomelane, respevtinely, are rarely found.

Calcareous rocks are minor constituent lithofacies as well as siliceous rocks in the area. The calcareous rocks foliated appear as layers intercalated within the basic schists and boundary between the basic schists and pelitic schists of the Pankehoronai unit under the suspension bridge in the Kamuikotan Gorge (Fig. 3-9a). They are about a meter in thickness, and show white or gray color. Rarely, calcareous rocks occur as small blocks or lenses in the pelitic and psammitic rocks, and such calcareous rocks seem to be psammitic rocks. These calcareous rocks are

completely recrystallized and some of them are subjected to ductile deformation (Fig. 3-9a). They almost consist only of calcite and no aragonite has been found in the calcareous rocks investigated.

4-4. Ultramafic rocks (Serpentinite)

Ultramafic rocks in the investigated area are mostly altered by the deformation and metamorphism, resulting to serpentinize except of a part. The serpentinites are divided into three types based on their forms in the field, such as massive serpentinite, flaked serpentinite and serpentine schist. The massive serpentinite is subdivided into one remaining a texture of peridotite and one having no original texture.

The former massive serpentinite is relatively solid. It composes of the north-south trending serpentinite body, bordering the Harushinai and Biei units, and cut the structure of both units. On the other hand, the latter massive serpentinite occurs as blocks with various sizes (less than several-ten meters in diameter) in the serpentinite melanges and sheared serpentinite zones along faults as unit boundaries. This serpentinite is commonly associated by abundant mesh-like veinlets filled with calcite. The flaked serpentinite mainly appears as matrixes of serpentinite melanges and sheared serpentinite zones. It is aggregates of chips or lenses with various sizes and is usually sheared. The serpentine schist occurs between the above sheared serpentinite zones along faults and the neighboring rocks, and as layers interleaved within the basic schist (of the Pankehoronai unit) in the north-bank of the Ishikari-gawa River nearby the Kamuikotan Gorge. The serpentine schist is subjected to deformation concordant with the neighboring basic schist, and contains small lenses and thin layers consisting of calcite.

The massive and solid serpentinite shows dark green or dark greenish gray in color. It consists mostly of olivine serpentinized as mesh and serpentine, suggesting that the protolith is dunite. In addition, because minor pseudomorphs of pyroxene are rarely observed, it seems

that the serpentinite of hartzburgite, lherzolite or wehrlite origin is present, too. The other serpentinites are black, deep green, light green and white in color. They are completely serpentinized, and their protoliths can not be identified. The serpentinites, highly sheared and foliated, are usually soft and show white or light green color.

5. Occurrence, textures and chemical composition of both igneous and metamorphic minerals

Major constituent minerals were analyzed by a JEOL electron-probe microanalyser JXA-733 with three wavelength-dispersive spectrometers at Faculty of Science, Ehime University and JXA-8600SX at Graduate School of Science and Technology, Niigata University. Chemical analyses of some amphiboles were carried out with a JEOL electron-probe microanalyser JSM-5400 using an energy-dispersive system at Ehime University. Analytical conditions were an accelerating voltage of 15 kV, specimen current of 5.0×10^{-9} A (4.0×10^{-10} A at the analyzer with energy-dispersive system) and beam diameter of 1-5 μm.

5-1. Basic rocks

Relic clinopyroxene

Igneous clinopyroxene is preserved in basaltic rocks from all units in the Kamuikotan Gorge area. In general, the amount and grain size decrease with increasing degree of recrystallization which resulted a development of visible schistosity. It has been replaced by metamorphic pyroxene, amphibole and chlorite that epitaxially overgrew at the fringe of relic crystals or along cleavages and irregular cracks (Fig. 3-7b). The boundary between igneous and replacing clinopyroxene under the microscope is usually plain but indistinct in some specimens. Relic clinopyroxene is commonly colorless and sometimes shows pale brownish pleochroism. The analyses of clinopyroxene are shown in Fig. 5-1 and appendix 1a.

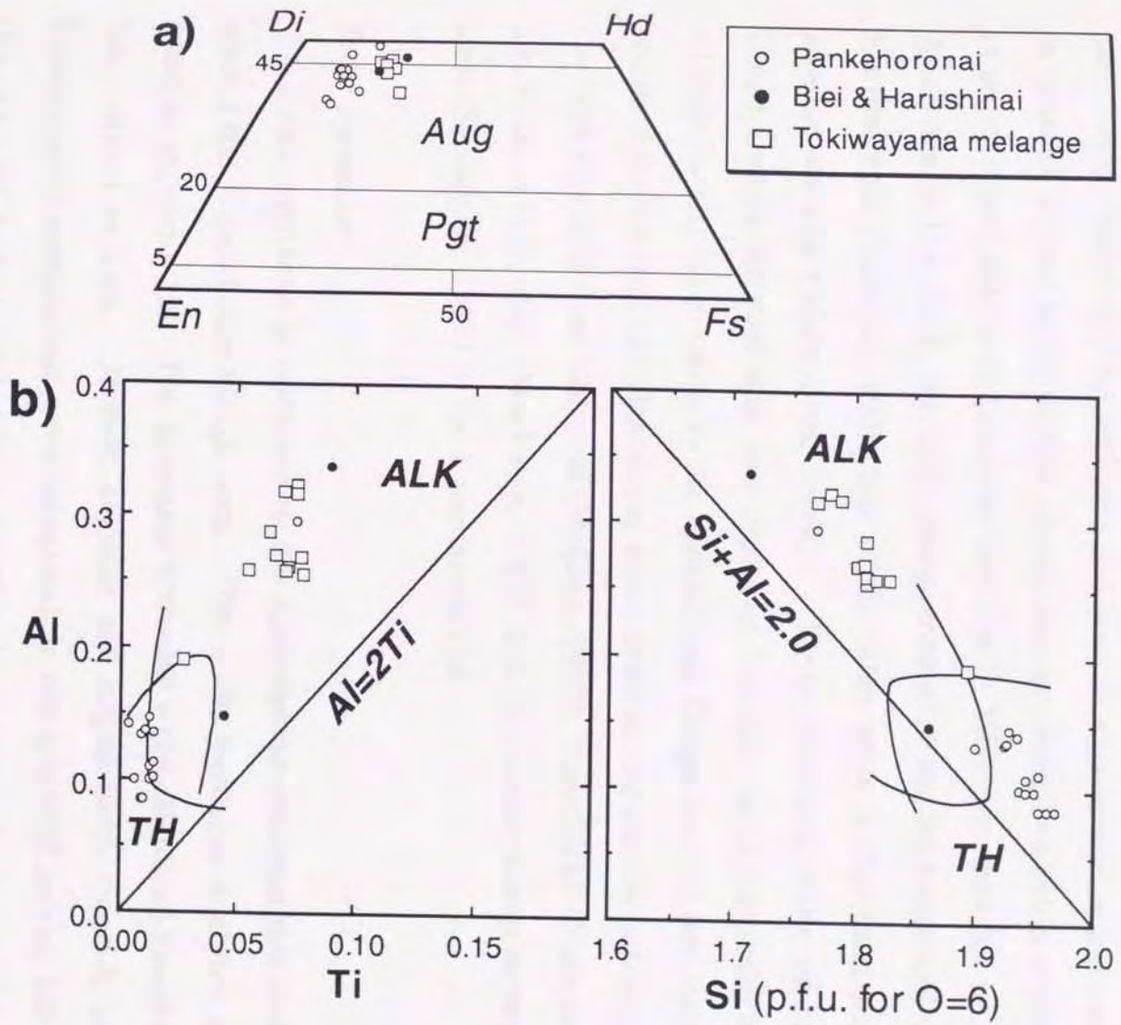

Fig. 5-1. Composition of a relic clinopyroxene in the metabasic rocks from all units in the Kamuikotan Gorge area. a) diopside-hedenbergite-enstatite-ferrossilite quadrangle diagram, b) Al versus Ti and Si diagrams.

The relic pyroxene is diopside or augite in composition (see Fig. 5-1a with the classification after Morimoto *et al.*, 1989), with high TiO_2 (0.20-3.11 wt.%) and Al_2O_3 (1.95-11.64 wt.%). Na_2O contents are less than 1.2 wt.%. Al_2O_3 is mainly combined with TiO_2 to form $CaAl_2TiO_6$ (Ti-tschrmaks) endmember, with minor amounts of $CaAl_2SiO_6$ (Ca-tschrmaks), $NaFe^{3+}Si_2O_6$ (aegirine) and $NaAlSi_2O_6$ (jadeite) components. In contrast, almost metamorphic clinopyroxenes described below are high in aegirine and jadeite components and low in TiO_2 (less than 0.4 wt.%). As shown in Fig. 5-1b, the relic clinopyroxene of the Pankehoronai unit has tholeiitic character, while that of the other units is characteristic of alkaline basalts (Maruyama, 1976). These chemical traits of relic clinopyroxene suggest that two types of basaltic rocks (tholeiite and alkaline basalt) are presents in the Kamuikotan Gorge area. Little date is obtained for the Biei and Harushinai units, however the similar conclusion has been reported from Shizunai (Nakano, 1985), Yubaridake (Nakagawa and Toda, 1987), Biei (Maekawa, 1986) and Horokanai-Kamietanbetsu areas (Shibakusa, 1991) in the Kamuikotan belt.

Sodic pyroxene

Sodic pyroxene is common in the Kamuikotan metamorphic rocks around the Kamuikotan Gorge area. The sodic pyroxene analyses are listed in appendix 1b. The structural formulae were calculated based on total cations as four. Jadeite, aegirine and augite (with diopside and hedenbergite) components were calculated as 100 x $Al^{VI}/(Ca+Na)$, 100 x $(Na-Al^{VI})/(Ca+Na)$, and 100 x $Ca/(Ca+Na)$, respectively. Other components, e.g., Ca- and Ti-tschrmaks, are disregarded because those amounts are negligible. The nomenclature of sodic pyroxene is based on the classification after Morimoto *et al.*(1989).

The modes of occurrence of sodic pyroxene are as follows: (a) replacement of primary igneous clinopyroxenes along rims and irregular cracks (Figs. 3-7b and 4-3a), (b) epitaxial overgrowths on primary clinopyroxene in albite-quartz veins, and (c) aggregates of acicular or needle crystals in albite-quartz veins. Sodic pyroxenes of type (a) are the most common through all units, especially from the Pankehoronai unit, in the Kamuikotan Gorge area. Those from the Pankehoronai unit are often turbid due to the presence of abundant fine-grained sphene and opaque mineral, and are occasionally surrounded by xenomorphic epidotes (Figs. 3-7b and 4-4). In well-recrystallized basic rocks, primary clinopyroxene are completely replaced by sodic pyroxenes. They can be distinguished from igneous clinopyroxene by their optical features such as pale yellow to yellow colors. Some of them are nearly colorless and resemble to relic clinopyroxene, but can be distinguished by distinct differences in composition. The sodic pyroxenes of type (b) show pleochroism from pale yellow to pale yellowish brown or light green. Those of type (c) occur as idiomorphic prisms, acicular or needle-like crystals and often form fan-shaped aggregates. Sodic pyroxenes of this type are usually colorless and sometimes show pleochroism from pale green to green. The sodic pyroxenes of type (c) occasionally coexist with quartz and albite, whereas those of type (b) are contact with only albite. Those of type (a) coexist with neither quartz nor albite.

The compositional variations of sodic pyroxenes from each unit are shown in Fig. 5-2. The chemical compositions of sodic pyroxene are varying by each crystal, specimen or type, and those showing notable pleochroism are rich in aegirine components. The sodic pyroxenes associated with quartz have more restricted compositions than those of the

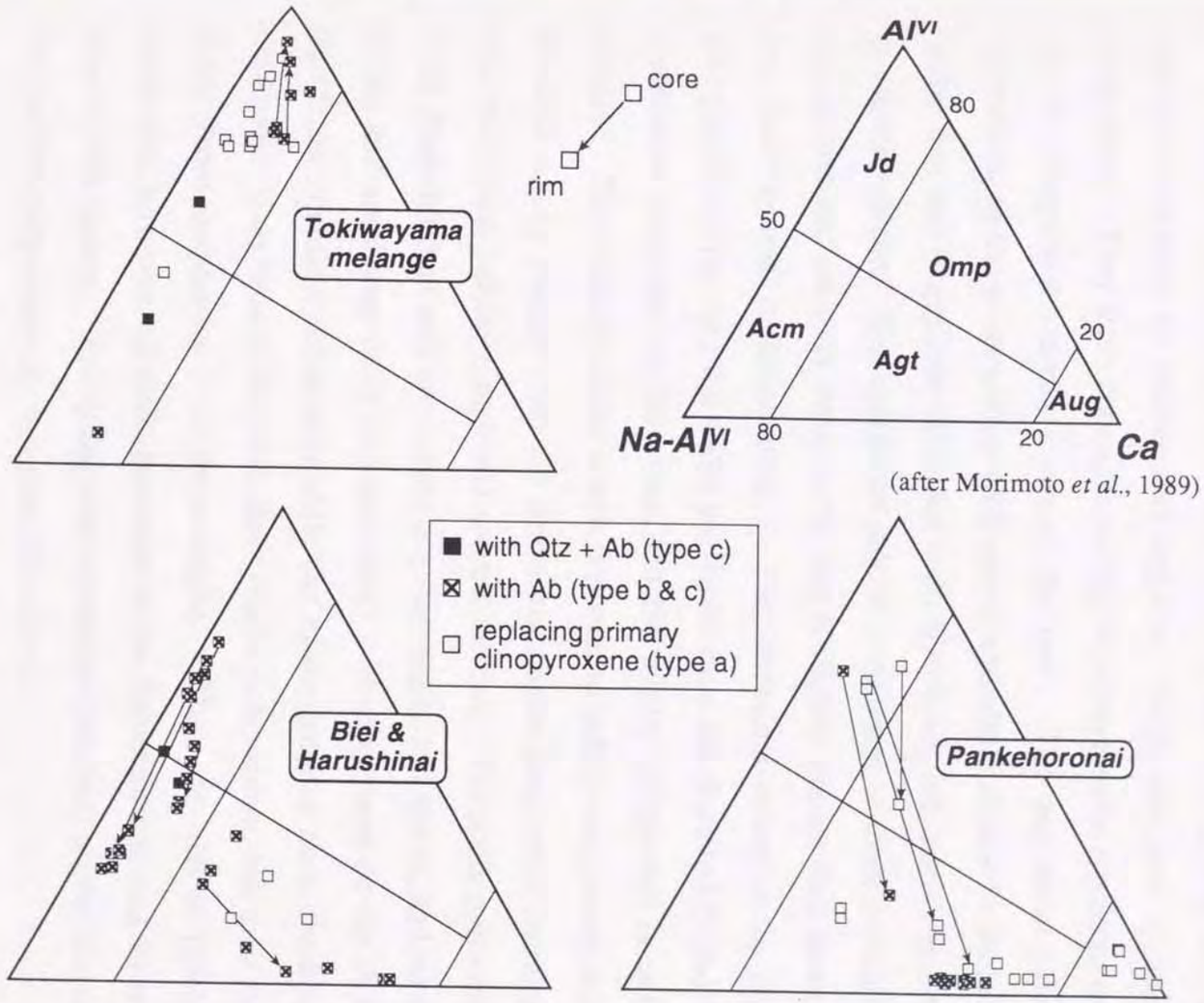

Fig. 5-2 Jadeite-acmite-augite diagram of sodic pyroxene from the basic rocks in all units around the Kamuikotan Gorge. Hereafter abbreviations of major minerals are followed by Kretz (1983).

others, and their compositions plot in the middle range between aegirine and jadeite. On the other hand, another sodic pyroxene has wide compositional variations from jadeite to augite, through aegirine.

The sodic pyroxenes from basic rocks in the Tokiwayama melange unit are restricted to jadeite and aegirine, which are poor in augite component. They have chemical zoning of a progressive type, and their jadeite component increases toward the rim. The maximum jadeite component of those coexisting with quartz and albite attains 56 mole %. In the Biei and Harushinai units, the sodic pyroxenes are jadeite, aegirine or aegirine-augite. The maximum jadeite component of those coexisting with quartz and albite is 49 mole %, and is slightly poorer than those in the Tokiwayama melange unit. The chemical zonation is of a retrogressive type, i.e., the sodic pyroxene rims are depleted in jadeite component compared to the cores, but the augite component is nealy constant. The sodic pyroxene which is poorer in jadeite component show different zoning pattern from the above, the augite component increases with decreasing jadeite component toward the rim. The sodic pyroxenes in the Pankehoronai unit are mainly aegirine-augite and augite, and rarely jadeite and omphacite (only one specimen). Most of them do not show significant chemical zonations, while the minor jadeites have chemical zonations. They tend to decrease their jadeite components, and their rim ranges from omphacite to aegirine-augite. They are rich in jadeite component, however, all sodic pyroxene in the Pankehoronai unit do not coexist with quartz. Excepting one specimen (jadeites) as the above, their jadeite components are less than 20 mole %.

Amphibole

Amphiboles are ubiquitous in basic rocks in all units around the Kamuikotan Gorge. Representative analyses of amphiboles are presented in appendix 1c. In present study, estimation of Fe^{2+} and Fe^{3+}, and calculated formulae in amphiboles were based on the assumption Si + Al + Ti + Fe + Mn + Mg = 13. The nomenclature of amphibole is based on the classification after Leake (1978).

Under the microscope, calcic and sodic amphiboles are identified. The former mainly occurs in basic rocks from the Pankehoronai unit, and is minor in those from the other units. The latter is common in the Biei, Harushinai and Tokiwayama melange units, and is often found in the Pankehoronai unit. As described above, amphiboles in the Pankehoronai unit are divided into two types that are different from the metamorphic stages (Ota, in submitting).

Most of calcic amphiboles from the study area are actinolite, which are commonly colorless or pale green, except amphiboles occuring in hornblendite or amphibolite blocks from the serpentinite melange, which is greenish magnesiohornblende. They appear as fibrous aggregates around relic clinopyroxene (Fig. 3-7a), as independent prismatic needles in the matrix with nematoblastic texture, and as tiny crystals dispersed in albite and quartz layers. Actinolites of the main stage in the Pankehoronai unit often surround sodic amphibole with pale blue or bluish violet in color (Figs. 3-7b and 3-9c). On the other hand, those of the initial stage are included within epidote porphyroblast, together with sodic amphiboles. The Al_2O_3 contents of these actinolites range from 0.1 to 1 wt. %. Some actinolites of the main stage in the Pankehoronai unit are close to the ideal formula, $Ca_2(Mg, Fe)_5Si_8O_{22}(OH)_2$. Actinolites from the Tokiwayama melange, Biei and Harushinai units, and those of

the initial stage in the Pankehoronai unit, however, contain some sodic amphibole endmember (Fig. 5-3).

Minor amount of sodic-calcic amphiboles with winchite composition, occur in the basic rocks of the Tokiwayama melange, Biei and Harushinai units. Winchite is sometimes rimmed by sodic amphibole. It is pale blue in color, so actinolite and winchite are difficult to distinguish under the microscope. Winchite contains up to 44 mole % sodic amphibole endmember.

As mentioned above, sodic amphiboles occur in all units around the Kamuikotan Gorge area. They occur as: (1) epitaxial overgrowths on igneous and metamorphic clinopyroxene (Figs. 3-7b and 4-3a); (2) as fine-grained acicular crystals in matrix or albite and quartz vein; (3) as fibrous aggregates interlayered on a mm-scale with phengite, chlorite and pumpellyite, which forms lenticular or layered aggregate; and (4) as inclusions within epidote porphyroblasts (Fig. 4-4). These sodic amphiboles show distinct pleochroism from pale blue to blue or from blue to bluish violet. In the Pankehoronai unit, sodic amphiboles of the initial stage show the mode of (1), (2) and (4), and those of (1) and (2) are entirely mantled by actinolite, formed during the main stage. The mode of (3) is limited the Tokiwayama melange unit. As shown in Fig. 5-3, sodic amphiboles have wide compositional variations from glaucophane to magnesioriebeckite, and contain up to 25 mole % actinolite endmember. The chemical compositions of sodic amphiboles, which are contact with the other mineral phases as discrete crystals, of the main stage in the Pankehoronai unit are restricted magnesioriebeckite, while those are mainly correspond to glaucophane or crossite in the other units. In any units, the sodic amphiboles in equilibrium with coexisting minerals exhibit progressive zonation with higher glaucophane content

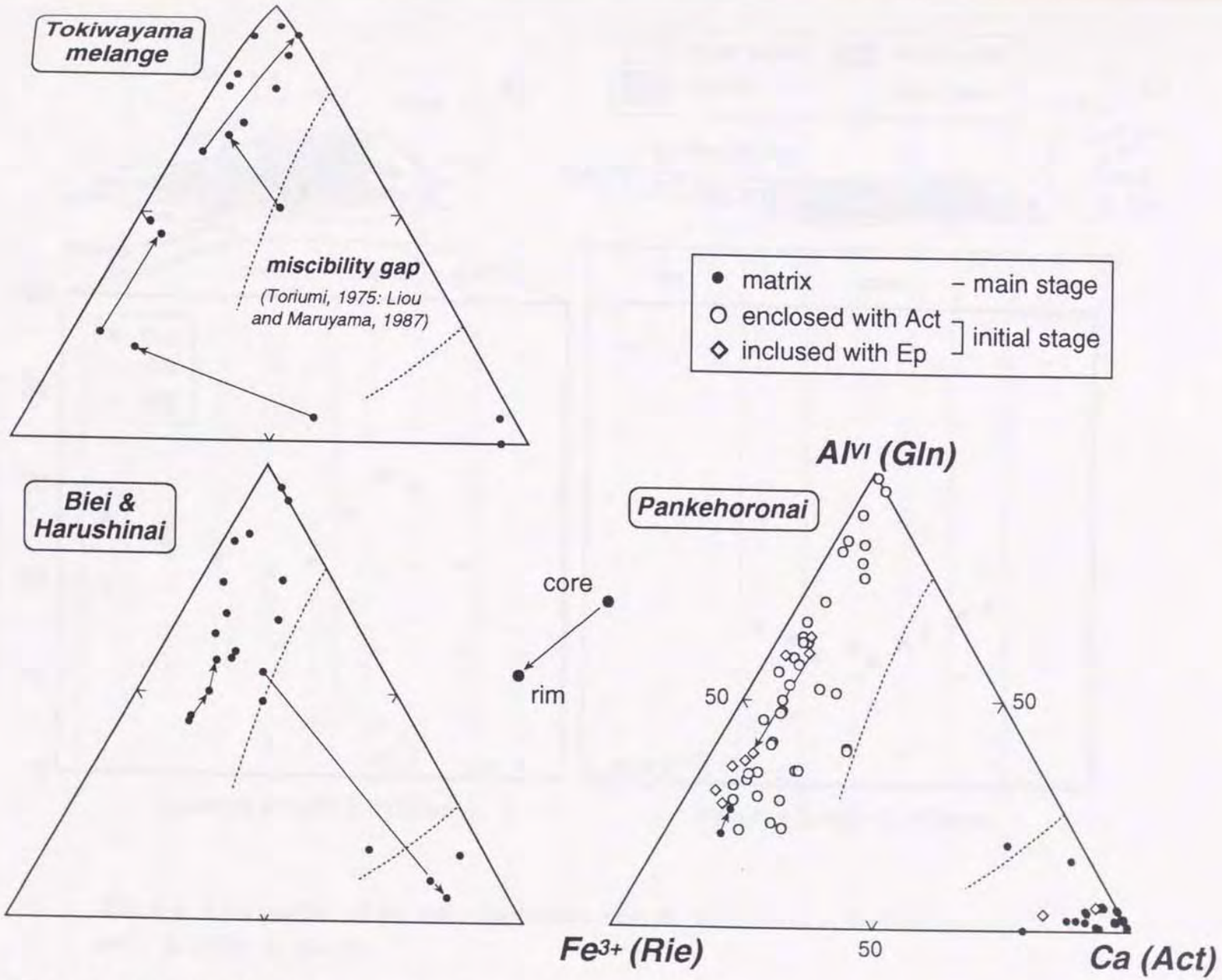

Fig. 5-3. Gln-Rie-Act diagram of sodic amphiboles from the metabasic rocks in all units around the Kamuikotan Gorge.

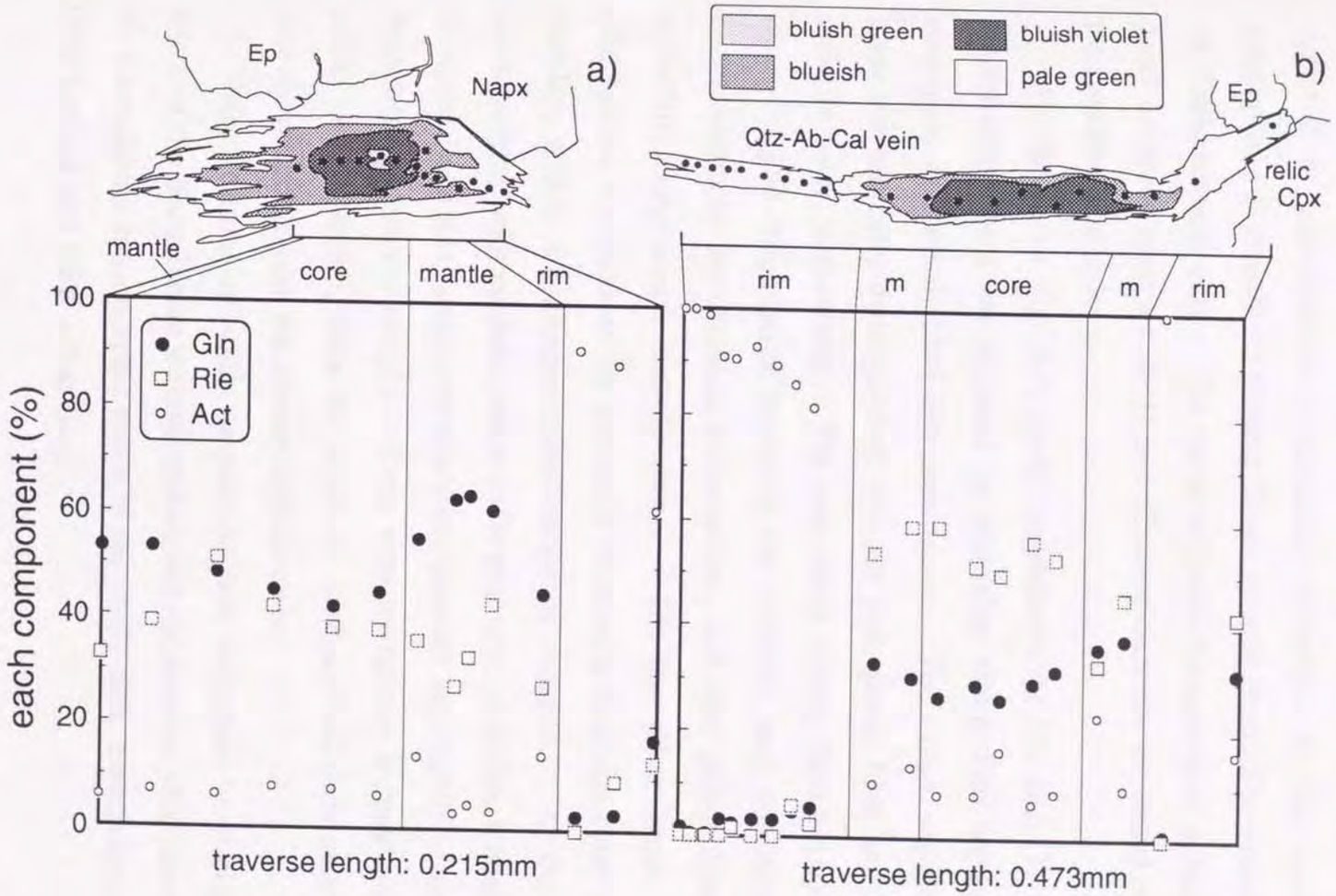

Fig. 5-4. Line profiles of the sodic amphiboles from the basic rocks in the Pankehoronai unit. **a**, K428. **b**, K4168.

towards the rims, except that some of them in the Biei unit have actinolite rims. On the other hand, the rims of sodic amphiboles of (4) are depleted in glaucophane components compared to the cores and glaucophane or crossite of (1) and (2) are entirely rimmed by actinolite in the Pankehoronai unit. The compositional changes were analyzed in detail for some crossites of (1) and (2) to characterize the initial stage in the Pankehoronai unit.

As shown in Fig. 5-4, sodic amphiboles of (1) and (2) in the Pankehoronai unit are replaced by actinolite along their fringes and cleavages, and are divided into some parts. Their rims, mantles and cores are optically distinguished, and are pale green, blue and bluish violet in color, respectively. The boundaries among them are optically clear. The boundaries between the mantles and the rims are discontinuous in the chemical compositions, and their glaucophane and actinolite components largely vary. On the other hand, their glaucophane components are gradually increasing from the cores to the mantles, within the compositional range of crossite. At the rims accompanying with epidote and/or sodic pyroxene, a similar tendency is recognized and their sodic amphibole components are slightly increasing toward the outermost margin. Some rims overgrown in quartz-albite-calcite vein, however, show the opposite tendency and their outermost rims are actinolite with the almost ideal formula.

These features of sodic amphiboles are important to clarify the nature of the Kamuikotan metamorphism and the metamorphic history of the Kamuikotan metamorphic rocks in the study area, especially in the Pankehoronai unit (Ota, submitting).

Lawsonite

Lawsonite commonly occurs in the basic rocks of the Tokiwayama melange unit, and occasionally appears in the Biei and Pankehoronai units. It is usually idioblastic lath and defines the schistosity together with chlorite and phengite. Lawsonite in the Tokiwayama melange unit coexists with sodic amphibole, pumpellyite or sodic pyroxene (Fig. 4-3a), although it does not contact with sodic amphibole in the Biei and Pankehoronai units. Some lawsonites that are relatively fine-grained in the Pankehoronai unit occur as decussate aggregates with hematite in amygdules, form lenticular aggregates in matrix, and scatter in albite and quartz vein. They have rounded shapes that it seems to be received a resorption after Gouchi (1983). Some lawsonites in vein are replaced by pumpellyite and phengite, and those aggregates in amygdules are cut by a veinlet of epidote and chlorite.

Chemical compositions of lawsonite are shown in Fig. 5-5 and appendix 1d. The compositions are close to the ideal structural formula, $CaAlSi_2O_8 \cdot 2H_2O$ with a noticeable substitution of Fe^{3+} for Al. The Fe_2O_3 content of lawsonite in the Biei unit is higher than that in the other units, reaches up to 2.6 wt.%. The compositional range of lawsonite in the Pankehoronai unit is included in that of the Tokiwayama melange unit. Although the Fe^{3+} contents of lawsonite vary considerably from grain to grain. Lawsonite in the Biei unit is associated with sodic pyroxene that is rich in Fe^{3+} (aegirine-jadeite or aegirine), while that coexisting with pumpellyite and sodic amphibole in the Tokiwayama melange unit is poorer in Fe^{3+} than the others. The appearances and compositions of pumpellyite, sodic pyroxene and sodic amphibole may affect the Fe^{3+}-Al substitution in lawsonite.

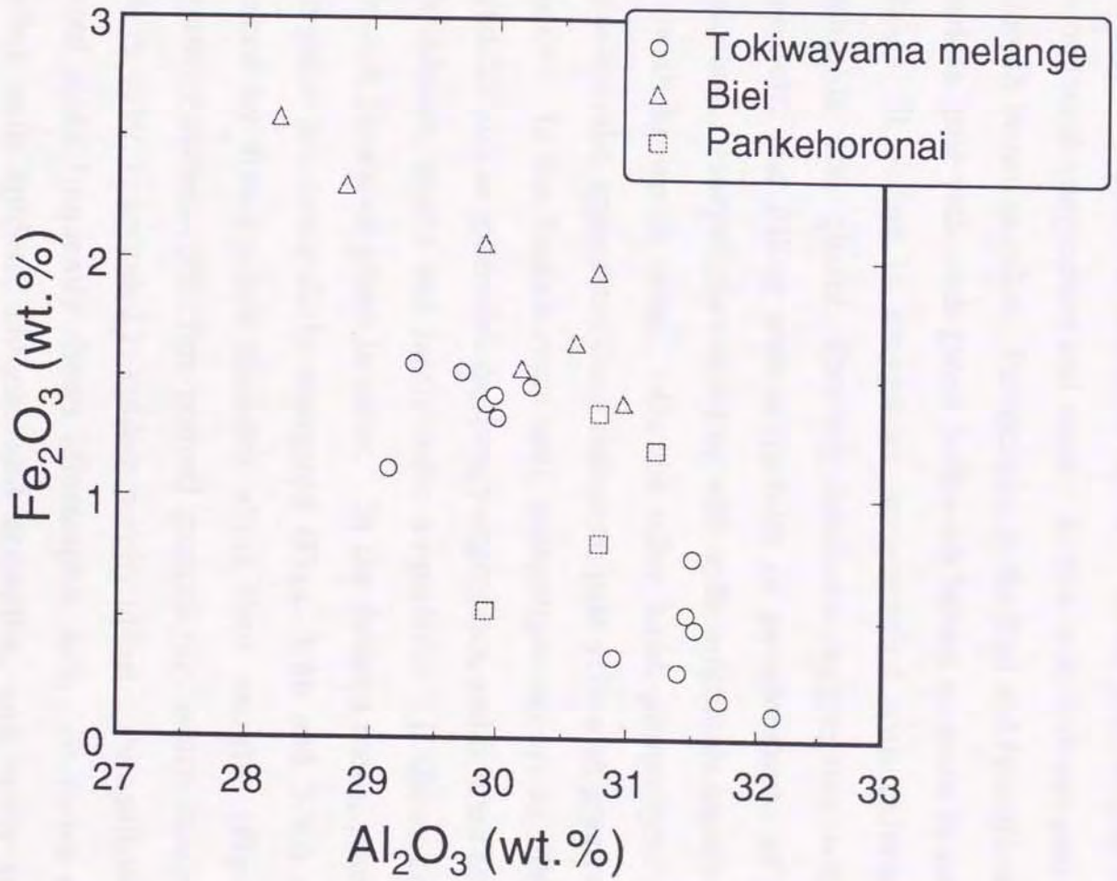

Fig. 5-5. Chemical composition of lawsonite shown in Fe_2O_3 versus Al_2O_3 diagram.

Pumpellyite

Pumpellyite appears widely in the basic rocks of all units, and displays a variety of forms and colors. In the Tokiwayama melange unit, it is colorless to pale yellowish green in color, and forms the schistosity with sodic amphibole dominant layers. Some pumpellyite occurs as monomineralic aggregates and veins. In this case, it shows pale green or yellowish brown in color. Pumpellyite in the Biei and Harushinai units is colorless, pale yellowish green, yellowish brown or green in color (Fig. 4-3a). It occurs in amygdules accompanied with chlorite, sodic amphibole and quartz, forming lenticular aggregates with sodic amphibole, and filling with amygdules or pseudomorphs of primary plagioclase. Pumpellyite coexisting with sodic amphibole mainly exhibits yellowish brown in color. On the other hand, pumpellyite forming monomineralic aggregates show colorless, pale yellowish green or green in color. In the Pankehoronai unit, pumpellyite occurs as filling with amygdules and as spherulitic or spongy aggregates, and is often associated with chlorite, quartz and rarely sodic amphibole. It shows colorless, yellowish brown or green in color. In the foliated rocks, pumpellyite aggregates are lenticularly elongated (Figs. 3-8b and 3-9c) and are replaced by fine-grained epidotes along their margins (Fig. 4-3b). Sometimes xenomorphic fine-grained pumpellyite, which exhibits pale green in color, is included in epidote porphyroblast. Pumpellyite in the foliated rocks frequently shows idiomorphic lath. It forms clusters together with epidote, chlorite and actinolite, and rarely replaces lawsonite in quartz and albite veins. Such an idiomorphic pumpellyite is colorless to pale green in color and shows optical zoning with deeper color in the core than the rim.

Representative analyses are given in appendix 1e. In the present study, structural formulae for pumpellyites have been recalculated by assuming total cations = 16 (Cooms *et al.*, 1976), and Fe^{3+} and Fe^{2+} were calculated based on O = 24.5. The compositional variation of pumpellyite is shown in Fig. 5-6. The Al-Fe*-Mg diagram after Cooms *et al.* (1976), where Fe* indicates total Fe as Fe^{2+}, suggests that the compositions of pumpellyite in the study area are mainly under the control of Fe^{3+}-Al substitution. The Mg content also is not constant, suggesting Mg-Fe^{2+} substitution, but its variety is relatively minor. The chemical composition of pumpellyite in the Pankehoronai unit is slightly higher in the Al content than that in the Tokiwayama melange, Biei and Harushinai units, although that in each unit considerably varies within a thin section according to the mode of occurrence or color. The pumpellyite showing deeper color, e.g., the cores of aggregate and lath-shaped crystal, contain lower Al and higher Fe* than that of the others with light color. The pumpellyite occurring as monomineralic vein, which exhibits colorless to pale green in color, in the Tokiwayama melange unit is higher in Al content than any pumpellyite in the analyzed specimens. The pumpellyite showing yellowish brown in color which is associated with sodic amphibole in the Biei unit and the pale greenish pumpellyite included with epidote porphyroblast in the Pankehoronai unit are rich in Fe* content within the same thin sections (Fig. 5-6a). In addition, the Fe^{3+} content of pumpellyite also shows the above tendency. The $X_{Fe^{3+}}$ ($=Fe^{3+}/(Fe^{3+}+Al)$) of pumpellyite in the Tokiwayama melange, Biei and Harushinai units, which reaches up to 0.26, is larger than that in the Pankehoronai unit (Fig. 5-6b). The pumpellyites with yellowish brown to green in color, which are the cores of aggregate and

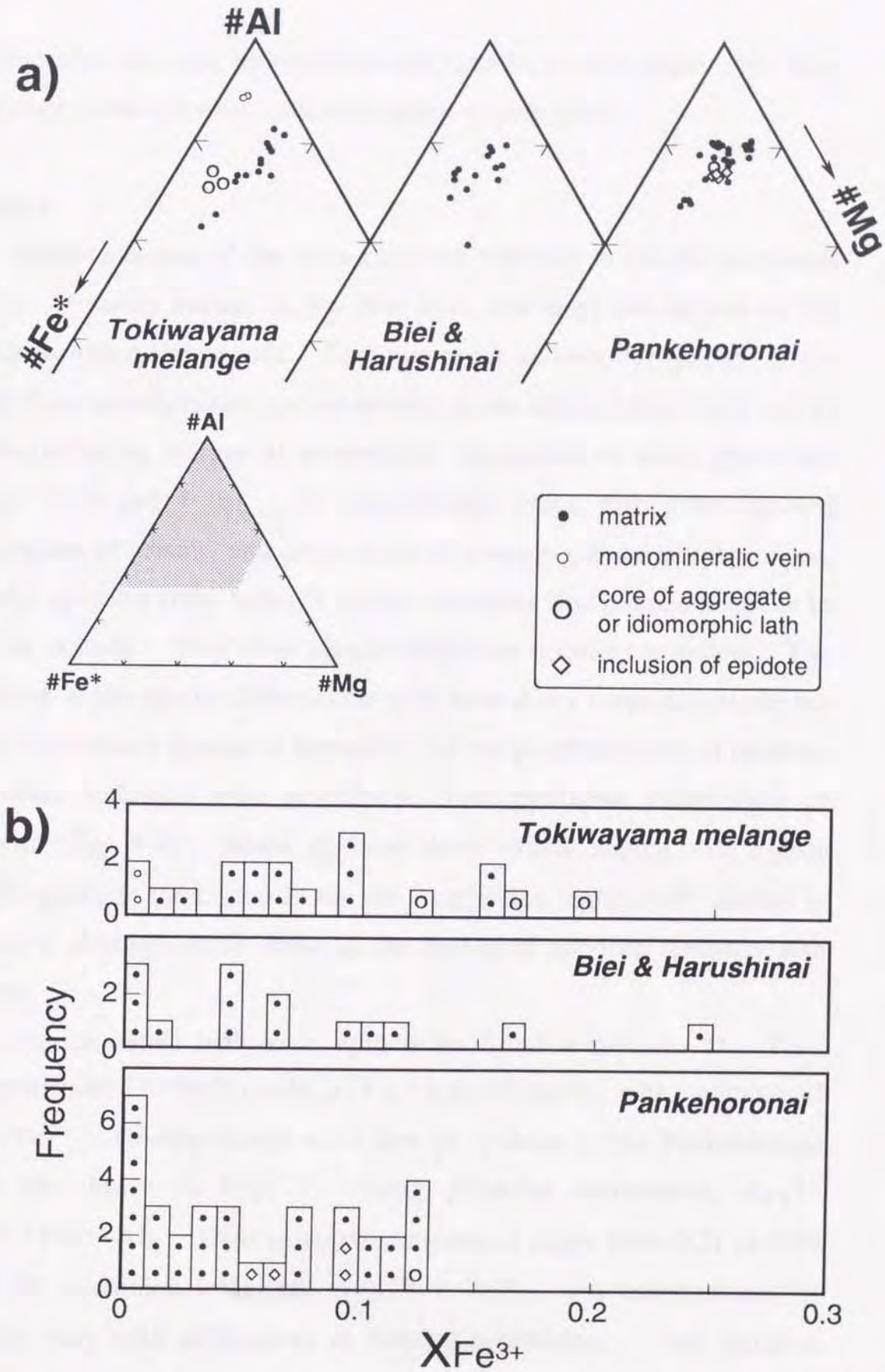

Fig. 5-6. Compositional variation of pumpellyite in the basic rocks. **a**. #Al-#Fe*-#Mg diagram, **b**. frequency distribution diagram of XFe^{3+}.

idiomorphic lath, and are included with epidote, contain higher Fe^{3+} than the others with colorless, yellowish green or pale green.

Epidote

Epidote is one of the most common minerals in the Pankehoronai unit. It rarely occurs in the Biei unit, and does not appear in the Tokiwayama melange unit. Epidotes occur as irregular patches in the matrix, as xenomorphic crystals around quartz-albite-calcite vein, and as replacing along margin of pumpellyite aggregates or sodic pyroxenes (Figs. 3-7b and 4-3b). In well-foliated rocks, they form layered aggregates of prisms, and often occur as coarser-grained porphyroblast. Rarely, epidotes show helicitic texture including fine-grained hematite in tabular crystals. They show pleochroism from colorless to yellow. The epidotes in the quartz-albite-calcite vein have dusty cores accompanying with fine-grained sphene or hematite, and the porphyroblasts of epidotes are often including sodic amphibole, sodic pyroxene, pumpellyite or chlorite (Fig. 4-4). Some epidotes show optical zoning with higher birefringence in the core than the rim, suggesting higher Fe^{3+} content in the core, although those showing the zoning of opposite tendency also appear.

Representative analyses of epidote are listed in appendix 1f. They are recalculated to the formula, $X_2Y_3(Al, Si)_3O_{12}(OH)$, with assuming all Fe is Fe^{3+}. Compositional variations of epidotes in the Pankehoronai unit are shown in Fig. 5-7 using pistacite component, $X_{Fe^{3+}} = Fe^{3+}/(Fe^{3+}+Al)$. Their pistacite components range from 0.21 to 0.39 with the maximum frequency at 0.30 to 0.32. The compositions of epidote vary with differences in mineral assemblage. The pistacite components of epidotes tend to decrease from hematite-bearing to sodic

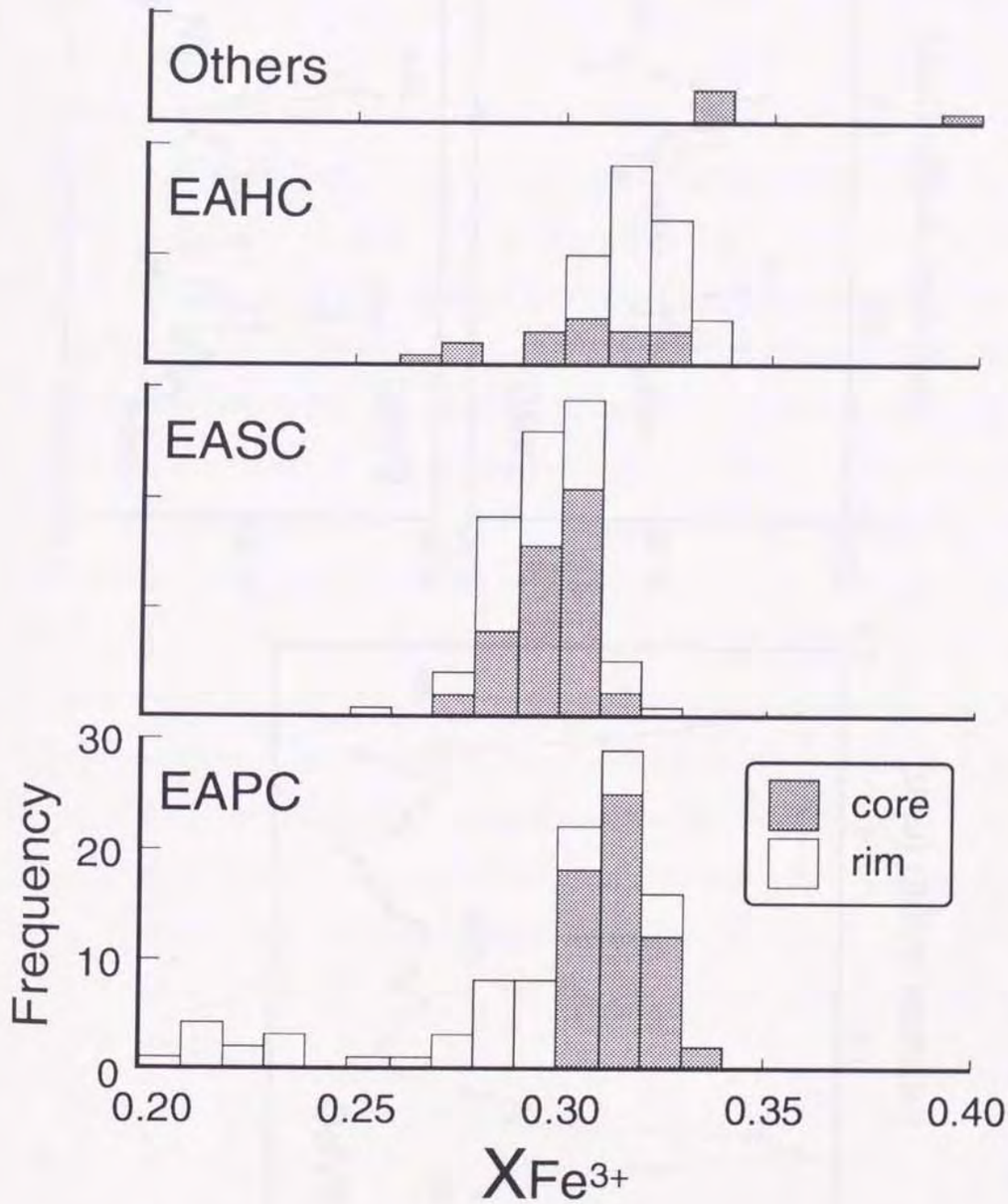

Fig. 5-7. Compositional variations of epidote shown in frequency distribution diagram of pistacite component; $X_{Fe^{3+}} = Fe^{3+}/(Fe^{3+}+Al)$.

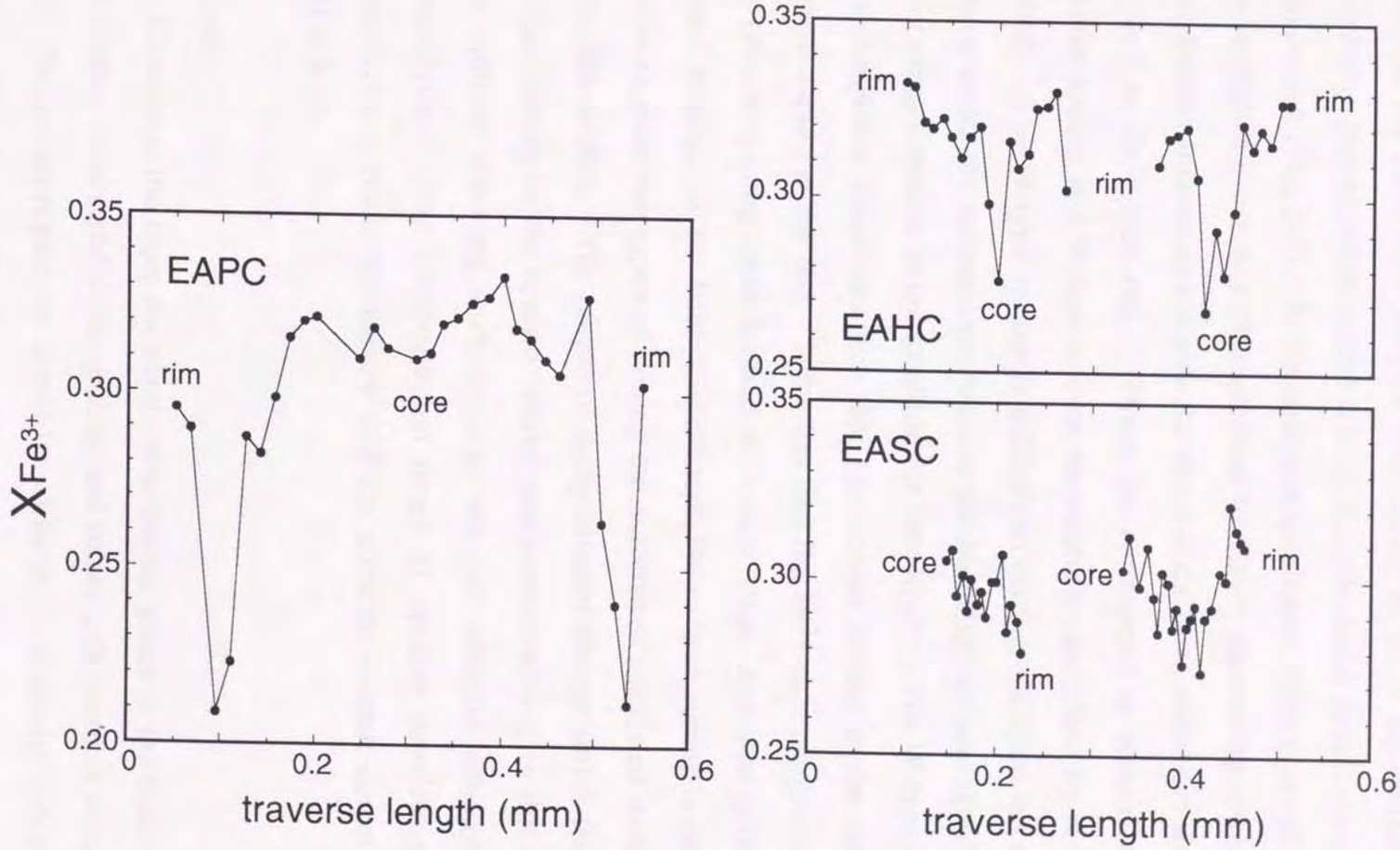

Fig. 5-8. Chemical variations from core to rim of pistacite component in epidotes.

pyroxene-bearing and pumpellyite-bearing rocks in this order, although those of the outermost margins considering to be in equilibrium with coexisting phases rather scatter due to variable zonal structures within a thin section (Fig. 5-8). In the analyzed specimens, three types of zoning are recognized; one is a characterized by $X_{Fe^{3+}}$ decreasing towards the rim, another increasing towards the rim and the third with Fe^{3+} rich core as well as Fe^{3+} rich rim. These are correspond to normal zoning, reverse zoning and W-type zoning, respectively, described by Nakajima (1982). The W-type zoning is difficult to distinguish from the reverse zoning under the microscope, because the birefringence and interference color are insensitive to composition for low $X_{Fe^{3+}}$. The W-type zoning is a composite zonal structure that has normal zoning in the core and reverse zoning at the rim. It implies that the Fe^{3+}-rich margin (also of the reverse zoning) was formed at a later stage than that producing normal zoning. In the Pankehoronai unit, the reverse zoning is common and more than two types of zoning are sometimes identified within the same thin section. The ranges of compositional change shrink from the W-type zoning to the reverse zoning and normal zoning in this order. The epidote showing such zonings are not directly contact with pumpellyite. The compositional range of epidote coexisting with pumpellyite is relatively narrow and the pistacite content ranges from 0.30 to 0.33.

Chlorite

Chlorite is the most abundant metamorphic phase in the basic rocks as a whole. It is usually fine-grained and shows pale green in color, and often forms aggregate in irregular shaped. Chlorite occurs as replacements of primary clinopyroxene or basaltic groundmass, and in

amygdules with pumpellyite. It occasionally defines a schistosity as layers with actinolite or lawsonite (Fig. 4-3). Some chlorite forms clusters with epidote, calcite and phengite around albite and quartz veins in the Pankehoronai unit. In highly foliated rocks, chlorite defines the schistosity as the layers together with epidote porphyroblast and as the arrangements of coarser-grained tabular crystal. Such chlorites show distinct pleochroism with yellow to green in color.

Chemical compositions of chlorite are listed in appendix 1g. The cation numbers per 28 oxygens are calculated by the assumption that all iron is ferrous. According to Hey's (1954) diagram, most of analyzed chlorites correspond to pycnochlorite and some of them do to brunsvigite or diabandite. As shown in Fig. 5-9, the chemical compositions of chlorite considerably vary in the X_{Mg} (= Mg/(Mg+Fe)) by the difference of mineral assemblage reflecting the bulk rock composition. Such a feature is distinct for chlorites in the basic rocks with high-variance assemblage (less than three phases) in the Pankehoronai unit, and their X_{Al} (= Al/(Al+Mg+Fe)) slightly increases with decreasing in the X_{Mg}. On the other hand, the X_{Al} of chlorites with low-variance assemblage is nearly constant for individual specimens and the X_{Mg} of them also occupies a relatively narrow range.

Calcite/Aragonite

Carbonate in the studied basic rocks is calcite and aragonite (Fig.4-2). Aragonite was stained by means of Feigl's solution and was identified under the microscope. Calcite appears throughout the all units and commonly occurs as xenomorphic crystal in albite and quartz vein. In the Pankehoronai unit, it often coexists with acicular actinolite, deeper colored chlorite, and coarser-grained epidote and phengite, while it never

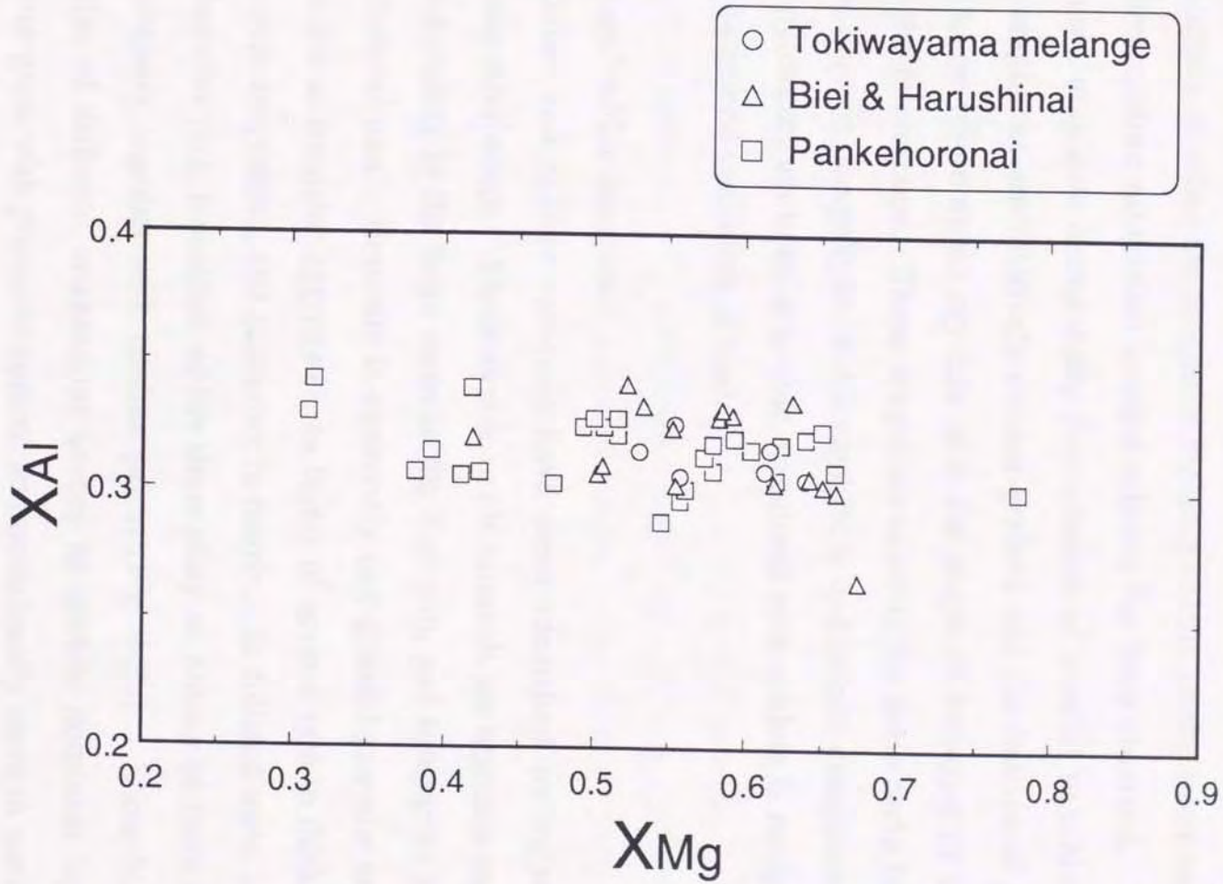

Fig. 5-9. Chemical compositions of chlorite in the basic rock shown in XAl versus XMg diagram.

occurs in the domain with pumpellyite and lawsonite. Aragonite occurs as aggregates of tiny crystals which replace along cleavages, fringes and boundaries of calcite grains. Some aragonite occurring in the Pankehoronai unit irregularly scatters within calcite grains. Although it is uncertain whether the aragonite replaces calcite or the latter includes the former, since no distinct textural relation has been observed. In the Biei unit, aragonite occasionally forms layers of parallel to schistosity. Such aragonites are relatively coarser-grained and the individual grains seem to be idiomorphic crystals with the shape of hexagon or square under the microscope. These aragonites occur in the basic rocks bearing deeper colored pumpellyite, sodic amphibole and jadeite component-rich sodic pyroxene, while no aragonite associated with epidote is recognized in the examined specimens at least.

Oxide and sulfide minerals

Oxide and sulfide minerals have been identified by means of reflecting microscope. Metamorphic oxide minerals are hematite and are detected mainly in the basic rocks in the Biei unit, and sometimes in the Pankehoronai unit. Hematite is commonly fine-grained granular crystal and occurs as irregular aggregates, as layers of several mm in thickness, filling with amygdules, and scattering in matrix. In foliated rocks of the Pankehoronai unit, hematites which show platy or blocky in form align on schistosity together with epidote prism (Fig. 4-3b). Some blocky hematites of different orientations scatter in epidote dominant layers. They intergrow with prismatic epidote and occasionally seem to surround the epidote. Sometimes the hematite cuts the elongations of acicular actinolite and lepidoblastic chlorite that define the schistosity. So far as

examined by the electron-probe microanalyser, the hematite is nearly pure Fe_2O_3 and contains low TiO_2 (about 1 wt.%).

Sulfide minerals are mainly pyrite in the basic rocks of the Pankehoronai unit. Minor accounts of them are usually square in form under the microscope and occur as scattering in matrix. They are partly or almost altered to limonite-like minerals.

Other minerals

Sphene is an accessory, but ubiquitous phase in most basic rocks throughout all units. It occurs as dusty aggregates of tiny granules in matrix and around both igneous and metamorphic clinopyroxenes with chlorite. In the foliated rocks of the Pankehoronai unit, sphene is relatively coarser and sometimes exhibits idiomorphic shape. Microprobe analyses of examined sphene are shown in appendix 1h. The chemical compositions indicate that the examined sphenes are close to Ti end-member component $CaTiSiO_5$ and contain low Al_2O_3 (0.85 - 2.73 wt.%) and Fe_2O_3 (0.75 - 2.71 wt.%). This tendency is particularly distinct for the sphene with epidote and actinolite in the foliated rocks. On the other hand, the sphenes in rocks bearing aegirine component-rich sodic pyroxene contain higher Fe^{3+} and Al than the others.

Phengite is the major potassium-bearing phase in the basic rocks of the study area. It forms schistosity together with chlorite and actinolite in the fine-grained rocks, e.g., metamorphosed volcanic sediments. The other phengite occurs as a minor phase in vein or amygdule. Phengites are usually fine-grained and rarely show pale green in color. Some of them in the Pankehoronai unit is coarser-grained and occurs as idiomorphic tabular crystals, which form clusters with prismatic epidote and deeper colored chlorite in albite-quartz-calcite vein. Compositions

of analyzed phengite are listed in appendix 1h, where calculating as O=22. The phengite in the examined specimens ranges in Fe*+Mg from 1.32 to 1.96, Al from 3.11 to 3.76, Si from 7.04 to 7.54 and Na from 0.003 to 0.03, except for one analyzed point (specimen K4-70). Similar to chlorite, the compositional variation is apparent within a thin section, controlled by the tschermak substitution (Mg, Fe^{2+})$SiAl_{-1}Al_{-1}$ (e.g., Miyashiro and Shido, 1985). The phengite in the Biei unit contain higher Fe*+Mg and lower Al than that in the Pankehoronai unit, although the significance of this tendency is uncertain. Because the above compositional variation is in part due to the bulk composition, in part the uncertainty in the Fe^{2+}/Fe^{3+} ratio and in part due to the persistence of earlier composition during progressive and/or retrogressive processes.

Stilpnomelane appears in the basic rocks bearing hematite, aegirine component-rich sodic pyroxene, and chlorite being low in X_{Mg}, and as idiomorphic acicular crystals. It shows pleochroism from pale brown to brown in color, and often forms radiating aggregates in matrix or albite and quartz domain.

Minor quartz occurs in most of the basic rocks studied and mainly in vein and as thin layers with albite. It is rare that quartz is mixed with matrix consisting of Ca-Al silicates, amphiboles, sodic pyroxene and chlorite.

Albite is ubiquitous and appears as minor phase in the basic rocks of all units. It commonly occurs with quartz in vein or lamina, and often coexists with sodic pyroxene and the other metamorphic phases in matrix. In the foliated rocks of the Pankehoronai unit, spotted albites (less than 1 mm in size) are observed. They occasionally show helicitic textures including with fine-grained actinolite and chlorite.

5-2. Pelitic and psammitic rocks

Phengite

Phengites are chief mineral phase in the pelitic and psammitic rocks, and constitute almost their fabrics such as schistosity, fold axial cleavage and so on. They occur as not only discrete metamorphic minerals on the S1-, S2- and S3-foliation but also constitutions of detrital grains remaining on the S1-foliation (Figs. 3-7b and 3-9c).

On the S1-foliation, detrital grains of quartz, feldspar (plagioclase and/or alkali-feldspar) and muscovite, and fragments of tuff are remaining. Detrital feldspars are partly replaced by tiny crystals of phengite with albite and minor calcite. Detrital grains of colorless muscovite are also recrystallized, however, the conversion of their chemical compositions is incomplete, as shown in their ranges and heterogeneity of compositions described below. The pale greenish fragments of tuff, the most coarse of the detritus, have similar natures to the detrital muscovites. Metamorphic phengites on the S1-foliations in pelitic rocks are commonly fine-grained and fibrous, and are accompanied with chlorite, albite and quartz. They include abundant carbonaceous materials and seem to be dusty. Phengites of the Tokiwayama melange unit are coarser-grained and often form platy bundles due to elongations during the later stage. The phengites, which intergrow with stilpnomelane, are clear and rarely show pale green color due to including no carbonaceous materials. Phengites on the S2-foliations occur as constitutions of C- and C'-surface of the S-C-C' structure. The phengites, which are fine-grained and fibrous, are associated with carbonaceous materials, chlorite and albites, and seem to be pale brown in color. Phengites on the foliations in pelitic schists of

the Pankehoronai and Tokiwayama melange units are relatively coarse-grained flakes and mainly colorless, and form layered domains with minor chlorites. In the Tokiwayama melange unit, the phengite are also associated with stilpnomelanes and minor actinolites. In addition, phengites of pressure shadows around detrital grains of muscovite and fragments of tuff are also regarded as those of the S2-foliation. They are fine-grained and are rarely associated with chlorites. The phengites are commonly colorless and some of them show pale green color. Metamorphic phengites on the S3-foliations in pelitic rocks of the Harushinai and Biei units are very fine-grained and are not accompanied with chlorites. They include abundant carbonaceous materials and seem to be dusty as well. Phengites of the Pankehoronai and Tokiwayama melange units are coarser-grained and form aggregates with small amounts of chlorite and carbonaceous material.

Besides of the above occurrences, metamorphic phengites occur as tiny needles in quartz-albite layers and as inclusions within spotted albites or porphyroblasts of sphenes. The quartz-albite layers correspond to the S1-foliations as bedding planes of the pelitic rocks and are cut by the S3-foliations, but textures suggesting the stage produced phengites in the layers have not been found. Although the spotted albites and porphyroblasts of sphenes often overgrow with cutting the S2-foliations, most of spotted albites with helicitic textures are post-tectonic against the S3-foliations. These textural relations suggest that the spotted albites and porphyroblasts of sphenes had been grown during and after the D3 stage, however, the stage formed phengites as inclusions is uncertain. The phengites described below are not included those in the uncertain stage.

Chemical compositions of phengite in the pelitic and psammitic rocks are shown in Figs. 5-10, 5-11 and 5-12, and appendix 2a. The

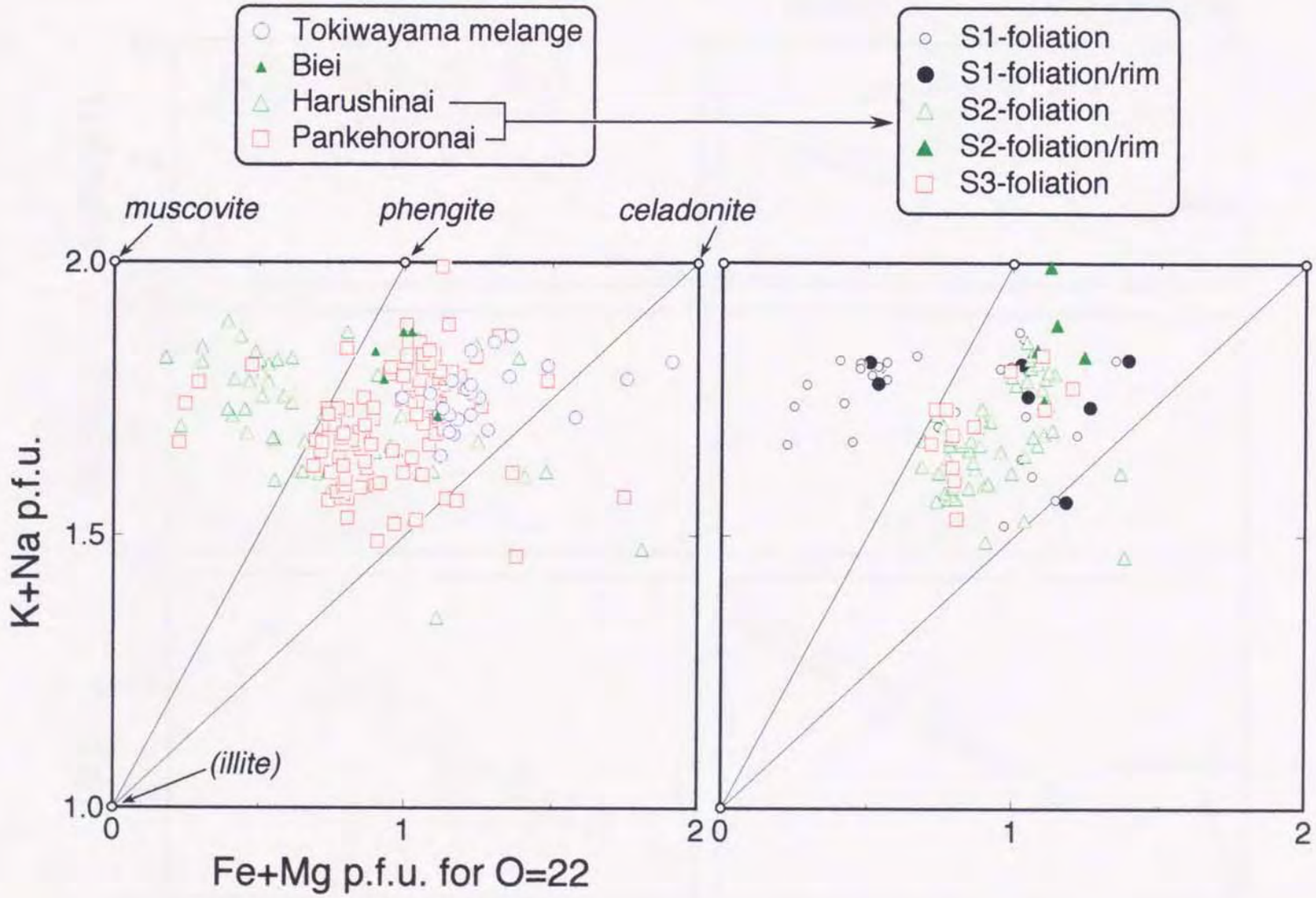

Fig. 5-10. Chemical compositions of phengite formed on the S1-, S2- and S3-foliation for the pelitic-psammitic rocks in the Kamuikotan Gorge area. **a.** (K+Na) versus (Fe+Mg) plots.

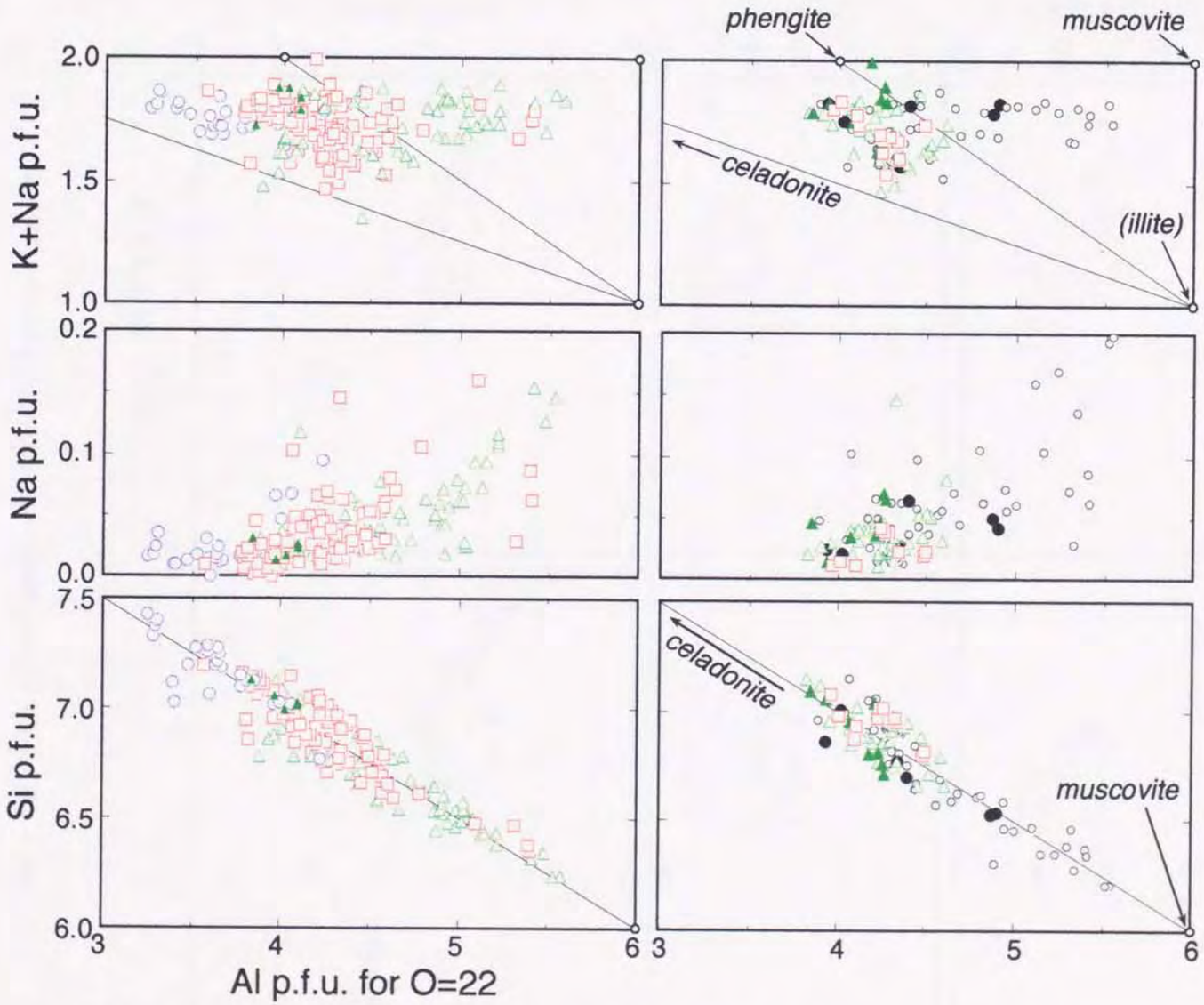

Fig. 5-10. b. (K+Na) versus Al plots. Symbols are the same as Fig. 5-10a.

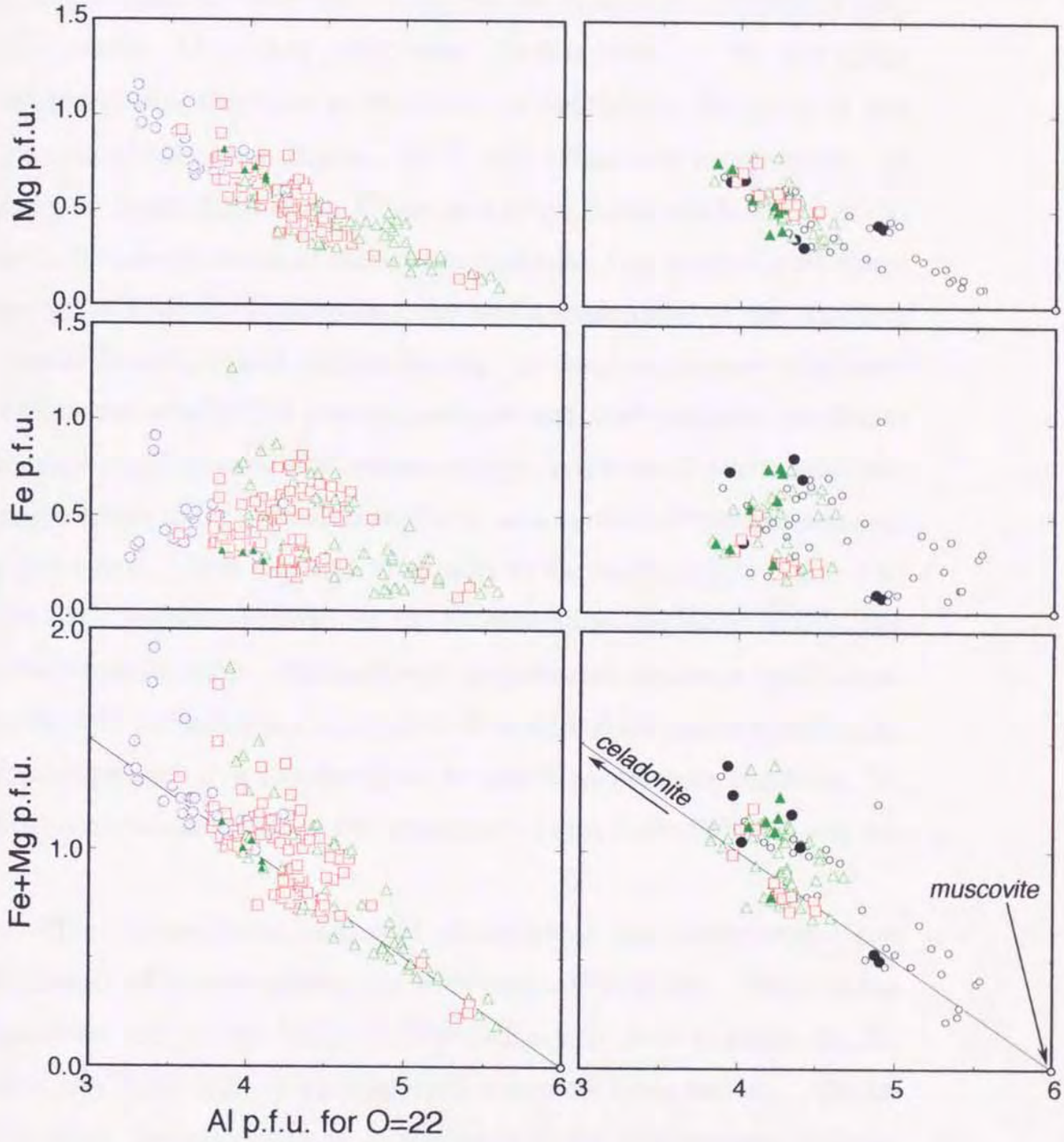

Fig. 5-10. c. (Fe+Mg) versus Al plots. Symbols are the same as Fig. 5-10a.

compositions of phengites obviously vary by differences of units and foliations (stages), controlled mainly by the tschermak substitution (Mg, Fe^{2+})$SiAl_{-1}Al_{-1}$ (Miyashiro and Shido, 1985). In low-grade metamorphism, the illite substitution (vacancy)Si(K, Na)$_{-1}$Al$_{-1}$ is also effective (Wang and Banno, 1987) and influences compositions of phengites in the Kamuikotan Gorge area (Figs. 5-10a and 5-10b). In this thesis, the atomic ratios of phengite are calculated by assuming all iron is ferrous and O=22. However, the slight departures of the analyses towards lower Al and higher Fe+Mg values (i.e., higher celadonite content characterized a low-temperature and high-pressure condition) from the stoichiometric line, shown in Figs. 5-10b and 5-10c suggest that the phengites in the Kamuikotan Gorge area contain substantial amounts of ferric iron. This fact clearly appears in the Al-Fe plot in Fig. 5-10c, with less correlation between Al and Fe contents on the lower Al side than on the opposite side. Although such a systematic tendency results from the Al-Fe^{3+} substitution and seems to be a critical feature in pelitic rocks metamorphosed at a low-temperature and high-pressure condition, its detail is abbreviated due to the uncertainty in the Fe^{2+}/Fe^{3+} ratio in this thesis.

The compositional ranges of phengites in the Pankehoronai and Harushinai units overlap over the wide range (Fig. 5-10). Those in the Harushinai unit are markedly variable and extend towards higher Al, Na and K+Na values (i.e., toward an ideal muscovite composition). On the other hand, the compositions of phengites in the Tokiwayama melange unit are apparently higher in Si and Fe+Mg than those of the other units, and are enriched in celadonite component (Fig. 5-10). The compositional ranges of phengites in the Biei unit occupy the middle field between those of the Tokiwayama melange unit and the Pankehoronai and

Harushinai units. The Si content and X_{Na} (=Na/(K+Na)) of phengites are 6.77-7.43 and 0.00-0.05 in the Tokiwayama melange unit, 7.00-7.13 and 0.01-0.02 in the Biei unit, 6.61-7.20 and 0.00-0.03 in the Pankehoronai unit, and 6.23-7.13 and 0.01-0.15 in the Harushinai unit, respectively (see appendix 2a). To examine the obvious compositional variations of phengites, particularly in the Pankehoronai and Harushinai units, in detail, the plots by each foliation are also shown in Fig. 5-10. The plots of the Pankehoronai and Harushinai units are not classified at these diagrams because the compositions of phengites on the foliations formed during the same stage have approximately similar ranges and tendencies of change despite a difference of units. Then, the diagrams in Fig. 5-10 indicate that phengites on the foliations of the later stage have less compositional variations than those on the foliations of the earlier stage. In other words, phengites on the S1-foliations have wide compositional ranging from so-called phengite to muscovite, while the compositions of phengites on the S2-foliations are mostly plotted within a relatively narrow range between phengite-illite and celadonite-illite joins. Finally, phengites on the S3-foliations have the most restricted compositions, which are slightly higher in Al than the typical phengite. The chemical zonations of phengites on the S1- and S2-foliations are concordant with the above tendency; the compositions increase in Si and Fe+Mg with decreasing in Al and Na toward the rims, and to become close to the compositions of phengites on the S3-foliations (Fig. 5-10).

Figs. 5-11 and 5-12 show the compositional variations of coexisting mineral phase in pelitic rocks. In the Pankehoronai and Harushinai units, phengites on the foliations formed during the earlier stage are commonly higher in Al, and coexist with chlorites with higher in Al and Fe/Mg ratio than those on the foliations formed during the later stage. Comparing

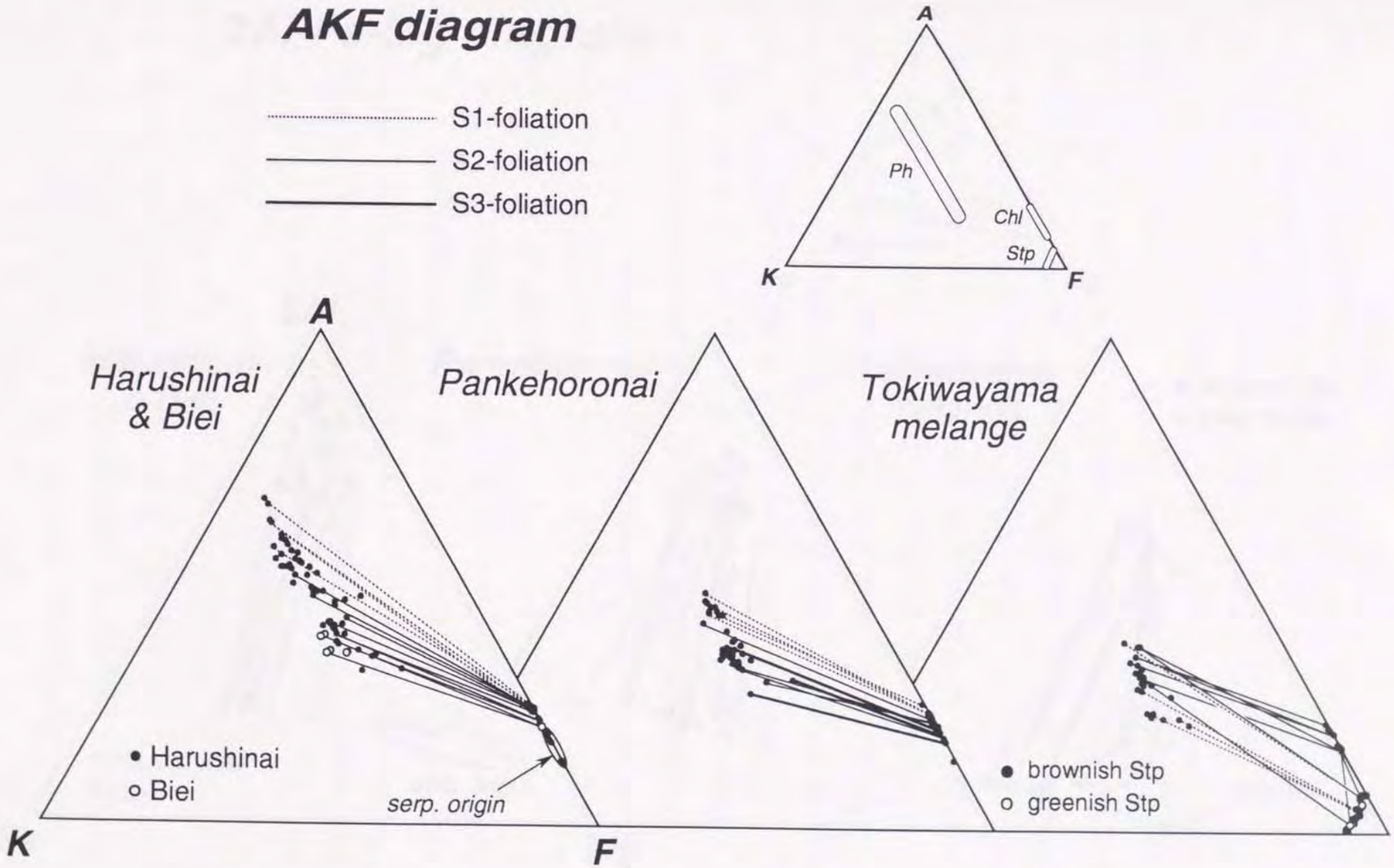

Fig. 5-11 AKF diagrams for the pelitic rocks in the Kamuikotan Gorge area. Tie-lines show pairs coexisting metamorphic mineral phase formed on the S1-, S2- and S3-foliation.

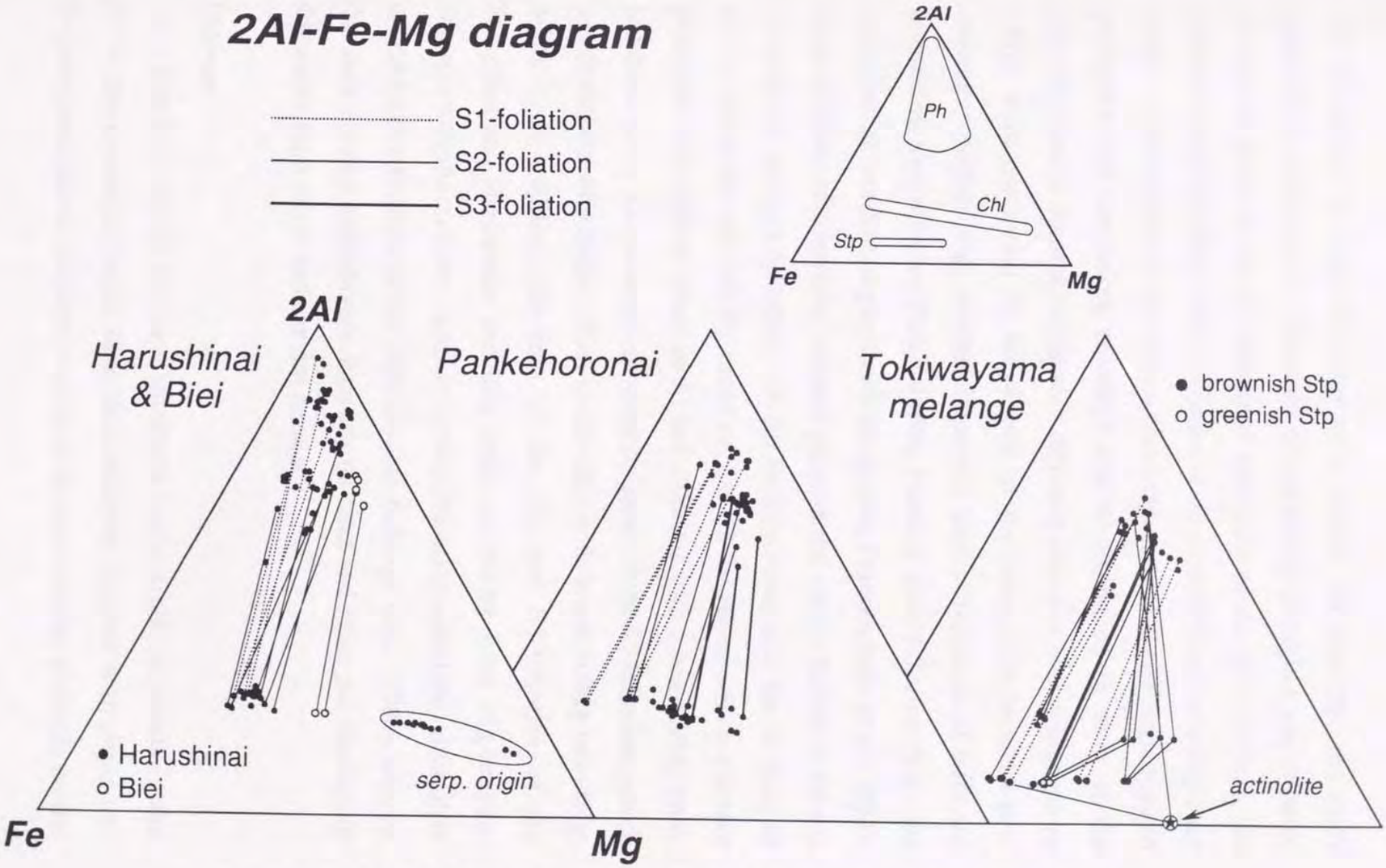

Fig. 5-12 2Al-Fe-Mg diagrams for the pelitic rocks in the Kamuikotan Gorge area, showing compositional variations of coexisting metamorphic mineral phase formed on the S1-, S2- and S3-foliation.

the phengites on each foliation with similar Al contents, the same tendency is recognized. Tie-lines of coexisting phengites and chlorite, except for pairs on the S1-foliations and parts of the S2-foliations, are sliding toward the Mg corner of triangle diagram without crossing each other. Consequently, the above chemically sympathetic variations of phengites and coexisting chlorites can be explained in term of the crystallization in local domains with different effective bulk compositions which were controlled by the degree of the interaction between pre-existing materials (e.g., detrital muscovite and/or fragments of tuff) and circulating metamorphic fluids during forming each foliation (e.g., the formation of interleaved phyllosilicate grains; Franceschelli et al., 1991). Some tie-lines of coexisting mineral pairs on the earlier foliations are cut by those on the later foliation. In the Pankehoronai unit, the tie-lines of the S1-foliations are cut by those of the S2-foliations which connect phengites with slightly lower in Al and chlorites with lower Fe/Mg ratio, and those of the S2-foliations are done by those of the S3-foliations which join phengites with higher in Al to chlorites with lower Fe/Mg ratio (Fig. 5-12). In addition, tie-lines of the S2- and S3-foliation of the Pankehoronai, Harushinai and Biei units are cut by joins of phengite-chlorite-stilpnomelane and/or phengite-stilpnomelane-actinolite assemblages restricted in the Tokiwayama melange unit. These suggest that such mineral assemblages, crossing tie-lines and joins, are chemically discordant each other, and can not coexist.

Chlorite

Chlorites, one of the most common metamorphic minerals in the pelitic and psammitic rocks, form the schistosity together with phengites. As mentioned above, chlorites coexist with metamorphic phengite on the

S1-, S2- and S3-foliation, where the chlorites on the S1-foliations include constitutions of detrital grains. On the S3-foliations in the pelitic rocks of the Harushinai and Biei units, no chlorites are observed and tiny crystals of phengites align. They are commonly fine-grained fibrous crystal, and appear colorless or pale green in color. Some chlorites, coexisting with stilpnomelane in the pelitic schists of the Tokiwayama melange unit, show the pleochroism of pale green to green. In the pelitic rocks of the Harushinai unit, chlorites derived from pebbles of serpentinite form lenticular aggregates surrounding the pebbles. The chlorites show pale greenish color and do not coexist with phengites.

Chemical compositions of chlorites in the pelitic and psammitic rocks are shown in Figs. 5-11, 5-12 and 5-13, and appendix 2b. All diagrams indicate that compositions of chlorites in the pelitic and psammitic rocks considerably change in X_{Mg}, due to the bulk control. In particular, the chlorites of serpentine origin are higher in X_{Mg} than any others. The compositions of chlorites from the Harushinai unit are restricted in relatively narrow range, while the compositional range of those from the Pankehoronai unit is considerably wide. The compositions of chlorites increase in MgO with decreasing in Al_2O_3 as well as those of coexisting phengites (Figs. 5-11 and 5-12). In the Tokiwayama melange unit, the compositions of chlorites markedly change by mineral assemblages, e.g., the chlorites coexisting with stilpnomelane and phengite are enriched in MgO. Generally, the Al_2O_3 content of chlorites coexisting with metamorphic phengites slightly increases with decreasing their X_{Mg} (Figs. 5-11 and 5-12). This is in part due to the differences of the bulk rock composition, as shown in the subparallel sliding of tie-lines in the 2Al-Fe-Mg diagram or the differences of mineral assemblages (Fig. 5-12). In the Harushinai and Pankehoronai units, however, some tie-lines of pairs

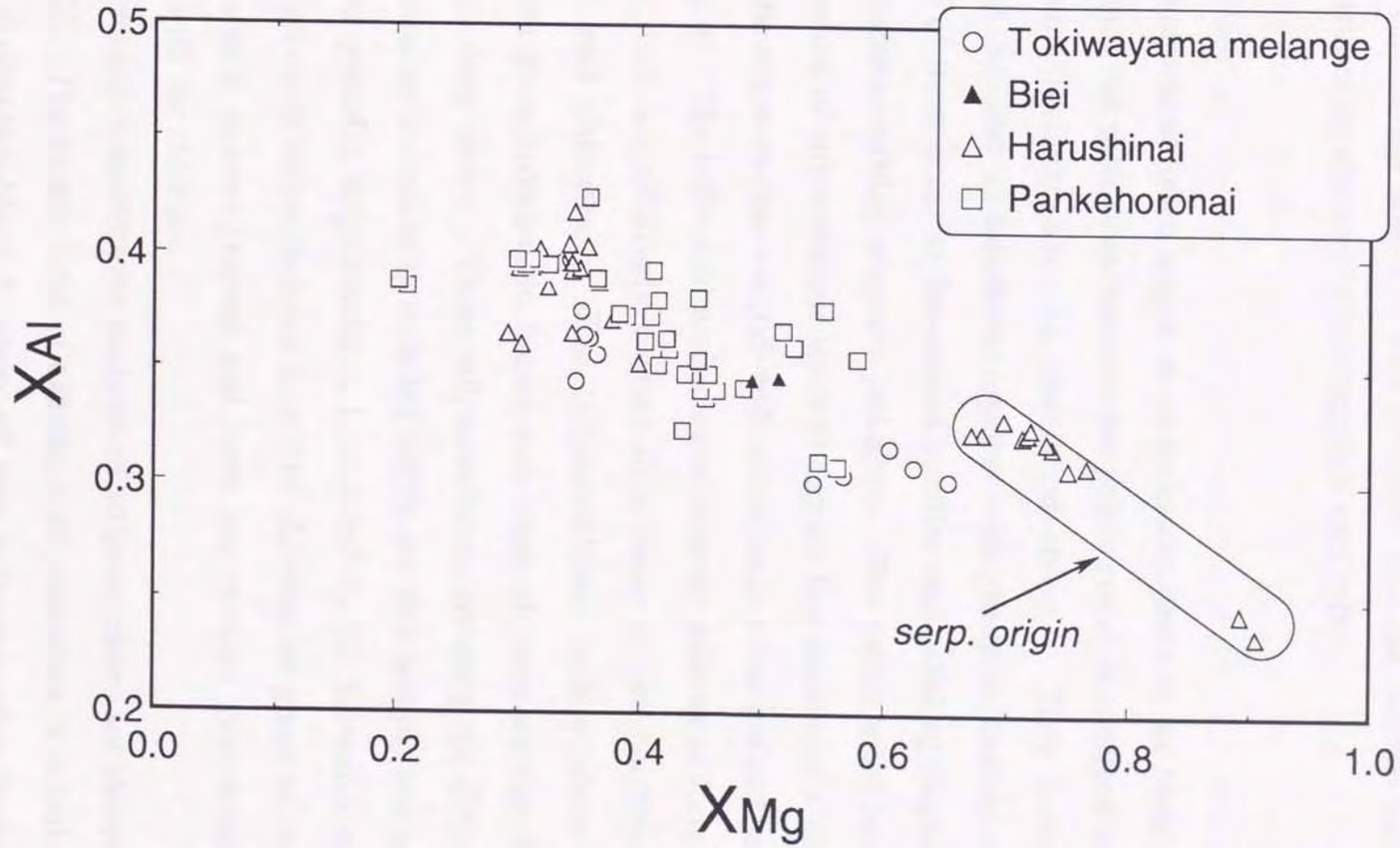

Fig. 5-13 Chemical compositions of chlorite in the pelitic-psammitic rocks shown in XAl versus XMg diagram. Abbreviations are the same as Fig. 5-9.

of phengite and chlorite on the S2- and S3-foliation (the later stage) intersect those of pairs of phengite and chlorite on the S1- and S2-foliation (the earlier stage). This indicates that the mineral pairs of different stages are chemically incompatible each other.

Stilpnomelane

Stilpnomelanes often appear as an accessory phase in the basic rock of each unit, but their occurrence in the pelitic rocks is confined to the Tokiwayama melange unit, as mentioned above. They form the schistosity (S1- and S2-foliations) together with phengites and chlorites, and some of them occur as fan-shaped bundles and radial aggregates in layers or veins consisting of quartz and albite. The pelitic schist bearing a large amount of stilpnomelane tends to contain less amount of chlorite, in which the stilpnomelane coexists with actinolite as a fine-grained needle and phengite. The individual grains are commonly acicular in form and the grain sizes are relatively coarser than those of the neighboring phengites and chlorites. The stilpnomelanes mainly show the pleochroism from colorless to brown and some of them do that from colorless to deep green. These stilpnomelanes, showing the different pleochroisms, are occasionally included within one thin section, and some of the deep greenish stilpnomelanes is mantled by the brownish ones. The deep greenish stilpnomelanes look like chlorites of green in color, but are usually coarser-grained and have the obvious pleochroisms compared with the chlorites.

Representative microprobe analyses of stilpnomelanes are shown in appendix 2c. The atomic ratio of examined stilpnomelane is calculated by Si+Al+Ti+Fe+Mn+Mg=7.5, where all iron is ferrous, after Eggleton (1972). The K_2O content ranges from 0.1 to 6.3 wt.%, and the Fe/Mg

ratio (Fig. 5-12) considerably varies by each specimen. The Al_2O_3 and SiO_2 content are approximately constant, ranging from 5.4 to 6.3, and from 44.4 to 51.0 wt.%, respectively, so the substitutions of Fe*+Mn+Mg by Al, and of tetrahedral Si by Al are not apparent. In the stilpnomelane showing optical zonation, the rim of brown in color is higher in FeO and lower in K_2O than the core of deep green. As mentioned above, the pelitic schists contained abundant stilpnomelane are poor in the amount of chlorite, and the assemblage phengite-stilpnomelane-actinolite tends to appear instead of phengite-chlorite-stilpnomelane (-sphene). The stilpnomelane in the former assemblage, i.e., one coexisting with actinolite, is the highest in FeO, while the stilpnomelane and chlorite in the latter assemblage are obviously enriched in MgO (Fig. 5-12).

Others

Quartz and albite are ubiquitous in the pelitic and psammitic rocks of all units, and commonly form veins or laminae. Fine-grained albites are often mixed with metamorphic phengites, chlorites and carbonaceous materials on the schistosity. In the foliated rocks of the Pankehoronai and Tokiwayama melange units, some quartz is elongated along the schistosity. Sometimes, spotted albites overgrown with cutting the schistosity (less than 2 mm in size), are observed in the pelitic schist of the Tokiwayama melange unit. The albites occasionally show helicitic textures including with fine-grained phengites and carbonaceous materials.

Sphenes appear as an accessory phase in the pelitic rocks of each unit. The occurrence of them in the psammitic rock is minor. Most sphenes are commonly very fine-grained granule, and form aggregates with carbonaceous materials. In the foliated rocks of the Pankehoronai

and Tokiwayama melange units, the sphenes tend to be a coarser-grained and elongated prism. Some of porphyroblastic sphenes includes finer-grained and xenomorphic phengite or chlorite in the pelitic schist of the Pankehoronai unit.

Carbonaceous materials are abundant in the pelitic rocks of all units. They are usually tiny and amorphous, and form aggregates. In relatively massive pelitic rocks of the Pankehoronai and Harushinai units, they are included within metamorphic phengites.

Although small amounts of the Ca-Al hydrosilicates and amphiboles occur in the pelitic and psammitic rocks, besides the above phases, their details are abbreviated.

6. Phengite K-Ar Ages

6-1. Dated specimens

Twenty-one phengites (Tokiwayama melange unit, 2 specimens; Pankehoronai unit, 8 specimens; Harushinai unit, 10 specimens; Biei unit, 1 specimen) separated from the Kamuikotan metamorphic rocks in study area were dated by the K-Ar method. Localities and mineral assemblages of dated specimens are shown in Fig.6-1 and Table 6-1.

Specimens that were systematically collected from each unit of the study area are pelitic-psammitic schist, siliceous schist and basic schist. These schists commonly have deformation microstructures as schistosity, shear plane, pressure shadow, crenulation fold, axial cleavage and so on. Pelitic-psammitic schists consist of pelitic layer that is black in color due to a large amount of carbonaceous material and psammitic layer or lens of several mm. They often intercalate quartz-albite layers ranging from a few to about 10 mm in thickness. Siliceous schists are pale green or gray in color, and alternate of phengite dominant layer of a few mm in thickness and quartz layers ranging from a few mm to several cm.

On the basis of microscopic observations, lepidoblastic phengite and chlorite form the foliation in pelitic-psammitic schists and siliceous schists. Pelitic-psammitic schists and siliceous schists contain some detritus. In the psammitic layer, detrital grains of muscovite, quartz and plagioclase are observed. Phengite in pelitic-psammitic schist is usually fine-grained, and occurs as aggregates alternated with chlorite. Under the plane polarized light of microscope, it shows pale green to colorless, sometimes brown or opaque due to the numerous inclusion of carbonaceous materials.

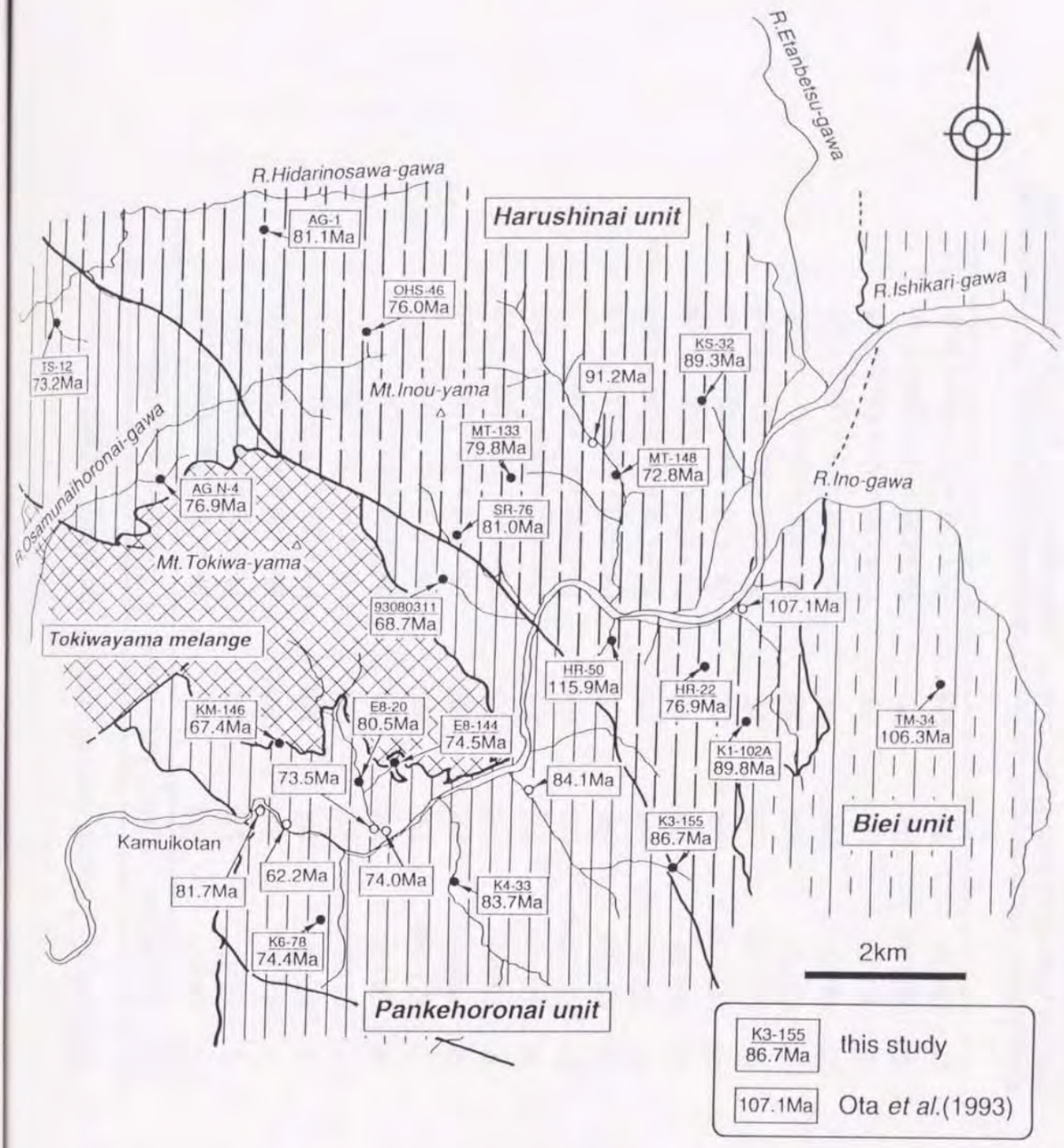

Fig. 6-1 Locality map of K-Ar dated specimens. Phengite K-Ar ages are also shown.

Table 6-1. Mineral assemblages of the dated samples.

No.	Sample No.	Unit	Rock name	Mineral assemblages
1	E8-117	SM	PS	Ph + Chl + Ab + Qtz + Carb
2	SR-21	SM	SS	Ph + Chl + Ab + Qtz + Stlp
3	K4-33	PK	PS	Ph + Chl + Ab + Qtz + Carb
4	K6-78	PK	MS	Ph + Chl + Ab + Act + Spn
5	E8-20	PK	SS	Ph + Chl + Ab + Qtz
6	E8-144	PK	SS	Ph + Chl + Ab + Qtz
7	KM-146	PK	SS	Ph + Chl + Ab + Qtz
8	93080311	PK	PS	Ph + Chl + Ab + Qtz + Carb
9	TS-12	PK	PS	Ph + Chl + Ab + Qtz + Carb
10	AG N-4	PK	PS	Ph + Chl + Ab + Qtz + Carb
11	K1-102A	HR	SS	Ph + Chl + Ab + Qtz
12	K3-155	HR	PS	Ph + Chl + Ab + Qtz + Carb
13	HR-22	HR	PS	Ph + Chl + Ab + Qtz + Carb + Spn
14	HR-50	HR	PS	Ph + Chl + Ab + Qtz + Carb
15	MT-133	HR	PS	Ph + Chl + Ab + Qtz + Carb
16	MT-148	HR	PS	Ph + Chl + Ab + Qtz + Carb
17	KS-32	HR	PS	Ph + Chl + Ab + Qtz + Carb
18	SR-76	HR	PS	Ph + Chl + Ab + Qtz + Carb
19	AG-1	HR	PS	Ph + Chl + Ab + Qtz + Carb
20	OHS-46	HR	PS	Ph + Chl + Ab + Qtz + Carb
21	TM-34	BI	MS	Ph + Chl + Ab + Act + Rcpx + Py

Abbreviations: SM, serpentinite melange (Tokiwayama melange) unit; PK, Pankehoronai unit; HR, Harushinai unit; BI, Biei unit; PS, pelitic-psammitic schist; SS, siliceous schist; MS, metabasic schist.

Basic schists are of volcanic sediments origin and the schistosity is mainly formed by actinolite, and lepidoblastic chlorite and phengite. They are well recrystallized, but contain a small amount of primary clinopyroxene, colorless or pale brownish augite (Table 6-1). Phengites in the schist are fine-grained crystals which are intergrown with actinolite, chlorite albite and sphene. Sometimes phengites form decussate aggregates in quartz and albite vein, which cut the schistosity. The modal amount of phengite in the basic schists is smaller than other specimens. On the basis of measurement by X-ray powder diffractmeter, the quantitative ratio of phengite in the bulk is several percents.

6-2. Preparation and analysis

The preparation of specimen and dating is carried out by the same procedure of Ota *et al.*(1993).

At first, rock specimens were roughly broken with a hammer and an iron mortar into pieces of a cm in size and all of visible psammitic parts intercalated in the pelitic-psammitic schists are removed. Broken specimens are crushed with a bowl mill, and an appropriate size fraction, depending on the size of each grain or aggregate of fine-grained phengite in the specimen was selected by sieving (Table 6-2). The sieved fraction was washed using distilled water and dried in an oven at about 80°C. Phengite was concentrated using an isodinamic separator, and the resultant specimen was treated with dilute HCl (about 2*N*) to dissolve out any chlorite within the grain boundary of phengite aggregate. The specimen was then wsahed repeatedly with distilled water, dried at about 80°C, and further concentrated by isodinamic separation techniques. Since most phengite is fine-grained, small crystals of actinolite, albite, quartz and carbonaceous materials which are intercalated phengite dominant part, could not completely be separated for some specimens, in particular basic schists, so their fractions are impure resulting lower potassium contents less than 5 wt.% (see Table 6-2).

Analyses of potassium and argon in the phengite separates, and calculations of age and error were carried out following the methods described by Nagao *et al.* (1984) and Itaya *et al.* (1991). Potassium was analyzed by flame photometry using a 2000 ppm Cs buffer. Separated phengite was decomposed by HF and HNO_3 treatment in a teflon beaker. Duplicate analyses were made for each specimen and the average value was used in the age calculation. Analytical uncertainty is ± 2 % at the 2-

Table 6-2. K-Ar ages of phengites separated from the metamorphic rocks and tectonic blocks in serpentinite of the Kamuikotan Gorge area.

No.	Sample No.	Unit Name	Rock name	Mesh size (μm)	K (wt.%)	Rad.^{40}Ar (10^{-8}ccSTP/g)	Non Rad.^{40}Ar (%)	K-Ar age (Ma)
1	E8-117	SM	PS	70/95	6.899±0.138	3430±34	5.7	123.8±2.7
2	SR-21	SM	SS	70/95	6.443±0.129	3439±33	2.7	132.6±2.8
3	K4-33	PK	PS	70/95	6.676±0.134	2220±22	5.4	83.7±1.8
4	K6-78	PK	MS	70/95	0.949±0.019	279.9±3.5	19.8	74.4±1.7
5	E8-20	PK	SS	70/95	7.917±0.158	2528±27	4.9	80.5±1.8
6	E8-144	PK	SS	70/95	6.168±0.123	1822±22	4.3	74.5±1.7
7	KM-146	PK	SS	70/95	6.463±0.129	1722±17	6.2	67.4±1.5
8	93080311	PK	PS	48/70	5.814±0.116	1579±18	5.6	68.7±1.6
9	TS-12	PK	PS	48/70	6.898±0.138	2001±21	3.9	73.2±1.6
10	AG N-4	PK	PS	48/70	6.021±0.120	1835±19	3.1	76.9±1.7
11	K1-102A	HR	SS	48/70	4.659±0.093	1664±18	2.7	89.8±2.0
12	K3-155	HR	PS	48/70	6.518±0.130	2246±24	3.0	86.7±1.9
13	HR-22	HR	PS	70/95	5.320±0.106	1622±17	5.1	76.9±1.7
14	HR-50	HR	PS	70/95	4.531±0.091	2104±21	4.5	115.9±2.5
15	MT-133	HR	PS	48/70	6.766±0.135	2143±24	4.8	79.8±1.8
16	MT-148	HR	PS	48/70	3.067±0.061	884.6±9.8	3.6	72.8±1.6
17	KS-32	HR	PS	48/70	3.572±0.071	1269±14	7.9	89.3±2.0
18	SR-76	HR	PS	48/70	5.806±0.116	1867±20	3.1	81.0±1.8
19	AG-1	HR	PS	48/70	4.677±0.094	1505±16	3.7	81.1±1.8
20	OHS-46	HR	PS	48/70	6.780±0.136	2043±23	3.9	76.0±1.7
21	TM-34	BI	MS	48/70	2.335±0.047	991.9±10.6	3.8	106.3±2.3

See text for details of the calculations.

Abbreviations same as Table 6-1.

sigma confidence level. Argon was analyzed on 15-cm radius, sector type mass spectrometer (HIRU) with a single collector system at Okayama University of Science (Itaya *et al.*, 1991). An isotopic dilution method with an argon-38 spike was used. The phengite separates were wrapped in aluminium foil, preheated in a vacuum at about 200°C and then argon was extracted at 1500°C in an ultra-high vacuum line. Reactive gases were removed by Ti-Zr scrubbers. The mass discrimination fuctor was checked with several different amounts of atmospheric argon each day before each set of four or five specimens were run on the mass spectrometer. Calibration of the isotopic ratios of the specimen gases was determined by interpolation of several mass discrimination factors determined with several different amounts of atmospheric argon according to the amount of ^{40}Ar in the extracted gas (Itaya *et al.*, 1991). Multiple runs of a standard (JG-1 biotite, 91 Ma) indicated that the uncertainty of argon analysis is about ± 1 % at the 2-sigma confidence level (Itaya *et al.*, 1991). Decay constants for ^{40}K to ^{40}Ar and to ^{40}Ca, and the ^{40}K abundance used in age calculation are 0.581 x 10^{-10}/year, 4.962 x 10^{-10} /year, and 0.0001167, respectively (Steiger and Jager, 1977).

6-3. Result of dating

The results of dating in this study are presented in Table 6-2, Figs. 6-1 and 6-2. Phengite K-Ar ages of the metamorphic rocks from study area show a wide range from 133Ma to 67Ma. As mentioned above, some specimens have a low potassium content which is due to mainly to impurities such as actinolite, albite, quartz and carbonaceous materials. But the low potassium content due to impurities does not significantly affect the phengite K-Ar ages (Itaya and Takasugi, 1988).

The ages of phengite from the Tokiwayama melange unit are 133Ma and 124Ma, and are the oldest in the study area. The ages of the Harushinai unit are dispersed from 116Ma to 73Ma, whereas phengite from the Pankehoronai unit yielded a relatively narrow and young range in age of 84Ma to 67Ma. The age in the Biei unit is 106Ma and is included in the range of the Harushinai unit.

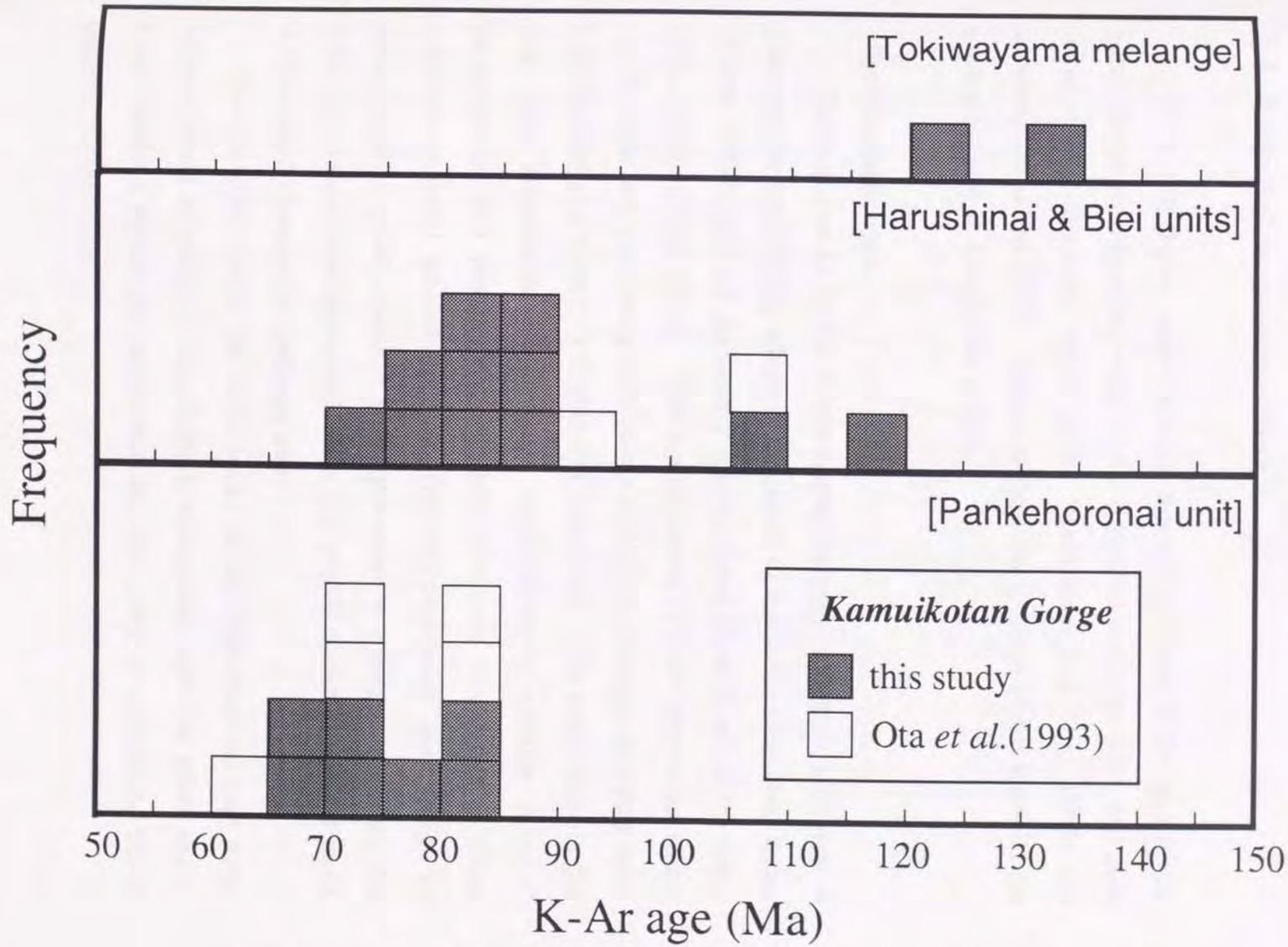

Fig. 6-2. Frequency distribution diagram of K-Ar ages of metamorphic rocks from all units in the Kamuikotan Gorge area.

7. Discussion

7-1. Kamuikotan metamorphism

Units, lithologies, index mineral assemblages and K-Ar ages of the Kamuikotan metamorphic rocks in the Kamuikotan Gorge area, and their metamorphic pressure types (after Sakakibara and Ota, 1994) are summarized as Table 7-1. Based on these data, nature of the Kamuikotan metamorphism is considered at first.

Mineral parageneses

The basic rocks in the Tokiwayama melange unit have lawsonite + glaucophane assemblage which corresponds to lawsonite-blueschist facies (Evans, 1990), and are apparently distinguished from those of the other units, as mentioned below. The compositions of sodic pyroxenes (max. Jd; 56 mole %), coexisting with quartz and albite, indicate that they have been formed at a extremely higher-P/T condition. The basic rocks in the Biei and Harushinai units have approximately similar mineral parageneses, and pumpellyite + sodic pyroxene + chlorite is most common mineral assemblages. The representative assemblage is pumpellyite + glaucophane + sodic pyroxene + chlorite, however, the sodic pyroxenes with quartz and albite has less Jd content (max. 49 mole %) than the Tokiwayama melange unit.

On the other hand, the basic rocks in the Pankehoronai unit have various kinds of mineral assemblages, comparing with the other units. More detailed petrologic treatments are necessary to understand these mineral parageneses.

Table 7-1. Correlation of units, lithologies, index mineral assemblages and K-Ar ages of the Kamuikotan metamorphic rocks in the Kamuikotan Gorge area and their metamorphic pressure types.

unit	lithology	mineral assemblage	metamorphic pressure type* (metamorphic facies)	K-Ar age (Ma)
Tokiwayama melange (TM) *[Tokiwayama -blueschist]*	(block) basic schist pelitic schist	Lws ± Pmp + Gln(Crt) + Napx + Chl Lws + Pmp + Napx + Chl	high-pressure type(1) (blueschist facies /Lws-Gln subfacies)	123.8-132.6
Biei (BI)	mainly basic rock	Pmp + Gln(Crt) ± Act + Napx + Chl Lws + Pmp + Napx + Chl Pmp + Act ± Napx + Chl Pmp + Napx + Chl	high-pressure type(2) (Pmp-Act facies/higher pressure subfacies)	106.3
Harushinai (HR)	pelitic rock psammitic rock basic rock			72.8-107.1
Pankehoronai (PK)	basic schist pelitic schist serpentinite	***[initial stage]*** Lws, Fe-Pmp Gln(Crt) ***[main stage]*** Ep + Hem + Act + Chl Ep ± Pmp + Act + Chl Pmp + Act ± Napx + Chl Ep + Act(Win) ± Napx + Chl	***[initial stage]*** (blueschist facies ?) ***[main stage]*** high-pressure intermediate group type (Pmp-Act facies)	? 62.2-84.1

** after Sakakibara and Ota (1994)*

Commonly, the petrologic system of basic rocks is discussed in terms of the components SiO_2-TiO_2-Al_2O_3-Fe_2O_3-FeO-MgO-CaO-Na_2O-K_2O-H_2O-CO_2. Quartz, albite, sphene and phengite are ubiquitous in investigated basic rocks; they are treated as excess phases for SiO_2, Na_2O, TiO_2, and K_2O, respectively. This simplification reduces the total number of components to five: Al_2O_3, Fe_2O_3, FeO-, MgO and CaO, assuming the fluid phase is in excess and consists mainly of H_2O in the calcite-free assemblages. As stated before, the X_{Mg} of chlorites in the studied basic rocks with low-variance (more than four mineral phases) assemblage occupies a relatively narrow range. Then, fixing the chlorite composition at constant X_{Mg}, the system can be further simplified to the four components Al_2O_3-Fe_2O_3-(FeO+MgO)-CaO. The mineral phases treated here are epidote, pumpellyite, actinolite, chlorite, hematite, sodic amphibole (crossite to riebeckite) and sodic pyroxene (aegirine-augite to sodic augite). A tetrahedron of A(Al_2O_3-Na_2O-3K_2O)–C(CaO)–F(FeO+MgO)–F3(Fe_2O_3) in Fig 7-1 shows mineral parageneses and compositional relations of the above seven mineral phases in the simplified four components system. Epidote, pumpellyite, actinolite, chlorite and hematite plot within the tetrahedron, but sodic amphibole and sodic pyroxene do outside. Pure acmite is plotted at an infinite point, and sodic pyroxenes are shown as solid solutions between augite and acmite.

The basic rocks in the Pankehoronai unit have various kinds of mineral assemblages derived from differences of Fe_2O_3 content and Fe/Mg ratio in the bulk compositions and metamorphic stages. In particular, the assemblages bearing hematites, sodic pyroxenes with higher aegirine components or sodic amphiboles with higher riebeckite components in the EPA zone, and those bearing epidotes in the SC zone

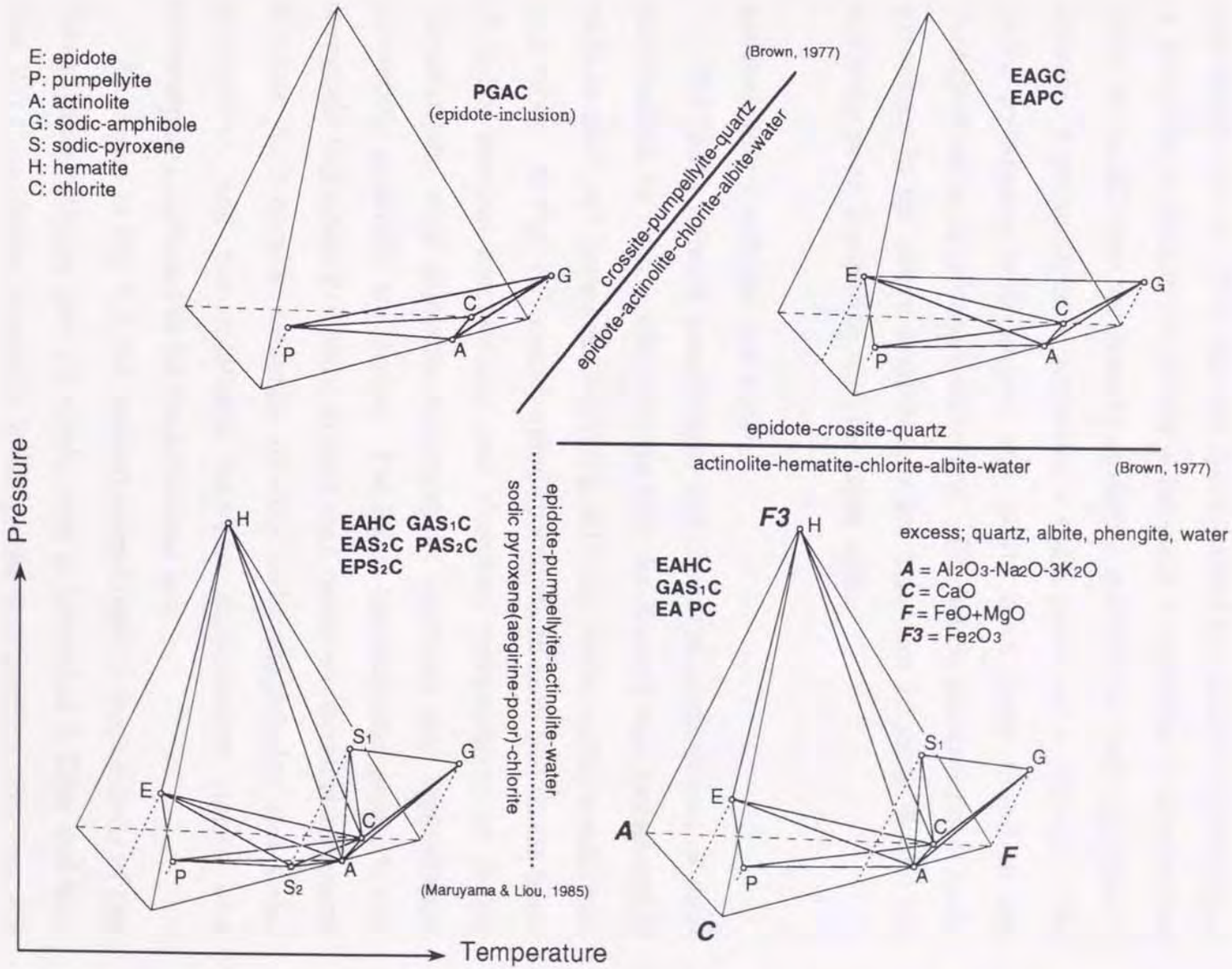

Fig. 7-1. A(Al_2O_3-Na_2O-$3K_2O$)–C(CaO)–F(FeO+MgO)–F3(Fe_2O_3) tetrahedron showing mineral parageneses in the basic rocks.

are subjected to influences of the bulk compositions, enriched Fe_2O_3 content (Fig. 7-1). Taking this into consideration, the main stage assemblages in the EPA zone are characterized by epidote + pumpellyite + actinolite + chlorite or epidote + hematite + actinolite + chlorite and those in the SC zone are done by epidote + actinolite + sodic pyroxene + chlorite or pumpellyite + actinolite + sodic pyroxene + chlorite. No sodic pyroxenes with quartz and albite have been found in the Pankehoronai unit, as described before. The jadeite components of sodic pyroxenes in the above assemblages are less than 20 mole % and are markedly poor, comparing with the other units.

Metamorphic conditions and history

The index mineral assemblages and chemical compositions of their constitutions in basic rocks indicate that the Kamuikotan metamorphic rocks in each unit have been formed at different metamorphic conditions, each other. In Fig. 7-2, metamorphic conditions in each unit on the basis of index mineral assemblages and chemical compositions of major constitutions, with available metamorphic reactions and approximate geothermal gradients, are shown. The figure also indicates prograde and retrograde individual P-T paths in each unit, based on chemical zonations of some metamorphic minerals (mainly sodic amphiboles and sodic pyroxenes), and the relations between deformation stages and metamorphic conditions in the Pankehoronai unit.

As shown in Fig. 7-2, the mineral assemblages in basic schists of the Tokiwayama melange unit are stable even at more than 6 Kbar and less than 200°C condition, unusually lower geothermal gradient (less than 10 °C/km), and the assemblages correspond to a typical lawsonite-blueschist facies (Evans, 1990). Hence, the metamorphic blocks in the Tokiwayama

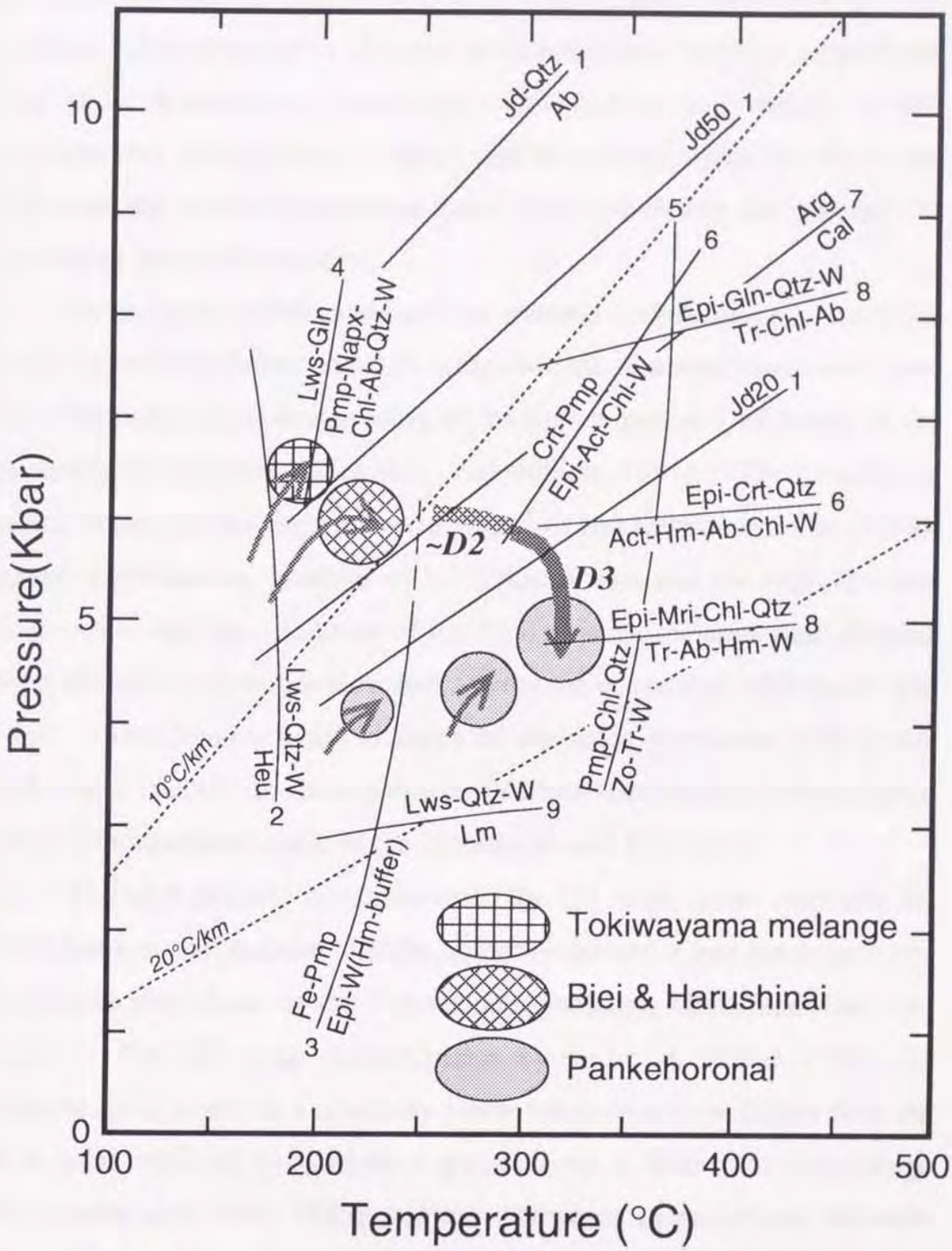

Fig. 7-2. Metamorphic conditions in each unit on the basis of index mineral assemblages and chemical compositions of major constitutions, with available metamorphic reactions and approximate geothermal gradients. The metamorphic reactions are referred from the following literatures; 1, Sakakibara(1991); 2, Nitsch(1968); 3, Schiffman and Liou(1983); 4, Maruyama and Liou (1988); 5, Nitsch(1971); 6, Brown(1977); 7, Johannes and Puhan(1971); 8, Maruyama et al.(1986); 9, Liou(1971).

melange unit belong to the high-pressure type 1 after Sakakibara and Ota (1994). The progressive changes in compositions of sodic amphiboles and sodic pyroxenes, coexisting with quartz and albite, in the Tokiwayama melange unit suggest that the metamorphic blocks in the Tokiwayama melange unit have been produced during the progressive increasing pressure condition.

The mineral assemblages and the mineral compositions in the basic rocks in the Harushinai and Biei units indicate that they have undergone the metamorphism corresponding to the higher pressure subfacies of the pumpellyite-actinolite facies (e.g., Sakakibara, 1991). The conditions, which belong to the high-pressure type 2 of Sakakibara and Ota (1994), denote a geothermal gradient of 10 °C/km or less and are slightly lower in pressure than the condition of the Tokiwayama melange unit, judging from the jadeite component in sodic pyroxene coexisting with quartz and albite. The compositional changes of the sodic pyroxenes with quartz and albite record the retrogressive process, decreasing metamorphic pressure/temperature ratio, in the Harushinai and Biei units.

The index mineral assemblages in the D3 stage (main stage) of the Pankehoronai unit indicate clearly higher temperature and lower pressure conditions than those of the Tokiwayama melange, Harushinai and Biei units. The SC zone characterized by sodic pyroxene + chlorite assemblage is stable at a relatively lower temperature conditions than the EPA zone defined by epidote + pumpellyite + actinolite assemblage (Maruyama and Liou, 1985), but the difference in conditions between these two zones is less apparent than possible to show in the diagram. The geothermal gradient in the D3 stage of the Pankehoronai unit is about 15 °C/km and the metamorphic temperature ranges from 200 °C to 300 °C, at about 5 Kbar. This corresponds to the pumpellyite-actinolite

facies and the Pankehoronai unit (main stage) is included by the high-pressure intermediate type after Sakakibara and Ota (1994).

For the initial stage of the Pankehoronai unit, no markedly assemblages have been found, but inclusions within epidote porphyroblasts are abundant (Fig. 4-4). Judging from available metamorphic reactions in Fig.7-1, mineral paragenesis of pumpellyite + sodic amphibole (crossite and/or glaucophane) of the Biei and Harushinai units are stable at a relatively higher P/T condition than mineral assembladge in the main stage (epidote + actinolite + chlorite) of the Pankehoronai unit (Brown, 1977). If crossite, actinolite, pumpellyite and chlorite as the inclusions had been coexisting with each other, this assemblages indicate the similar metamorphic conditions to the Biei and Harushinai units. Textures of sodic amphibole and hematite, and compositional changes in $X_{Fe^{3+}}$ of sodic amphibole and epidote (Figs. 4-3b, 5-3, 5-4, 5-7 and 5-8) in the basic rocks of the Pankehoronai unit imply that oxygen fugacity in the system may have increased during metamorphism, with constant temperature and pressure conditions (e.g., Robinson et al., 1982; Spear, 1993). The relations between deformation structures and their constituent minerals (Figs. 3-9c and 4-4), however, suggest that the metamorphic P-T conditions have changed with time. Therefore, it is suggested that the basic rocks of the Pankehoronai unit initially had been metamorphosed under low grade condition with a relatively high ratio of P/T during the D2 stage, corresponding to the metamorphic condition of the Biei and Harushinai units, and were subsequently converted to assemblages of the main stage (the D3 stage) by a combination of decline in the P/T ratio and increasing oxygen fugacity (Ota, submitting).

As shown in Fig. 7-2, parts of the Pankehoronai unit have been undergone higher P/T condition similar to the Biei and Harushinai units in earlier stage (the D2 stage), consequently subjected to decompression and heating (the D3 stage). This retrogressive change of the geothermal gradient infers that parts of the Pankehoronai unit have been heated at their exhumation process. On the other hand, no reheating retrogressive history is observed in the Biei, Harushinai and Tokiwayama melange units, and the only Pankehoronai unit has a unique history.

7-2. K-Ar dating of low grade metamorphic rocks: approximate age of multi-origin micas as endmember

Metamorphic history and K-Ar age of multi-origin micas

The maximum temperature of the Kamuikotan metamorphic rocks in this area is about 300 °C, as mentioned before, while the closure temperature for muscovite is about 350 °C (Jäger, 1979). In this case, phengite K-Ar ages in the Kamuikotan Gorge area are regarded as so-called metamorphic peak ages (Fig. 1-4), however, it must be confirmed whether or not an assumption on such a definition is satisfied.

As described before, the pelitic rocks in this area contain some detritus and have deformation structures, i.e., foliations consisting mainly of phengite, formed in different stages. Such conditions are illustrated in Fig. 7-3. The incomplete recrystallization by low-grade metamorphism, with heterogeneous deformation, produses metamorphic minerals on the newer foliations, but compositional conversions of minerals on the pre-existing foliations are not complete in many cases. As a result, parts formed at different stages are preserved in the low-grade metamorphic rocks. Mixing rates of such parts in the rocks change by degrees of advance the deformation and associated recrystallization. For examples, advances of deformation structures during the D3 stage in the Pankehoronai unit are different from those in the Harushinai unit. The F3-folds observed in the Harushinai unit are open and/or close folds, and the S1- and S2-foliations, bent by the F3-folds, are controlled the regional structure. On the other hand, the F3-folds in the Pankehoronai unit are mainly close to tight folds. The structures in the Pankehoronai unit are limited by the S3-foliations as the axial cleavages of F3-folds, and the rocks in this unit contain more parts formed during the later stage (D3

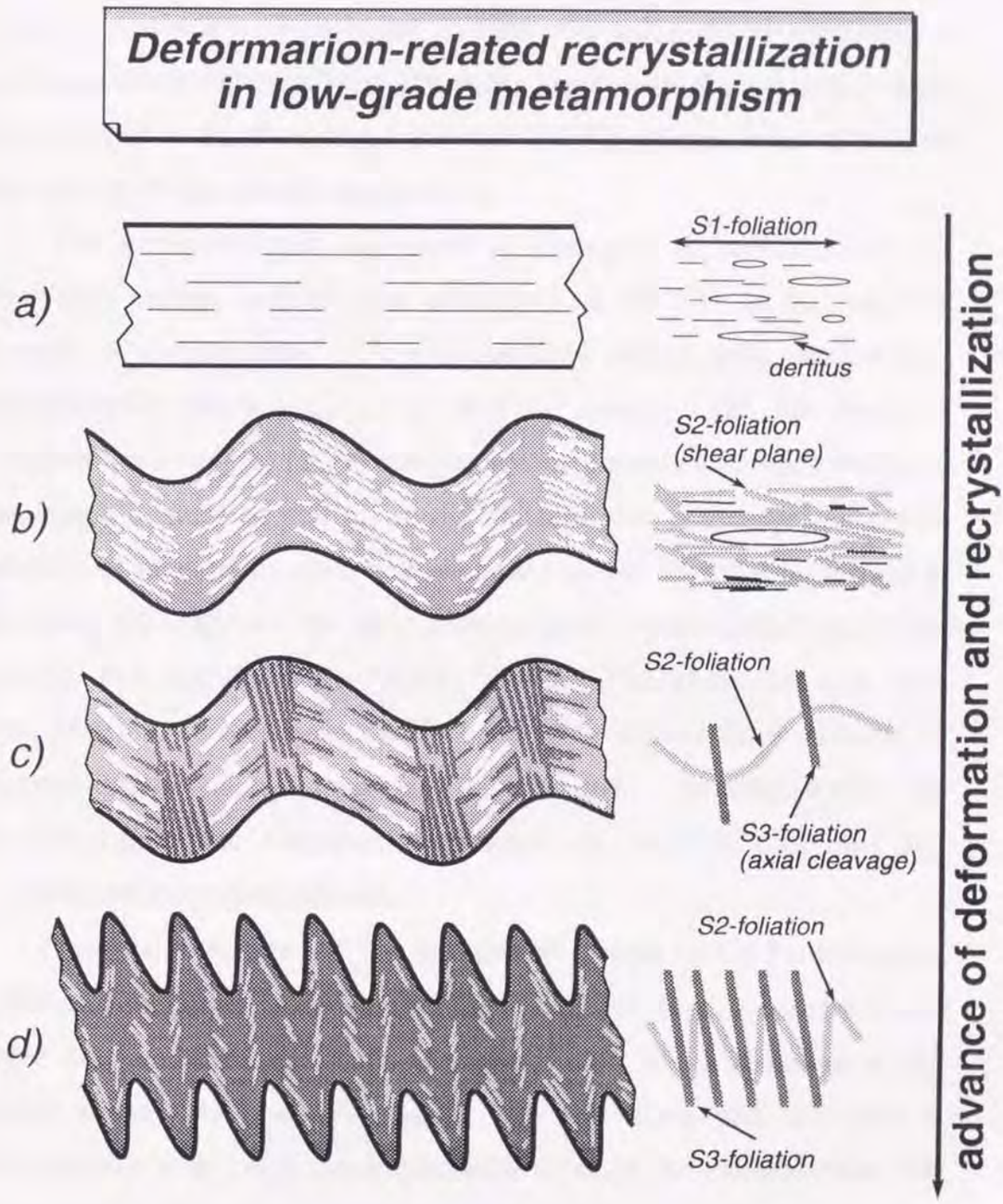

Fig. 7-3. Schematic diagram showing process of recrystallization in low-grade metamorphic rocks. Note that the mixing ratio of parts formed during different stages changes, depending on degrees of deformation with recrystallization.

stage) than those in the Harushinai unit. Here, the condition of c) and d) shown in Fig. 7-3 correspond to that of the Harushinai and Pankehoronai units, respectively. If phengites in parts selected as dating specimens is not completely recrystallized, the rocks composed of parts which have been formed in different stages may not show a specific time, defined by the concept of the closure temperature.

The compositional variations of phengite in pelitic rocks, as described before, indicate that phengites on the S1- or S2-foliations formed at earlier stage have compositions mixed with detritus and metamorphic phyllosilicates at various rates. On the basis of compositional ranges, i.e., heterogeneity, of phengites on each foliation, the mixed degrees of detritus in the metamorphic phases decrease with advance of recrystallization, and phengites on the S3-foliation formed at the latest D3 stage are the most homogeneous composition (Fig. 5-10). Taking the metamorphic history in the Pankehoronai unit into consideration, it seems that such a tendency results from advance of recrystallization due to increasing temperature. In other words, the disappearance the chemical influence of detritus indicates the comprehensive recrystallization.

Phengite K-Ar ages of the metamorphic rocks in the Pankehoronai and Harushinai units range from 62 Ma to 116 Ma (Figs. 6-1 and 6-2, and Table 6-2), and the ages of the Harushinai unit, which foliations of the earlier stage (D1 and D2 stages) are well preserved, occupies a considerably wide range comparing with those of the Pankehoronai unit dominated by foliations of the latest stage (D3 stage). Then, the degrees of recrystallization at the D3 stage are investigated for actually dated fractions concentrated phengites. The results are shown in Figs. 7-4 and 7-5. These diagrams show that the specimens with older ages have more

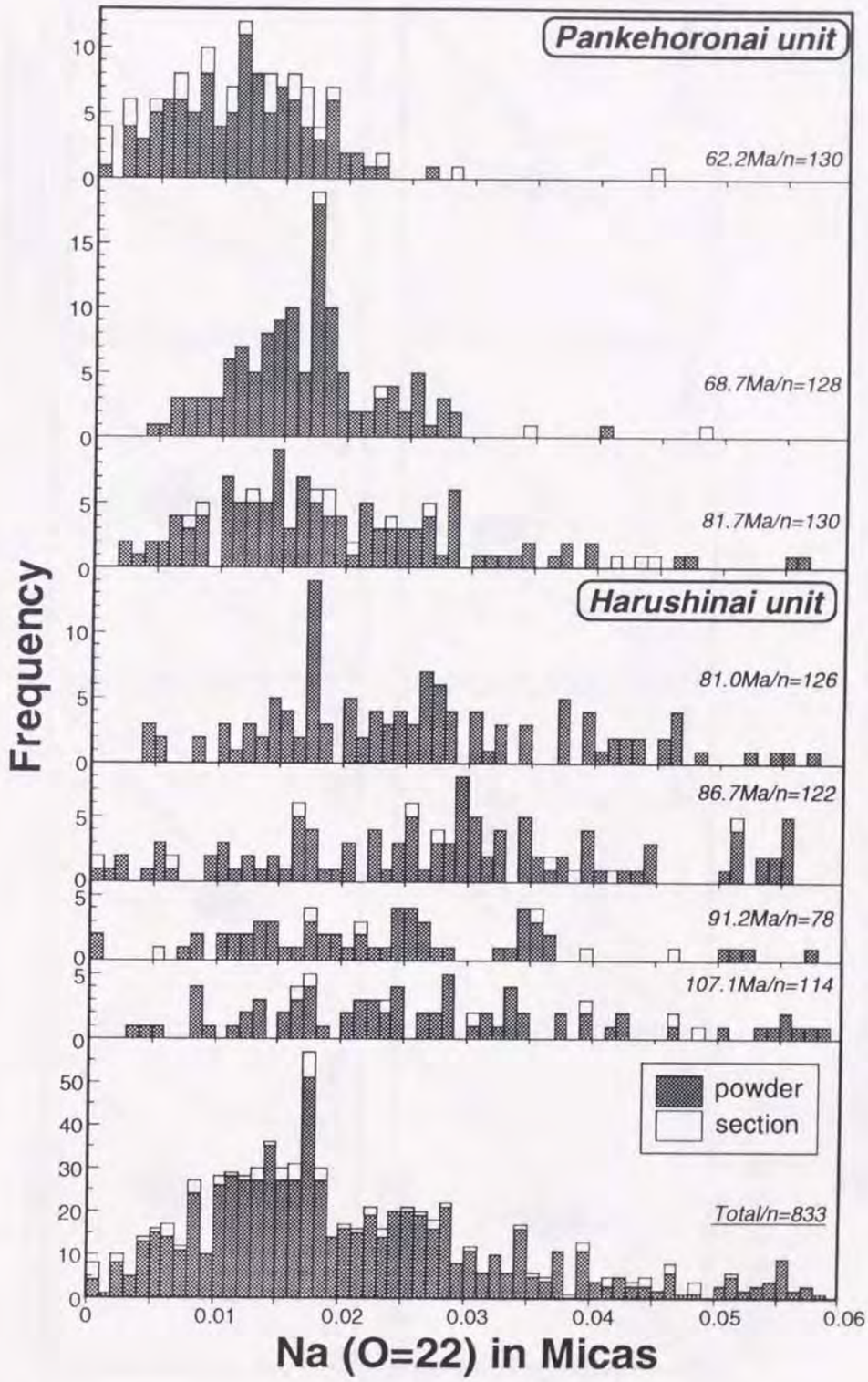

Fig. 7-4. Compositional variations of phengite in pelitic rocks in the Kamuikotan Gorge area. **a**. frequency distribution diagram of Na content in micas in the powder specimen and thin section.

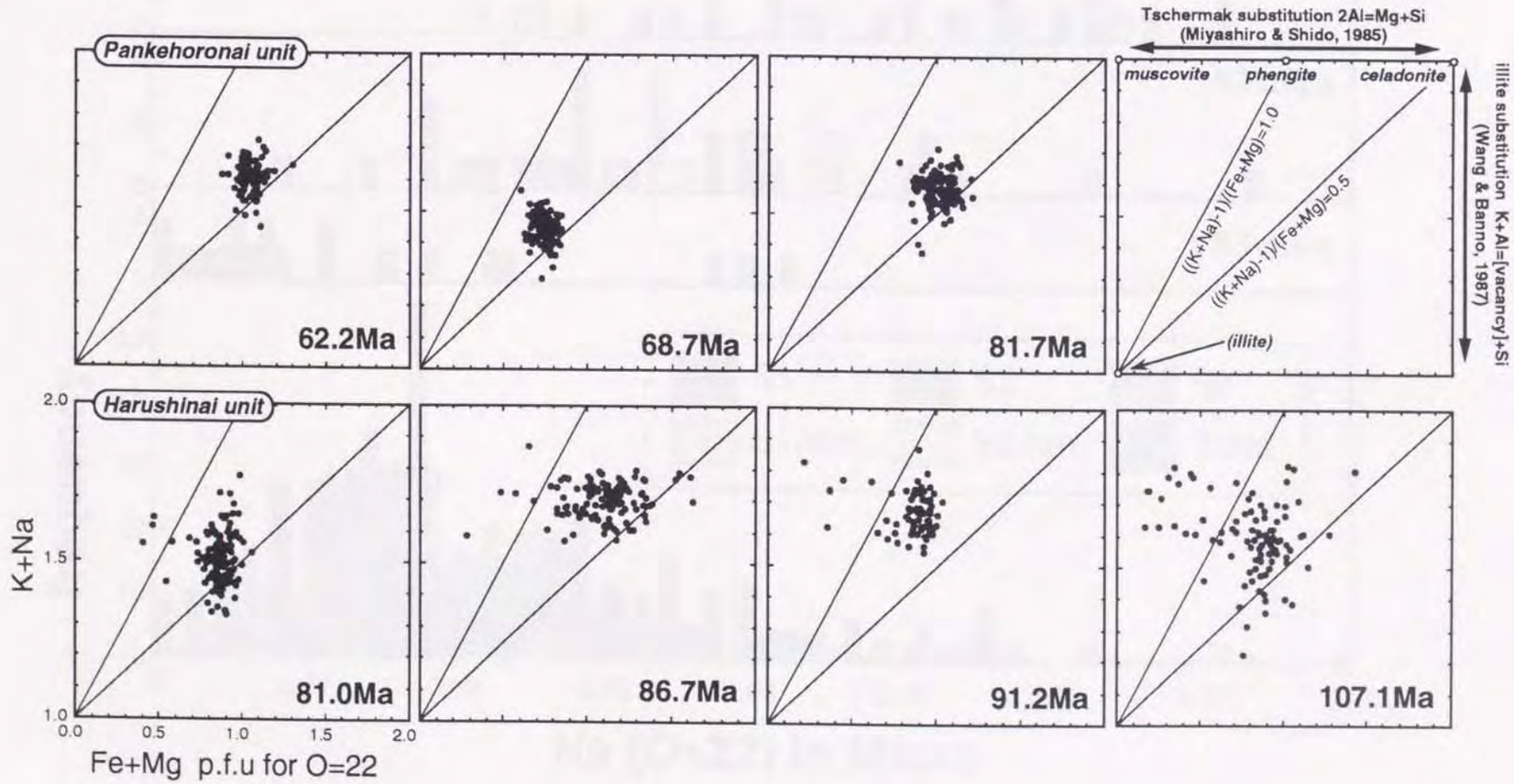

Fig. 7-4. b. Compositional variations of phengite in each dated specimens and major two substitutions of micas in pelitic rocks.

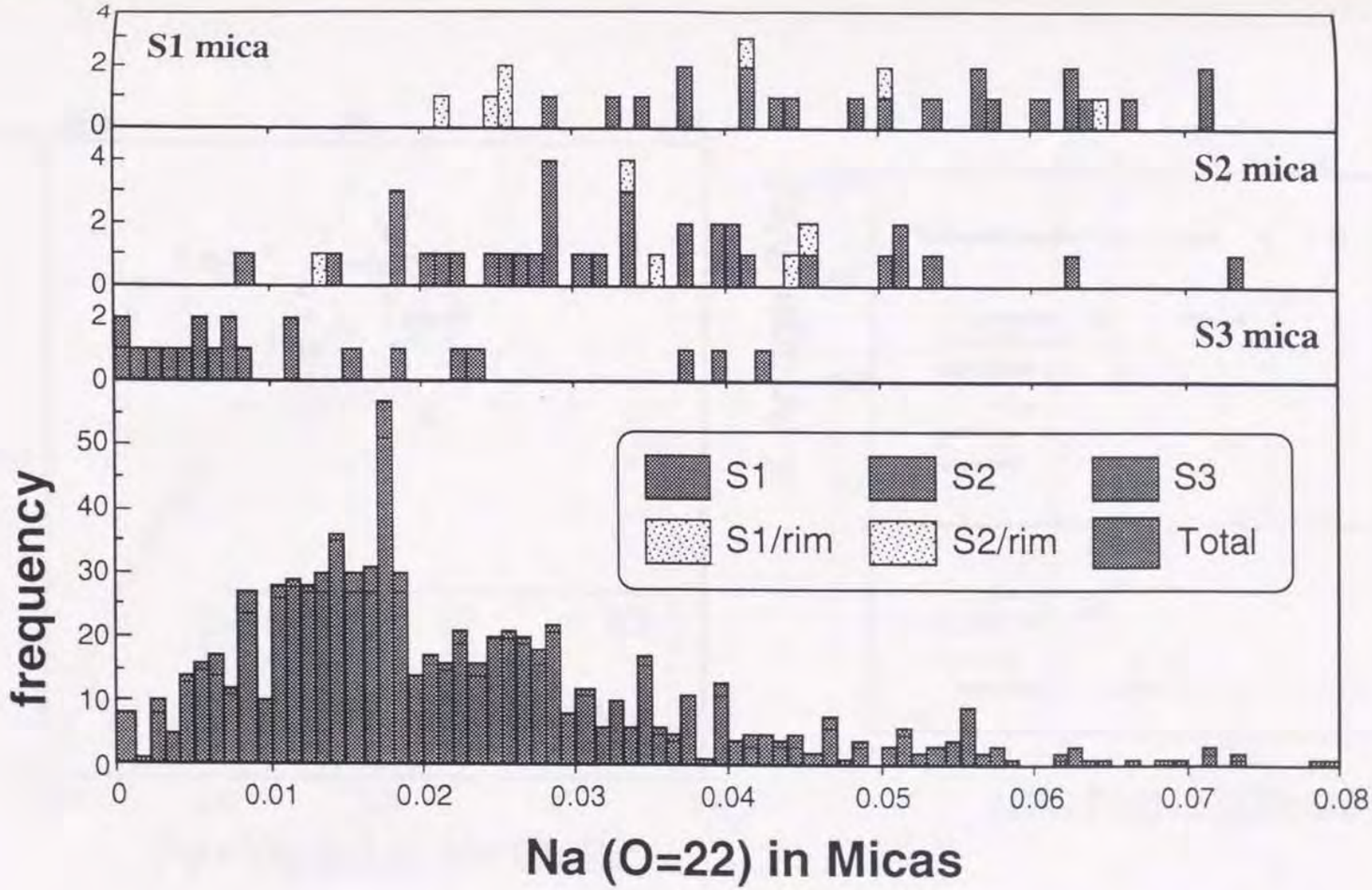

Fig. 7-5. Compositional variations of phengite in pelitic rocks in the Kamuikotan Gorge area. **a**. frequency distribution diagram of Na content in micas on each foliation.

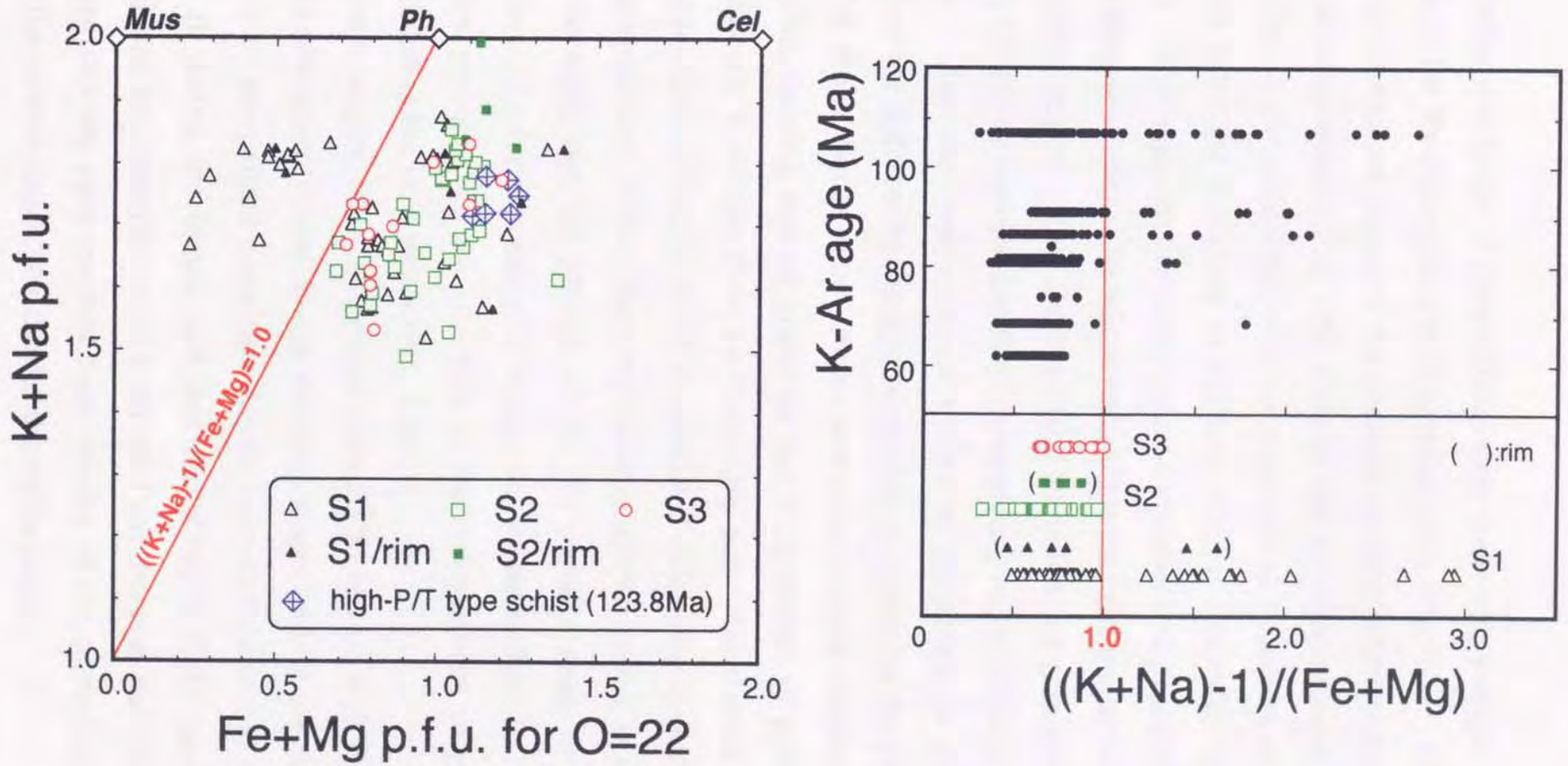

Fig. 7-5. b. Compositional variations of phengites on each foliation in thin sections and in powder specimens. Note that micas on the foliations formed at the earlier stages and those in the specimens shown the older K-Ar ages have considerably wide compositional ranges.

comprehensive range of compositions than those with younger ages as a whole of the Pankehoronai and Harushinai units (Fig. 7-4). Comparing with compositional ranges of the phengite on each foliation and those in each dated specimens (Fig. 7-5), it seems that the compositional ranges of phengites in the dated specimens are subjected to influences of phengite derived from the foliations at different stages, especially the earlier stages. This suggests that compositional variations of phengites in each dated specimens change by mixed rates of the phengite on the foliations at the earlier stages. The compositional variations of phengites on the earlier foliations indicate that they incompletely recrystallize at the later stages. But the compositional ranges of phengites on the earlier foliations are different by the ages of specimens containing the phengites. Fig. 7-6 shows modes of occurrence and compositional variations of the phengites, forming detrital grains on the S1-foliations of pelitic rocks with different K-Ar ages from the Harushinai unit. The detrital grains in both specimens are recrystallized to associated with metamorphic chlorite. The compositions of the phengites forming detrital grains in specimen with the older age are plotted within the peculiar range to the S1-foliations, i.e., corresponding to muscovite, whereas those in specimen with the younger age are changing to the compositions of phengites formed during the later stages (Fig. 7-6b).

These suggest that the apparent phengite K-Ar ages shift by mixing rates of phengites formed during different stages and by compositional changes of pre-existed phengites due to recrystallizations at the later stages in dating specimens, and that the phengite K-Ar ages of the Kamuikotan metamorphic rocks from the Pankehoronai and Harushinai units are mixture ages resulted from mixing of the phengites formed during the various stages, in paticular the earlier stages.

Hr-22 (Hr/76.9Ma)

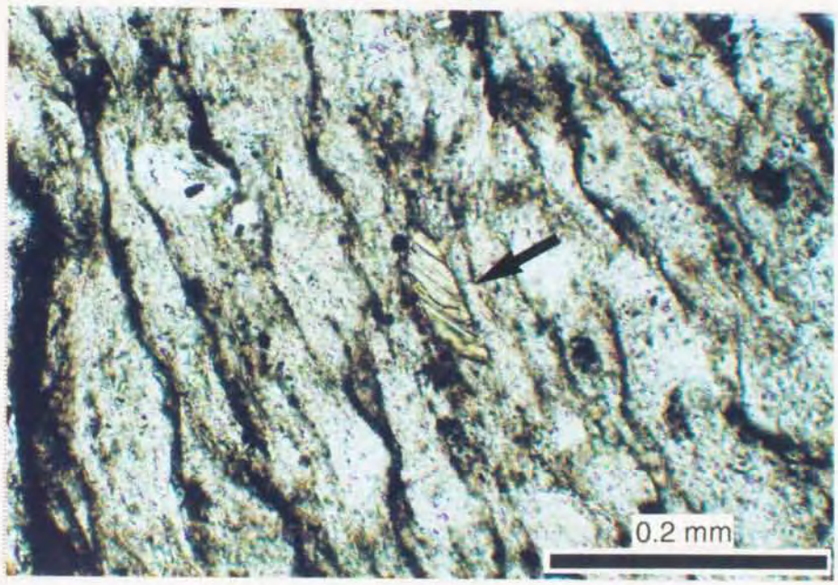

K-5-2 (Hr/107.1Ma)

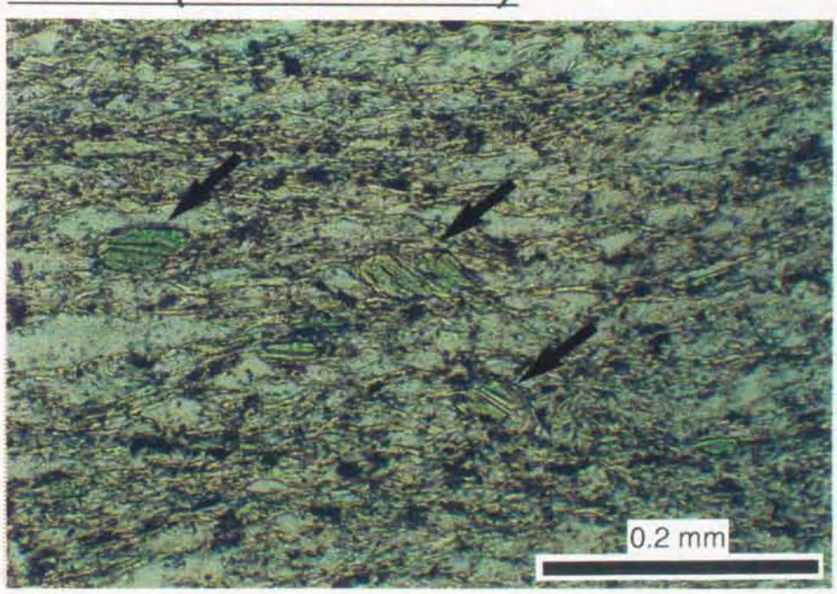

Fig. 7-6. a. Photomicrographs showing modes of occurrence of detrital grains in pelitic rocks with different K-Ar ages from the Harushinai unit. Arrows show the detrital grains remaining on the S1-foliations.

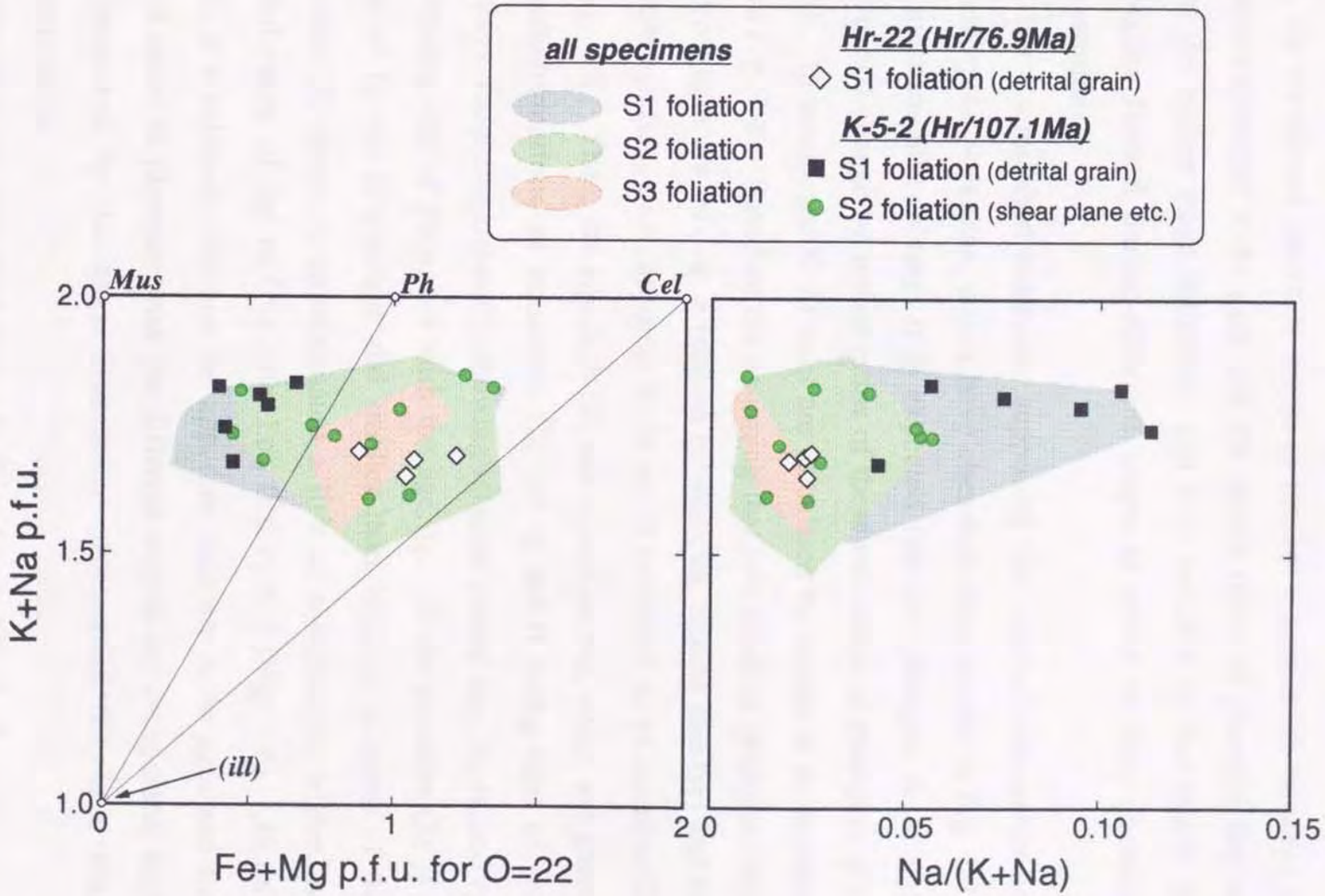

Fig. 7-6. b. Compositional variations of micas composing of detrital grains in pelitic rocks with different K-Ar ages from the Harushinai unit. Compositional ranges of micas on each foliation are also shown. See text for details.

Approximate age of multi-origin micas as endmember

As mentioned above, it seems to present a correlation between an apparent phengite K-Ar ages and the mixed ratios of phengite derived from the earlier stage foliations, and it is possible to distinguish the phengites formed during different stages in terms of their chemical compositions.

For a simplified examples, supposing that detrital muscovites and metamorphic phengites, which have chemical traits shown in Fig. 7-7a, are mechanically mixing, it is expected that the phengite K-Ar ages determined change by mixed ratios of these two kinds of phengites (Fig. 7-7b). In actual, the K-Ar ages are calculated by means of an equation (1) in Fig. 7-8. Based on the assuming that two kinds of phengites with different ages are mixing, a relation between the mixing rate (r_1) and the mixture age (t_{mix}), i.e., apparent K-Ar age is presented as an equation (2) in Fig. 7-8. Then, the equation (2) and equations (4), which are gotten by transformations of equations (3) for t_0 and t_1 being ages of end members, reduce equation (5) showing relation among t_{mix}, t_0, t_1, and r_1, the mixing rate of phengites with the age, t_1. In the equation (5), if a value of (t_1-t_0) is constant and smaller than 100 Ma, a curve of the equation (5) shows is approximated a line of equation (6) within the limited range of the mixing rate, i.e., $0 \leq r_1 \leq 1$ (Fig. 7-8). In this study, if a relations between the apparent phengite K-Ar ages and the mixed ratios of phengite with the different origins are recognized, they are presented by the linear correlation of equation (6), as a first approximation.

Based on the definition shown in Figs. 7-9 and 7-10, phengites with various origins in actually dated fraction specimens are classified into

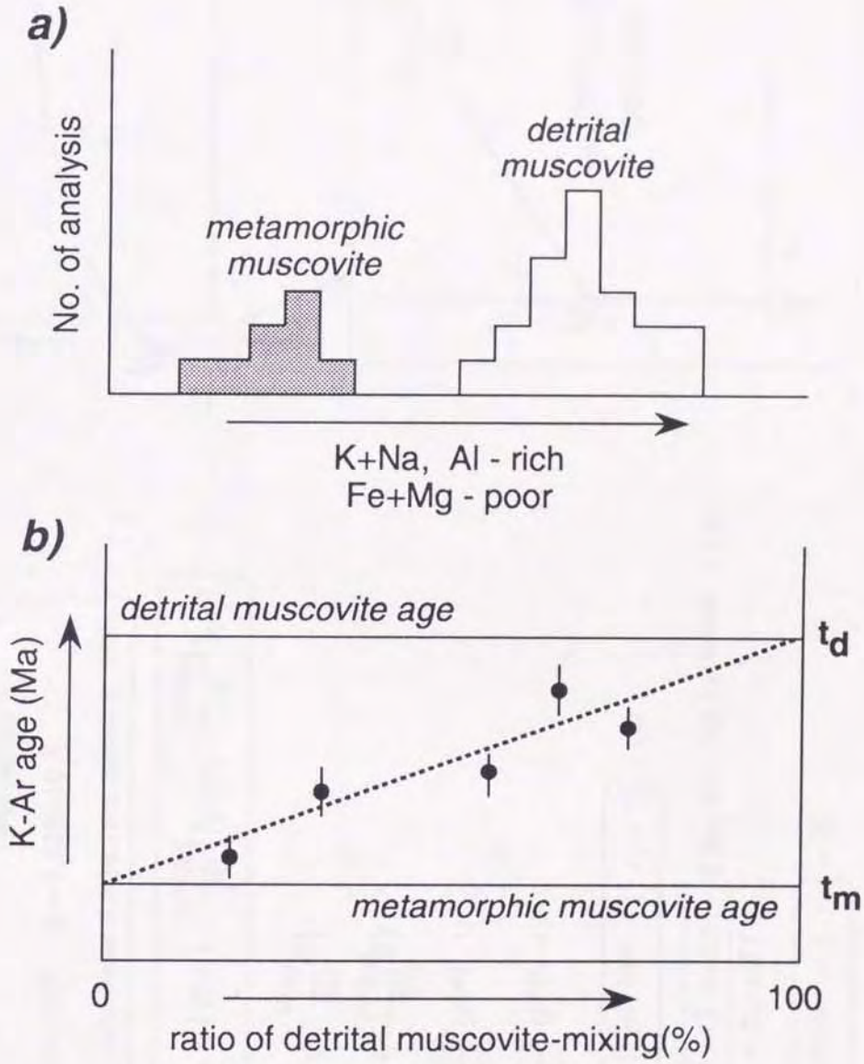

Fig. 7-7. a. Compositional variations of low-grade metamorphic and detrital micas, and **b**. hypothetical correlation between apparent K-Ar ages and mixing ratios of these micas.

$$t\,(\mathrm{Ma}) = a \cdot ln\left\{1 + b \cdot \frac{[^{40}\mathrm{Ar}]\ (10^{-8}\mathrm{ccSTP/g})}{[\mathrm{K}]\ (\mathrm{wt\%})}\right\} \quad -(1)$$

$$a = 1.804\times10^{3} \qquad b = 1.428\times10^{-4}$$

(after Nagao & Itaya, 1988; Itaya et al., 1991)

$$t_{mix} = a \cdot ln\left[1 + b\left\{(1-r_1)\cdot\left(\frac{[^{40}\mathrm{Ar}]}{[\mathrm{K}]}\right)_0 + r_1 \cdot \left(\frac{[^{40}\mathrm{Ar}]}{[\mathrm{K}]}\right)_1\right\}\right] \quad -(2)$$

$$\begin{cases} t_0 = a \cdot ln\left(1 + b \cdot \dfrac{[^{40}\mathrm{Ar}]_0}{[\mathrm{K}]}\right) \\ t_1 = a \cdot ln\left(1 + b \cdot \dfrac{[^{40}\mathrm{Ar}]_1}{[\mathrm{K}]}\right) \end{cases} \quad -(3)$$

$$\begin{cases} \left(\dfrac{[^{40}\mathrm{Ar}]}{[\mathrm{K}]}\right)_0 = \dfrac{1}{b}\cdot\left(e^{t_0/a} - 1\right) \\ \left(\dfrac{[^{40}\mathrm{Ar}]}{[\mathrm{K}]}\right)_1 = \dfrac{1}{b}\cdot\left(e^{t_1/a} - 1\right) \end{cases} \quad -(4)$$

$$t_{mix} = t_0 + a \cdot ln\left[\left\{e^{(t_1-t_0)/a} - 1\right\}\cdot r_1 + 1\right] \quad -(5)$$

$$0 \leqq \left\{e^{(t_1-t_0)/a} - 1\right\}\cdot r_1 \ll 1 \;\cdots\; 0 \leqq r_1 \leqq 1,\ 0 \leqq \left\{e^{(t_1-t_0)/a} - 1\right\} \ll 1$$

$$ln\,(x+1) \fallingdotseq x \leftarrow 0 \leqq x \ll 1$$

$$t_{mix} = t_0 + a \cdot \left\{e^{(t_1-t_0)/a} - 1\right\}\cdot r_1 \quad -(6)$$

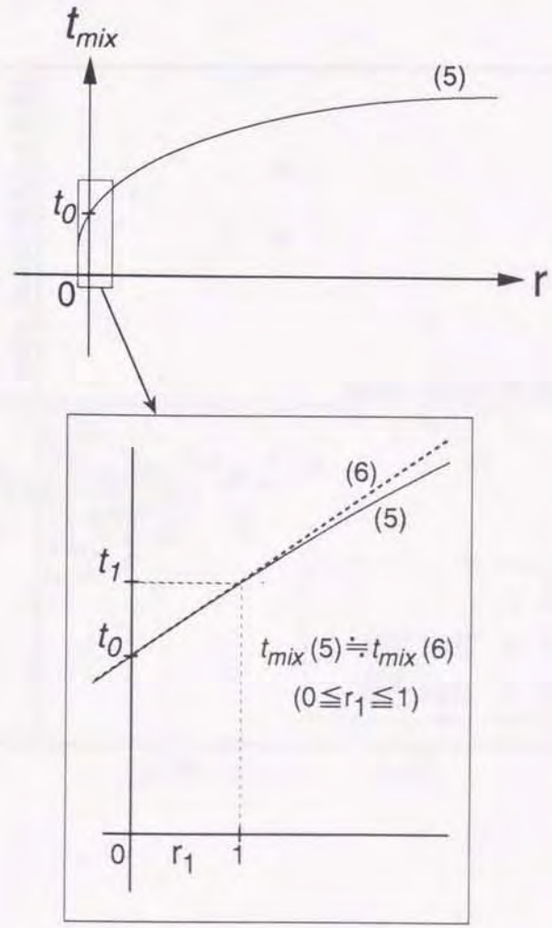

Fig. 7-8. Approximate correlation between apparent K-Ar ages and mixing ratios of micas with different K-Ar ages. See text for details.

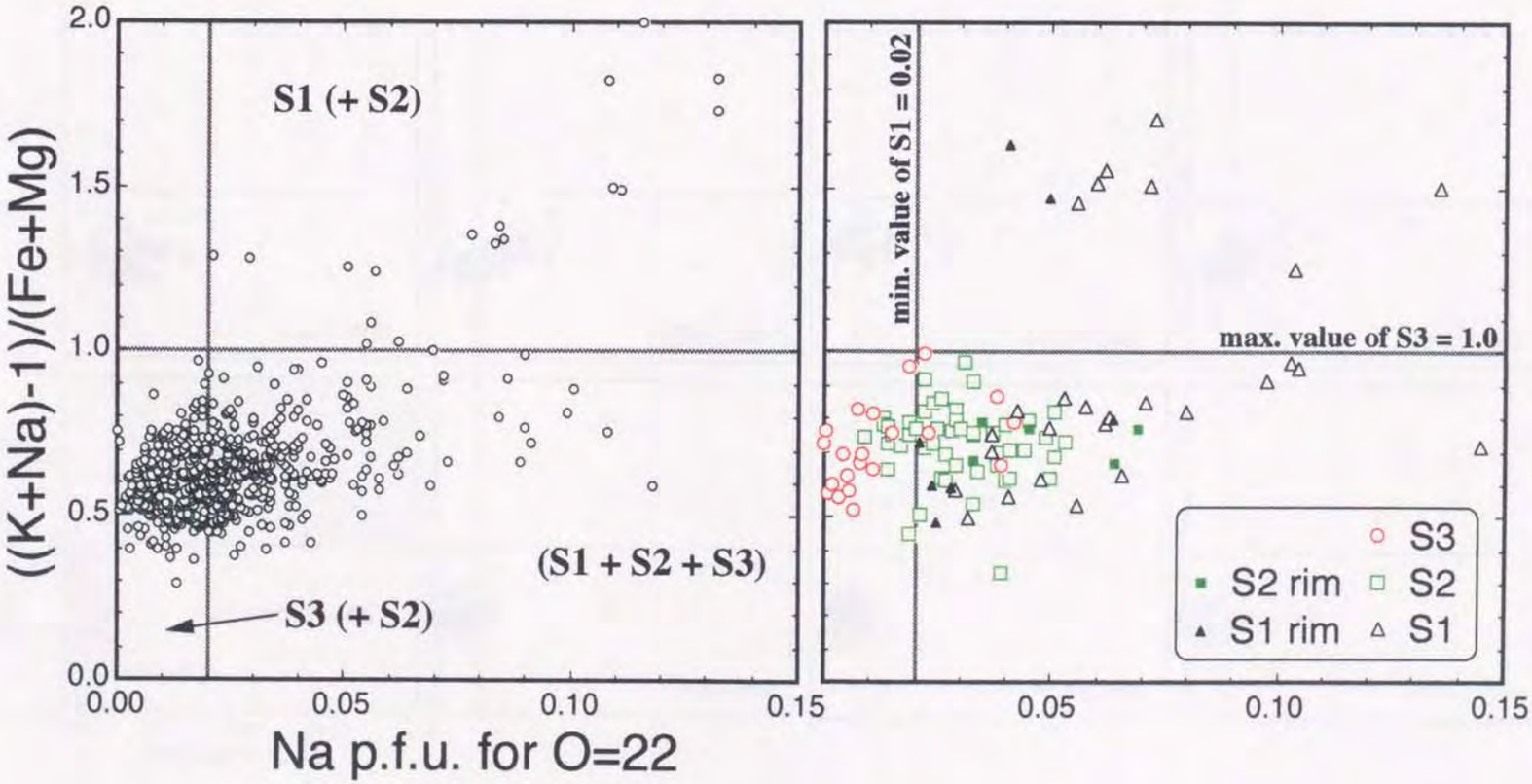

Fig. 7-9. The definitions of compositional ranges of phengites on each foliation. **left**: compositional variations in all of powder specimens, **right**: compositional variations of phengites on each foliation.

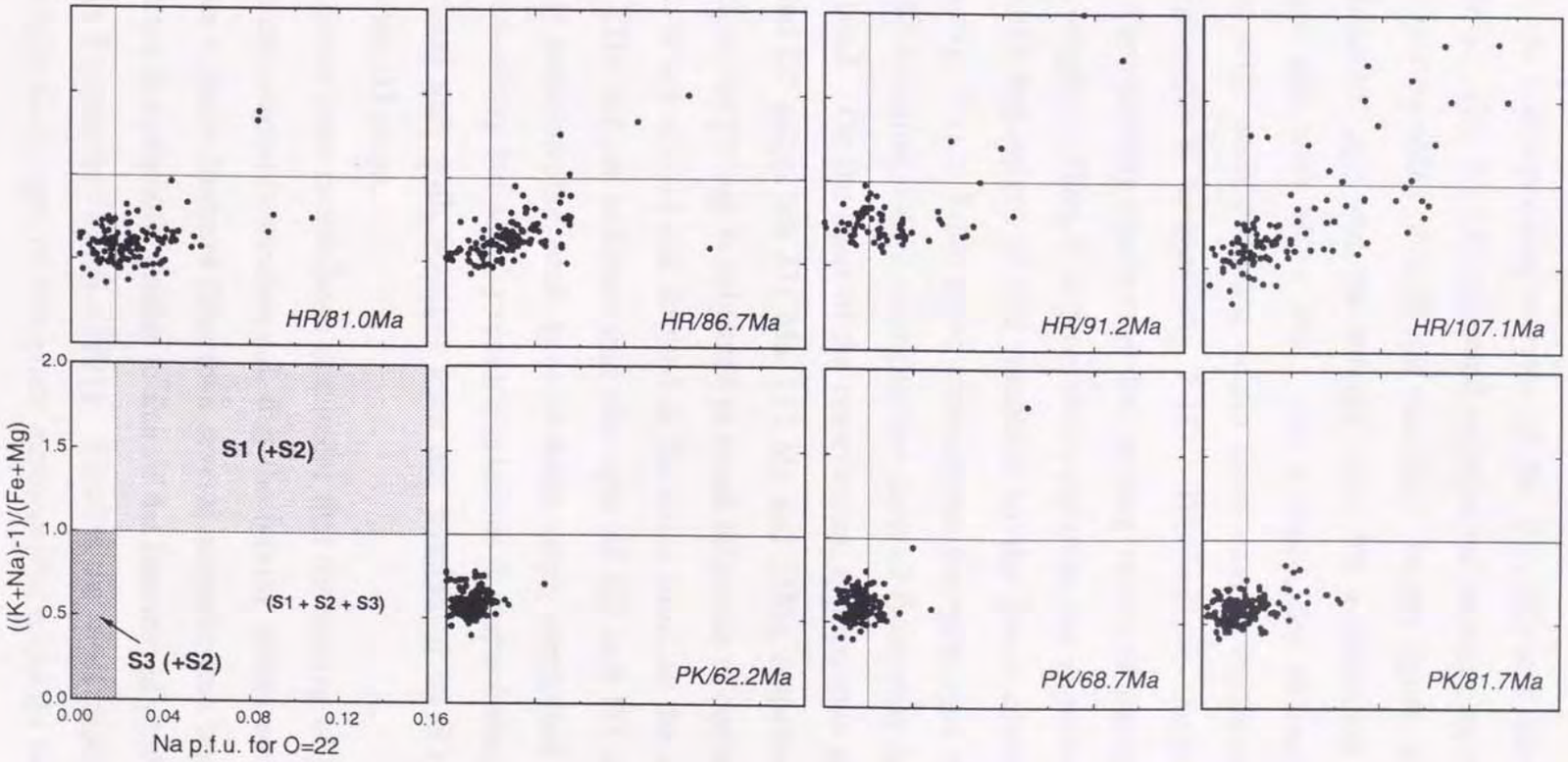

Fig. 7-10. The definitions of compositional ranges of phengites for each specimen dated.

three groups corresponding to ones of the S1-, S2- and S3-foliations, respectively. Fig. 7-11 is presented correlations between apparent K-Ar ages and mixing ratios of each end member. In this figure, how to plot of the apparent age and the mixing ratio for a specimen from the Harushinai unit with 107.1 Ma. As a result, the mixing ratios of phengites with each different origin have exactly relationship with apparent phengite K-Ar ages (Fig. 7-11). This indicates the phengite K-Ar ages considerably change by the mixing ratios of phengites with different origins. Then, it is possible to calculate the approximate ages of each different origin as end members by the linear correlations as shown in Fig. 7-11. From those correlations, phengite ages of the S1-, S2- and S3-foliation, i.e., a phengite age derived from only one origin, are calculated. On the basis of the correlations, approximate ages of the D1, D2 and D3 stages are 231 Ma, 112 Ma and 58Ma, respectively (Fig. 7-11). Since the D1 age is subjected to much influence of detritus, which the origin is not always one formed at the same time, so the age is not treated. The author believes that the ages of D2 and D3 stages are significant metamorphic peak ages in each stage, supported not only phengite chemistry but also by textural relations that specimens from the Pankehoronai unit with younger ages are dominated by S3-foliation formed at the D3 stage.

The above liner correlations document that the mixing of phengites with different origins is mechanical, that the mixing orders are small as the same as a probe diameter (less than several micrometers), and that the mixing nature is extremely similar to that of the interleaved phyllosilicate grains after Franceschelli et al. (1991). Finally, the most important fact is that phengite K-Ar ages of low-grade metamorphic rocks do not show a

Correlations between apparent K-Ar ages and mixing ratios of each end member

Endmember	Calc. age (Ma)	Approximate equation
S1	231	t_{S1}(Ma)= 77.9+1.53 * r_{S1}(%) R^2=0.98
S2	112	t_{S2}(Ma)= 59.7+0.52 * r_{S2}(%) R^2=0.62
S3	58	t_{S3}(Ma)=108.1-0.50 * r_{S3}(%) R^2=0.80

Apparent age (Ma)	No. of analysis	Ratio (%) S3	S2	S1	Recalc. age (Ma) [+/- apparent age]
107.1	97	24.7	56.7	18.6	121 [+14]
91.2	71	35.2	54.9	9.9	105 [+14]
86.7	112	28.6	66.9	4.5	102 [+15]
81.0	118	38.1	59.5	2.4	94 [+13]
81.7	126	59.3	40.7	0.0	80 [-2]
68.7	122	77.1	23.0	0.0	70 [-1]
62.2	104	94.2	5.8	0.0	61 [-1]

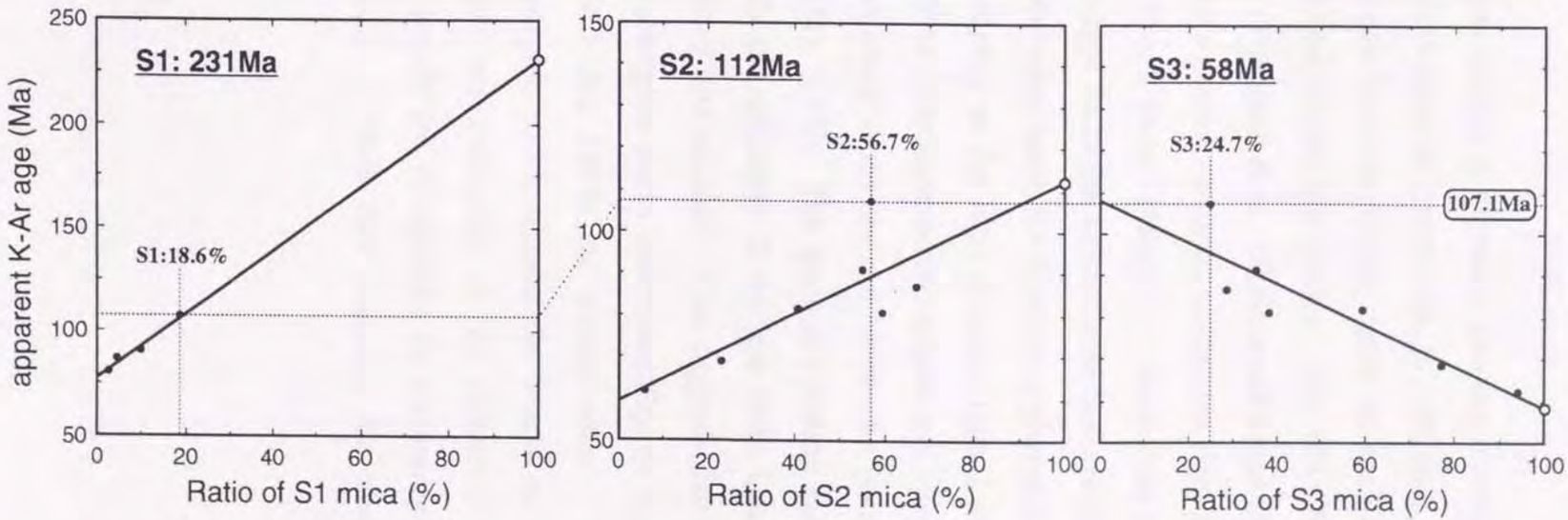

Fig. 7-11. Correlation between the apparent age and the mixing ratio with each different origin and approximate ages of each end member calculated by the linear correlations.

specific time because the portions formed at the same time are obviously small and it is extremely difficult to separate completely, in most case.

Fig. 7-12 shows the relations between mixing ratios of each end member and ^{40}Ar-^{39}Ar incremental-release age spectra. The ^{40}Ar-^{39}Ar incremental-release age spectra (Takigami et al., 1992; unpublished data) of heterogeneous specimens have a pattern elevating toward the right side (higher temperature step) and do not show "plateau". These data also support that the phengite K-Ar ages from the Kamuikotan metamorphic rocks, dated in this study. On the other hand, the fraction of phengites in Mitsuishi siliceous schist, belonging to the high-pressure type 1 after Sakakibara and Ota (1994), of ^{40}Ar-^{39}Ar incremental-release age spectra (Takigami et al., 1992; unpublished data) do not show the pattern elevating toward the right side (Fig. 7-13). The (pseudo-) plateau age is approximately concordant with the phengite K-Ar age after Ota et al.(1993), taking the analyzing error into account. This suggests that the phengite K-Ar ages from metamorphic rocks corresponding to high-pressure type 1 (Sakakibara and Ota, 1994) are worthy ones. As mentioned before, these metamorphic rocks, such as the blocks in the Tokiwayama melange unit, are not subjected to the influence of retrogressive recrystallization which are recognized in metamorphic rocks of the Pankehoronai unit. This fact supports the above interpretation.

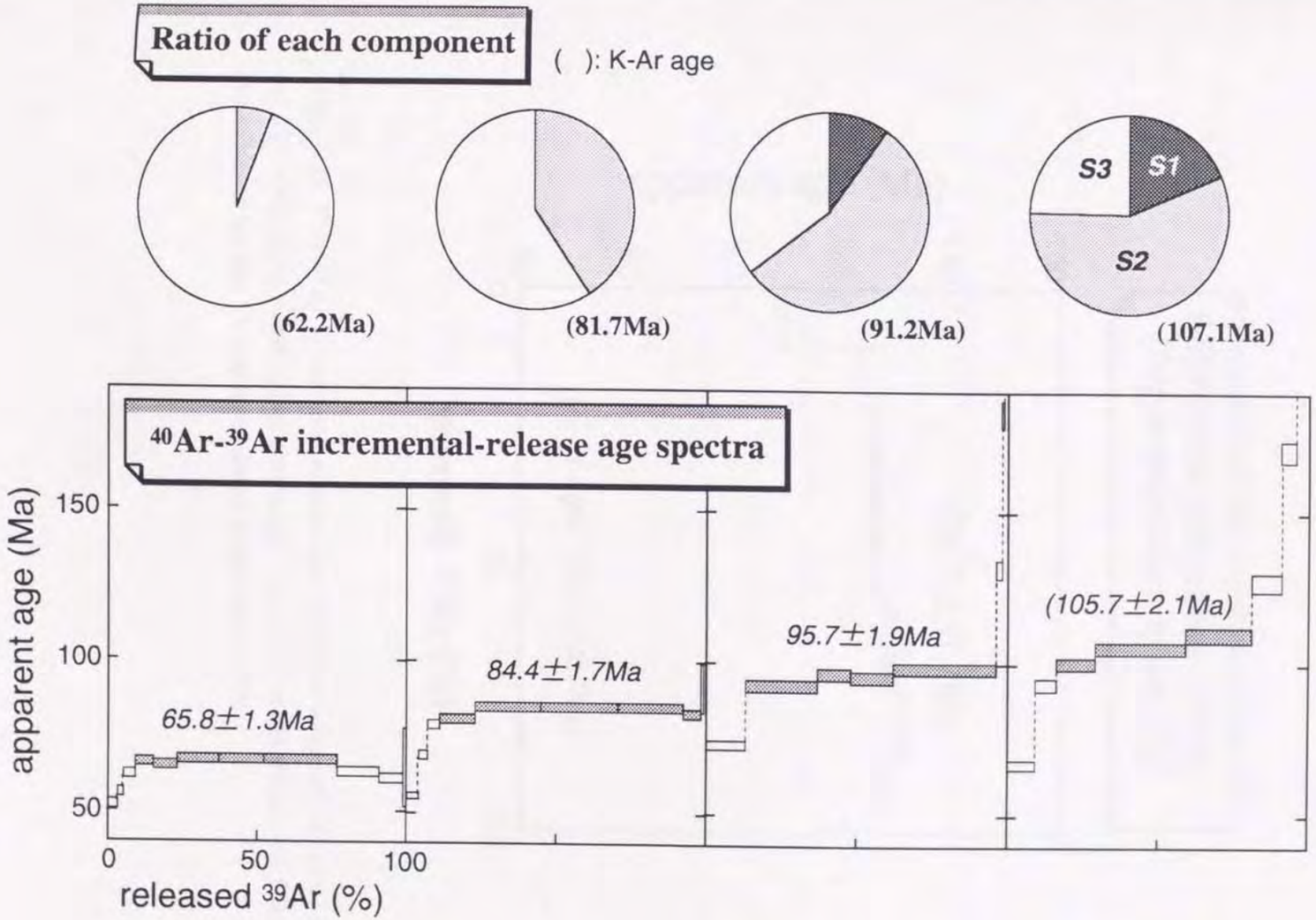

Fig. 7-12. Relations between mixing ratio of each end member and ^{40}Ar-^{39}Ar incremental-release age spectra. Note that heterogeneous specimens do not show "plateau".

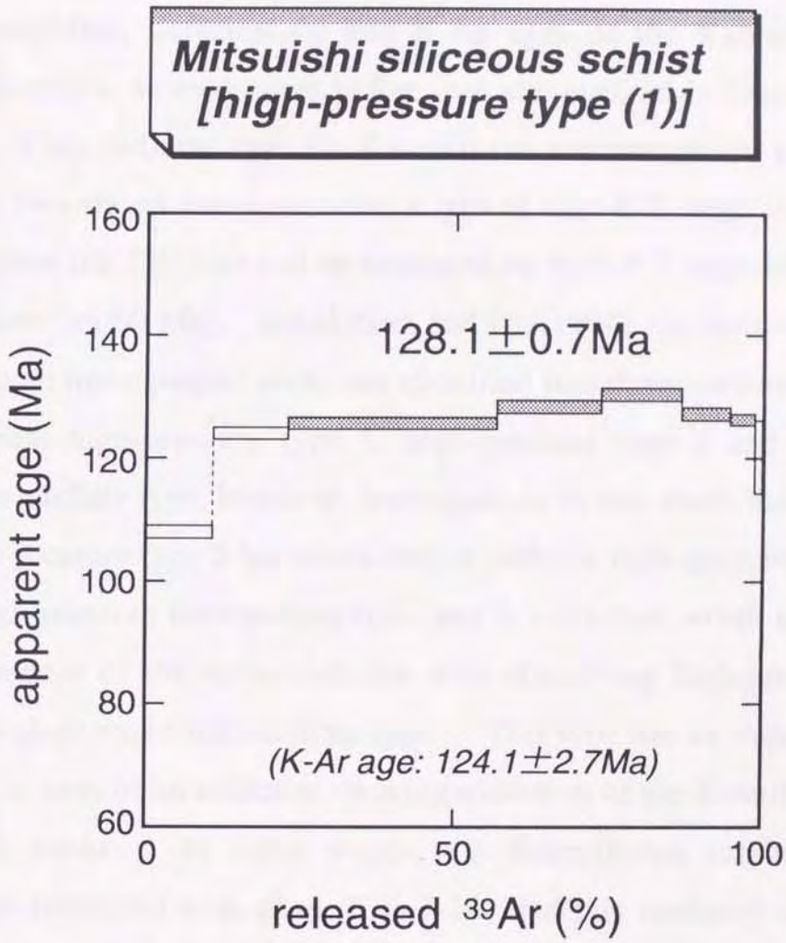

Fig. 7-13. ^{40}Ar-^{39}Ar incremental-release age spectra of Mitsuishi siliceous schist (Ota et al.,1991) belonging to the high-pressure type 1 classified by Sakakibara and Ota (1994). This specimen is Sp. No. 15 which was dated by Ota et al.(1993).

7-3. Evolution of the Kamuikotan metamorphic rocks from Kamuikotan Gorge area

Metamorphism, deformation and K-Ar ages of the Kamuikotan metamorphic rocks, as mentioned before, are summarized in Figs. 7-14 and 7-15. They indicate that the Kamuikotan metamorphism can be divided into two stages fundamentally: a typical high-P/T stage in early Cretaceous time (ca 120 Ma) and an intermediate high-P/T stage in early Paleogene time (ca 60 Ma). Sakakibara and Ota(1994) has insisted that the Kamuikotan metamorphic rocks are classified into three metamorphic pressure types: high-pressure type 1, high-pressure type 2 and high-pressure intermediate type, however, investigations in this study indicates that the high-pressure type 2 has characters of both the high-pressure type 1 and the high-pressure intermediate type, and is not a type which can be divided by means of the same criterion with classifying high-pressure type 1 and high-pressure intermediate type. This type has an important significance in term of an indicator showing evolution of the Kamuikotan metamorphic rocks. In other words, the Kamuikotan subduction geotherm has increased with time (Fig. 7-14) and this tendency is the principal nature of the Kamuikotan metamorphic rocks.

Finally, the processing formation of the Kamuikotan metamorphic rocks based on the results of this study and available data from various viewpoints is illustrated as Fig. 7-16.

In earliest Cretaceous time (Fig. 7-16a), the Kamuikotan metamorphism has begun together with northwestward subduction of the Sorachi plateau (Kimura et al., 1994) on the Izanagi plate with Triassic age, judging from radiolarian biostratigraphic data after Hori and Sakakibara (1994). In this time, the subduction rate has suddenly become

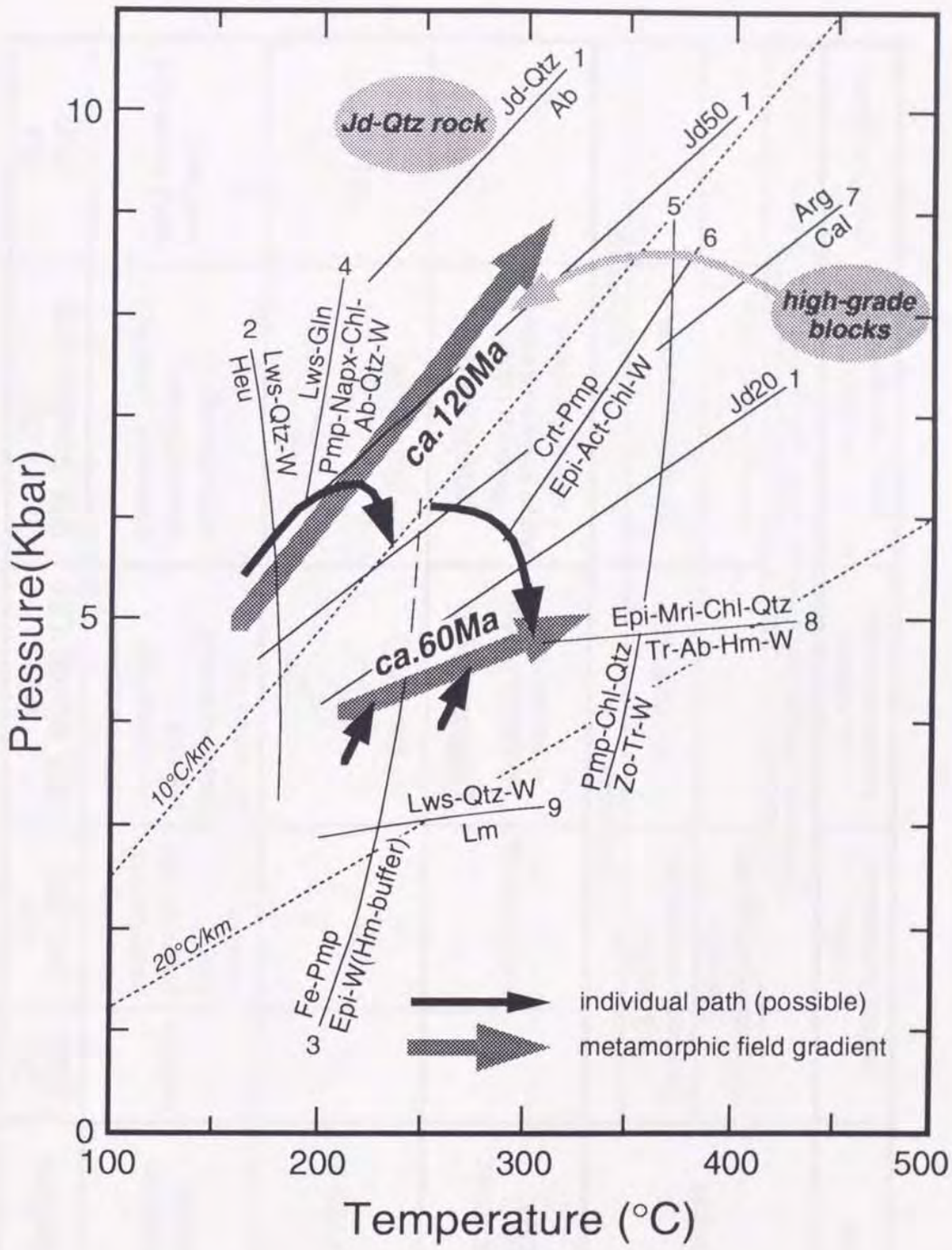

Fig. 7-14. Summarized P-T diagram showing history of various metamorphic rocks in the Kamuikotan metamorphic belt. Metamorphic conditions and history of jadeite-quartz rock (Takayama, 1986) and high-grade blocks (Shibakusa, 1991) are also shown. Note that metamorphic field gradients of coherent high-P/T metamorphic rocks are changing with time.

Deformation	D0 (S0)	D1 (F1, S1)	D2 (F2, S2=Si, L2)	D3 (F3, S3=Sm, L3)	D4 (F4)
Deformation structure	bedding	schistosity intrafolial fold ptygmatic fold boudin fracture	asymmetric close fold crenulation fold kink fold pressure solution S-C structure	asymmetric close fold crenulation fold axial cleavage	upright open fold kink band
Type of strain	(?)		 (top to NE)	 (top to SSW)	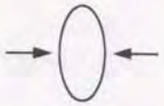
Metamorphic Facies		(Pmp-Act Facies)	**[initial stage]** Blueschist Facies *- max pressure -*	**[main stage]** Pmp-Act Facies (higher temperature subfacies) *- max temperature -*	
Tectonics	subduction			exhumation	
	accretion (formation of melange)		underplating	formation of nappe	
	Transit of the Farallon-Izanagi ridge			*Transit of the Kula-Pacific ridge*	
	Westward conversion of motion of the Izanagi-Kula plate				
Time	ca.130Ma (earliest Cretaceous)		ca. 120Ma (early Cretaceous)	ca. 60Ma (early Paleogene)	(late Paleogene)

Fig. 7-15. Summary of deformation, metamorphism and tectonics of the Kamuikotan high-P/T metamorphic rocks in central Hokkaido.

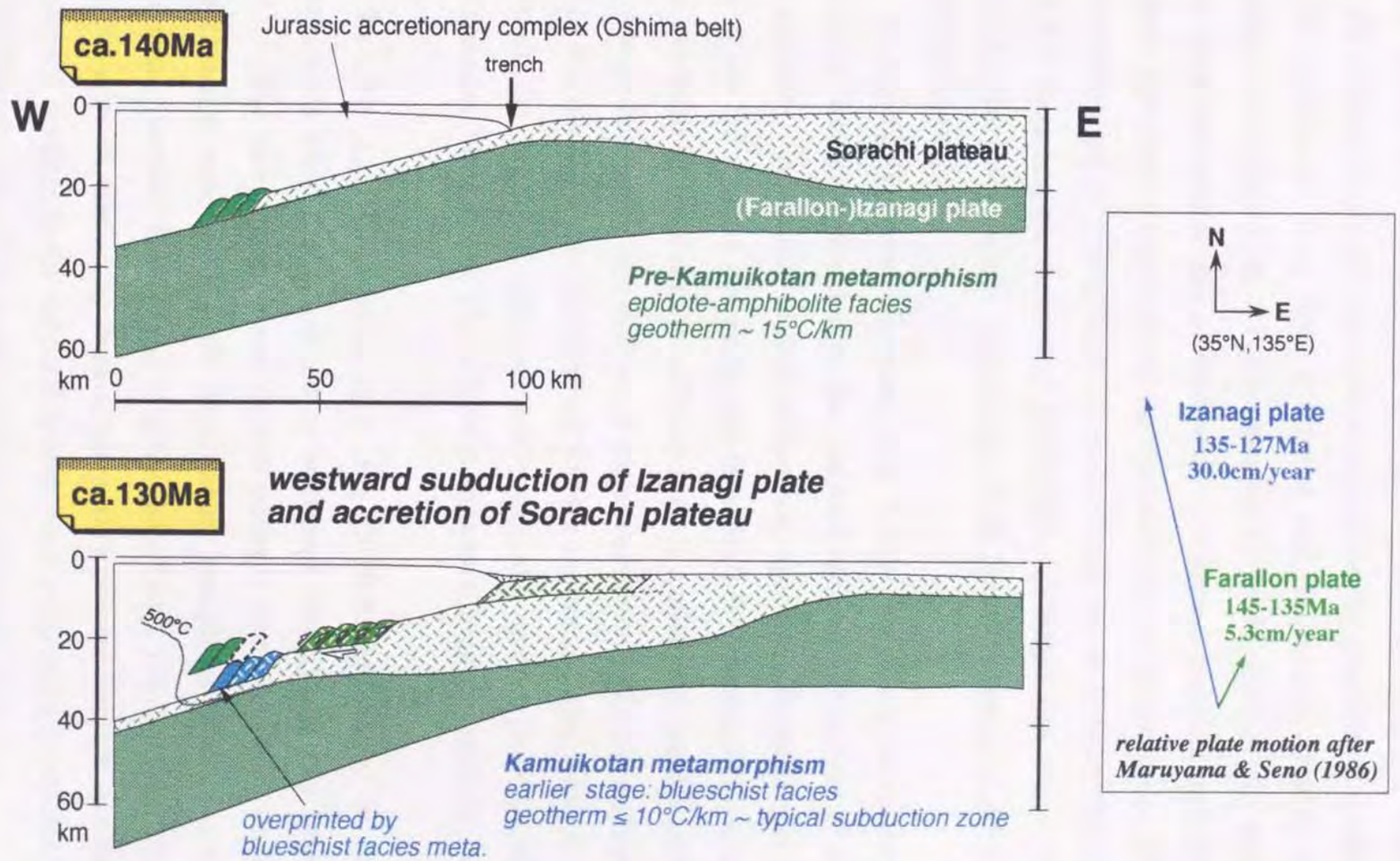

Fig. 7-16. A model showing formation and exhumation processes of the Kamuikotan high-P/T metamorphic rocks. See text for details. **a**. earliest Cretaceous (140-130Ma).

faster (about 30 cm/year; Maruyama and Seno, 1986) than the before. By the subduction of old and cold oceanic plate, the geothermal gradient in the subduction zone have decreased and resulted in forming the representative blueschists. Pre-formed higher-grade metamorphic rocks have been refrigerated due to decreasing geothermal gradient, and parts of them have been overprinted by the blueschist facies assemblages. The radiometric ages of typical high-P/T metamorphic rocks indicate that the high-P/T metamorphic rocks have immediately exhumed after that. The major driving force may be a buoyancy of the Sorachi plateau subducted, with huge amounts.

In late Early Cretaceous time (Fig. 7-16b), strike slip faults have formed at forearc basin due to the sinistral oblique subduction of the Izanagi plate. According to their radiometric ages and estimated ages as time of the D2 stage in this study, the most high-P/T metamorphic rocks have exhumed before this time and have been at a relatively shallow level. What serpentine sands and detritus of metamorphic minerals are included within the middle Yezo Group,being forearc sediments, also imply that parts of the high-P/T metamorphic rocks and exotic higher-grade metamorphic blocks have exposed with serpentinite on the earth in that time.

In early Late Cretaceous time (Fig. 7-16c), the motion of the Izanagi-Kula plate has converted to westward (Maruyama and Seno, 1986). The sedimentation and growth patterns of accretionary prism have changed, resulting that the accretionary complexes dominated by continental materials have begun to grow (Kiyokawa, 1992). After this time, the ages of subducting oceanic plate have become younger and the geothermal gradient in the subduction zone have progressively increased. The subduction rates of the oceanic plate have gradually decreased.

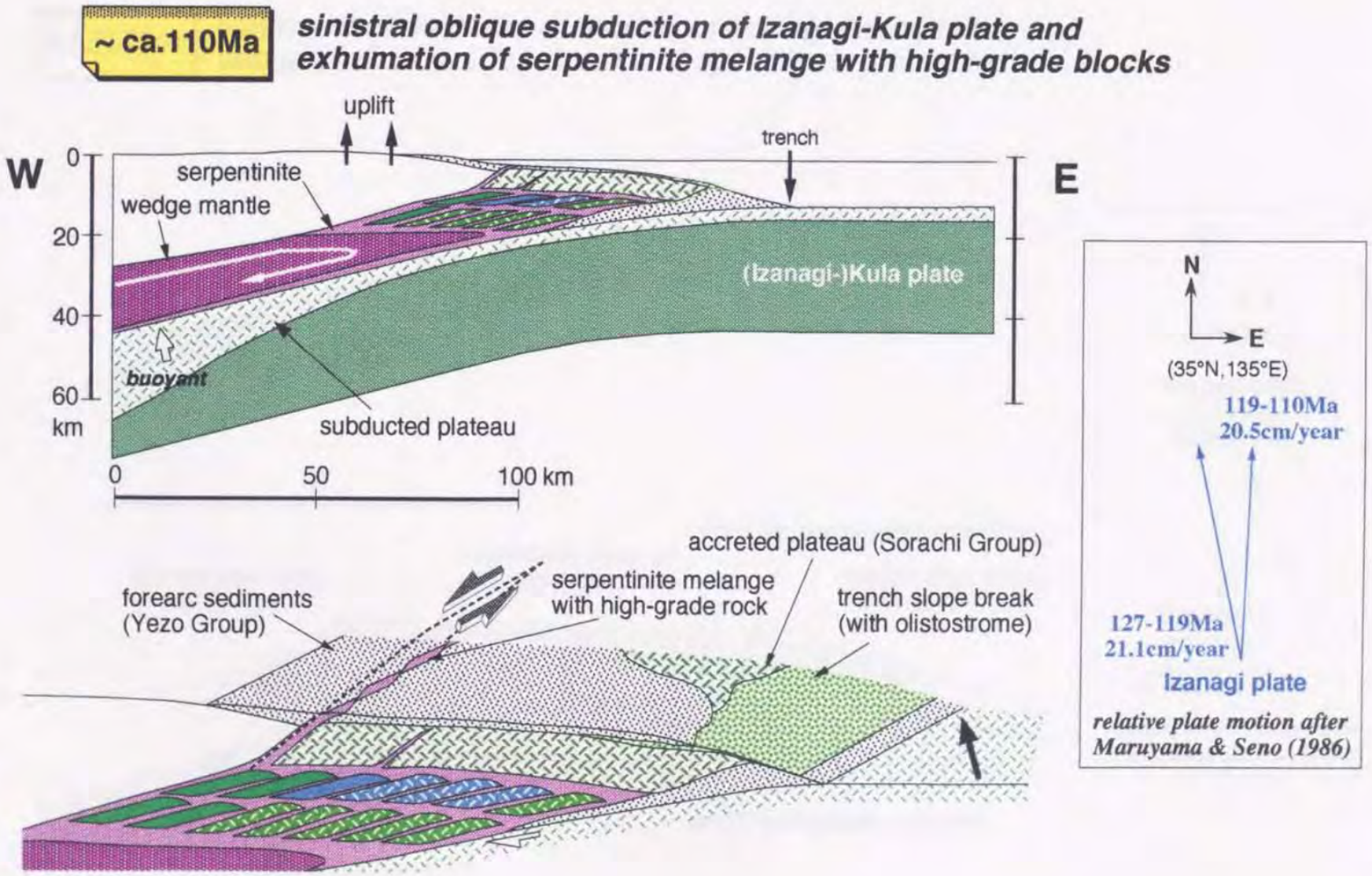

Fig. 7-16. b. late Early Cretaceous (ca. 110Ma).

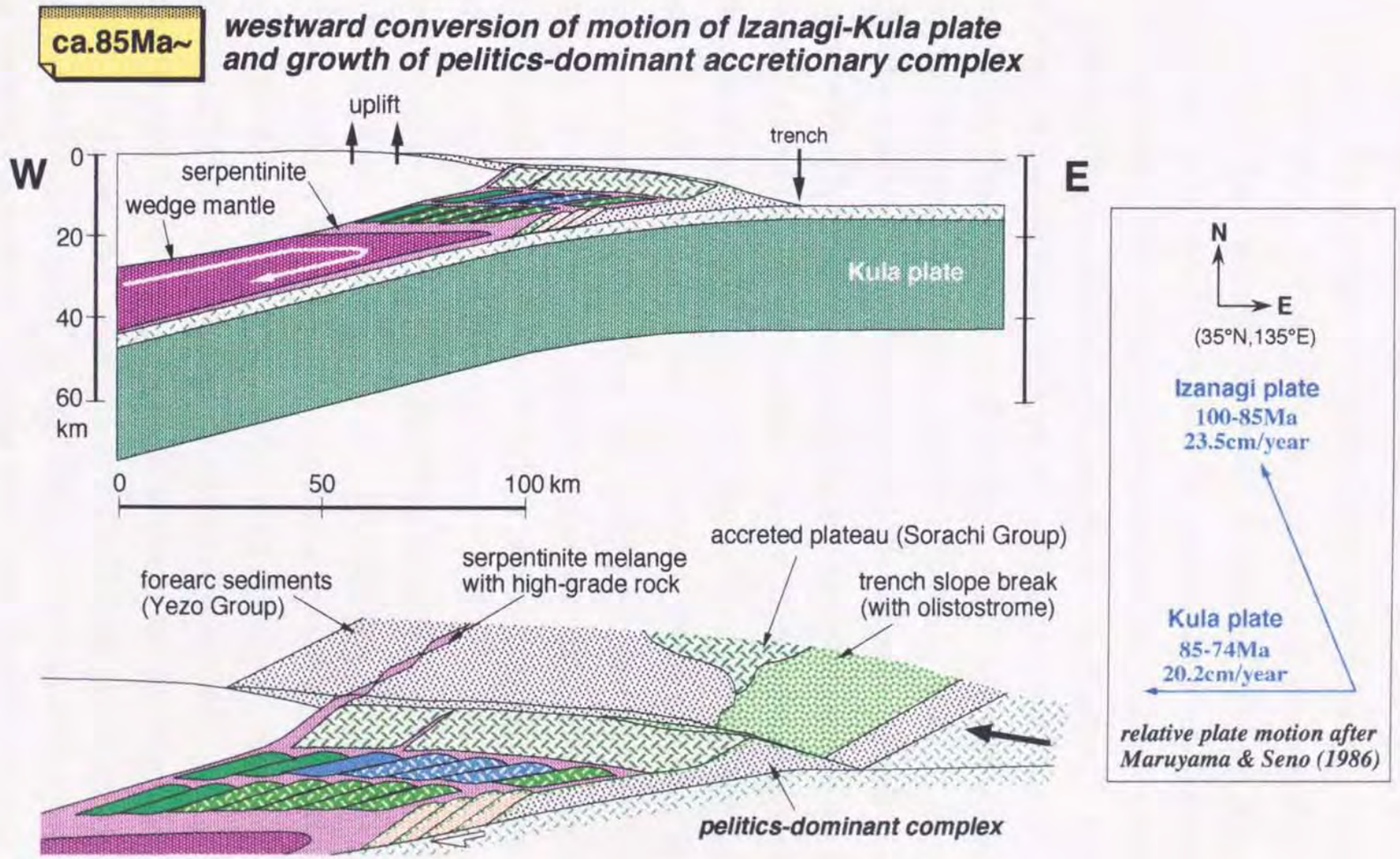

Fig. 7-16. c. early Late Cretaceous (ca. 85Ma).

In early Paleogene time, estimated as time of the D3 stage (Fig. 7-16d), the Kula-Pacific ridge has approached around Hokkaido. The geothermal gradient in the subduction zone have increased and the metamorphic rocks belonging to high-P/T intermediate type (e.g., Pankehoronai unit) have been produced at the lower part of the accretionary prism. They have exhumed with formation of nappe and have attained the metamorphic peak during the exhumation. The exhumation of metamorphic rocks at this time may result from the buoyancy of the Kula-Pacific plate with young age, sufficiently developed accretionary complex, and underplating to the lower level of such accretionary complex. The delamination at the boundary between the Kula and Pacific plates (so-called the Kula-Pacific ridge) may have been effective to the exhumation of metamorphic rocks. Some of high-P/T metamorphic rocks (e.g., Harushinai and Biei units), which had already exhumed at a shallow level, have been subjected to the influence of increasing geothermal gradient in the subduction zone. But the metamorphic sequenses at the present structural upper level (e.g., Horokanai unit; Sakaibara and Ota, 1994) have been suffered no influence of recovering the geothermal gradient.

It is suggested that complex natures of the Kamuikotan metamorphic rocks have produced by such a process, which the ages of subducting plates have gradually become younger and the relaxation of geothermal gradient under the subduction zone, formed the metamorphic rocks, have been activated during Early Cretaceous to Early Paleogene time.

Besides, the Kamuikotan subduction geotherm has increased with time (Fig. 7-14) and this tendency is the principal nature of the Kamuikotan metamorphic rocks, as stated before. On the other hand, the relation between metamorphic field gradient and individual P-T paths of

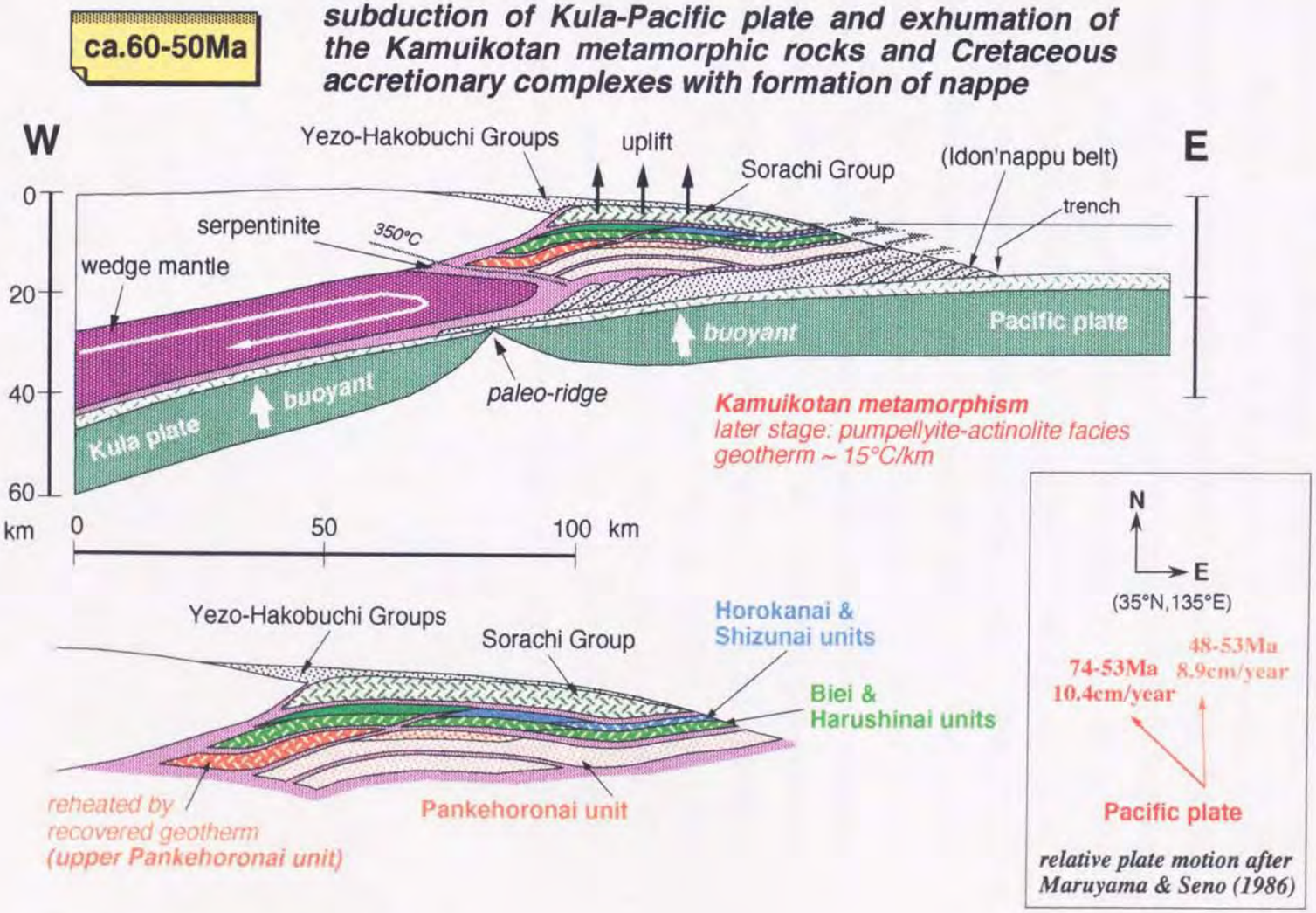

Fig. 7-16. d. early Paleogene (60-50Ma).

the Sanbagawa metamorphic rocks (Nakamura and Enami, 1994) is different from that of the Kamuikotan metamorphic rocks (Fig. 7-17). In the Sanbagawa metamorphic belt, the individual P-T paths of all mineral zones are forming only one metamorphic facies series and the systematic change of the individual P-T paths indicate that the Sanbagawa subduction geotherm has decreased with time (Fig. 7-17). These two metamorphic rocks have formed in Cretaceous time, related to the subduction of the Izanagi plate toward the eastern margin of the Asian continent. The changes of their individual P-T paths with time indicate that the high-P/T metamorphisms have advanced within the subduction zones which have a non-steady-state geotherm. Difference of evolution of the above two metamorphic rocks may be related to difference of the subduction modes, depending on the tectonic setting of the overriding continental plates, proposed by Kimura et al. (1990), with some uncertainties. Current uncertainties on the tectonics of the high-P/T metamorphic belts in the subduction zones will reveal on the way of integrating discussions for various tectonics related to the subduction zones.

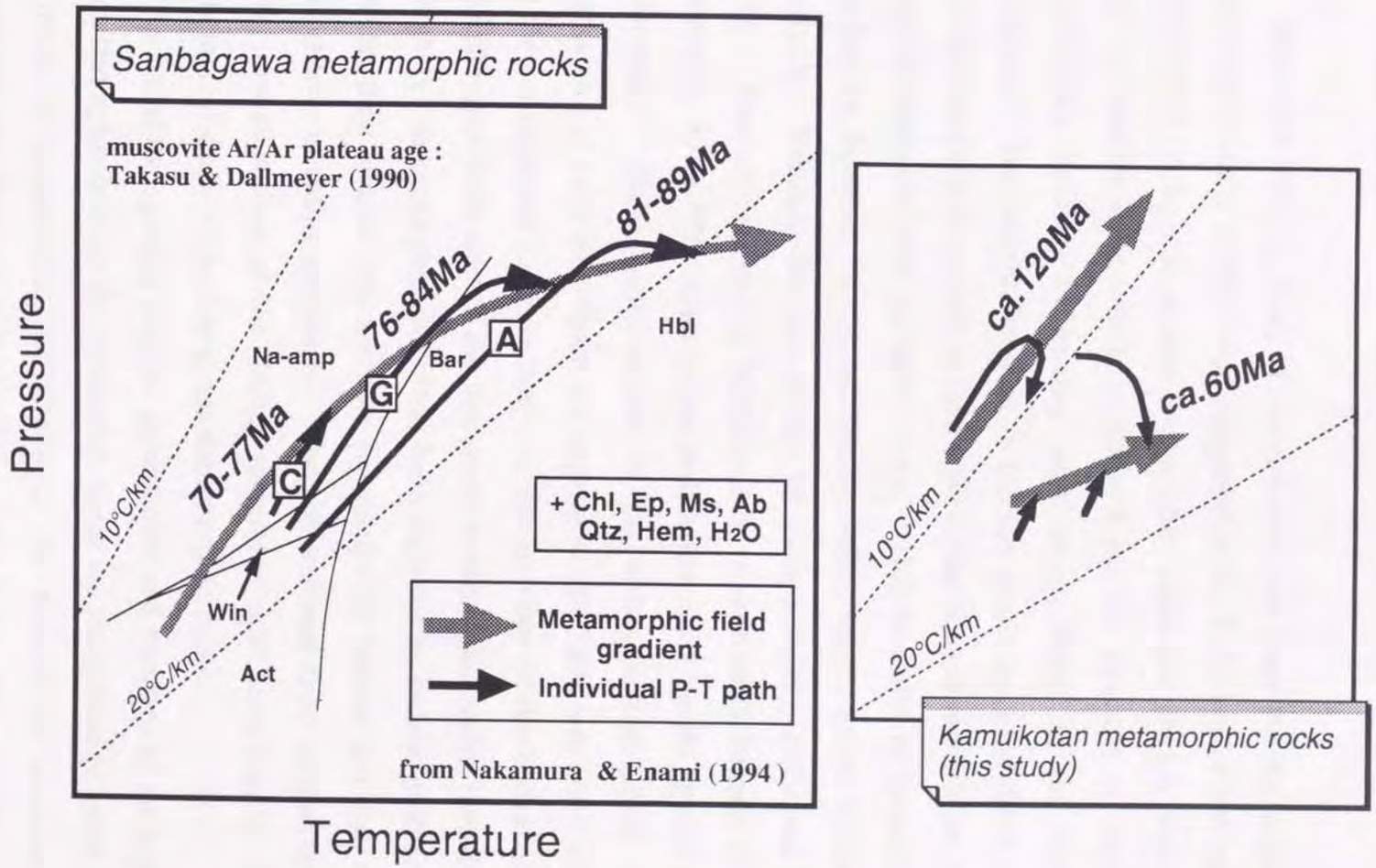

Fig. 7-17. The relations between metamorphic field gradients and individual P-T paths. Note that the change with time of the Sanbagawa geothermal gradients shown by individual P-T paths is different from that of the Kamuikotan geothermal gradients.

8. Conclusion

Minutely investigations of dated specimens from the Kamuikotan metamorphic rocks in this study suggest that the K-Ar age of low-grade metamorphic rocks is a mixture age in many cases and always does not show a specific time which is defined by the concept of closure temperature, because of mixing multi-origin micas in the dating specimens. The recrystallization in the low-grade metamorphism less than the pumpellyite-actinolite facies preserves the earlier textures and forms considerably heterogeneous rocks. This is useful to investigate their history, however for the radiometric dating, such a nature becomes a demerit. Because the ages change by parts selecting specimens for dating. Recently, the dating techniques on a very small domain (e.g., spot-fusion ^{40}Ar-^{39}Ar laser-probe techniques on a single grain) are developed. Their contributions in the chronological study are remarkable but such techniques are expensive and have less convenient than the conventional K-Ar method. In the previous works, discordance of the phengite K-Ar ages of the low-grade metamorphic rocks, including the high-P/T metamorphic rocks, has been regarded as serious problems, however, their sources are not only the analytical method but also the heterogeneity in dating specimens. The conventional K-Ar method with careful investigations of the dating specimens will contribute to the chronological study of the low-grade metamorphic rocks.

As stated the opening chapter, generalities and varieties of the high-P/T metamorphic belts in the subduction zones are recognized in terms of the mode of occurrence, the structure, the amount of associated serpentinite, the range of radiometric age, the P-T paths of individual rocks, and so on. From these view points, the formation and exhumation

mechanism of the high-P/T metamorphic rocks have been discussed to date.

The increasing the Kamuikotan metamorphic P/T gradient with time indicate that the Kamuikotan metamorphism has advanced within the subduction zones which have a non-steady-state geotherm, and the radiometric ages of the Kamuikotan high-P/T metamorphic rocks, subjected to regional deformation, do not show a specific time. Thus, the exhumation of high-P/T metamorphic rocks is not always continuous, even if their radiometric ages successively change. The persistence of high-P/T assemblages in the high-P/T metamorphic rocks requires the rapid exhumation without recovering the geothermal gradient. Although the P-T paths of individual high-P/T metamorphic rocks have changed with time, such changes result from the non-steady-state geotherm of the subduction zone. The exhumation of high-P/T metamorphic rocks which are contained their ages within a specific range is certainly episodic and may be rapid. Platt (1986) has emphasized underplating of pre-subducted materials and extensional tectonics derived from the underplating, and insisted the unroofing model. The conclusion for radiometric ages in this study, however, indicates that the exhumation of high-P/T metamorphic rocks is exactly episodic, and does not assist the extension model proposed by Platt (1986). Consequently, this study supports the wedge extrusion model, proposed by Maruyama (1990) and Maruyama et al.(1994), as the exhumation mechanism of the high-P/T metamorphic belts in the subduction zones.

Acknowledgments

I wish to express my sincere gratitude to Associate Professor Sumio Miyashita of Niigata University for his valuable suggestions and discussions, and critical reading of the manuscript. I greatly appreciate Associate Professor Masayuki Sakakibara of Ehime University, who advised, encouraged and provided invaluable discussions at the various stages of this study. I am grateful to Professor Tetsumaru Itaya of Okayama University of Science for his permission and instruction of the K-Ar dating, and valuable suggestions and discussions about the chronological study. I would like to thank Associate Professor Tsuyoshi Toyoshima of Niigata University for his helpful guidance, advice, and discussion in the structural analysis.

I also wish to thank Dr. Toshiaki Shimura of Niigata University for his helpful suggestions and discussions. I would like to thank Dr. Takashi Arai of the same university for his advice and fruitful discussions. I wish to thank Dr. Hidehiko Shibakusa of Ikueu High School, Professor Teruo Watanebe of Hokkaido University and Dr. Hiroyuki Takeshita of Okayama University of Science for useful discussions. I would like to thank Associate Professor Yutaka Takigami of Kanto Gakuen University for permission to cite unpublished data of the Ar-Ar dating. I am grateful to Mr. Hisashi Ofuka of Co., Ltd. TOKEN GEOTECH, who discussed the geology of study area and provided the dating specimens. I am indebted to Professor Koichi Tazaki of Ehime University for his instruction of preparation of dating specimens and useful advice, and to Professor Kenji Shuto of Niigata University for his encouragement and helpful advice.

I would like to thank students of Okayama University of Science for assistance with K-Ar dating and useful discussions. I also acknowledge the intellectual stimulation provided by my colleagues and students in Niigata, Ehime and Hokkaido Universities.

I would like to express my gratitude to Mr. and Mrs. Kurashima resident to Asahikawa, Hokkaido for assistance of various kinds during the field work. Finally, I am sincerely thankful that the late my father has encouraged me in my studies.

References

Arai, T. and Miyashita, S., 1994, Shear deformation and metamorphism of the Poroshiri Ophiolite in the Shunbetsu River region, the Hidaka belt, Hokkaido, Japan. *Jour. Geol. Soc. Japan*, 100, 162-176.*

Asahina, T. and Komatsu, M., 1979, The Horokanai opholitic complex in the Kamuikotan tectonic belt, Hokkaido, Japan. *Jour. Geol. Soc. Japan.*, 85, 317-330.

Brown, E.H., 1977, Phase equilibria among pumpellyite, lawsonite, epidote and associated minerals in low grade metamorphic rocks. *Contrib.Mineral.Petrol.*, 64, 123-136.

Coombs, D.S., Nakamura, Y. and Vaugnat, M., 1976, Pumpellyite-actinolite facies schists of Taveyanne Formation near Loeche, Valais, Switzerland. *Jour. Petrol.*, 17, 440-471.

Dewey, J.F. and Bird, J.M., 1970, Mountain belts and the new global tectonics. *Jour. Geophys. Res.*, 75, 2625-2647.

Eggleton, R.A., 1972, The cristal structure of stilpnomelane. Part II. The full cell. *Mineral. Mag.*, 38, 693-711.

Ernst, W.G., 1988, Tectonic history of subductionzones inferred from retrograde blueschist *P-T* paths. *Geology*, 16, 1081-1084.

Evans, B.W., 1990, Phase relations of epidote-blueschists. *Lithos,* 25, 3-23.

Franceschelli,M., Memmi, I. and Gianelli G., 1991, Re-eqilibration of detrital muscovite and the formation of interleaved phyllosilicate grains in low temperature metamorphism, northern Apennines, Italy. *Contrib. Mineral Petrol.*, 109, 151-158.

Gouchi, N., 1983, Kamuikotan metamorphic rocks in the Kamuikotan gorge area, west of Ashikawa, Hokkaido. *Jour. Japan. Assoc. Min. Petr. Econ. Geol.*, 78, 383-393.*

Gouchi, N., Omata, M., Katoh, T., Itaya, T. and Watanabe, T., 1992, K-Ar ages of white mica fractions from the Susunai metamorphic rocks in Sakhalin, far east Russia. *Jour. Fac. Sci. Hokkaido Univ.* Ser. IV, 23, 2, 281-286.

Hashimoto, M., 1985, Two geological types of glaucophanitic terranes in Japan. *Jour. Japan. Assoc. Min. Pet. Econ. Geol.*, 80,113-117.*

Hey, M.H., 1954, A new review of the chlorites. *Miner. Mag.*, 30, 277-292.

Hirajima, T., Isono, T. and Itaya, T., 1992, K-Ar age and chemistry of white mica in the Sanbagawa metamorphic rocks in the Kanto Mountains, central Japan. *Jour. Geol. Soc. Japan*, 98, 5, 445-455.*

Hori, S.R. and Sakakibara, M., 1994, A chert-clastic sequence spanning the late Triassic-early Cretaceous period of the Kamuikotan Complex in the Shizunai area, south-central Hokkaido, Japan. *Jour. Geol. Soc. Japan,* 100, 8, 575-583.

Imaizumi, M., 1984, Metamorphism and mode of occurrence of metabasites in the Kamuikotan terrain of the Horokanai Pass area, Hokkaido. *Jour. Japan. Assoc. Miner. Petrol. Econ.*, 79, 1-19.*

Imaizumi, M. and Uyeda, Y., 1981, On the K-Ar ages of the Rocks of two kinds existed in the Kamuikotan metamorphic rocks located in the Horokanai district, Hokkaido. *Jour. Japan. Assoc. Miner. Petrol. Econ.*, 76, 88-92.*

Imaizumi, M. and Kanehira, K., 1980, Jadeite from the Kamuikotan tectonic belt, Hokkaido. *Jour. Geol. Soc. Japan*, 86, 629-633.

Ishibashi, M., 1939, On the rocks in vicinity of Horai-san, Mitsuishi in the province of Hidaka. *Bull. Geol. Surv.Hokkaido*, 10, 7-34.**

Ishizuka, H., 1985, Prograde metamorphism of the Horokanai ohiolite in the Kamuikotan zone, Hokkaido, Japan. *Jour. Petro.*, 26, 391-417.

Ishizuka, H. and Imaizumi, M., 1980, Epidote-garnet amphibolite from the Horokanai pass area in the Kamuikotan tectonic belt, Hokkaido. *Jour. Geol. Soc. Japan,* 86, 15-24.

Ishizuka, H., Imaizumi, M., Gouchi, N. and Banno, S., 1983a, The Kamuikotan zone in Hokkaido, Japan: tectonic mixing of high-pressure and low-pressure metamorphic rocks. *Jour. Metamorphic. Geol.*, 1, 263-275.

Ishizuka, H., Okamura, M. and Saito, Y., 1983b, Latest Jurassic radiolarian from the Horokanai ophiolite in the Kamuikotan zone, Hokkaido, Japan. *Jour. Geol. Soc. Japan*, 89, 731-732.

Ishizuka, H., Imaizumi, M. and Hirono, A., 1989, Tectonics on the formation of the Kamuikotan zone based on the geology and structure of the high-pressure metamorphic rocks. *Mon. Earth*, 11, 6, 350-354.**

Isozaki, Y. and Itaya, T., 1990, Chronology of Sanbagawa metamorphism. *Jour. Metamorphic. Geol.*, 8, 401-411.

Isozaki, Y., Maruyama, S. and Furuoka, F., 1990, Accreted oceanic materials in Japan. *Tectonophysics*, 181, 179-205.

Isozaki, Y. and Itaya, T., 1991, Pre-Jurassic klippe in northern Chichibu Belt in west-central Shikoku, Southwest Japan -Kurosegawa Terrane as a tectonic outlier of the pre-Jurassic rocks of the Inner Zone. *Jour. Geol. Soc. Japan*, 97, 6, 431-450.*

Isozaki, Y. and Maruyama, S., 1991, Studies on orogeny based on plate tectonics in Japan and new geotectonic subdivision of the Japanese Islands. *Jour. Geography*, 100, 697-761.*

Itaya, T. and Takasugi, H., 1988, Muscovite K-Ar ages of the Sambagawa schists, Japan and argon depletion during cooling and deformation. *Contr. Miner. Petrol.*, 100, 281-290.

Itaya, T., Nagao, K., Inoue, K., Honjou, Y., Okada, T. and Ogata, A., 1991, Argon isotope analysis by a newly developed mass spectrometric system for K-Ar dating. *Mineral. Jour.*, 15, 5, 203-221.

Iwasaki, I., Watanabe, T. and Itaya, T., 1991, Eocene K-Ar ages for white mica in the Kamuikotan belt, Hokkaido, Japan. *Joint Ann.*

Meet; Soc. Mining Geol. Japan, Japan. Miner. Petrol. Econ. Geol. and Mineral. Soc. Japan, Abstract. 78.**

Iwasaki, I., Shibakusa, H., Gouchi, N. and Watanabe, T., 1994, Kamuikotan Belt (Central part). *the 101 th Ann. Meet. the Geol. Soc. Japan, Excursion guidebook,* 139-159.**

Jäger, E., 1979, Introduction to geochronology. *In Jäger, E. and Hunziker, J.C., eds., Lectures in isotope geology, Springer, Berlin,* 1-12.

Johannes, W. and Puhan, D., 1971, The calcite-aragonite transition, reinvestigated. *Contri. Mineral. Petrol.*, 31, 225-228.

Katoh, Y.,Niida, K. andWatanabe, T., 1979, Serpentinite melange around Mt.Shirikomadake in the Kamuikotan Structural Belt, Hokkaido. *Jour. Geol. Soc. Japan,* 85, 279-285.*

Kawamura, M., Tajika, J., Kawamura, T. and Kato, Y., 1986, Constitution and occurrences of the Paleozoic and Mesozoic fromations in SW Hokkaido, northern Japan. *In Geology and Tectonics of Hokkaido, Monogr. Assoc. Geol. Collab. Japan,* 31, 17-32.*

Kawamura, M., Ohtsu, S., Terada, T. and Yasuda, N., 1994, Geology and internal structure of the Jurassic Oshima accretionary complex. *the 101 th Ann. Meet. the Geol. Soc. Japan, Excursion guidebook*, 175-195.**

Kiminami, K., 1983, Sedimentary history of the late Cretaceous-Paleocene Nemuro Group, Hokkaido,Japan: a forearc basin of the Paleo-Kuril arc-trench system. *Jour. Geol. Soc. Japan*, 89, 607-624.

Kiminami, K., 1986, Cretaceous tectoniucs of Hokkaido and the environs of the Okhotsk Sea. *Monogr. Assoc. Geol. Collab. Japan,* 31, 403-418.*

Kiminami, K., Komatsu, M., Niida, K. and Kito, N., 1986, Tectonic divisions and stratigraphy of the Mesozoic rocks of Hokkaido, Japan. *Monogr. Assoc. Geol. Collab. Japan*, 31, 1-15.*

Kimura, G., 1986, Oblique subduction and forearc tectonics. *Geology,* 14, 404-407

Kimura, G., Miyashita, S. and Miyasaka S., 1983, Collision tectonics in Hokkaido and Sakhalin. *In Hashimoto, M. and Uyeda, S.(eds), Accretion tectonics in the Circum-Pacific regions., TERRAPUB, Tokyo,* 123-134.

Kimura, G., Takahashi, M. and Kuno, M., 1990, Mesozoic collision-extrusion tectonics in eastern Asia. *Tectonophysics,* 181, 15-23.

Kimura, G., Sakakibara, M., Ofuka, H., Ishizuka, S., Okamura, M., Melonikov, O.A. and Lushchenko, Y., 1992, A deep section of accretionary complex: Susunai Complex in Sakhalin Island, Northwest Pacific Margin. *The Isalnd Arc,* 1, 166-175.

Kimura, G., Sakakibara, M. and Okamura,M., 1994, Plumes in central Panthalassa? Deductions from accretes oceanic fragments in Japan. *Tectonics*, 13, 905-916.

Kito, N., 1987, Stratigraphic relation between greenstones and clastic sedimentary rocks in the Kamuikotan Belt, Hokkaido, Japan. *Jour. Geol. Soc. Japan*, 93, 21-35.**

Kiyokawa, S., 1992, Geology of the Idonnappu belt, central Hokkaido, Japan: evolution of a Cretaceous accretionary complex. *Tectonics*, 11, 1180-1206.

Kokubu, H., Kawamura, M., Nakagawa, M., Katoh, T., Toda, H., Sakakibara, M. and Reserch Group of the Kamuikotan Belt., 1990, Reexamination on the geological units of the Biei Complex, Kamuikotan Belt. *the 97 th Ann. Meet. Geol. Soc. Japan, Abstract*, 319.**

Komatsu, M., 1985, Structural framework of the axial zone of Hokkaido - its constitution, characters and tectonics. *Mem. Geol. Soc. Japan.*, 25, 137-155.*

Komatsu, M., Arita, K., Miyashita, S., Maeda, J. and Motoyoshi, Y., 1979, The boundary between the Western Zone and the Main Zone of the Hidaka Metamorphic Belt. *the 86 th Ann. Meet. Geol. Soc. Japan, Abstract*, 289.**

Komatsu, M., Miyashita, S. and Arita, K., 1986, Composition and structure of the Hidaka metamorphic belt, Hokkaido -historical review and present status. *Geology and Tectonics of Hokkaido, Monogr. Assoc. Geol. Collab. Japan*, 31, 189-203.*

Komatsu, M., Shibakusa, H., Miyashita, S., Ishizuka, H., Osanai, Y. and Sakakibara, M., 1992, Subduction and collision related high and low

P/T metamorphic belts. *the 29th IGC Field Trip Guide Book,* 5, 1-61.

Kontani, Y., Kiminami, K., Tajika, J. and Maniwa, K., 1986, Cretaceous sedimentary rocks in the Tokoro and Nemuro belts, Hokkaido. *Geology and Tectonics of Hokkaido, Monogr. Assoc. Geol. Collab. Japan,* 31, 157-171.*

Kretz, R., 1983, Symbols for rock-forming minerals. *Am. Mineral.* 68, 277-279.

Leake , B.E., 1978, Nomenclature of amphiboles. *Am. Mineral.*, 63, 1023-1052.

Liou, J.G., 1971, P-T stabilities of laumontite, wairakite, lawsonite and related minerals in the system $CaAl_2Si_2O_8$-SiO_2-H_2O. *Jour. Petrol.*, 12, 379-411.

Liou, J.G. and Maruyama, S., 1987, Paragenesis of amphiboles in blueschist facies metamorphism. *Jour. metamorphic Geol.*, 5, 371-395.

Liou, J.G., Zhang, R.Y. and Ernst, W.G., 1994, An introduction to ultrahigh-pressure metamorphism. *The Island Arc*, 3, 1-24.

Lister, G.S. and Snoke, A.W., 1984, S-C Mylonites. *Jour. Struct. Geol.*, 6, 6, 617-638.

Maekawa, H., 1983, Submarine sliding deposits and their modes of occurence of the Kamuikotan metamorphic rocks on the Biei area, Hokkaido, Japam. *Jour. Fac. Sci., Univ. Tokyo,* Ser. II, 20, 489-507.

Maekawa, H., 1986a, A low P/T metamorphic episode in the Biei area, Kamuikotan blueschist terrane, Japan. *In Evans, B.W. and Brown, E.H.(eds), Blueschists and eclogites, Geol. Soc. Amer. Memoir,* 164, 395-406.

Maekawa, H., 1986b, Processing formation of the Kamuikotan metamorphic rocks from Biei and surrounding areas, central Hokkaido. In Geology and Tectonics of Hokkaido. *Monogr. Assoc. Geol. Cooab. Japan,* 31, 107-118.*

Maruyama, S., 1976, Chemical natures of the Sawadani greenstone complex in Chichibu belt, eastern Shikoku. *Jour. Geol. Soc. Japan,* 82, 183-197.*

Maruyama, S., 1990, Denudation process of high-pressure metamorphic belt. *the 97 th Ann. Meet. Geol. Soc. Japan, Abstract,* 484.**

Maruyama, S. and Liou, J.G., 1985, The stability of Ca-Na pyroxene in low-grade metabasites of high-pressure intermediate facies series. *Am. Mineral.,* 70, 16-29.

Maruyama, S. and Liou, J.G., 1988, Petrology of Franciscan metabasites along the jadeite-glaucophane type facies series, Cazadero, California. *Jour. Petrol.*, 29, 1-37.

Maruyama, S. and Seno, T., 1986, Orogeny and relative plate motions: Example of the Japanese Islands. *Tectonophysics,* 127, 305-329.

Maruyama, S., Cho, M. and Liou, J.G., 1986, Experimental investigations of blueschist-greenschist transition equilibria: pressure dependence of Al_2O_3 contents in sodic amphiboles - a new geobarometer. *In*

Evans, B.W. and Brown, E.H.(eds), Blueschists and eclogites, Geol. Soc. Amer. Memoir, 164, 1-16.

Maruyama, S., Liou, J.G. and Zhang, R.Y., 1994, Tectonic evolution of the ultrahigh-pressure(UHP) and high-pressure(HP) metamorphic belts from central China. *The Isaland Arc,* 3, 112-121.

Matsuda, T. and Isozaki, Y., 1991, Well-documented travel history of Mesozoic pelagic chert, from mid-oceanic ridge to subduction zone. *Tectonics,* 10, 475-499.

Miyashiro, A. and Shido, F., 1985, Tschermak substitution in low- and middle-grade pelitic schists. *Jour. Petrol.*, 26, 449-448.

Miyashita, S., 1983, Reconstruction of the ophiolite succession in the Western zone of the Hidaka metamorphic belt, Hokkaido. *Jour. Geol. Soc. Japan,* 89, 69-86.*

Mizuochi, Y., 1982, Stratigraphy and structure of the Kamuikotan metamorphic rocks in the West of Asahikawa city. *the 89 th Ann. Meet. Geol. Soc. Japan, Abstract,* 429.**

Mizuochi, Y., 1983MS, Metamorphic rocks in the Kamuikotan Belt in the westward area from Asahikawa, central Hokkaido. *Master thesis, Dept. Mineral Geol., Akita Univ.,* 78p.*

Morimoto, N., Fabries, J., Ferguson, A.K., Ginzburg, I.V., Ross, M., Seifert, F.A., Zussman, J., Aoki, K. and Gottardi, G., 1989, Nomenclature of pyroxenes. *Mineral. Jour.*, 14, 5, 198-221.

Motoyama, N., 1991MS, Structual study of around the Kamuikotan Gorge. *Dept. Geol. Mineral, Niigata Univ.*, 64p.**

Nagao, K., Nishido, H., Itaya, T. and Ogata, K., 1984, An age determination by K-Ar method. *Bull. Hiruzen Res. Inst.*, 9, 19-38.**

Nakagawa, M. and Toda, H., 1987, Geology and petrology of Yubari-dake serpentinite melange in the Kamuikotan tectonic belt, central Hokkaido, Japan. *Jour. Geol. Soc. Japan,* 93, 733-748.

Nakagawa, M. and Nakano, N., 1987, K-Ar dating and its significance of Kamuikotan mafic schist from Mitsuishi river, southern central Hokkaido, Japan. *Earth Science (Chikyu Kagaku),* 41, 4, 244-247.**

Nakajima, T., 1982, Phase relations of pumpellyite-actinolite facies metabasites in the Sanbagawa metamorphic belt in central Shikoku, Japan. *Lithos*, 15, 267-280.

Nakamura, C. and Enami, M., 1994, Prograde amphiboles in hematite-bearing basic and quartz schists in the Sanbagawa belt, central Shikoku: relationship between metamorphic field gradient and *P-T* paths of individual rocks. *Jour. metamorphic Geol.*, 12, 841-852.

Nakano, N., 1981, Metamorphism of greenstones in the Kamuikotan zone and Hidaka western marginal tectonic zone in the Shizunai-Mitsuishi district, Hokkaido. *Jour. Geol. Soc. Japan,* 87, 211-224.*

Nakano, N., 1985, Petrological character of metabasalts from the southern Kamuikotan zone, central Hokkaido. *Jour. Reserch, Dai-ni High School of Tokyo University of Agriculture,* No.3, 33-63.**

Nanayama, F., 1992, Stratigraphy and facies of the Paleocene Nakanogawa Group in the southern part of central Hokkaido, Japan. *Jour. Geol. Soc. Japan,* 98, 11, 1041-1059.*

Niida, N. and Kito, N., 1986, Cretaceous arc-trench systems in Hokkaido. *Monography Assoc. Geol. Colla. Japan,* 31, 379-402.*

Nitsch, K.H., 1968, Die stabilitat von lawsonit. *Naturwissenschaffen*, 55, 388.

Nitsch, K.H., 1971, Stabilitatsbezichungen von prenit and pumpellyit-haltigen paragenesen. *Contri. Mineral. Petrol.*, 30, 240-260.

Ofuka, H., 1994MS, Structual analysis of the Kamuikotan metamorphic rocks in the Kamuikotan gorge area, west of Asahikawa city, central Hokkaido, Japan. *Master thesis, Dept. Earth Sci., Ehime Univ.*, 92p*

Okada, H., 1983, Collision orogenesis and sedimentation in Hokkaido, Japan. *In Hashimoto, M. and Uyeda, S. eds., Accretion tectonics in the Circum-Pacific regions, TERRAPUB, Tokyo,* 107-122.

Omata, M., 1991MS, Geology and rock deformation around the Etanbetsu pass, the Kamuikotan belt, Hokkaido, Japan. *Master thesis, Dept. Geol. Mineral, Hokkaido Univ.**

Onuki, H. and Takanashi, Y., 1986, Notes on the petrography and rock-forming mineralogy (17) - chemical variation of pumpellyite in two metabasites. *Jour. Japan. Assoc. Miner. Petrol. Econ. Geol.*, 81, 272-280.

Osanai, Y., Komatsu, M. and Owada, M., 1991, Metamorphism and granitic genesis in the Hidaka Metamorphic Belt, Hokkaido, Japan. *Jour. Metamorphic Geol.*, 9, 111-124.

Ota, T., 1993MS, Regional metamorphism of Kamuikotan metamorphic rocks in the Kamuikotan gorge area, west of Ashikawa, Hokkaido. *Master thesis, Dept. Earth Sci., Ehime Univ.,* 91p*

Ota, T., Sakakibara, M., Itaya, T. and Takigami, Y., 1991, K-Ar and Ar-Ar ages of Kamuikotan metamorphic rocks, Hokkaido. *the 98 th Ann. Meet. Geol. Soc. Japan, Abstract,* 435.**

Ota, T., Sakakibara, M. and Itaya, T., 1993, K-Ar ages of the Kamuikotan metamorphic rocks, Hokkaido, Japan. *Jour. Geol. Soc. Japan,* 99, 335-345.*

Platt, J.P., 1986, Dynamics of orogenic wedges and the uplift of high-pressuremetamorphic rocks. *Geol. Soc. Am. Bull.* 97, 1037-1053.

Robinson, P., Spear, F. S., Schumacher, J. C., Laird, J., Klein, C., Evans, B. W. and Doolan, B. L., 1982, Phase relations of metamorphic amphiboles: natural occurrence and theory. *Reviews in Mineralogy. Mineral. Soc. Am.* 9B, 1-227.

Sakakibara, M., 1991, Metamorphic petrology of the northern Tokoro metabasites, eastern Hokkaido, Japan. *Jour. Petrol.*, 32, 333-364.

Sakakibara, M., Niida, K., Toda, H., Kito, N., Kimura, G., Tajika, J., Katoh, T., Yoshida, A. and Research Group of the Tokoro Belt, 1986, Nature and tectonic history of the Tokoro belt. *Monogr. Assoc. Geol. Cooab. Japan,* 31, 173-187.*

Sakakibara, M., Ofuku, H., Kimura, G., Ishizuka, H., Miyashita, M., Okamura, M. and Melinikov, O.A., 1992, Metamorphic evolution of

the Susunai metamorphic rocks in soutern Sakhalin. *the 29 th IGC Abstracts,* 2, 588.

Sakakibara, M. and Ota, T., 1994, Metamorphic evolution of the Kamuikotan high- pressure and low temperature metamorphic rocks in central Hokkaido, Japan. *Jour. Geophys. Res.*, 99, 22221-22235.

Scaillet, S., Feraud, G., Lagabrielle, Y., Ballevre, M. and Ruffet, G., 1990, $^{40}Ar/^{39}Ar$ laser-probe dating by step-heating and spot-fusion of phengites from the Dora-Maira nappe of the western Alps, Italy. *Geology*, 18, 741-744.

Scaillet, S., Feraud, G., Ballevre, M. and Amouric M., 1992, Mg/Fe and [(Mg,Fe)Si-Al_2] compositional control on argon behaviour in hig-pressure white micas: A $^{40}Ar/^{39}Ar$ continuous laser-probe study from the Dora-Maira nappe of the internal western Alps, Italy. *Geochim. Cosmochim. Acta,* 56, 2851-2872.

Schiffman, P. and Liou, J.G., 1983, Synthesis of Fe-pumpellyite and its stability relations with epidote. *Jour. metamorphic Geol.*, 1, 91-101.

Shibakusa, H., 1974, Glaucophane schists in the Horokanai are in the Kamuikotan metamorphic belt. *Jour. Geol. Soc. Japan,* 80, 341-353.**

Shibakusa, H., 1989, Lawsonite-pumpellyite-epidote stabilities in glaucophane schists in the Horokanai-Kamietanbetsu area of Kamuikotan Zone, Hokkaido, Japan. *Mineral. Petrol.*, 40, 241-256.

Shibakusa, H., 1991, Petrological study of the Kamuikotan metamorphic rocks in the Horokanai-Kamietanbetsu area, central Hokkaido, Japan. *Ph.D. thesis, Dept. Geol. Mineral., Kyoto Univ.* 140pp.

Shibakusa, H. and Itaya, T., 1992, K-Ar ages of glaucophane schists and associated rocks from the Horokanai-Kamietanbetsu area in the Kamuikotan zone, Hokkaido, northern Japan. *Jour. Geol. Soc. Japan,* 98, 1061-1064.

Shido, F. and Seki, Y., 1959, Notes on rock-forming minerals (11) Jadeite and hornblende from the Kamuikotan metamorphic belt. *Jour. Geol. Soc. Japan,* 65, 673-677.

Spear, F. S., 1993, Metamorphic Phase Equilibria and Pressure-Temperature-Time Paths. *Mineral. Soc. Am. Monograph.* pp.799.

Steiger, R. and Jäger, E., 1977, Subcommission on geochronology convension on the use of decay constants in geo- and cosmo-chronology. *Earth Planet. Sci. Lett.*, 36, 359-362.

Takasu, A. and Dallmeyer, R.D., 1990, ^{40}Ar-^{39}Ar mineral age constraints for the tectonothermal evolution of the Sambagawa metamorphic belt, central Shikoku, Japan: a Cretaceous accretionary prism. *Tectonophysics*, 185, 111-139.

Takayama, M., 1986, Mode of occurence and significiance of jadeite in the Kamuikotan metamorphic rocks, Hokkaido, Japan. *Jour. Metamorphic Geol.*, 4, 445-454.

Takayama, M., 1988, Regional metamorphism of the Kamuikotan metamorphic rocks in hte Kamuikotan Gorge area. *Jour. Japan. Miner. Petrol. Econ. Geol.*, 27, 175-190.*

Takigami, Y., Ota, T., Sakakibara, M., Itaya, T. and Ishizuka, H., 1992, ^{40}Ar-^{39}Ar and K-Ar ages of Kamuikotan metamorphic rocks from Hokkaido, Japan. *the 29 th IGC Abstracts,* 2, 589.

Uemura, T. and Long, X., 1987, Kink bands in rocks. *Jour. Geol. Soc. Japan,* 93, 9, 681-699.*

Uemura, T., Uda, T. and Motoyama, N., 1991, Deformation sequence of the Kamuikotan area. *the 98 th Ann. Meet. Geol. Soc. Japan, Abstract,* 286.**

Uyeda, H., Kawamura, M., Katoh, T. and Nakagawa, M., 1994, Geology of accretionary complexes in the southern Idon'nappu and Kamuikotan belts, and "Nappe tectonics". *the 101 th Ann. Meet. the Geol. Soc. Japan, Excursion guidebook,* 161-174.**

Watanabe, T., Shibakusa, H. and Nakagawa, M., 1986, Characteristics of metamorphism and outline of melange in the Kamuikotan zone. *Geology and Tectonics of Hokkaido, Monogr. Assoc. Geol. Collab. Japan,* 31, 97-106.*

(* in Japanese with English abstract, ** in Japanese)

Appendix

Microprobe analyses of minerals

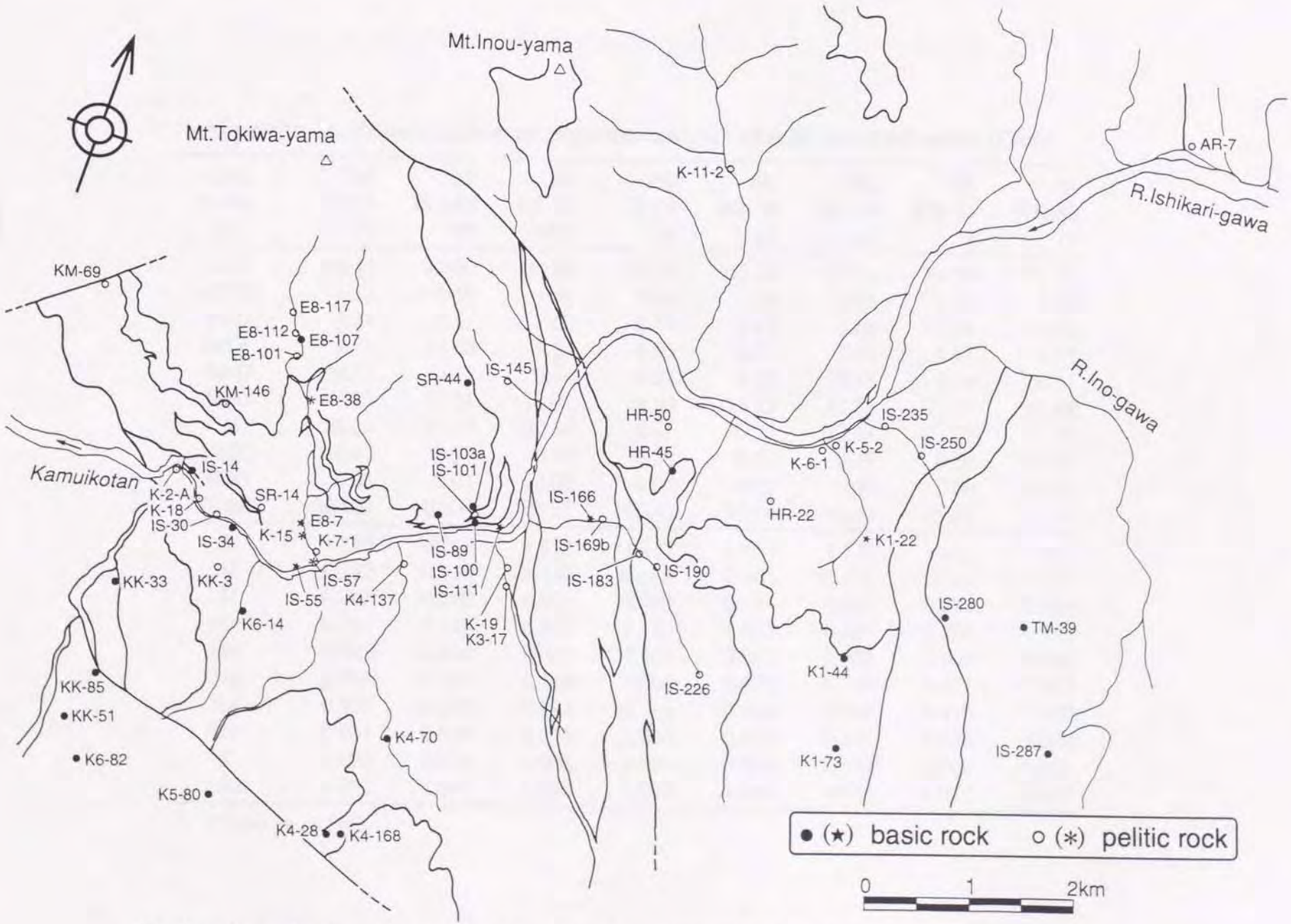

Fig. Localities of analyzed specimens. Symbols in parentheses show boulders.

Appendix 1a. Representative microprobe analyses of relic clinopyroxenes (O=6)

Unit	TM	BI	BI	PK	PK	PK	PK	PK
Sp.No.	IS-55	IS-280	K1-73	IS-14	K4-28	K4-70	KK-51	KK-85
No.	18	35	SG1	19	41	27	8	14
SiO2	48.49	45.08	50.39	54.48	52.27	47.15	44.59	51.45
Al2O3	6.52	7.55	3.41	2.00	2.30	6.68	11.64	3.07
TiO2	2.24	3.11	1.60	0.35	0.49	2.66	1.06	0.33
FeO*	9.11	10.80	9.34	5.95	6.89	7.29	8.51	6.17
MnO	0.17	0.13	0.24	0.22	0.21	0.16	0.14	0.11
MgO	12.75	11.54	14.07	18.69	16.15	12.75	11.15	16.64
CaO	20.24	21.29	20.56	18.51	20.71	22.44	21.75	21.73
Na2O	0.47	0.53	0.76	0.28	0.42	0.43	0.39	0.23
K2O	0.03	0.01	0.00	0.00	0.00	0.00	0.00	0.02
Total	100.02	100.04	100.37	100.48	99.44	99.56	99.23	99.75
Si	1.809	1.713	1.878	1.967	1.937	1.770	1.682	1.901
Al	0.287	0.338	0.150	0.085	0.101	0.296	0.517	0.134
Ti	0.063	0.089	0.045	0.009	0.014	0.075	0.030	0.009
Fe*	0.284	0.343	0.291	0.180	0.213	0.229	0.269	0.191
Mn	0.005	0.004	0.008	0.007	0.007	0.005	0.004	0.004
Mg	0.709	0.654	0.782	1.006	0.892	0.713	0.627	0.917
Ca	0.809	0.867	0.821	0.716	0.822	0.903	0.879	0.860
Na	0.034	0.039	0.055	0.020	0.030	0.031	0.029	0.016
K	0.002	0.000	0.000	0.000	0.000	0.000	0.000	0.001
Total	4.002	4.047	4.030	3.990	4.016	4.022	4.037	4.033

* Total Fe as FeO.

Appendix 1b. Representative microprobe analyses of sodic pyroxenes (O=6)

Unit	TM	TM				TM			
Assem.	LSC	LPSC				LGPSC			
Sp.No.	IS-111	E8-7				E8-107			
No.	S3	4	5	7	9	7	8	11	12
Type**	a	a	a	a	a	b	b	b	b
								rim-	-------core
SiO2	55.79	59.46	60.13	59.24	60.29	58.65	58.76	60.02	58.25
Al2O3	6.95	18.67	19.72	16.71	21.12	16.99	18.88	22.40	17.01
TiO2	0.84	0.00	0.23	0.03	0.00	0.00	0.01	0.19	0.01
FeO*	18.76	6.32	5.40	9.79	3.56	5.73	5.41	2.47	6.40
MnO	0.15	0.08	0.07	0.07	0.05	0.15	0.09	0.04	0.03
MgO	1.87	0.87	0.77	0.60	0.61	2.31	2.07	0.74	1.96
CaO	2.29	1.45	1.20	1.15	1.29	3.90	2.92	0.93	3.24
Na2O	12.45	14.33	14.21	14.15	14.05	12.62	12.98	14.35	12.59
K2O	0.02	0.02	0.03	0.02	0.01	0.03	0.01	0.02	0.04
Total	99.12	101.20	101.76	101.76	100.98	100.38	101.13	101.16	99.53
Si	2.031	2.024	2.036	2.029	2.049	2.028	2.008	2.024	2.035
Al	0.299	0.750	0.787	0.674	0.845	0.692	0.760	0.890	0.700
Ti	0.023	0.000	0.006	0.001	0.000	0.000	0.000	0.005	0.000
Fe*	0.571	0.180	0.153	0.280	0.101	0.166	0.155	0.070	0.187
Mn	0.005	0.002	0.002	0.002	0.001	0.004	0.003	0.001	0.001
Mg	0.102	0.044	0.039	0.030	0.031	0.119	0.105	0.037	0.102
Ca	0.089	0.053	0.044	0.042	0.047	0.144	0.107	0.034	0.121
Na	0.879	0.946	0.933	0.940	0.926	0.846	0.860	0.937	0.852
K	0.001	0.001	0.001	0.001	0.000	0.001	0.001	0.001	0.002
Total	4.000	4.000	4.000	4.000	4.000	4.000	4.000	4.000	4.000
Jd	31	75	81	69	87	70	79	92	72
Acm	60	20	15	27	8	16	10	5	16
Aug	9	5	4	4	5	15	11	4	12

* Total Fe as FeO. ** See text.

Appendix 1b (continue)

Unit	BI				BI				BI	BI
Assem.	PSC				PSC				LSC	PGSC
Sp.No.	Is-280				Is-287				K1-44	K1-73
No.	32	33	44	S5	S3	S4	S6	S7	S2	S1
Type**	b	b	b	c	b	b	b	b	c	a
	rim-	-------core			core-	---------rim	rim	core		
SiO2	52.50	54.56	52.82	55.29	58.77	55.61	55.99	57.69	57.11	56.28
Al2O3	0.76	4.84	13.60	6.96	16.61	6.26	5.38	14.96	11.46	3.45
TiO2	0.21	0.11	0.18	0.16	0.00	0.19	0.17	0.01	0.16	0.03
FeO*	21.65	19.92	16.39	16.95	9.73	21.86	23.04	11.83	15.30	17.74
MnO	1.24	0.11	0.10	0.11	0.06	0.01	0.04	0.05	0.00	0.08
MgO	3.75	3.16	3.89	3.26	0.40	0.90	0.89	0.25	0.82	11.19
CaO	12.34	6.29	1.39	6.25	0.48	1.38	1.32	0.54	1.01	5.87
Na2O	6.99	10.46	11.48	10.02	13.81	12.88	13.15	13.96	13.81	5.74
K2O	0.00	0.00	0.07	0.01	0.03	0.02	0.02	0.01	0.05	0.03
Total	99.44	99.45	99.92	99.01	99.89	99.11	100.00	99.30	99.72	100.41
Si	2.000	2.006	1.880	2.031	2.054	2.036	2.036	2.037	2.028	2.057
Al	0.035	0.210	0.571	0.301	0.684	0.271	0.231	0.622	0.480	0.148
Ti	0.006	0.003	0.005	0.005	0.000	0.005	0.005	0.000	0.004	0.001
Fe*	0.689	0.612	0.488	0.521	0.285	0.669	0.700	0.349	0.454	0.542
Mn	0.039	0.003	0.003	0.004	0.002	0.000	0.001	0.002	0.000	0.003
Mg	0.212	0.173	0.206	0.179	0.021	0.050	0.048	0.013	0.043	0.610
Ca	0.503	0.248	0.053	0.246	0.018	0.054	0.051	0.021	0.039	0.230
Na	0.516	0.745	0.792	0.714	0.936	0.914	0.927	0.956	0.950	0.407
K	0.000	0.000	0.003	0.000	0.001	0.001	0.001	0.001	0.002	0.002
Total	4.000	4.000	4.000	4.000	4.000	4.000	4.000	4.000	4.000	4.000
Jd	3	21	53	31	72	28	24	64	49	23
Acm	47	54	40	43	26	66	71	34	48	41
Aug	49	25	6	26	2	6	5	2	4	36

Appendix 1b (continue)

Unit	PK	PK	PK				PK		PK	
Assem.	EPSC	ESC	PSC				EASC		GASC	
Sp.No.	Is-14	Is-34	Is-166				K4-28		KK-33	
No.	15	38	24	25	28	29	42	2	7	8
Type**	a	a	a	a	b	b	a	b	a	a
			core-	--------rim	rim-	--------core			rim-	--------core
SiO2	53.95	54.54	58.12	54.80	55.49	58.74	53.22	53.01	54.67	54.58
Al2O3	0.96	3.48	16.27	3.49	5.01	16.84	1.33	0.57	4.30	3.81
TiO2	0.00	0.06	0.00	0.18	0.23	0.00	0.00	0.00	0.17	0.10
FeO*	14.23	14.93	9.46	15.46	15.68	9.45	11.32	15.90	18.96	19.93
MnO	0.37	0.13	0.03	0.28	0.19	0.05	0.38	0.18	0.13	0.11
MgO	9.06	7.92	0.90	6.66	5.05	0.51	10.28	7.77	4.27	3.88
CaO	17.15	13.26	2.85	12.54	9.87	1.62	20.91	14.53	7.94	8.24
Na2O	4.18	6.80	13.34	6.92	8.94	14.11	1.82	5.86	9.70	9.68
K2O	0.10	0.04	0.01	0.00	0.02	0.00	0.03	0.00	0.04	0.00
Total	100.00	101.16	100.98	100.33	100.48	101.32	99.29	97.81	100.18	100.33
Si	2.009	1.974	2.013	2.011	2.013	2.019	2.010	2.007	1.996	1.998
Al	0.042	0.148	0.664	0.151	0.214	0.682	0.060	0.026	0.185	0.164
Ti	0.000	0.002	0.000	0.005	0.006	0.000	0.000	0.000	0.005	0.003
Fe*	0.443	0.451	0.274	0.475	0.476	0.272	0.357	0.503	0.579	0.610
Mn	0.012	0.004	0.001	0.009	0.006	0.001	0.012	0.006	0.004	0.004
Mg	0.503	0.427	0.046	0.364	0.273	0.026	0.579	0.439	0.232	0.211
Ca	0.685	0.514	0.106	0.493	0.384	0.060	0.846	0.590	0.310	0.323
Na	0.302	0.477	0.895	0.492	0.629	0.940	0.133	0.430	0.687	0.687
K	0.005	0.002	0.000	0.000	0.001	0.000	0.002	0.000	0.002	0.000
Total	4.000	4.000	4.000	4.000	4.000	4.000	4.000	4.000	4.000	4.000
Jd	4	12	66	15	21	68	6	3	18	16
Acm	26	36	23	35	41	26	8	40	51	52
Aug	69	52	11	50	38	6	86	58	31	32

Appendix 1c. Representative microprobe analyses of amphiboles (O=23)

Unit	TM				TM		TM		TM		TM			
Assem.	PGSC				LPGSC		LPGSC		LPGS		PGC			
Sp.No.	IS-89				IS-100		IS-103a		E8-107		SR-44 (metahornblendite)			
No.	G1	G2	G3	G4	G1	G2	22	23	2	15	G1	G2	G4	G5
Mineral	Crt	Gln	Gln	Crt	Mrb	Crt	Gln	Gln	Gln	Gln	Win	Mrb	Mg-Hbl	Act
Note														
	core-------rim		rim-------core		core-------rim						core-------rim		core-------rim	
SiO2	56.86	57.76	57.94	57.09	55.68	56.05	57.27	55.66	57.83	57.78	55.04	55.12	47.51	57.46
Al2O3	5.90	8.64	11.02	7.71	2.92	5.37	9.56	8.77	9.84	10.19	1.80	2.54	8.17	0.15
TiO2	0.03	0.01	0.14	0.11	0.00	0.27	0.46	0.28	0.33	0.23	0.01	0.01	1.78	0.00
FeO*	16.80	14.88	13.17	16.52	22.71	18.05	12.95	14.32	13.25	11.99	14.80	21.09	11.39	6.96
MnO	0.22	0.18	0.13	0.08	0.16	0.18	0.08	0.04	0.18	0.19	0.60	0.43	0.17	0.26
MgO	9.25	9.08	7.65	8.46	8.13	8.81	8.72	8.67	8.96	8.98	14.38	9.22	15.46	20.27
CaO	3.23	1.10	1.16	0.64	0.66	0.76	0.34	1.25	0.35	1.25	7.65	1.68	10.33	13.18
Na2O	5.41	6.70	6.83	6.94	6.52	6.56	6.85	6.49	7.09	6.53	3.27	6.45	3.28	0.13
K2O	0.11	0.01	0.01	0.01	0.01	0.03	0.00	0.03	0.02	0.04	0.09	0.04	0.25	0.02
Total	97.81	98.36	98.05	97.56	96.79	96.08	96.23	95.51	97.85	97.18	97.64	96.58	98.34	98.43
Si	8.047	7.981	8.051	8.001	8.010	8.010	8.024	7.939	7.975	8.030	7.821	7.974	6.773	7.955
Al	0.984	1.407	1.805	1.274	0.495	0.904	1.579	1.474	1.599	1.669	0.301	0.433	1.373	0.024
Ti	0.003	0.001	0.015	0.012	0.000	0.029	0.048	0.030	0.034	0.024	0.001	0.001	0.191	0.000
Fe*	1.988	1.719	1.530	1.936	2.732	2.157	1.517	1.708	1.528	1.394	1.759	2.551	1.358	0.806
Mn	0.026	0.021	0.015	0.009	0.019	0.022	0.009	0.005	0.021	0.022	0.072	0.053	0.021	0.030
Mg	1.951	1.870	1.585	1.768	1.744	1.877	1.821	1.844	1.842	1.861	3.046	1.988	3.285	4.184
Ca	0.490	0.163	0.173	0.096	0.102	0.116	0.051	0.191	0.052	0.186	1.165	0.260	1.578	1.955
Na	1.484	1.795	1.840	1.886	1.819	1.818	1.861	1.795	1.896	1.760	0.901	1.809	0.907	0.035
K	0.020	0.002	0.002	0.002	0.002	0.005	0.000	0.005	0.004	0.007	0.016	0.007	0.045	0.004
Total	14.994	14.960	15.014	14.984	14.922	14.940	14.912	14.991	14.951	14.953	15.082	15.077	15.530	14.994
Gln	50	71	90	64	26	47	83	71	81	86	6	20	-	0
Rie	22	26	0	31	76	50	16	20	19	4	40	64	-	6
Act	25	8	9	5	5	6	3	10	3	10	58	13	-	98

* Total Fe as FeO

Appendix 1c. (continue)

Unit	BI(SM)			BI								BI	
Assem.	LPGSC			PGSC								PGC	
Sp.No.	K1-22			K1-73								TM-39	
No.	G1	G2	G3	G1	G2	G3	G7	G8	G9	G10	G11	G1	G3
Mineral	Crt	Gln	Gln	Crt	Gln	Crt	Crt	Crt	Crt	Crt	Crt	Act	Win
Note													
									core-	----------	-------rim		
SiO2	56.42	56.31	55.67	56.66	58.48	56.73	57.62	57.06	56.62	57.19	58.57	54.87	55.97
Al2O3	7.44	9.57	7.55	4.88	9.80	7.51	6.61	5.33	6.01	6.52	6.98	1.41	2.40
TiO2	0.27	0.00	0.02	0.10	0.09	0.05	0.02	0.06	0.04	0.03	0.01	0.04	0.06
FeO*	16.59	16.37	16.80	17.29	13.19	15.57	14.68	14.48	15.84	15.94	15.05	17.24	17.07
MnO	0.14	0.05	0.08	0.04	0.03	0.03	0.03	0.03	0.08	0.07	0.07	0.50	0.14
MgO	8.86	6.52	7.57	9.59	8.71	8.88	10.05	11.19	10.52	10.05	10.42	12.26	12.41
CaO	1.87	0.22	2.36	1.54	0.47	1.10	1.72	3.00	1.83	1.87	1.53	9.62	8.28
Na2O	6.41	7.07	5.72	6.46	7.05	6.49	6.41	5.90	6.10	6.23	6.70	1.91	2.68
K2O	0.05	0.02	0.05	0.03	0.00	0.05	0.03	0.05	0.03	0.02	0.04	0.29	0.15
Total	98.05	96.13	95.82	96.59	97.82	96.41	97.17	97.10	97.07	97.92	99.37	98.14	99.16
Si	7.921	8.041	8.042	8.070	8.076	8.025	8.080	8.045	7.938	7.971	8.016	7.954	7.931
Al	1.231	1.611	1.286	0.819	1.595	1.252	1.092	0.886	0.993	1.071	1.126	0.241	0.401
Ti	0.029	0.000	0.002	0.011	0.009	0.005	0.002	0.006	0.004	0.003	0.001	0.004	0.006
Fe*	1.948	1.955	2.030	2.059	1.523	1.842	1.721	1.707	1.857	1.858	1.723	2.090	2.023
Mn	0.017	0.006	0.010	0.005	0.004	0.004	0.004	0.004	0.009	0.008	0.008	0.061	0.017
Mg	1.854	1.388	1.630	2.036	1.793	1.873	2.101	2.352	2.199	2.088	2.126	2.649	2.622
Ca	0.281	0.034	0.365	0.235	0.070	0.167	0.258	0.453	0.275	0.279	0.224	1.494	1.257
Na	1.745	1.957	1.602	1.784	1.888	1.780	1.743	1.613	1.658	1.684	1.778	0.537	0.736
K	0.009	0.004	0.009	0.005	0.000	0.009	0.005	0.009	0.005	0.004	0.007	0.054	0.027
Total	15.035	14.995	14.977	15.024	14.957	14.956	15.006	15.075	14.938	14.966	15.009	15.085	15.021
Gln	58	81	65	41	81	64	55	44	48	53	56	10	17
Rie	28	14	14	38	11	29	24	24	47	37	30	13	22
Act	14	2	19	12	4	9	13	23	14	14	11	75	63

Appendix 1c. (continue)

Unit	HR						PK					
Assem.	PGSC						EASC					
Sp.No.	HR-45						K4-28					
No.	G3	G6	G7	G8	GL1	GL2	37	38'	37'	46	47	51
Mineral	Gln	Gln	Gln	Gln	Gln	Gln	Crt	Gln	Gln	Act	Gln	Crt
Note							enc. Act	enc. Act	enc. Act		enc. Act	enc. Act
								core-	----------	-------rim		
SiO2	56.02	55.30	57.10	56.36	56.45	57.66	57.31	58.29	57.64	54.86	57.04	57.46
Al2O3	8.47	1.70	10.85	6.25	8.87	10.07	6.79	10.47	9.51	0.59	8.21	7.23
TiO2	0.10	0.08	0.09	0.11	0.05	0.35	0.05	0.00	0.27	0.00	0.16	0.07
FeO*	17.82	15.35	14.76	17.85	16.90	14.63	14.55	10.82	11.86	10.57	13.67	14.47
MnO	0.06	0.16	0.06	0.09	0.13	0.05	0.09	0.07	0.07	0.16	0.12	0.09
MgO	6.44	12.40	6.50	8.35	7.19	7.13	10.00	9.58	9.78	17.08	9.32	9.87
CaO	0.54	9.71	0.58	2.70	1.97	0.91	0.60	0.78	1.26	12.21	0.58	0.75
Na2O	6.80	1.23	6.95	5.78	6.36	6.70	7.00	6.49	6.40	0.56	6.97	7.01
K2O	0.05	0.05	0.03	0.05	0.05	0.00	0.00	0.05	0.04	0.02	0.00	0.03
Total	96.30	95.98	96.92	97.54	97.97	97.50	96.39	96.55	96.83	96.05	96.07	96.98
Si	8.035	8.094	8.065	8.028	7.985	8.086	8.054	8.060	8.005	7.925	8.037	8.039
Al	1.432	0.293	1.806	1.049	1.479	1.664	1.125	1.706	1.557	0.100	1.363	1.192
Ti	0.011	0.009	0.010	0.012	0.005	0.037	0.005	0.000	0.028	0.000	0.017	0.007
Fe*	2.138	1.879	1.743	2.126	1.999	1.716	1.710	1.251	1.377	1.277	1.611	1.693
Mn	0.007	0.020	0.007	0.011	0.016	0.006	0.011	0.008	0.008	0.020	0.014	0.011
Mg	1.377	2.706	1.369	1.773	1.516	1.491	2.095	1.975	2.025	3.678	1.958	2.058
Ca	0.083	1.523	0.088	0.412	0.299	0.137	0.090	0.116	0.187	1.890	0.088	0.112
Na	1.891	0.349	1.903	1.596	1.744	1.822	1.907	1.740	1.723	0.157	1.904	1.901
K	0.009	0.009	0.005	0.009	0.009	0.000	0.000	0.009	0.007	0.004	0.000	0.005
Total	14.983	14.881	14.996	15.018	15.052	14.959	14.998	14.864	14.918	15.050	14.992	15.019
Gln	73	16	91	52	73	85	56	92	81	1	68	59
Rie	21	5	0	22	10	0	33	10	14	5	23	29
Act	4	81	4	21	15	7	5	6	10	94	4	6

Appendix 1c. (continue)

Unit	PK										PK		
Assem.	EAC										PAC		
Sp.No.	K4-168										K6-14		
No.	4	6	7	9	11	12	16	17	18	20	38	39	40
Mineral	Act	Act	Act	Act	Crt	Crt	Crt	Crt	Crt	Act	Act	Act	Act
Note					enc.Act	enc.Act	enc.Act	enc.Act	enc.Act				
	rim-	----------	----------	----------	----------	----------	----------	-----core	core-	-------rim			
SiO2	56.03	56.32	56.18	56.35	56.07	56.72	55.88	56.34	56.61	55.03	56.85	56.55	57.17
Al2O3	0.08	0.29	0.38	0.63	4.43	3.66	3.67	3.78	4.38	0.34	0.46	0.30	0.33
TiO2	0.05	0.13	0.00	0.11	0.09	0.07	0.28	0.16	0.18	0.09	0.07	0.03	0.09
FeO*	7.00	7.51	6.96	7.71	14.54	14.08	16.19	15.71	13.04	12.10	10.89	11.88	12.35
MnO	0.21	0.45	0.23	0.45	0.28	0.31	0.20	0.17	0.31	0.31	0.18	0.21	0.19
MgO	19.13	18.89	19.23	18.62	12.22	12.88	11.45	11.38	12.54	16.22	17.55	16.59	16.24
CaO	12.90	11.88	12.18	11.30	1.39	1.78	0.92	1.14	3.03	12.46	12.49	12.12	12.30
Na2O	0.56	0.95	0.97	1.22	6.96	6.24	7.18	6.67	5.90	0.52	0.39	0.24	0.24
K2O	0.03	0.10	0.00	0.10	0.00	0.00	0.00	0.01	0.00	0.00	0.11	0.09	0.09
Total	95.99	96.52	96.13	96.49	95.98	95.74	95.77	95.36	95.99	97.07	98.99	98.01	99.00
Si	8.030	7.995	7.998	7.983	7.925	7.987	7.966	8.034	8.019	7.943	7.958	8.011	8.050
Al	0.014	0.049	0.064	0.105	0.738	0.607	0.617	0.635	0.731	0.058	0.076	0.050	0.055
Ti	0.005	0.014	0.000	0.012	0.010	0.007	0.030	0.017	0.019	0.010	0.007	0.003	0.010
Fe*	0.839	0.892	0.829	0.913	1.719	1.658	1.930	1.874	1.545	1.461	1.275	1.407	1.454
Mn	0.025	0.054	0.028	0.054	0.034	0.037	0.024	0.021	0.037	0.038	0.021	0.025	0.023
Mg	4.087	3.997	4.081	3.932	2.575	2.704	2.433	2.419	2.648	3.490	3.662	3.503	3.409
Ca	1.981	1.807	1.858	1.715	0.211	0.269	0.141	0.174	0.460	1.927	1.873	1.840	1.856
Na	0.156	0.261	0.268	0.335	1.907	1.704	1.984	1.844	1.620	0.146	0.106	0.066	0.066
K	0.005	0.018	0.000	0.018	0.000	0.000	0.000	0.002	0.000	0.000	0.020	0.016	0.016
Total	15.142	15.086	15.126	15.068	15.118	14.972	15.125	15.020	15.080	15.073	14.999	14.922	14.937
Gln	1	2	3	4	33	30	29	32	37	0	2	3	3
Rie	0	2	0	6	53	59	56	53	33	2	6	8	2
Act	99	90	93	86	11	14	7	9	23	96	95	97	97

Appendix 1c. (continue)

Unit	PK								PK		PK	
Assem.	EPAC								GASC		EAHC	
Sp.No.	K6-82								KK-33		KK-51	
No.	15	17	21	22	21	22	23	25	11	12	10	16
Mineral	Act	Act	Crt	Crt	Crt	Crt	Act	Act	Mrb	Mrb	Mrb	Mrb
Note			inc.Ep	inc.Ep	inc.Ep	inc.Ep	inc.Ep	chl layer			enc.Act	enc.Act
			rim-	------core					core-	-------rim		
SiO2	55.33	55.01	54.98	55.42	56.25	54.89	55.09	54.11	55.78	56.19	56.02	56.79
Al2O3	1.00	0.64	4.27	6.54	7.31	6.90	0.83	0.98	2.57	2.90	3.86	3.11
TiO2	0.00	0.00	0.01	0.05	0.00	0.11	0.00	0.01	0.05	0.02	0.01	0.06
FeO*	14.64	14.32	20.41	19.41	17.72	19.26	14.37	13.42	21.01	20.77	13.37	13.19
MnO	0.29	0.37	0.20	0.16	0.15	0.17	0.30	0.29	0.16	0.11	0.08	0.09
MgO	14.43	13.79	7.72	6.72	7.22	6.73	14.41	14.59	9.70	9.50	14.40	14.44
CaO	11.98	11.96	0.90	0.84	0.74	0.36	11.83	11.71	1.27	1.15	1.82	2.32
Na2O	0.63	0.29	6.53	6.83	6.50	7.07	0.53	0.62	6.97	7.16	7.02	6.77
K2O	0.05	0.07	0.00	0.02	0.03	0.04	0.09	0.10	0.01	0.00	0.00	0.00
Total	98.35	96.45	95.02	95.99	95.92	95.53	97.45	95.83	97.52	97.80	96.57	96.76
Si	7.947	8.070	8.052	8.045	8.073	7.983	7.973	7.949	7.967	8.005	7.806	7.927
Al	0.169	0.111	0.737	1.119	1.237	1.183	0.142	0.170	0.433	0.487	0.634	0.512
Ti	0.000	0.000	0.001	0.005	0.000	0.012	0.000	0.001	0.005	0.002	0.001	0.006
Fe*	1.759	1.757	2.500	2.356	2.127	2.342	1.739	1.649	2.510	2.475	1.558	1.539
Mn	0.035	0.046	0.025	0.020	0.018	0.021	0.037	0.036	0.019	0.013	0.009	0.011
Mg	3.090	3.016	1.685	1.454	1.545	1.459	3.109	3.195	2.065	2.018	2.991	3.005
Ca	1.844	1.880	0.141	0.131	0.114	0.056	1.835	1.843	0.194	0.176	0.271	0.347
Na	0.175	0.082	1.854	1.922	1.809	1.994	0.149	0.177	1.930	1.978	1.896	1.833
K	0.009	0.013	0.000	0.004	0.005	0.007	0.017	0.019	0.002	0.000	0.000	0.000
Total	15.028	14.976	14.995	15.057	14.928	15.057	15.000	15.039	15.126	15.153	15.167	15.180
Gln	6	6	37	56	64	58	6	6	20	24	22	22
Rie	3	0	51	30	30	36	4	2	65	58	66	55
Act	92	96	7	7	6	3	93	92	10	9	14	17

Appendix 1d. Representative microprobe analyses of lawsonite (O=8).

Unit	TM			TM		TM				TM				
Assem.	LPGSC			LPGSC		LPSC				LGSC				
Sp.No.	IS-100			IS-103a		IS-111				E8-107				
No.	L1	L2	L3	30	31	L1	L2	L3	L4	9	10	13	14	16
Note														
SiO2	37.82	38.87	38.80	38.19	38.64	38.92	39.13	37.71	38.95	39.28	39.43	40.25	39.59	39.45
Al2O3	29.70	29.97	30.00	31.40	31.52	29.33	29.90	29.13	30.26	32.15	31.72	31.50	31.47	30.90
TiO2	0.19	0.15	0.08	0.06	0.00	0.30	0.21	0.06	0.48	0.16	0.47	0.17	0.22	0.03
Fe2O3*	1.52	1.43	1.34	0.28	0.46	1.56	1.39	1.12	1.47	0.11	0.16	0.76	0.52	0.34
MnO	0.01	0.00	0.00	0.00	0.00	0.00	0.00	0.00	0.04	0.00	0.00	0.08	0.16	0.17
MgO	0.33	0.02	0.00	0.01	0.04	0.11	0.00	0.00	0.02	0.04	0.04	0.13	0.16	0.15
CaO	16.57	16.46	16.70	17.29	17.67	17.29	16.89	17.02	16.94	16.15	16.61	16.93	16.70	16.88
Na2O	0.00	0.00	0.00	0.00	0.00	0.00	0.01	0.00	0.00	0.00	0.01	0.05	0.02	0.00
K2O	0.01	0.01	0.00	0.00	0.00	0.08	0.00	0.04	0.03	0.04	0.02	0.03	0.00	0.00
Total	86.15	86.91	86.92	87.23	88.33	87.59	87.53	85.08	88.19	87.93	88.46	89.90	88.84	87.92
Si	2.039	2.070	2.067	2.026	2.027	2.067	2.072	2.059	2.050	2.052	2.052	2.067	2.056	2.071
Al	1.887	1.881	1.884	1.963	1.949	1.836	1.866	1.874	1.877	1.979	1.946	1.907	1.926	1.912
Ti	0.008	0.006	0.003	0.002	0.000	0.012	0.008	0.002	0.019	0.006	0.018	0.007	0.009	0.001
Fe3+*	0.062	0.057	0.054	0.011	0.018	0.062	0.055	0.046	0.058	0.004	0.006	0.029	0.020	0.014
Mn	0.000	0.000	0.000	0.000	0.000	0.000	0.000	0.000	0.002	0.000	0.000	0.003	0.007	0.008
Mg	0.027	0.002	0.000	0.001	0.003	0.009	0.000	0.000	0.002	0.003	0.003	0.010	0.012	0.012
Ca	0.957	0.939	0.953	0.983	0.993	0.984	0.958	0.996	0.955	0.904	0.926	0.932	0.929	0.949
Na	0.000	0.000	0.000	0.000	0.000	0.000	0.001	0.000	0.000	0.000	0.001	0.005	0.002	0.000
K	0.001	0.001	0.000	0.000	0.000	0.005	0.000	0.003	0.002	0.003	0.001	0.002	0.000	0.000
Total	4.980	4.955	4.961	4.985	4.990	4.975	4.960	4.980	4.965	4.951	4.954	4.962	4.963	4.966

* Total Fe as Fe2O3.

Appendix 1d. (continue)

Unit	BI							PK	PK		
Assem.	LSC							PC	GASC		
Sp.No.	K1-44							K5-80	KK-33		
No.	L1	L2	L3	L4	LW1	LW2	LW3	6	1	3	4
Note								aggregate	in vein	in vein	in vein
SiO2	39.13	38.65	39.63	39.07	39.79	40.62	40.79	39.13	39.21	40.29	39.24
Al2O3	29.91	28.28	30.19	28.80	30.61	30.98	30.79	29.90	30.78	31.22	30.78
TiO2	0.59	0.90	0.14	0.90	0.18	0.12	0.02	0.00	0.04	0.01	0.01
Fe2O3*	2.06	2.58	1.53	2.29	1.64	1.39	1.94	0.53	0.82	1.20	1.36
MnO	0.37	0.71	0.11	0.30	0.00	0.00	0.01	0.00	0.00	0.00	0.04
MgO	0.07	0.09	0.02	0.05	0.04	0.02	0.03	0.00	0.09	0.05	0.03
CaO	16.35	16.22	16.54	16.29	17.25	16.86	16.79	17.03	17.04	16.92	16.84
Na2O	0.00	0.00	0.00	0.00	0.01	0.01	0.01	0.00	0.04	0.03	0.01
K2O	0.00	0.01	0.00	0.00	0.00	0.04	0.00	0.00	0.01	0.02	0.00
Total	88.48	87.44	88.16	87.70	89.52	90.04	90.38	86.59	88.03	89.74	88.31
Si	2.056	2.066	2.080	2.073	2.062	2.085	2.088	2.087	2.060	2.074	2.058
Al	1.852	1.781	1.868	1.801	1.870	1.874	1.857	1.880	1.906	1.894	1.902
Ti	0.023	0.036	0.006	0.036	0.007	0.005	0.001	0.000	0.002	0.000	0.000
Fe3+*	0.081	0.104	0.061	0.091	0.064	0.054	0.075	0.021	0.033	0.046	0.053
Mn	0.016	0.032	0.005	0.013	0.000	0.000	0.000	0.000	0.000	0.000	0.002
Mg	0.005	0.007	0.002	0.004	0.003	0.002	0.002	0.000	0.007	0.004	0.002
Ca	0.920	0.929	0.930	0.926	0.958	0.927	0.921	0.973	0.959	0.933	0.946
Na	0.000	0.000	0.000	0.000	0.001	0.001	0.001	0.000	0.004	0.003	0.001
K	0.000	0.001	0.000	0.000	0.000	0.003	0.000	0.000	0.001	0.001	0.000
Total	4.954	4.956	4.950	4.945	4.965	4.949	4.946	4.962	4.971	4.957	4.965

Appendix 1e. Representative microprobe analyses of pumpellyite (O=24.5)

Unit	TM		TM		TM	TM					TM		TM	
Assem.	LPASC		PGSC		LPGSC	LPGSC					LPSC		PGAC	
Sp.No.	IS-55		IS-89		IS-100	IS-103a					IS-111		SR-44	
No.	32	31	P1	P3	P1	24	27	28	29	32	P1	P2	P1	P2
Note						rim-	------core	rim-	------core					
SiO2	38.11	38.38	37.55	37.80	37.54	37.61	36.35	37.75	36.94	38.08	37.47	37.76	37.69	37.68
Al2O3	26.06	26.48	21.51	22.18	22.49	25.65	21.42	25.81	21.97	26.38	19.57	19.12	24.25	23.58
TiO2	0.08	0.13	0.08	0.00	0.00	0.14	0.00	0.11	0.00	0.00	0.00	0.05	0.02	0.06
FeO*	2.77	3.11	7.32	6.94	5.31	2.03	9.60	3.75	8.45	2.48	9.96	11.74	3.48	4.60
MnO	0.56	0.60	0.38	0.34	0.38	1.28	0.05	0.58	0.17	1.04	0.26	0.25	0.24	0.39
MgO	0.92	0.83	2.56	2.55	3.28	3.55	1.69	3.68	2.21	3.04	2.62	2.38	2.95	3.13
CaO	22.46	22.38	21.60	21.90	21.49	21.77	22.94	22.22	22.31	21.21	21.84	21.99	22.32	22.62
Na2O	0.25	0.11	0.15	0.19	0.08	0.42	0.00	0.37	0.25	0.63	0.03	0.04	0.16	0.15
K2O	0.02	0.04	0.17	0.02	0.01	0.00	0.00	0.02	0.01	0.01	0.05	0.05	0.03	0.00
Total	91.23	92.06	91.32	91.92	90.58	92.45	92.05	94.29	92.31	92.87	91.80	93.38	91.14	92.21
Si	6.246	6.249	6.202	6.191	6.199	6.008	6.010	5.926	6.047	6.055	6.212	6.189	6.150	6.097
Al	5.034	5.081	4.187	4.281	4.377	4.829	4.174	4.776	4.239	4.944	3.824	3.694	4.663	4.497
Ti	0.010	0.016	0.010	0.000	0.000	0.017	0.000	0.013	0.000	0.000	0.000	0.006	0.002	0.007
Fe*	0.380	0.423	1.011	0.951	0.733	0.271	1.327	0.492	1.157	0.330	1.381	1.609	0.475	0.622
Mn	0.078	0.083	0.053	0.047	0.053	0.173	0.007	0.077	0.024	0.140	0.037	0.035	0.033	0.053
Mg	0.225	0.201	0.630	0.623	0.807	0.845	0.417	0.861	0.539	0.721	0.648	0.582	0.718	0.755
Ca	3.944	3.904	3.823	3.843	3.802	3.726	4.064	3.738	3.913	3.614	3.879	3.862	3.902	3.921
Na	0.079	0.035	0.048	0.060	0.026	0.130	0.000	0.113	0.079	0.194	0.010	0.013	0.051	0.047
K	0.004	0.008	0.036	0.004	0.002	0.000	0.000	0.004	0.002	0.002	0.011	0.010	0.006	0.000
Total	16.000	16.000	16.000	16.000	16.000	16.000	16.000	16.000	16.000	16.000	16.000	16.000	16.000	16.000
#Al	89	89	72	73	74	81	71	78	71	82	65	63	80	77
#Fe*	7	7	17	16	12	5	22	8	19	6	24	27	8	11
#Mg	4	4	11	11	14	14	7	14	9	12	11	10	12	13
XFe3+**	0.00	0.00	0.10	0.09	0.05	0.05	0.16	0.09	0.15	0.03	0.17	0.20	0.02	0.07

* Total Fe as FeO. ** see text for calculation

Appendix 1e. (continue)

Unit	BI		BI(SM)		BI		BI		HR		PK	PK(SM)			
Assem.	PSC		LPGSC		PGSC		PGAC		PGASC		EPSC	PSC			
Sp.No.	IS-280		K1-22		K1-73		TM-39		HR-45		Is-14	IS-166			
No.	P1	P2	P1	P3	P1	P3	P1	P2	P1	P2	23	P2	P3	P4	P8
Note															
SiO2	37.08	37.47	37.88	37.57	36.21	36.15	37.02	36.99	38.32	38.68	37.68	38.06	37.54	37.41	37.44
Al2O3	21.99	23.34	24.23	24.05	22.34	21.47	23.33	19.53	22.81	25.32	22.43	23.35	21.43	21.22	21.16
TiO2	0.87	0.05	0.06	0.01	0.00	0.06	0.09	0.04	0.04	0.14	0.08	0.04	0.03	0.05	0.00
FeO*	7.95	7.95	4.41	5.04	8.47	9.65	5.02	10.88	5.42	3.32	5.66	6.60	9.54	9.42	9.27
MnO	0.10	0.13	0.10	0.21	0.04	0.05	0.13	0.18	0.23	0.77	0.27	0.39	0.08	0.13	0.12
MgO	1.68	1.82	2.58	2.71	1.84	2.18	3.28	4.37	3.76	3.27	3.48	2.84	2.18	2.52	2.32
CaO	21.71	21.71	22.20	22.39	22.51	22.20	22.70	20.93	21.25	21.51	23.13	21.28	21.47	21.39	21.48
Na2O	0.20	0.17	0.24	0.13	0.06	0.06	0.11	0.14	0.19	0.43	0.08	0.11	0.00	0.00	0.00
K2O	0.00	0.00	0.01	0.01	0.00	0.02	0.01	0.03	0.16	0.01	0.04	0.00	0.00	0.00	0.00
Total	91.58	92.64	91.71	92.12	91.47	91.84	91.69	93.09	92.18	93.45	92.85	92.67	92.27	92.14	91.79
Si	6.146	6.113	6.162	6.096	5.995	5.976	6.024	6.006	6.199	6.138	6.070	6.169	6.185	6.163	6.194
Al	4.295	4.488	4.645	4.599	4.359	4.183	4.474	3.737	4.349	4.736	4.259	4.461	4.161	4.120	4.126
Ti	0.108	0.006	0.007	0.001	0.000	0.007	0.011	0.005	0.005	0.017	0.010	0.005	0.004	0.006	0.000
Fe*	1.102	1.085	0.600	0.684	1.173	1.334	0.683	1.477	0.733	0.441	0.763	0.895	1.314	1.298	1.283
Mn	0.014	0.018	0.014	0.029	0.006	0.007	0.018	0.025	0.032	0.103	0.037	0.054	0.011	0.018	0.017
Mg	0.415	0.443	0.626	0.656	0.454	0.537	0.796	1.058	0.907	0.774	0.836	0.686	0.535	0.619	0.572
Ca	3.855	3.795	3.869	3.892	3.993	3.932	3.958	3.641	3.683	3.657	3.993	3.696	3.790	3.776	3.808
Na	0.064	0.054	0.076	0.041	0.019	0.019	0.035	0.044	0.060	0.132	0.025	0.035	0.000	0.000	0.000
K	0.000	0.000	0.002	0.002	0.000	0.004	0.002	0.006	0.033	0.002	0.008	0.000	0.000	0.000	0.000
Total	16.000	16.000	16.000	16.000	16.000	16.000	16.000	16.000	16.000	16.000	16.000	16.000	16.000	16.000	16.000
#Al	74	75	79	77	73	69	75	60	73	80	73	74	69	68	69
#Fe*	19	18	10	12	20	22	11	24	12	7	13	15	22	21	21
#Mg	7	7	11	11	8	9	13	17	15	13	14	11	9	10	10
XFe3+**	0.06	0.07	0.02	0.05	0.13	0.17	0.10	0.26	0.07	0.02	0.13	0.05	0.10	0.12	0.11

Appendix 1e. (continue)

Unit	PK		PK		PK				PK		PK			
Assem.	PAC		PC		PAC				EAPC		EAPC			
Sp.No.	K4-70		K5-80		K6-14				K6-82		K6-82F			
No.	31	32	2	3	26	34	35	36	19	20	5	33	36	37
Note	Chl-side		core-	-------rim					inc.Ep	inc.Ep			core-	-------rim
SiO2	37.56	38.31	36.83	37.17	38.18	38.35	38.40	38.18	37.67	37.55	37.09	37.50	36.53	37.91
Al2O3	23.46	24.64	25.05	25.17	24.91	26.02	24.95	25.56	22.65	22.48	24.91	24.96	23.52	25.08
TiO2	0.04	0.01	0.03	0.05	0.07	0.04	0.09	0.12	0.03	0.02	0.02	0.04	0.00	0.02
FeO*	4.42	2.76	5.20	4.92	2.57	2.38	3.11	2.77	6.54	6.12	4.24	4.56	6.12	4.53
MnO	0.29	0.19	0.23	0.29	0.47	0.57	0.42	0.47	0.31	0.40	0.30	0.40	0.23	0.30
MgO	3.10	3.32	1.94	2.27	3.73	3.68	3.94	3.47	2.68	2.92	2.75	2.86	2.57	2.41
CaO	21.85	22.22	22.36	22.43	22.43	22.41	22.15	21.99	22.56	22.49	23.42	23.08	23.13	22.85
Na2O	0.21	0.25	0.02	0.01	0.31	0.27	0.28	0.30	0.03	0.04	0.14	0.14	0.13	0.21
K2O	0.00	0.00	0.00	0.00	0.00	0.01	0.03	0.01	0.00	0.00	0.04	0.00	0.00	0.00
Total	90.93	91.70	91.66	92.31	92.67	93.73	93.37	92.87	92.47	92.02	92.90	93.53	92.23	93.31
Si	6.156	6.187	6.025	6.027	6.089	6.042	6.082	6.082	6.129	6.128	5.948	5.979	5.938	6.065
Al	4.532	4.690	4.830	4.810	4.682	4.832	4.657	4.799	4.343	4.324	4.707	4.690	4.505	4.729
Ti	0.005	0.001	0.004	0.006	0.008	0.005	0.011	0.014	0.004	0.002	0.003	0.004	0.000	0.002
Fe*	0.606	0.373	0.711	0.667	0.343	0.314	0.412	0.369	0.890	0.835	0.568	0.608	0.832	0.606
Mn	0.040	0.026	0.032	0.040	0.063	0.076	0.056	0.063	0.043	0.055	0.040	0.054	0.032	0.041
Mg	0.757	0.799	0.473	0.549	0.887	0.864	0.930	0.824	0.650	0.710	0.658	0.679	0.623	0.575
Ca	3.837	3.845	3.919	3.897	3.832	3.783	3.759	3.753	3.933	3.932	4.024	3.942	4.029	3.916
Na	0.067	0.078	0.006	0.003	0.096	0.082	0.086	0.093	0.009	0.013	0.043	0.043	0.041	0.066
K	0.000	0.000	0.000	0.000	0.000	0.002	0.006	0.002	0.000	0.000	0.008	0.000	0.000	0.001
Total	16.000	16.000	16.000	16.000	16.000	16.000	16.000	16.000	16.000	16.000	16.000	16.000	16.000	16.000
#Al	77	80	80	80	79	80	78	80	74	74	79	78	76	80
#Fe*	10	6	12	11	6	5	7	6	15	14	10	10	14	10
#Mg	13	14	8	9	15	14	16	14	11	12	11	11	10	10
XFe3+**	0.04	0.00	0.02	0.03	0.04	0.03	0.05	0.02	0.08	0.09	0.09	0.08	0.13	0.04

Appendix 1f. Representative microprobe analyses of epidote (O=12.5)

Unit	PK		PK					PK		
Assem.	ESC		EASC					EAPC		
Sp.No.	Is-34		K4-28					K6-82		
No.	41	42	40	44	65	68	70	E1	E2	E6
					core-	----------	-------rim	rim-	------core	
SiO2	38.22	37.98	37.39	37.53	38.64	38.22	38.17	38.00	37.79	37.44
Al2O3	18.29	20.79	21.29	21.25	21.53	21.92	21.78	20.88	21.37	20.64
TiO2	0.03	0.00	0.00	0.03	0.00	0.09	0.12	0.00	0.04	0.00
Fe2O3*	18.49	16.35	15.31	15.09	14.93	14.02	13.78	15.18	14.92	15.60
MnO	0.06	0.02	0.11	0.05	0.04	0.13	0.24	0.13	0.49	0.09
MgO	0.22	0.00	0.01	0.00	0.07	0.02	0.01	0.01	0.00	0.00
CaO	23.08	23.24	22.35	23.14	22.47	23.50	22.71	22.81	22.12	22.36
Na2O	0.10	0.02	0.00	0.00	0.11	0.00	0.01	0.00	0.00	0.01
K2O	0.02	0.04	0.00	0.02	0.00	0.00	0.00	0.02	0.01	0.01
Total	98.51	98.44	96.46	97.11	97.79	97.88	96.83	97.03	96.74	96.15
Si	3.084	3.041	3.040	3.035	3.086	3.053	3.075	3.072	3.060	3.058
Al	1.739	1.962	2.040	2.026	2.027	2.064	2.068	1.989	2.039	1.987
Ti	0.002	0.000	0.000	0.002	0.000	0.005	0.008	0.000	0.002	0.000
Fe3+*	1.123	0.985	0.937	0.918	0.897	0.843	0.835	0.923	0.909	0.959
Mn	0.004	0.001	0.008	0.003	0.003	0.009	0.017	0.009	0.034	0.006
Mg	0.026	0.000	0.001	0.000	0.008	0.002	0.001	0.001	0.000	0.000
Ca	1.995	1.994	1.947	2.005	1.923	2.012	1.961	1.976	1.919	1.957
Na	0.016	0.003	0.000	0.000	0.017	0.000	0.002	0.000	0.000	0.002
K	0.002	0.004	0.000	0.002	0.000	0.000	0.000	0.002	0.001	0.001
Total	7.992	7.990	7.972	7.992	7.960	7.988	7.967	7.973	7.964	7.970
XFe3+	0.39	0.33	0.31	0.31	0.31	0.29	0.29	0.32	0.31	0.33

* Total Fe as Fe2O3

Appendix 1f. (continue)

Unit	PK			PK					PK	
Assem.	EAPC			EAHC					EAC	
Sp.No.	K6-82F			KK-51					KK-85	
No.	2	14	21	46	47	48	49	57	16	18
		rim	rim	rim-	-------core	-------core	--------rim			
SiO2	37.21	38.17	37.95	37.10	36.97	37.21	36.79	37.79	37.11	38.06
Al2O3	22.07	25.68	25.45	21.31	22.03	22.09	21.45	21.09	21.55	21.35
TiO2	0.01	0.12	0.00	0.04	0.08	0.56	0.13	0.08	0.04	0.00
Fe2O3*	15.11	11.03	11.13	15.68	14.66	13.20	15.52	15.32	15.52	15.99
MnO	0.30	0.10	0.09	0.10	0.23	0.03	0.19	0.25	0.30	0.01
MgO	0.02	0.03	0.01	0.01	0.03	0.02	0.02	0.02	0.00	0.03
CaO	23.01	22.48	21.99	22.56	22.52	23.65	23.08	22.94	22.91	23.01
Na2O	0.00	0.00	0.04	0.00	0.00	0.00	0.00	0.00	0.00	0.00
K2O	0.00	0.00	0.00	0.00	0.00	0.00	0.00	0.00	0.00	0.01
Total	97.72	97.62	96.66	96.79	96.51	96.77	97.16	97.48	97.43	98.46
Si	2.992	3.009	3.018	3.013	3.002	3.008	2.984	3.046	2.999	3.037
Al	2.092	2.386	2.386	2.040	2.109	2.105	2.050	2.003	2.052	2.008
Ti	0.000	0.007	0.000	0.003	0.005	0.034	0.008	0.005	0.002	0.000
Fe3+*	0.914	0.654	0.666	0.958	0.896	0.803	0.947	0.929	0.944	0.960
Mn	0.021	0.006	0.006	0.007	0.016	0.002	0.013	0.017	0.021	0.001
Mg	0.002	0.003	0.002	0.001	0.003	0.003	0.003	0.002	0.000	0.004
Ca	1.983	1.898	1.874	1.964	1.960	2.049	2.006	1.981	1.983	1.968
Na	0.000	0.001	0.006	0.000	0.000	0.000	0.000	0.000	0.000	0.000
K	0.000	0.000	0.000	0.000	0.000	0.000	0.000	0.000	0.000	0.001
Total	8.004	7.964	7.959	7.985	7.991	8.004	8.010	7.983	8.001	7.979
XFe3+	0.30	0.22	0.22	0.32	0.30	0.28	0.32	0.32	0.32	0.32

Appendix 1g. Representative microprobe analyses of chlorite (O=28)

Unit	TM			TM	TM		BI	BI		BI	
Assem.	LPGSC			LPGSC	LPSC		PSC	SC		LSC	
Sp.No.	IS-100			IS-103a	IS-111		IS-280	IS-287		K1-44	
No.	C2	C3	C4	34	C1	C2	40	C2	C3	C1	C4
Note											
SiO2	29.11	27.91	28.09	29.56	29.09	29.42	28.84	28.03	29.31	28.06	28.07
Al2O3	17.04	18.45	17.28	17.52	17.36	17.38	17.22	17.84	18.80	18.28	18.54
TiO2	0.00	0.00	0.00	0.00	0.00	0.00	0.00	0.01	0.01	0.01	0.00
FeO*	19.87	24.00	21.12	25.18	20.30	24.66	29.87	21.48	19.47	24.01	21.85
MnO	0.59	0.41	0.57	0.28	0.83	0.95	0.35	0.46	0.41	0.48	0.87
MgO	19.62	16.73	18.78	15.96	18.27	17.37	12.20	16.91	18.72	16.75	17.32
CaO	0.00	0.00	0.00	0.19	0.05	0.00	0.21	0.08	0.06	0.06	0.05
Na2O	0.03	0.02	0.00	0.00	0.01	0.00	0.07	0.01	0.01	0.00	0.00
K2O	0.03	0.00	0.03	0.01	0.02	0.01	0.33	0.07	0.08	0.00	0.01
Total	86.29	87.52	85.87	88.70	85.93	89.79	89.09	84.89	86.87	87.65	86.71
Si	6.049	5.840	5.919	6.113	6.085	6.018	6.114	5.977	6.011	5.865	5.874
Ti	0.000	0.000	0.000	0.000	0.000	0.000	0.000	0.002	0.002	0.002	0.000
Al	4.173	4.550	4.291	4.270	4.280	4.190	4.302	4.483	4.544	4.503	4.573
Fe*	3.453	4.200	3.722	4.355	3.551	4.218	5.295	3.830	3.339	4.197	3.824
Mn	0.104	0.073	0.102	0.049	0.147	0.165	0.063	0.083	0.071	0.085	0.154
Mg	6.077	5.219	5.899	4.921	5.697	5.297	3.855	5.375	5.723	5.219	5.403
Ca	0.000	0.000	0.000	0.042	0.011	0.000	0.048	0.018	0.013	0.013	0.011
Na	0.012	0.008	0.000	0.000	0.004	0.000	0.029	0.004	0.004	0.000	0.000
K	0.008	0.000	0.008	0.003	0.005	0.003	0.089	0.019	0.021	0.000	0.003
Total	19.876	19.890	19.941	19.753	19.781	19.890	19.795	19.792	19.729	19.883	19.842
XMg	0.64	0.55	0.61	0.53	0.62	0.56	0.42	0.58	0.63	0.55	0.59
XAl	0.30	0.33	0.31	0.32	0.32	0.31	0.32	0.33	0.33	0.32	0.33

* Total Fe as FeO.

Appendix 1g.(continue)

Unit	BI		BI		HR		PK	PK	PK(SM)		
Assem.	PGSC		PGAC		PGASC		EPSC	ESC	PSC		
Sp.No.	K1-73		TM-39		HR-45		IS-14	IS-34	IS-166		
No.	C1	C2	C1	C2	C1	C2	22	40	30	C6	C7
Note											
SiO2	29.53	29.48	29.24	30.10	29.45	29.15	28.20	31.36	28.70	27.78	28.43
Al2O3	17.38	17.54	16.84	14.69	16.74	16.67	17.83	17.24	16.46	16.47	16.56
TiO2	0.00	0.02	0.01	0.00	0.00	0.02	0.00	0.00	0.00	0.00	0.00
FeO*	19.51	20.08	20.72	18.73	26.52	24.15	21.54	12.51	24.50	32.44	28.23
MnO	0.13	0.16	0.28	0.17	0.25	0.25	0.34	0.21	0.27	0.30	0.27
MgO	21.29	20.26	18.93	21.74	15.14	16.92	18.46	24.85	17.28	11.26	14.24
CaO	0.06	0.08	0.16	0.10	0.12	0.25	0.12	0.17	0.03	0.14	0.20
Na2O	0.02	0.01	0.03	0.03	0.01	0.02	0.05	0.13	0.04	0.00	0.00
K2O	0.01	0.02	0.02	0.00	0.04	0.02	0.01	0.02	0.00	0.00	0.00
Total	87.93	87.65	86.23	85.56	88.27	87.45	86.55	86.49	87.28	88.39	87.93
Si	5.990	6.015	6.098	6.265	6.171	6.103	5.896	6.219	6.040	6.030	6.058
Ti	0.000	0.003	0.002	0.000	0.000	0.003	0.000	0.000	0.000	0.000	0.000
Al	4.155	4.218	4.139	3.604	4.134	4.114	4.394	4.029	4.083	4.213	4.159
Fe*	3.310	3.426	3.614	3.260	4.648	4.229	3.766	2.075	4.312	5.889	5.030
Mn	0.022	0.028	0.049	0.030	0.044	0.044	0.060	0.035	0.048	0.055	0.049
Mg	6.438	6.162	5.885	6.746	4.730	5.281	5.754	7.346	5.421	3.644	4.523
Ca	0.013	0.017	0.036	0.022	0.027	0.056	0.027	0.036	0.007	0.033	0.046
Na	0.008	0.004	0.012	0.012	0.004	0.008	0.020	0.050	0.016	0.000	0.000
K	0.003	0.005	0.005	0.000	0.011	0.005	0.003	0.005	0.000	0.000	0.000
Total	19.939	19.879	19.840	19.940	19.769	19.844	19.920	19.795	19.928	19.864	19.864
XMg	0.66	0.64	0.62	0.67	0.50	0.56	0.60	0.78	0.56	0.38	0.47
XAl	0.30	0.31	0.30	0.26	0.31	0.30	0.32	0.30	0.30	0.31	0.30

Appendix 1g.(continue)

Unit	PK		PK		PK		PK		PK	PK	
Assem.	EASC		PC		PAC		EAPC		EAPC	GASC	
Sp.No.	K4-28		K5-80		K6-14		K6-82		K6-82F	KK-33	
No.	49	36	4	5	24	27	17	29	3	2	9
Note								inc.Ep			
SiO2	28.58	28.39	25.17	25.58	28.63	29.56	26.65	26.79	27.56	27.74	28.41
Al2O3	17.53	18.17	17.45	18.04	17.58	17.56	17.92	18.18	18.31	18.13	18.22
TiO2	0.00	0.01	0.00	0.00	0.00	0.01	0.00	0.00	0.04	0.00	0.00
FeO*	18.93	20.68	34.47	33.42	23.20	21.42	25.68	25.30	27.16	28.79	22.13
MnO	0.29	0.18	0.46	0.48	0.27	0.23	0.37	0.46	0.54	0.32	0.29
MgO	20.53	19.16	8.73	8.60	17.43	19.61	15.37	15.20	14.83	11.67	18.12
CaO	0.10	0.02	0.04	0.10	0.12	0.09	0.03	0.14	0.14	0.22	0.08
Na2O	0.00	0.00	0.00	0.00	0.00	0.00	0.00	0.00	0.01	0.23	0.01
K2O	0.00	0.04	0.00	0.00	0.00	0.02	0.00	0.01	0.00	0.02	0.00
Total	85.96	86.65	86.32	86.22	87.23	88.50	86.02	86.08	88.59	87.12	87.26
Si	5.931	5.890	5.708	5.761	5.979	6.014	5.753	5.767	5.802	5.986	5.897
Ti	0.000	0.002	0.000	0.000	0.000	0.002	0.000	0.000	0.006	0.000	0.000
Al	4.287	4.443	4.664	4.788	4.327	4.211	4.559	4.612	4.544	4.611	4.458
Fe*	3.285	3.588	6.538	6.294	4.052	3.644	4.636	4.554	4.783	5.196	3.842
Mn	0.051	0.032	0.088	0.092	0.048	0.040	0.068	0.084	0.097	0.058	0.051
Mg	6.351	5.926	2.952	2.887	5.426	5.948	4.946	4.878	4.655	3.754	5.607
Ca	0.022	0.004	0.010	0.024	0.027	0.020	0.007	0.032	0.031	0.051	0.018
Na	0.000	0.000	0.000	0.000	0.000	0.000	0.000	0.000	0.004	0.096	0.004
K	0.000	0.011	0.000	0.000	0.000	0.005	0.000	0.003	0.000	0.006	0.000
Total	19.927	19.894	19.960	19.846	19.858	19.883	19.968	19.929	19.922	19.759	19.877
XMg	0.66	0.62	0.31	0.31	0.57	0.62	0.52	0.52	0.49	0.42	0.59
XAl	0.31	0.32	0.33	0.34	0.31	0.31	0.32	0.33	0.32	0.34	0.32

Appendix 1h. Representative microprobe analyses of sphene (O=5) and phengite (O=22)

Mineral	sphene					phengite								
Unit	BI	PK	PK		PK	BI		PK	PK	PK		PK	PK	
Assem.	PSC	PASC	EAPC		RASC	PSC		EPSC	ESC	PAC		RASC	EAC	
Sp.No.	IS-280	K6-14	K6-82F		KK-33	IS-280		IS-14	IS-34	K4-70		KK-33	KK-85	
No.	34	29	29	30	6	38	39	21	43	33	34	5	17	21
SiO2	31.55	29.88	31.11	30.90	32.44	53.82	51.42	54.93	52.16	49.32	56.04	50.98	52.55	51.95
Al2O3	2.73	2.19	0.85	0.81	1.74	21.00	19.83	21.50	23.65	26.83	19.63	21.51	22.44	22.28
TiO2	33.24	39.32	38.62	37.43	36.50	0.01	0.01	0.04	0.03	0.00	0.00	0.05	0.17	0.16
Fe2O3*	2.91	1.37	0.75	0.79	2.08									
FeO*						5.80	7.53	2.22	3.96	4.64	2.17	4.51	3.86	4.81
MnO	0.01	0.00	0.00	0.01	0.00	0.06	0.04	0.07	0.00	0.03	0.05	0.03	0.00	0.00
MgO	0.70	0.08	0.01	0.00	0.14	4.54	5.24	5.86	4.32	2.51	5.62	4.54	4.73	4.99
CaO	27.65	26.80	29.79	30.17	28.32	0.20	0.14	0.06	0.08	0.12	0.09	0.10	0.15	0.16
Na2O	0.05	0.08	0.01	0.04	0.19	0.12	0.10	0.08	0.12	0.38	0.01	0.07	0.05	0.05
K2O	0.04	0.11	0.07	0.06	0.14	10.06	9.79	10.48	10.81	9.58	10.06	10.21	10.55	10.17
Total	98.88	99.83	101.19	100.22	101.55	95.61	94.10	95.24	95.13	93.41	93.67	92.00	94.50	94.57
Si	1.038	0.975	1.006	1.011	1.040	7.255	7.135	7.306	7.039	6.768	7.539	7.129	7.126	7.068
Al	0.106	0.084	0.032	0.031	0.066	3.336	3.243	3.370	3.761	4.339	3.112	3.545	3.586	3.573
Ti	0.823	0.965	0.939	0.921	0.880	0.001	0.001	0.004	0.003	0.000	0.000	0.005	0.017	0.016
Fe3+*	0.072	0.034	0.018	0.020	0.050									
Fe*						0.654	0.874	0.247	0.447	0.532	0.244	0.527	0.438	0.547
Mn	0.000	0.000	0.000	0.000	0.000	0.007	0.005	0.008	0.000	0.003	0.006	0.004	0.000	0.000
Mg	0.034	0.004	0.000	0.000	0.007	0.912	1.084	1.162	0.869	0.513	1.127	0.947	0.956	1.012
Ca	0.975	0.937	1.032	1.057	0.972	0.029	0.021	0.009	0.012	0.018	0.013	0.015	0.022	0.023
Na	0.003	0.005	0.001	0.003	0.012	0.031	0.027	0.021	0.031	0.101	0.003	0.019	0.013	0.013
K	0.002	0.005	0.003	0.003	0.006	1.730	1.733	1.778	1.861	1.677	1.726	1.822	1.825	1.765
Total	3.053	3.007	3.032	3.046	3.032	13.956	14.122	13.904	14.024	13.952	13.770	14.013	13.983	14.018

* Total Fe as Fe2O3 or FeO.

Appendix 2a. Representative microprobe analyses of phengite (O=22).

Unit	TM			TM		TM				TM		TM			
Sp.No.	K-15			IS-57'		E8-101				E8-112'		E8-117			
No.	MUS3	MUS4	MUS5	5	6	1	2	4	15	1	2	M1	M3	M4	M5
Note									+Stlp						
SiO2	55.18	55.19	54.78	54.05	55.29	53.70	53.27	50.97	55.01	52.83	52.75	53.90	51.64	52.95	49.41
Al2O3	20.93	20.92	20.84	23.12	23.14	22.03	22.84	20.62	20.43	23.67	24.26	22.90	23.31	22.74	26.17
TiO2	0.00	0.04	0.00	0.01	0.09	1.49	0.02	0.08	0.00	0.00	0.00	0.02	0.01	0.02	0.33
FeO*	3.14	2.92	2.99	4.24	3.21	3.75	4.43	7.14	2.41	4.28	3.49	3.57	4.77	4.45	4.90
MnO	0.07	0.12	0.12	0.05	0.03	0.02	0.00	0.00	0.03	0.05	0.04	0.07	0.03	0.01	0.04
MgO	4.76	5.19	5.79	3.43	4.06	3.94	3.59	4.43	5.37	3.45	3.44	3.52	3.43	3.53	2.92
CaO	0.01	0.00	0.01	0.04	0.05	0.05	0.00	0.00	0.03	0.00	0.00	0.06	0.10	0.09	0.00
Na2O	0.14	0.09	0.07	0.04	0.06	0.05	0.07	0.04	0.06	0.06	0.08	0.06	0.05	0.09	0.35
K2O	10.64	10.80	10.51	9.79	9.97	10.26	10.56	9.98	10.29	9.82	10.09	9.90	9.91	9.77	9.66
Total	94.86	95.28	95.10	94.77	95.90	95.29	94.78	93.26	93.63	94.16	94.15	94.00	93.25	93.65	93.78
Si	7.400	7.373	7.330	7.250	7.290	7.192	7.198	7.120	7.432	7.148	7.120	7.273	7.096	7.211	6.770
Al	3.308	3.294	3.286	3.655	3.596	3.477	3.637	3.395	3.253	3.775	3.859	3.642	3.775	3.650	4.226
Ti	0.000	0.004	0.000	0.001	0.009	0.150	0.002	0.008	0.000	0.000	0.000	0.002	0.001	0.002	0.034
Fe*	0.352	0.326	0.334	0.476	0.354	0.420	0.501	0.834	0.272	0.484	0.394	0.403	0.548	0.507	0.561
Mn	0.008	0.013	0.013	0.006	0.003	0.002	0.000	0.000	0.003	0.006	0.005	0.008	0.003	0.001	0.005
Mg	0.952	1.034	1.156	0.686	0.798	0.787	0.723	0.923	1.082	0.696	0.692	0.708	0.703	0.717	0.596
Ca	0.001	0.001	0.002	0.006	0.007	0.007	0.000	0.000	0.004	0.000	0.000	0.009	0.015	0.013	0.000
Na	0.036	0.024	0.018	0.010	0.015	0.013	0.018	0.011	0.016	0.016	0.021	0.016	0.013	0.024	0.093
K	1.819	1.841	1.793	1.675	1.677	1.753	1.820	1.778	1.774	1.695	1.738	1.704	1.737	1.697	1.689
Total	13.875	13.910	13.933	13.764	13.749	13.802	13.900	14.069	13.836	13.820	13.829	13.764	13.891	13.822	13.974
XMg	0.730	0.760	0.776	0.591	0.693	0.652	0.591	0.525	0.799	0.590	0.637	0.637	0.562	0.586	0.515
XNa	0.040	0.027	0.020	0.012	0.017	0.014	0.020	0.012	0.017	0.017	0.023	0.017	0.015	0.026	0.103

* Total Fe as FeO

Appendix 2a. (continue)

Unit	TM			TM			BI				HR				HR	
Sp.No.	KM-69			SR-14			AR-7				K-5-2				K-6-1	
No.	13	14	15	22	23	24	MUS3	MUS5	6	8	3	4	5	7	MUS5	MUS6
Note																
SiO2	50.66	55.23	54.12	51.46	50.67	50.96	52.07	51.57	51.93	52.76	52.46	49.41	49.74	48.39	46.88	51.54
Al2O3	21.95	22.73	22.70	25.26	24.29	24.59	25.84	25.23	25.76	24.14	25.23	25.86	30.91	32.96	30.17	26.07
TiO2	0.00	0.04	0.00	0.06	0.09	0.01	0.00	0.00	0.00	0.05	0.04	0.00	0.08	0.46	0.19	0.24
FeO*	4.48	3.34	3.12	2.45	2.73	2.89	2.21	2.68	2.26	2.71	4.39	7.52	1.68	2.45	2.78	4.19
MnO	0.15	0.04	0.00	0.00	0.02	0.03	0.00	0.00	0.00	0.01	0.05	0.03	0.00	0.00	0.04	0.08
MgO	5.12	4.63	4.37	3.48	3.93	3.83	3.24	3.57	3.37	4.01	2.80	1.87	1.82	0.90	2.37	2.92
CaO	0.00	0.06	0.03	0.00	0.07	0.00	0.00	0.00	0.04	0.00	0.11	0.00	0.02	0.02	0.04	0.02
Na2O	0.00	0.07	0.11	0.25	0.25	0.17	0.09	0.06	0.09	0.12	0.09	0.06	0.18	0.36	0.22	0.45
K2O	9.65	9.96	10.10	9.68	9.43	9.08	10.53	10.71	10.22	9.78	9.26	10.45	9.56	9.66	10.34	10.21
Total	92.01	96.10	94.55	92.64	91.48	91.56	93.99	93.82	93.67	93.58	94.43	95.20	93.99	95.20	93.02	95.71
Si	7.064	7.279	7.257	7.018	7.015	7.028	7.015	6.995	7.011	7.126	7.055	6.779	6.646	6.426	6.442	6.897
Al	3.607	3.531	3.587	4.060	3.963	3.997	4.102	4.033	4.099	3.843	3.999	4.181	4.867	5.159	4.885	4.111
Ti	0.000	0.004	0.000	0.006	0.009	0.001	0.000	0.000	0.000	0.005	0.004	0.000	0.008	0.046	0.019	0.024
Fe*	0.522	0.368	0.350	0.279	0.316	0.333	0.249	0.304	0.255	0.306	0.494	0.863	0.188	0.272	0.319	0.469
Mn	0.018	0.004	0.000	0.000	0.002	0.004	0.000	0.000	0.000	0.001	0.006	0.003	0.000	0.000	0.005	0.009
Mg	1.064	0.910	0.874	0.707	0.811	0.787	0.651	0.721	0.678	0.807	0.561	0.382	0.363	0.178	0.485	0.582
Ca	0.000	0.008	0.004	0.000	0.010	0.000	0.000	0.000	0.006	0.000	0.016	0.000	0.003	0.003	0.006	0.003
Na	0.000	0.018	0.029	0.066	0.067	0.045	0.025	0.016	0.024	0.031	0.023	0.016	0.047	0.093	0.059	0.117
K	1.716	1.675	1.728	1.684	1.666	1.598	1.810	1.854	1.760	1.685	1.589	1.829	1.630	1.637	1.813	1.743
Total	13.991	13.798	13.828	13.821	13.860	13.794	13.851	13.924	13.832	13.806	13.747	14.053	13.751	13.813	14.032	13.954
XMg	0.671	0.712	0.714	0.717	0.720	0.703	0.723	0.704	0.727	0.725	0.532	0.307	0.659	0.396	0.603	0.554
XNa	0.000	0.020	0.032	0.073	0.075	0.051	0.027	0.018	0.026	0.035	0.026	0.018	0.052	0.103	0.065	0.130

Appendix 2a. (continue)

Unit	HR		HR			HR			HR							
Sp.No.	K-11-2		IS-183			IS-190			IS-226							
No.	MUS1	MUS2	10	13	14	4	5	6	M1	M4	M8	M11	M13	M14	M16	17
Note												S2	S2	S2	S2	
												rim	-----core	rim	-----core	
SiO2	52.41	49.48	50.97	47.99	47.19	49.12	48.94	50.25	49.27	48.24	50.14	48.67	47.32	51.96	49.29	52.47
Al2O3	25.20	32.08	29.97	33.33	35.93	28.17	29.67	30.30	31.34	31.69	24.59	27.13	27.86	25.35	26.56	26.05
TiO2	0.09	0.26	0.16	0.39	0.31	0.34	0.32	0.12	0.82	0.71	0.22	0.28	0.29	0.11	0.25	0.08
FeO*	3.73	2.04	1.86	1.57	0.88	3.00	5.09	2.72	0.83	0.98	6.73	6.17	6.18	3.38	5.81	2.59
MnO	0.00	0.00	0.01	0.00	0.00	0.03	0.00	0.04	0.01	0.01	0.03	0.03	0.04	0.05	0.02	0.00
MgO	2.63	1.67	1.77	1.13	0.45	1.88	2.10	2.20	2.08	2.15	3.14	1.53	1.44	3.31	1.92	3.05
CaO	0.07	0.02	0.05	0.01	0.00	0.02	0.04	0.03	0.00	0.08	0.11	0.06	0.01	0.00	0.04	0.12
Na2O	0.13	0.31	0.18	0.44	1.08	0.29	0.20	0.11	0.16	0.23	0.07	0.24	0.20	0.08	0.23	0.07
K2O	9.43	9.46	9.15	10.46	9.18	9.39	9.76	9.13	10.51	10.27	9.09	9.98	10.28	10.08	10.08	9.54
Total	93.70	95.33	94.12	95.32	95.02	92.24	96.12	94.90	95.02	94.36	94.12	94.09	93.62	94.32	94.20	93.97
Si	7.083	6.533	6.778	6.376	6.229	6.746	6.539	6.668	6.536	6.453	6.877	6.698	6.571	7.004	6.763	7.034
Al	4.015	4.993	4.697	5.219	5.589	4.560	4.672	4.739	4.900	4.996	3.975	4.401	4.559	4.027	4.295	4.116
Ti	0.009	0.026	0.016	0.039	0.031	0.035	0.032	0.012	0.082	0.071	0.023	0.029	0.030	0.011	0.026	0.008
Fe*	0.421	0.225	0.207	0.174	0.097	0.345	0.569	0.302	0.092	0.110	0.772	0.710	0.718	0.381	0.667	0.290
Mn	0.000	0.000	0.001	0.000	0.000	0.003	0.000	0.004	0.001	0.001	0.003	0.003	0.005	0.006	0.002	0.000
Mg	0.530	0.329	0.351	0.224	0.089	0.385	0.418	0.435	0.411	0.429	0.642	0.314	0.298	0.665	0.393	0.610
Ca	0.010	0.003	0.007	0.001	0.000	0.003	0.006	0.004	0.000	0.011	0.016	0.009	0.001	0.000	0.006	0.017
Na	0.035	0.079	0.046	0.113	0.276	0.077	0.052	0.028	0.041	0.060	0.019	0.064	0.054	0.021	0.061	0.018
K	1.625	1.594	1.552	1.773	1.546	1.645	1.664	1.546	1.779	1.753	1.591	1.752	1.821	1.733	1.764	1.632
Total	13.730	13.781	13.656	13.919	13.857	13.800	13.951	13.738	13.842	13.884	13.917	13.981	14.057	13.849	13.977	13.725
XMg	0.557	0.593	0.629	0.562	0.477	0.528	0.424	0.590	0.817	0.796	0.454	0.307	0.293	0.636	0.371	0.677
XNa	0.039	0.088	0.052	0.126	0.307	0.086	0.058	0.031	0.046	0.066	0.021	0.071	0.060	0.023	0.068	0.020

Appendix 2a. (continue)

Unit	HR								HR				PK			
Sp.No.	IS-235								IS-250				K-2-A			
No.	M3	M4	M6	M8	M9	M10	18	20	7	10	11	12	10	11	12	13
Note									S2	S2	S1	S1				
											in psm	in psm				
SiO2	48.36	48.92	48.80	47.77	46.79	47.40	49.15	51.58	48.59	48.14	47.45	48.79	53.43	52.87	52.69	53.42
Al2O3	30.75	32.18	32.50	35.09	35.32	34.51	31.10	29.12	31.11	31.56	32.22	31.72	23.95	23.79	26.21	24.81
TiO2	0.00	0.01	0.54	0.03	0.01	0.18	0.00	0.01	0.26	0.05	0.36	0.03	0.01	0.01	0.07	0.03
FeO*	2.37	3.97	1.58	0.85	1.40	1.29	2.35	1.53	2.57	2.11	2.38	1.73	3.08	3.09	3.19	3.08
MnO	0.09	0.04	0.03	0.02	0.00	0.04	0.04	0.00	0.03	0.01	0.00	0.04	0.03	0.04	0.03	0.01
MgO	1.92	0.87	1.17	0.71	0.77	0.83	1.14	2.10	1.62	1.13	1.20	1.32	3.75	3.85	3.58	3.60
CaO	0.06	0.04	0.07	0.03	0.00	0.00	0.01	0.06	0.00	0.01	0.00	0.01	0.02	0.01	0.02	0.03
Na2O	0.27	0.23	0.36	0.49	0.57	0.60	0.07	0.06	0.16	0.09	0.27	0.28	0.07	0.03	0.17	0.10
K2O	9.24	9.93	9.58	9.29	10.00	9.78	10.60	10.24	10.41	10.15	9.74	9.40	10.29	10.26	9.86	10.27
Total	93.06	96.19	94.63	94.28	94.86	94.63	94.46	94.70	94.75	93.25	93.62	93.32	94.63	93.95	95.82	95.35
Si	6.558	6.484	6.487	6.337	6.228	6.310	6.601	6.847	6.520	6.530	6.418	6.568	7.165	7.147	6.969	7.106
Al	4.915	5.027	5.092	5.486	5.541	5.415	4.922	4.556	4.920	5.046	5.136	5.033	3.785	3.790	4.086	3.890
Ti	0.000	0.001	0.054	0.003	0.001	0.018	0.000	0.001	0.026	0.005	0.037	0.003	0.001	0.001	0.007	0.003
Fe*	0.269	0.440	0.176	0.094	0.156	0.144	0.264	0.170	0.288	0.239	0.269	0.195	0.345	0.349	0.353	0.343
Mn	0.010	0.004	0.003	0.002	0.000	0.005	0.005	0.000	0.003	0.001	0.000	0.005	0.003	0.005	0.003	0.001
Mg	0.388	0.172	0.232	0.140	0.153	0.165	0.228	0.416	0.324	0.229	0.242	0.265	0.750	0.776	0.706	0.714
Ca	0.009	0.006	0.010	0.004	0.000	0.000	0.001	0.009	0.000	0.001	0.000	0.001	0.003	0.001	0.003	0.004
Na	0.071	0.059	0.093	0.126	0.147	0.155	0.018	0.015	0.042	0.024	0.071	0.073	0.018	0.008	0.044	0.026
K	1.599	1.679	1.625	1.572	1.698	1.661	1.816	1.734	1.782	1.757	1.681	1.614	1.760	1.769	1.664	1.743
Total	13.819	13.871	13.772	13.766	13.923	13.872	13.855	13.748	13.906	13.832	13.853	13.756	13.831	13.846	13.835	13.830
XMg	0.591	0.281	0.569	0.598	0.495	0.534	0.464	0.710	0.529	0.488	0.473	0.576	0.685	0.690	0.667	0.676
XNa	0.079	0.066	0.103	0.140	0.163	0.172	0.020	0.017	0.046	0.026	0.079	0.081	0.020	0.009	0.048	0.029

Appendix 2a. (continue)

Unit	PK				PK										
Sp.No.	K-7-1				K-18										PK K-19
No.	mus4	b2	b3	11	1	3	6	17	MS1	MS5	MS6	MS8	MS9	MS11	mus2
Note									S3	S3	S1	S2	S2	S3	
											in-qz	rim	-----core		
SiO2	53.08	50.50	49.42	51.86	52.27	52.99	50.38	52.27	47.91	50.63	51.39	52.68	50.86	51.47	52.09
Al2O3	25.10	25.24	29.05	25.45	25.10	24.51	24.40	23.87	22.64	25.62	23.94	25.00	24.60	25.12	23.54
TiO2	0.06	0.10	0.21	0.06	0.00	0.02	0.07	0.12	0.00	0.05	0.06	0.06	0.06	0.04	0.07
FeO*	3.53	4.74	4.17	3.61	3.25	2.65	2.87	3.09	5.78	3.91	5.19	3.01	4.83	3.50	4.26
MnO	0.11	0.14	0.11	0.00	0.04	0.03	0.06	0.04	0.23	0.08	0.10	0.02	0.06	0.05	0.08
MgO	3.13	2.80	2.40	3.16	3.58	3.69	3.26	3.86	4.97	3.73	4.46	3.60	3.48	3.47	3.21
CaO	0.05	0.13	0.01	0.01	0.04	0.00	0.00	0.08	0.00	0.11	0.00	0.01	0.00	0.00	0.04
Na2O	0.05	0.18	0.23	0.10	0.02	0.01	0.04	0.06	0.06	0.04	0.08	0.05	0.11	0.06	0.06
K2O	10.17	9.54	10.15	9.92	10.11	10.27	10.38	10.23	8.51	10.18	10.23	10.60	9.80	10.51	10.22
Total	95.28	93.37	95.75	94.17	94.41	94.17	91.46	93.62	90.10	94.35	95.45	95.03	93.80	94.22	93.57
Si	7.081	6.925	6.614	7.001	7.033	7.124	7.016	7.100	6.855	6.868	6.942	7.051	6.953	6.976	7.121
Al	3.946	4.079	4.582	4.049	3.980	3.884	4.005	3.821	3.818	4.096	3.811	3.944	3.963	4.013	3.793
Ti	0.006	0.010	0.021	0.006	0.000	0.002	0.007	0.012	0.000	0.005	0.006	0.006	0.006	0.004	0.007
Fe*	0.394	0.544	0.467	0.408	0.366	0.298	0.334	0.351	0.692	0.444	0.586	0.337	0.552	0.397	0.487
Mn	0.012	0.016	0.012	0.000	0.005	0.003	0.007	0.005	0.028	0.009	0.011	0.002	0.007	0.006	0.009
Mg	0.622	0.572	0.479	0.636	0.718	0.740	0.677	0.782	1.060	0.754	0.898	0.718	0.709	0.701	0.654
Ca	0.007	0.019	0.001	0.001	0.006	0.000	0.000	0.012	0.000	0.016	0.000	0.001	0.000	0.000	0.006
Na	0.013	0.048	0.060	0.026	0.005	0.003	0.011	0.016	0.017	0.011	0.021	0.013	0.029	0.016	0.015
K	1.731	1.669	1.733	1.708	1.735	1.761	1.844	1.773	1.553	1.762	1.763	1.810	1.709	1.817	1.782
Total	13.812	13.883	13.970	13.836	13.848	13.814	13.902	13.871	14.022	13.965	14.039	13.883	13.929	13.930	13.874
XMg	0.612	0.513	0.506	0.609	0.663	0.713	0.669	0.690	0.605	0.630	0.605	0.681	0.562	0.639	0.573
XNa	0.014	0.053	0.066	0.029	0.006	0.003	0.012	0.018	0.018	0.012	0.023	0.014	0.032	0.018	0.016

Appendix 2a. (continue)

Unit	PK			PK				PK		PK		PK		PK		PK
Sp.No.	IS-30			IS-101				IS-145		IS-169b		K3-17		K4-137		KK-3
No.	1	2	4	13	14	17	18	9	10	6	10	1	4	MUS6	MUS7	MUS2
Note	S2	S2	S1	S2	S2	S1	S1									
SiO2	53.20	52.66	52.89	50.43	50.53	49.75	47.61	51.43	50.65	52.88	51.95	50.03	51.80	51.54	52.00	52.79
Al2O3	24.26	24.56	25.13	28.25	28.24	26.25	27.06	27.36	26.68	27.79	27.71	28.80	28.59	24.43	23.88	22.19
TiO2	0.03	0.00	0.00	0.15	0.05	1.31	0.07	0.02	0.06	0.00	0.11	0.08	0.07	0.00	0.00	0.00
FeO*	3.43	2.89	2.93	2.41	2.03	2.78	5.63	3.32	3.20	1.79	1.85	4.36	2.30	3.82	3.81	3.48
MnO	0.07	0.00	0.02	0.08	0.08	0.08	0.01	0.00	0.02	0.01	0.00	0.04	0.07	0.04	0.06	0.00
MgO	3.29	3.41	3.30	2.47	2.52	2.63	1.85	2.13	2.12	2.97	2.93	1.83	2.31	2.77	2.76	4.52
CaO	0.02	0.09	0.01	0.00	0.00	0.00	0.00	0.04	0.00	0.03	0.04	0.00	0.02	0.00	0.00	0.00
Na2O	0.07	0.10	0.04	0.07	0.08	0.07	0.19	0.06	0.09	0.13	0.15	0.10	0.08	0.00	0.00	0.03
K2O	10.31	10.17	10.49	9.97	9.94	9.44	10.11	9.99	10.43	10.11	9.74	10.07	9.65	10.79	10.44	10.69
Total	94.68	93.88	94.81	93.83	93.47	92.31	92.53	94.35	93.25	95.71	94.48	95.31	94.89	93.39	92.94	93.71
Si	7.144	7.111	7.081	6.797	6.820	6.829	6.660	6.912	6.915	6.948	6.911	6.710	6.868	7.064	7.140	7.200
Al	3.839	3.909	3.965	4.488	4.492	4.247	4.461	4.334	4.293	4.304	4.345	4.553	4.468	3.946	3.864	3.566
Ti	0.003	0.000	0.000	0.015	0.005	0.135	0.007	0.002	0.006	0.000	0.011	0.008	0.007	0.000	0.000	0.000
Fe*	0.385	0.326	0.328	0.272	0.229	0.319	0.659	0.373	0.365	0.197	0.206	0.489	0.255	0.438	0.437	0.397
Mn	0.008	0.000	0.002	0.009	0.009	0.009	0.001	0.000	0.002	0.001	0.000	0.005	0.008	0.005	0.006	0.000
Mg	0.659	0.686	0.659	0.496	0.507	0.538	0.386	0.427	0.431	0.582	0.581	0.366	0.457	0.566	0.564	0.920
Ca	0.003	0.013	0.001	0.000	0.000	0.000	0.000	0.006	0.000	0.004	0.006	0.000	0.003	0.000	0.000	0.000
Na	0.018	0.026	0.010	0.018	0.021	0.019	0.052	0.016	0.024	0.033	0.039	0.026	0.021	0.000	0.000	0.008
K	1.766	1.752	1.792	1.714	1.712	1.653	1.804	1.713	1.816	1.695	1.653	1.723	1.632	1.886	1.828	1.860
Total	13.826	13.824	13.838	13.810	13.795	13.749	14.030	13.783	13.853	13.764	13.751	13.880	13.718	13.906	13.842	13.951
XMg	0.631	0.678	0.668	0.646	0.689	0.628	0.369	0.534	0.541	0.747	0.738	0.428	0.642	0.564	0.563	0.698
XNa	0.020	0.029	0.012	0.020	0.023	0.021	0.057	0.017	0.026	0.037	0.043	0.029	0.023	0.000	0.000	0.009

Appendix 2b. Representative microprobe analyses of chlorite (O=28).

Unit	TM		TM			TM				BI		HR		HR
Sp.No.	KM-69		SR-14			E8-117				AR-7		K-5-2		K-6-1
No.	11	12	18	19	25	C1	C2	C3	C4	5	7	1	2	CHL
SiO2	29.71	28.97	28.56	29.03	28.05	25.76	26.43	25.70	26.62	27.27	27.00	25.75	25.68	29.56
Al2O3	16.45	17.09	17.15	16.83	17.74	19.10	19.32	19.94	18.61	19.03	19.15	19.94	19.72	17.88
TiO2	0.00	0.00	0.00	0.00	0.00	0.02	0.00	0.00	0.00	0.06	0.00	0.00	0.03	1.83
FeO*	24.83	23.98	20.49	19.01	21.43	30.93	30.57	31.72	32.57	25.76	24.76	34.75	34.64	28.87
MnO	0.32	0.33	0.10	0.12	0.21	0.41	0.60	0.59	0.73	0.47	0.45	1.36	1.40	1.15
MgO	16.50	17.52	19.08	20.05	18.36	9.97	9.62	9.72	9.76	14.19	14.86	8.09	8.45	8.53
CaO	0.00	0.06	0.01	0.00	0.01	0.04	0.02	0.00	0.00	0.00	0.01	0.00	0.00	0.56
Na2O	0.03	0.01	0.04	0.04	0.09	0.09	0.07	0.01	0.02	0.02	0.01	0.03	0.00	0.08
K2O	0.06	0.02	0.00	0.01	0.05	0.05	0.13	0.10	0.03	0.02	0.02	0.04	0.04	0.34
Total	87.90	87.98	85.43	85.09	85.94	86.37	86.76	87.78	88.34	86.82	86.26	89.96	89.96	88.80
Si	6.199	6.023	6.006	6.078	5.903	5.699	5.800	5.611	5.797	5.811	5.765	5.586	5.572	6.260
Al	4.045	4.187	4.251	4.153	4.400	4.981	4.997	5.131	4.776	4.779	4.819	5.098	5.043	4.463
Ti	0.000	0.000	0.000	0.000	0.000	0.003	0.000	0.000	0.000	0.010	0.000	0.000	0.005	0.292
Fe*	4.333	4.169	3.603	3.328	3.771	5.723	5.610	5.792	5.931	4.591	4.422	6.304	6.286	5.113
Mn	0.057	0.058	0.018	0.021	0.037	0.077	0.112	0.109	0.135	0.085	0.081	0.250	0.257	0.205
Mg	5.132	5.430	5.982	6.258	5.760	3.288	3.147	3.164	3.168	4.508	4.730	2.616	2.733	2.694
Ca	0.000	0.013	0.002	0.000	0.002	0.009	0.005	0.000	0.000	0.000	0.002	0.000	0.000	0.127
Na	0.012	0.004	0.016	0.016	0.037	0.039	0.030	0.004	0.008	0.008	0.004	0.013	0.000	0.033
K	0.016	0.005	0.000	0.003	0.013	0.014	0.036	0.028	0.008	0.005	0.005	0.011	0.011	0.092
Total	19.793	19.889	19.878	19.856	19.923	19.834	19.736	19.839	19.824	19.797	19.830	19.877	19.907	19.280
XMg	0.542	0.566	0.624	0.653	0.604	0.365	0.359	0.353	0.348	0.495	0.517	0.293	0.303	0.345

* Total Fe as FeO.

Appendix 2b. (continue)

Unit	HR		HR		HR	HR				HR		HR
Sp.No.	IS-183		IS-190		IS-226	IS-235				IS-250		HR-22
No.	11	14	21	22	18	15	17	C2	C3	8	9	1
SiO2	25.26	25.17	24.10	25.23	26.73	26.86	28.44	25.68	26.23	25.47	25.30	26.20
Al2O3	21.41	21.25	21.34	21.63	20.26	21.55	18.43	21.09	21.57	20.72	20.94	21.48
TiO2	0.00	0.00	0.01	0.00	0.03	0.03	0.74	0.01	0.00	0.00	0.00	0.05
FeO*	30.84	30.56	32.58	29.68	30.31	30.51	28.75	29.78	29.02	31.53	29.62	30.86
MnO	0.57	0.60	0.68	0.67	0.88	0.66	0.35	0.48	0.46	0.84	0.76	1.03
MgO	8.67	9.08	7.86	8.71	10.27	8.96	10.77	9.69	9.11	8.55	9.59	8.07
CaO	0.00	0.00	0.00	0.01	0.00	0.01	0.05	0.01	0.02	0.00	0.04	0.11
Na2O	0.00	0.01	0.02	0.05	0.03	0.00	0.00	0.00	0.00	0.00	0.00	0.06
K2O	0.01	0.02	0.00	0.05	0.06	0.37	0.13	0.32	0.45	0.06	0.03	0.14
Total	86.76	86.69	86.59	86.03	88.57	88.95	87.66	87.06	86.86	87.17	86.28	88.00
Si	5.544	5.526	5.377	5.555	5.722	5.718	6.074	5.590	5.687	5.596	5.561	5.668
Al	5.538	5.499	5.611	5.613	5.112	5.406	4.639	5.411	5.512	5.366	5.424	5.476
Ti	0.000	0.000	0.002	0.000	0.005	0.005	0.119	0.002	0.000	0.000	0.000	0.008
Fe*	5.661	5.611	6.079	5.465	5.427	5.431	5.135	5.421	5.262	5.794	5.445	5.584
Mn	0.106	0.112	0.129	0.125	0.160	0.119	0.063	0.089	0.084	0.156	0.141	0.189
Mg	2.837	2.972	2.614	2.859	3.278	2.843	3.429	3.145	2.945	2.801	3.142	2.604
Ca	0.000	0.000	0.000	0.002	0.000	0.002	0.011	0.002	0.005	0.000	0.009	0.026
Na	0.000	0.004	0.009	0.021	0.012	0.000	0.000	0.000	0.000	0.000	0.000	0.025
K	0.003	0.006	0.000	0.014	0.016	0.100	0.035	0.089	0.124	0.017	0.008	0.039
Total	19.689	19.730	19.820	19.656	19.732	19.625	19.506	19.748	19.619	19.730	19.732	19.618
XMg	0.334	0.346	0.301	0.343	0.377	0.344	0.400	0.367	0.359	0.326	0.366	0.318

Appendix 2b. (continue)

Unit	HR								PK		PK	
Sp.No.	HR-50								K-2-A		K-7-1	
No.	C1	C2	C4	C5	C8	C10	C12	C14	8	9	9	10
SiO2	24.40	24.84	30.56	29.67	30.13	29.93	32.73	29.69	27.75	27.07	24.83	25.18
Al2O3	22.04	21.76	17.74	18.84	18.55	18.93	14.35	18.35	17.83	19.84	19.68	20.76
TiO2	0.07	0.03	0.21	0.16	0.00	0.00	0.01	0.00	0.07	0.00	6.28	0.06
FeO*	31.46	30.83	13.16	16.40	14.87	15.55	6.57	17.34	29.82	29.74	24.21	29.26
MnO	0.94	0.89	0.38	0.51	0.47	0.48	0.07	0.48	0.67	0.58	1.23	1.51
MgO	9.00	9.38	24.17	21.45	23.47	22.54	31.44	20.83	12.86	13.00	7.59	9.38
CaO	0.00	0.00	0.22	0.10	0.02	0.00	0.03	0.03	0.00	0.00	0.05	0.01
Na2O	0.00	0.02	0.00	0.04	0.00	0.03	0.03	0.01	0.00	0.01	0.01	0.03
K2O	0.07	0.07	0.10	0.06	0.04	0.02	0.02	0.02	0.00	0.01	0.10	0.01
Total	87.98	87.82	86.54	87.23	87.55	87.48	85.25	86.75	89.00	90.25	83.98	86.20
Si	5.319	5.401	6.092	5.969	5.987	5.970	6.394	6.031	5.895	5.658	5.491	5.555
Al	5.663	5.576	4.168	4.467	4.344	4.450	3.304	4.393	4.464	4.887	5.129	5.397
Ti	0.011	0.005	0.031	0.024	0.000	0.000	0.001	0.000	0.011	0.000	1.045	0.010
Fe*	5.736	5.606	2.194	2.759	2.471	2.594	1.073	2.946	5.298	5.198	4.477	5.398
Mn	0.174	0.164	0.064	0.087	0.079	0.081	0.012	0.083	0.121	0.103	0.230	0.282
Mg	2.925	3.040	7.183	6.433	6.952	6.702	9.156	6.308	4.073	4.050	2.502	3.085
Ca	0.000	0.000	0.047	0.022	0.004	0.000	0.006	0.007	0.000	0.000	0.012	0.002
Na	0.000	0.008	0.000	0.016	0.000	0.012	0.011	0.004	0.000	0.004	0.004	0.013
K	0.019	0.019	0.025	0.015	0.010	0.005	0.005	0.005	0.000	0.003	0.028	0.003
Total	19.848	19.820	19.806	19.790	19.847	19.814	19.962	19.777	19.862	19.903	18.918	19.745
XMg	0.338	0.352	0.766	0.700	0.738	0.721	0.895	0.682	0.435	0.438	0.359	0.364

Appendix 2b. (continue)

Unit	PK						PK		PK		PK		
Sp.No.	K-18						K-19		IS-30		IS-101		
No.	11	CHL2	CHL3	CHL4	CHL7	CHL10	3	4	3	5	15	16	20
SiO2	26.26	27.77	25.58	26.75	26.54	26.89	26.46	27.24	26.48	26.81	24.80	24.49	24.47
Al2O3	18.93	18.71	20.31	20.17	19.55	19.40	21.97	20.53	19.25	19.88	20.84	21.19	20.99
TiO2	0.00	0.44	0.49	0.58	0.41	0.00	0.03	0.03	0.01	0.02	0.00	0.00	0.00
FeO*	27.75	26.14	29.45	28.29	28.42	27.59	28.17	22.15	29.37	29.42	30.74	31.83	31.05
MnO	0.78	0.63	0.58	0.72	0.82	0.83	0.68	0.73	0.62	0.46	1.02	1.05	1.04
MgO	13.44	13.81	10.53	10.96	11.76	12.55	11.02	17.01	11.72	11.22	8.20	7.83	8.14
CaO	0.00	0.15	0.22	0.31	0.22	0.00	0.00	0.00	0.00	0.01	0.00	0.00	0.00
Na2O	0.00	0.01	0.01	0.01	0.00	0.00	0.05	0.07	0.06	0.01	0.00	0.01	0.00
K2O	0.00	0.05	0.01	0.00	0.00	0.05	0.22	0.02	0.11	0.21	0.08	0.10	0.02
Total	87.16	87.71	87.18	87.79	87.72	87.31	88.60	87.78	87.62	88.04	85.68	86.50	85.71
Si	5.661	5.870	5.558	5.719	5.695	5.765	5.589	5.633	5.717	5.745	5.542	5.455	5.479
Al	4.810	4.661	5.201	5.082	4.944	4.902	5.470	5.004	4.898	5.021	5.489	5.563	5.540
Ti	0.000	0.070	0.080	0.093	0.066	0.000	0.005	0.005	0.002	0.003	0.000	0.000	0.000
Fe*	5.003	4.621	5.351	5.058	5.100	4.947	4.976	3.831	5.303	5.272	5.745	5.930	5.815
Mn	0.142	0.113	0.107	0.130	0.149	0.151	0.122	0.128	0.113	0.083	0.193	0.198	0.197
Mg	4.319	4.352	3.411	3.493	3.762	4.011	3.470	5.244	3.772	3.584	2.732	2.600	2.717
Ca	0.000	0.034	0.051	0.071	0.051	0.000	0.000	0.000	0.000	0.002	0.000	0.000	0.000
Na	0.000	0.004	0.004	0.004	0.000	0.000	0.020	0.028	0.025	0.004	0.000	0.004	0.000
K	0.000	0.013	0.003	0.000	0.000	0.014	0.059	0.005	0.030	0.057	0.023	0.028	0.006
Total	19.935	19.739	19.766	19.650	19.767	19.791	19.712	19.878	19.861	19.773	19.725	19.780	19.754
XMg	0.463	0.485	0.389	0.408	0.425	0.448	0.411	0.578	0.416	0.405	0.322	0.305	0.318

Appendix 2b. (continue)

Unit	PK		PK		PK		PK		PK		PK		
Sp.No.	IS-145		IS-169b		K3-17		K4-137		KK-3		KM-146		
No.	7	8	7	9	2	3	1	2	CHL1	CHL2	1	2	3
SiO2	24.68	24.14	26.51	26.17	25.31	25.09	25.76	24.55	29.12	28.50	28.83	29.60	27.52
Al2O3	20.42	20.47	21.30	20.71	21.32	21.39	18.98	20.97	17.30	17.25	20.71	20.68	21.34
TiO2	0.05	0.02	0.00	0.00	0.00	0.00	0.00	0.02	0.00	0.00	0.16	0.13	0.09
FeO*	36.19	36.26	26.97	27.97	31.06	32.21	27.71	31.03	24.53	23.85	24.66	21.71	24.96
MnO	0.91	0.92	0.90	0.89	1.13	1.16	0.69	1.18	0.22	0.00	0.52	0.58	0.55
MgO	5.35	5.14	12.26	11.16	8.39	7.67	9.60	7.82	16.62	17.20	15.45	15.01	15.11
CaO	0.00	0.00	0.00	0.00	0.00	0.00	4.23	0.00	0.10	0.13	0.04	0.11	0.03
Na2O	0.00	0.00	0.02	0.00	0.00	0.00	0.07	0.02	0.01	0.00	0.06	0.06	0.05
K2O	0.06	0.04	0.23	0.06	0.05	0.15	0.31	0.07	0.02	0.00	0.28	0.35	0.01
Total	87.66	86.99	88.19	86.96	87.26	87.67	87.35	85.66	87.92	86.93	90.72	88.23	89.66
Si	5.547	5.482	5.605	5.647	5.546	5.512	5.638	5.505	6.065	5.990	5.813	6.033	5.631
Al	5.409	5.479	5.308	5.266	5.506	5.539	4.896	5.542	4.247	4.273	4.920	4.968	5.145
Ti	0.008	0.003	0.000	0.000	0.000	0.000	0.000	0.003	0.000	0.000	0.025	0.019	0.013
Fe*	6.802	6.887	4.769	5.047	5.692	5.918	5.072	5.819	4.273	4.192	4.157	3.700	4.271
Mn	0.173	0.177	0.161	0.163	0.210	0.216	0.128	0.224	0.039	0.000	0.089	0.100	0.096
Mg	1.792	1.740	3.864	3.590	2.741	2.512	3.132	2.614	5.161	5.389	4.644	4.561	4.610
Ca	0.000	0.000	0.000	0.000	0.000	0.000	0.992	0.000	0.022	0.030	0.009	0.025	0.006
Na	0.000	0.000	0.008	0.000	0.000	0.000	0.030	0.009	0.002	0.000	0.022	0.025	0.019
K	0.017	0.012	0.062	0.017	0.014	0.042	0.087	0.020	0.006	0.000	0.072	0.091	0.003
Total	19.749	19.781	19.777	19.729	19.708	19.739	19.973	19.736	19.816	19.874	19.750	19.522	19.794
XMg	0.209	0.202	0.448	0.416	0.325	0.298	0.382	0.310	0.547	0.562	0.528	0.552	0.519

Appendix 2c. Representative microprobe analyses of stilpnomelane (O=13.5).

Unit	TM														
Sp.No.	K-15		IS-57'		E8-38				E8-101	E8-112'		KM-69		SR-14	
No.	12	13	19	20	2	4	5	10	14	3	4	16	17	20	21
Note						core	------rim	+ act							
	brown	brown	brown	brown	brown	green	brown	brown	brown	brown	brown	green	green	brown	brown
SiO2	46.55	49.10	46.46	46.17	48.06	46.56	47.15	49.54	46.15	46.05	44.35	48.10	47.01	50.97	50.51
Al2O3	5.83	6.07	5.95	5.78	5.75	5.58	5.56	5.77	5.47	5.98	5.72	5.82	5.69	6.25	6.27
TiO2	0.01	0.00	0.00	0.00	0.01	0.00	0.00	0.00	0.44	0.00	0.00	0.00	0.02	0.00	0.03
FeO*	20.49	21.74	28.39	28.12	25.27	24.33	26.20	24.79	26.56	26.94	26.29	24.86	24.14	19.28	19.56
MnO	3.24	3.26	0.62	0.64	0.63	0.70	0.64	0.64	0.76	0.76	0.82	1.18	1.23	0.97	0.98
MgO	9.39	10.68	5.89	5.98	8.63	8.39	8.42	9.01	6.82	6.41	6.14	8.85	8.82	12.69	13.46
CaO	0.14	0.13	0.01	0.03	0.14	0.05	0.07	0.07	0.02	0.02	0.00	0.00	0.03	0.00	0.03
Na2O	0.23	0.20	0.04	0.04	0.33	0.31	0.22	0.05	0.19	0.25	0.32	0.21	0.22	0.04	0.04
K2O	2.33	1.31	0.69	0.84	1.85	4.77	2.94	0.14	1.40	1.89	6.34	3.60	1.04	0.40	0.30
Total	88.21	92.49	88.05	87.60	90.67	90.69	91.20	90.01	87.81	88.30	89.98	92.62	88.20	90.60	91.18
Si	3.999	3.955	4.027	4.029	4.033	4.033	3.986	4.081	4.027	4.024	4.011	4.011	4.002	4.058	3.980
Al	0.590	0.576	0.608	0.594	0.569	0.570	0.554	0.560	0.563	0.616	0.610	0.572	0.571	0.586	0.582
Ti	0.001	0.000	0.000	0.000	0.001	0.000	0.000	0.000	0.029	0.000	0.000	0.000	0.001	0.000	0.002
Fe*	1.472	1.464	2.058	2.052	1.773	1.762	1.853	1.708	1.938	1.969	1.988	1.734	1.718	1.284	1.289
Mn	0.236	0.222	0.046	0.047	0.045	0.051	0.046	0.045	0.056	0.056	0.063	0.083	0.089	0.065	0.065
Mg	1.203	1.282	0.761	0.778	1.080	1.083	1.061	1.106	0.887	0.835	0.828	1.100	1.119	1.506	1.581
Ca	0.013	0.011	0.001	0.003	0.013	0.005	0.006	0.006	0.002	0.002	0.000	0.000	0.003	0.000	0.003
Na	0.038	0.031	0.007	0.007	0.054	0.052	0.036	0.008	0.032	0.042	0.056	0.034	0.036	0.006	0.006
K	0.255	0.135	0.076	0.094	0.198	0.527	0.317	0.015	0.156	0.211	0.732	0.383	0.113	0.041	0.030
Total	7.807	7.677	7.584	7.603	7.764	8.084	7.860	7.529	7.690	7.755	8.288	7.917	7.652	7.547	7.539
XMg	0.450	0.467	0.270	0.275	0.378	0.381	0.364	0.393	0.314	0.298	0.294	0.388	0.394	0.540	0.551

* Total Fe as FeO.